University of Alberta

ROBUST CONTROL OF LARGE SCALE SYSTEMS WITH APPLICATION TO AN INDUSTRIAL INTEGRATED ENERGY PLANT

by

Adarsha Swarnakar 

A thesis submitted to the Faculty of Graduate Studies and Research in partial fulfillment of the requirements for the degree of

Doctor of Philosophy

Department of Electrical and Computer Engineering

Edmonton, Alberta
Fall 2008

Your file Votre référence
ISBN: 978-0-494-46434-2
Our file Notre référence
ISBN: 978-0-494-46434-2

Live as if you were to die tomorrow. Learn as if you were to live forever.

– Mahatma Gandhi

To my parents

Abstract

In engineering applications like power systems and robotics, the systems consist of many interconnected subsystems. In some situations, due to fault or maintenance issues, these subsystems are disconnected and again connected (structurally perturbed) to carry out the required job. Moreover, during operation, when a disturbance affects the plant and causes variation in the process variables, namely, frequency of generators or angle of robot arms, most probably the operator adjusts the controller parameters to overcome this disturbance. In this situation, one can ask two practically important questions: "Is it possible to maintain overall stability under structural perturbations (connective stability) or when the controllers are detuned capriciously? How much of the performance loss of the system is due to these scenarios?"

During the last three decades, many research efforts designed a controller for each subsystem in a plant, this is called decentralized design. The controllers were synthesized for stability under load fluctuations and for other objectives. However, due to complexity, there are few clear and effective design techniques for connective stability and/or for stability under arbitrary control loop detuning. Furthermore, every system possesses some degree of nonlinearity and structured controller design for nonlinear systems is an active area of investigation.

The approach of this thesis is to utilize mathematical tools, namely, structured singular values, properties of norms, different optimization techniques, transformation methods, and matrix operations to cast the design of controllers into a convex optimization framework (in some cases, quasi-convex) which is readily solvable by available numerical software. These algorithms are clear and computationally efficient. An additional goal is to develop new conditions for reducing the performance loss of a decentralized control system. The

work here verifies the theoretical design algorithms developed in this thesis as applied to Syncrude control problems. This plant is highly nonlinear and the controllers presently working cannot overcome problems such as: a) due to arbitrary tuning of the controllers and sudden load variations, the 900-pound header pressure undergoes oscillations which the controllers are incapable to damp out quickly and b) controlling the load fluctuations requires large quantities of natural gases, a major economic concern.

Acknowledgements

The work in this thesis was done during the last three and half years under the esteemed supervision of Dr. Horacio J. Marquez and Dr. Tongwen Chen. I am thankful to them for their technical suggestions, assistance, cautiously reviewing manuscripts related to my PhD work, and I feel privileged working under their guidance.

It was a pleasure to work in the Advanced Control Laboratory where I had the opportunity to learn and share ideas with my colleagues Jingbo, Yu, Jing, Mostafa, Ali, Reza, and Vahid and my seniors Amr, Danlei, Guofeng and Jiandong. I would also like to thank Dr. Vinay Kariwala of Nanyang Technological University, Singapore and Dr. Feng Tao of Rutter Hinz Inc for valuable technical suggestions and comments on the chapter 4 of this thesis.

I appreciate the research grant from Syncrude Canada Ltd. and Natural Sciences and Engineering Research Council of Canada during the first three years and British Columbia Transmission Corporation afterwards that was provided to me by Dr. Horacio J. Marquez and Dr. Tongwen Chen as a research assistantship. The funding was instrumental in providing me the opportunity to attend conferences, which led me to continually learn about new technological developments and to meet renowned researchers in my field. I am also gratified to the Instrument Society of America and the University of Alberta to support my research.

Table of Contents

List of Tables

List of Figures

Nomenclature

The abbreviations, symbols and notations used in this thesis are included here. This is done to maintain a uniformity for technical persons of two different disciplines: control systems and power plant. Some of them are standard and can be found in [3, 50]. Matrices are denoted by boldface upper case, vectors by boldface lower case, and all other variables are in italics.

Greek Symbols

$\pi(\cdot)$	Region of attraction
δ	Distance to uncontrollability or unobservability
α	Degree of robustness
γ	Performance parameter
η	Set of laguerre coefficients
κ	Euclidian condition number of a matrix, transfer matrix
μ	Structured singular value
ρ	Spectral radius
λ	Lagrange parameter
λ_{max}	Maximum eigenvalue
ω_{nmax}	Maximum undamped natural frequency
α_{min}	Minimum decay rate
σ	Singular value
$\bar{\sigma}$	Maximum singular value
$\underline{\sigma}$	Minimum singular value
ω	frequency
$\mathbf{\Delta}$	Uncertainty matrix

Abbreviations

iff	if and only if
w.r.t	with respect to
via	through
vs	versus
AM	Auto manual
ARE	Algebraic riccati equation
BBD	Bordered block diagonal
BLT	Biggest log-modulus tuning
BMI	Bilinear matrix inequality

CCL	Cone complementary linearization
CL	Closed loop
DIC	Decentralized integral controllability
DNA	Direct nyquist array
FD	Forced draught
FE	Flow element
FRC	Flow recorder controller
FT	Flow transmitter
FY	Flow relay
GRC	Generating rate constraint
HPI	Hydrocarbon processing industry
HP	High pressure
ID	Induced draught
IM	Interaction measure
IMC	Internal model control
IP	Intermediate pressure
ITAE	Integral time absolute error
KKT	Karush-Kuhn-Tucker
LCV	Level control valve
LHP	Left half of the complex plane
LIC	Level indicator controller
LMI	Linear matrix inequality
LP	Low pressure
LQR	Linear quadratic regulator
LT	Level transmitter
LTI	Linear time invariant
LY	Level relay
OTSG	Once-through steam generator
MATLAB	Matrix Laboratory
MIMO	Multi input multi output
MPC	Model predictive control
NI	Niederlinski index
NP	Non-polynomial time
PI	Proportional integral
PID	Proportional integral derivative
PRC	Pressure recorder controller
PT	Pressure transmitter
PZ	Pole zero
QP	Quadratic programming
RGA	Relative gain array
RHP	Right half of the complex plane
ROC	Rate optimal control
SISO	Single input single output
SS	State space
SYNSIM	Syncrude simulation package
TT	Temperature transmitter
UB	Utility boiler
YALMIP	Yet another LMI parser

Notations

$\dot{(\cdot)}$	Derivative w.r.t time
$\|\cdot\|_p$	p-norm of vectors, matrices or transfer functions
$(\cdot)^T$	Transpose of a matrix
$\mathrm{Re}(\cdot)$	Real part
$\det(\cdot)$	Determinant of a matrix or transfer matrix
$\mathrm{tr}(\cdot)$	Trace of a matrix
$\mathrm{diag}(\cdot)$	Diagonal part of a matrix
$\min(\cdot)$	Minimization of a function
$\mathbb{R}$	Set of real numbers
$\bar{\mathbf{Q}}$	State weighting matrix
$\bar{\mathbf{R}}$	Control weighting matrix
N_p	Prediction horizon
N_c	Control horizon
a	Scaling factor
j	Imaginary number
s	Laplace parameter
$\mathbf{u}$	Variables to be manipulated or control signals
$\mathbf{y}$	Variables to be controlled or measurements
$\mathbf{A}$	State matrix
$\mathbf{B}$	Input matrix
$\mathbf{C}$	Output matrix
$\mathbf{D}$	Feedthrough matrix or scaling matrix
$\mathbf{L}$	Observer gain matrix
$\mathbf{I}$	Identity matrix
$\mathbf{K}(s)$	Controller or compensator
$\mathbf{G}(s)$	System transfer matrix from $\mathbf{u}$ to $\mathbf{y}$
$\tilde{\mathbf{G}}(s)$	(Block) diagonal part of $\mathbf{G}(s)$
$\mathbf{S}(s)$	Sensitivity function
$\mathbf{R}(s)$	Control sensitivity function
$\mathbf{H}(s)$	Complementary sensitivity function
$\mathcal{RH}_\infty$	Subspace of real rational transfer matrices with poles on the left half of the s-plane
$\Re^{m\times n}$	Space of real numbers with dimension $m \times n$
$N(\alpha, \mathbf{F}(s))$	Net number of clockwise encirclements of the point $(\alpha, 0)$ by the image of Nyquist D contour under $\mathbf{F}(s)$
$\star$	Terms that are induced by symmetry
$+-$	Biasing station
■	End of proof

Norms

$\mathcal{H}_\infty$ norm: For a stable system $\mathbf{G}(s)$ [91]

$$\|\mathbf{G}(s)\|_\infty = \sup_{\omega\in\mathbb{R}} \bar{\sigma}(\mathbf{G}(j\omega))$$

$\mathcal{L}_\infty$ norm: It is similar to $\mathcal{H}_\infty$ norm, but for an unstable system $\mathbf{G}(s)$ with no poles on

the imaginary axis.

Chapter 1

Introduction

1.1 Overview of Multi-Loop Control Systems

Interconnected systems appear in a number of fields such as power systems, chemical processes, space structures, and robotics, to name a few. During the last few decades, research in the field of large-scale interconnected systems has concentrated on decentralized robust control strategies [31, 44, 46, 56, 70, 81, 82, 84, 85, 87, 120, 123, 125]. An incentive to design decentralized control methods is that splitting the large scale systems into low order subsystems and subsequent controller design for each subsystem lead to a decrease in an overall computational effort. Although, it is not always possible to respect this desideratum, other reasons for this preference include [5, 31, 32, 36, 42, 49, 82, 84, 85, 88, 91]:

- *Modeling effort*: In the case of multivariable design, a good process model of the overall system is mandatory. The model must be maintained and renewed and the corresponding optimization problem should be modified when alterations occur in the process [88]. In a decentralized scheme, the designer needs to know only the model of each subsystem and the controllers can be obtained and tuned easily with some prior knowledge of process interactions (either by intuition or experiment). It is even possible to tune controllers online by selecting a few parameters, e.g., gain, integral time constant, or reset rate, without destabilizing the overall system [88, 91]. Therefore, in some process industries centralized architectures are avoided in support of simple structured (diagonal, block diagonal, BBD) controllers [36, 42].

- In power systems, robotics, and space structures, very often interconnected systems do not remain as a single entity in an working environment. In many cases (faults, operational requirements), subsystems are disconnected and again connected to

perform the required task [84]. Under such structural reconfigurations, what is required is a control strategy that can guarantee *connective* stability (stability in the presence of structural perturbations) of the overall system [82, 84], and/or attain a desired *performance* in the face of uncertainty in interconnections [31, 49].

- In power systems, where subsystems are geographically separated from each other, there are also frequent changes in power generation. This deregulated environment leads to unforeseen malfunctions in the subsystems. Under these situations, it is necessary to develop decentralized control strategies that keep processes operating well under varying operating conditions and in the presence of different disturbances [5, 85].

- Failure tolerance capability and ease of understanding has led to acceptance of decentralized control by operators in the industry.

The design of the aforementioned control system includes [89]: 1) selection of suitable pairings and 2) design of (block) decentralized controllers. So far in process industries, the RGA [15] and Rijnsdrop's interaction measure [76] have been found to be practical means of removing impracticable pairings (step 1). For the control design (step 2), past research efforts boil down to the following four categories [7, 21, 50, 51, 57, 65, 68, 89, 112]

a) *Simultaneous design*: In this approach, the controller is assumed to be of a predetermined structure (like state space form, PID, PI, etc.) with some parameters to be designed. By using different optimization techniques, parameters are obtained by minimizing the suitable norms ($\mathcal{H}_2$, $\mathcal{H}_\infty$) of the CL system [50, 51]. A shortcoming of this approach is its relative complexity and, in some cases, the non-convexity of the resulting optimization problem [7, 50, 51].

b) *Detuning method*: In this technique, the controller for each subsystem is first designed by ignoring interactions among different loops. Next, the controllers are detuned with some knowledge of the interactions (obtained by prior experiments) until a prespecified stability condition is satisfied [57]. In [65] a similar approach called the BLT method was proposed where the controllers were first designed using the Ziegler-Nichols method. This provides an appropriate starting point of the next tuning step. Then, the controllers are detuned by regulating a variable that divides the controller gain and multiplies the reset time. This parameter provides a tradeoff between stability and performance, because increase in its value leads to sluggish

response but brings more stability to the system. Due to the fact that it is easily understandable, the method is widely accepted in industry, however, it is applicable to open loop stable linear systems *only* [57].

c) *Sequential loop closing*: In this case, each block of the controller is designed one after the other. At first, the controller related to a fast loop (inner loop) is designed and the loop is closed. Then, the controller corresponding to the next loop is designed based on this closed loop system information [50, 51, 89]. Due to its simplicity, this method is now being widely used in industry. However, when the lower level loops fail, the failure tolerance of the remaining loops cannot be guaranteed [21, 57, 68, 89, 112].

d) *Independent design*: In this method, the control design is based on the (block) diagonal elements of the system. The controller in each loop is designed by stipulating the form of each CL transfer function, resulting in an IMC-PID type controller [57]. If the interaction is less than a certain bound, this method can maintain stability of the overall closed loop system. Since information about the controllers in other loops is not used, the design is conservative but the nominal stability of the remaining loops is guaranteed if *any* loop fails [35, 50, 51, 57, 89].

Shortcomings of decentralized control systems include closed loop performance degradation due to interactions, and, in many cases, non-convexity of the optimization problem at the design phase [79]. This thesis provides some insight into approaches a) and d) above and tries to solve problems in these methods. Thus the work is mainly focussed on the control design and it is assumed that suitable loop pairings between measured variables and the corresponding manipulated variables have been already decided in advance. However, in chapter 4 there is some discussion on the pairing problem.

1.2 Structure and Outline of the Thesis

This section presents the structure and outline of this thesis.

1.2.1 Thesis Overview

In chapter 2 the following class of nonlinear interconnected systems [70, 84, 85, 87, 120, 125]

$$\dot{\mathbf{x}}_i = \mathbf{A}_i\mathbf{x}_i + \mathbf{B}_i\mathbf{u}_i + \mathbf{G}_i\mathbf{h}_i(\mathbf{x}),\ \ \mathbf{y}_i = \mathbf{C}_i\mathbf{x}_i,\ \ i = 1, 2, 3, \ldots, N$$

is considered, and decentralized observer-based controllers and dynamic output feedback controllers based on measurements are designed. Here, $\mathbf{x}_i \in \Re^{n_i}$ are the states, $\mathbf{u}_i \in \Re^{m_i}$ are the inputs, $\mathbf{y}_i \in \Re^{p_i}$ are the outputs, and $\mathbf{h}_i(\mathbf{x})$ are interconnections. This problem was recognized in 2001 by [84] and numerous efforts were made by [70, 95, 125] to design decentralized observer-based control laws; however, an algorithm to design these controllers remained to be created, because a non-convex optimization problem can only give a *local* solution. In this chapter, a thorough literature survey is performed on the theory and applications of this class of system and LMI tools are utilized to cast the design problem into a convex optimization framework. This algorithm is computationally efficient, gives a global minimum *if* it exists, and maximizes the robustness of CL system against uncertain nonlinear perturbations. Performance issues are also considered in chapter 2.

In chapter 3 the design of controllers in which some information is shared among subsystems is considered. In the overlapping control law, the local controllers use shared states to improve the stability and performance of the overall closed loop system. In this chapter, motivations arose by following the work of [87, 122]. These authors did a thorough survey of limitations related to past work and proposed a less restrictive static state feedback control design in the LMI framework. The method was applied to a platoon of unmanned vehicles where two different kinds of overlapping, namely, Type I and Type II (Fig. 1.1) were taken into account. For Type I, the input matrix and the control law have the following forms [122]:

$$\mathbf{B} = \begin{bmatrix} \mathbf{B}_{11} & 0 \\ \mathbf{B}_{21} & \mathbf{B}_{22} \\ 0 & \mathbf{B}_{32} \end{bmatrix}, \quad \mathbf{K} = \begin{bmatrix} \mathbf{K}_{11} & \mathbf{K}_{12} & 0 \\ 0 & \mathbf{K}_{22} & \mathbf{K}_{23} \end{bmatrix}, \tag{1.1}$$

and in Type II $\mathbf{B_{21}} = \mathbf{B_{22}} = 0$. However, in the Type II overlapping case, some parameters in the optimization problem were selected on a trial and error basis to convert the nonlinear optimization problem into LMIs. Moreover, for both Type I and Type II overlapping a structured Lyapunov function was considered, which may cause infeasibility and decrease in the degree of robustness. Inspired by these restrictions, a *general* algorithm that takes into account a wide panorama of open NP-hard problems [12] in overlapping control such as state feedback, static output feedback, and full order as well as reduced order dynamic output feedback control designs is proposed. There is no need to select parameters by trial and error or to use structured Lyapunov functions. The algorithm is applicable to other structures of the controllers, namely, decentralized design or control design when state information is shared by a number of subsystems and BBD structure [87]. The results are generalized to N nonlinear interconnected systems.

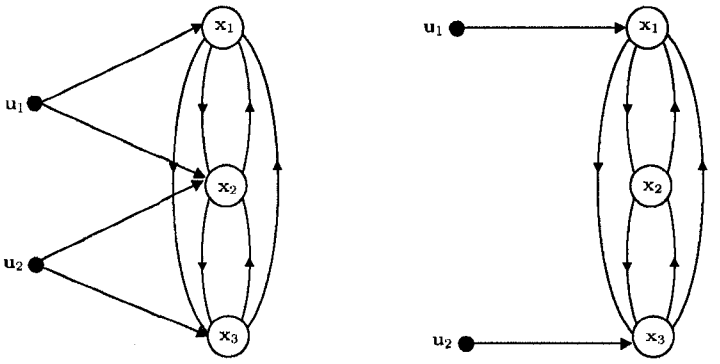

Figure 1.1: Type I and Type II overlapping [122].

To bring some disparity between different techniques used in this thesis, chapter 4 deals with a frequency domain design method. The method is based on an independent design for linear systems where the controller in each loop is designed without using information of other controllers. The challenge is to find a (block) diagonal approximated system that possesses the same number of unstable poles as the plant. This problem was considered in 1986 by [35] and many efforts were placed, however, utilization of this technique is restricted to open loop *stable* systems. In this chapter, different properties of norms, congruence transformations, and reciprocal variant of the projection lemma are utilized to provide an easily understandable and programmable approach to this problem. This contribution is important in the sense that the solution of this problem leads to a generalization of all the past results of independent designs (based on μ-IM [57, 63, 89], and many others) to *unstable* systems. New results are also presented such as finding an upper bound of the CL performance requirement due to decentralized architecture and derivation of conditions under which closing one loop does not propel the zeros of other parts to cross the imaginary axis.

Despite this flurry of theoretical developments, different applications are considered to show that the theory is of practical interest. In chapter 2 a nonlinear interconnected model of a boiler-turbine system [5, 6] is studied and the developed control framework is successfully applied to this unit. In chapter 3 a two area power system is considered and the development of a nonlinear model is described for a utility boiler-header system for Syncrude Canada Ltd. Throughout the modeling phase, a nonlinear simulation package of Syncrude called SYNSIM is used, which includes the nonlinearities in the plant. This package was developed to simulate unpredictable perturbed situations and to analyze

stability and performance. At present, SYNSIM is extensively used by engineers because the match between plant measurements and predictions achieved by SYNSIM is good. The developed model is successfully validated with the data from SYNSIM.

In Sections 1.2.2-1.2.3 some basic concepts of power plant operation and Syncrude integrated energy systems (where the control problems were found) are presented. A reader knowledgeable in power plant control and instrumentation may pass over these sections without loss of continuity.

1.2.2 Power Plant Technology

Industrial boilers are highly interconnected; their main task is to generate steam for producing electricity and exporting the electrical energy to the grid [61]. The generated steam may also be supplied to utilities, other processes or a residential unit. A schematic of a steam boiler system is shown in Fig. 1.2 (a simplified diagram is available in [61]). The figure can be split into three parts: fire, water, and electrical. On the fire side, the heat is produced by burning fossil fuels (coal, methane, ethane, etc.), from the exhaust of gas turbines, or by harnessing the heat from radioactive decay of nuclear fuels. On the water side, feedwater passes through an economizer (which exchanges heat between incoming feedwater and outgoing flue gas) and is supplied to the boiler drum. The feedwater then proceeds to the mud drum through downcomers, and the mud drum dispenses the water to risers (by natural or forced circulation). The heat supplied to the risers is used to boil water. Saturated steam (300°C) is then separated from the water in the drum and directed to superheaters and waterwall headers to achieve a superheated steam (500°C) that flows to a header. An attemperator between superheaters sprays cold water to control the temperature. On the electrical side, the superheated steam passes through turbines to convert the heat energy into mechanical energy and then to electrical energy in the generators. The condensed steam from the low pressure turbines flows to a condenser (DM-makeup), low pressure heaters, deaerators (to remove air from water), high pressure heaters, and a feed control station which distributes it to an economizer. The plant operation is based on the well-known Rankine cycle, a thermodynamic cycle that involves chemical engineering, physics, thermodynamics, and mechanical and electrical engineering. As shown in Fig. 1.3, processes in the Rankine cycle can be broken down into the following parts:

- 2-3– condensate is heated and water is pumped to the boiler drum at 140°C,

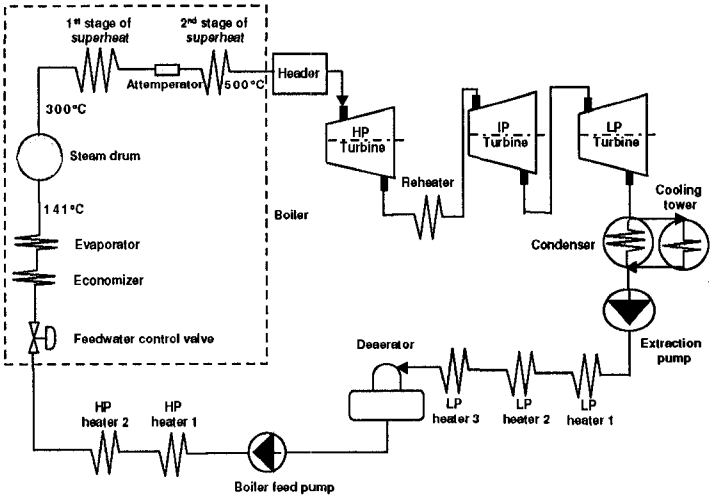

Figure 1.2: Operation of power generating plant.

- 3-3'– feedwater is heated to a saturation temperature in the drum,
- 3'-4– feedwater converted to steam at a saturation temperature,
- 4-4'– steam is superheated in the primary and secondary superheaters,
- 4'-5– steam is expanded in the HP turbine,
- 5-5'– steam is heated in reheaters (situated between HP and IP turbines),
- 5'-1– steam is expanded in IP and LP turbines, and
- 1-2– LP exhaust steam is converted to condensate by cooling water.

The efficiency of the plant depends on the area of the temperature versus entropy diagram in Fig. 1.3.

As shown in Fig. 1.4, a part of the interconnected system at the Syncrude plant consists of UBs (UB 201-UB 203), CO-type boilers (C.O.1 and C.O.2), and OTSGs (OTSG1 and OTSG2) developed by Innovative Technologies, Ontario. The plant has four divisions: mining, extraction, upgrading, and utilities. Steam from different boilers is collected in the 900# (900 pounds or 6.306 MPa) header and is used in: 1) cokers for extracting bitumen from oil sands, 2) other low pressure headers (600#, 150#, 50#) for extraction, upgrading (conversion of bitumen heavy oil into lighter components like naphtha, diesel oil), building heating, etc., and 3) turbines (G1, G2, G4 and G6) for generating electricity. The difference

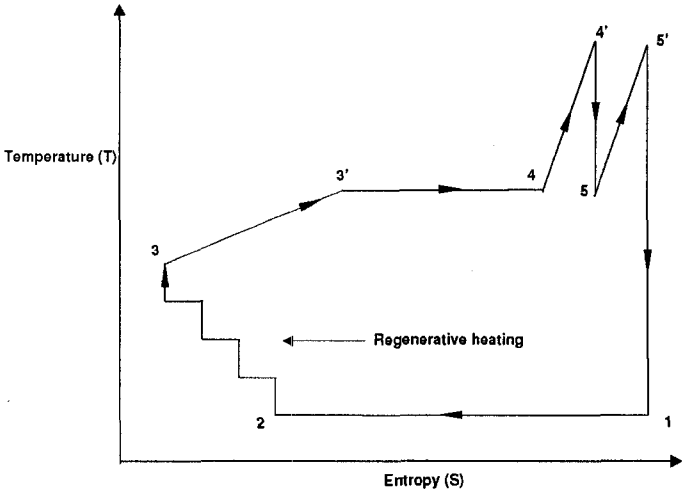

Figure 1.3: Ideal Rankine thermodynamic cycle [117].

between UB and CO-type boiler lies in the type of fuel used; UBs burn natural gases such as methane and ethane and CO boilers exploit coker-off gases. OTSGs exchange heat (without drums) between incoming feedwater and outgoing hot gases from G3 and G5. However, the working principle of UBs and CO-type boilers is the same, as shown in Fig. 1.2. Due to boiler characteristics (time constants, fuel used), utility boilers maintain the 900# header pressure, CO boilers have self loops for the steam flow, and OTSGs maintain their own steam temperatures. The let down stations reduce steam pressure and act as interfaces between headers.

Recently, a new UE-1 system consisting of two CO boilers (CO3, CO4) was introduced in the plant to take care of additional load demands. In Fig. 1.4, G3 and G5 are gas turbines, G1, G2, and G4 are back pressure steam turbines (sensitive to 50# back pressure), and G6 is a condensing turbine. The 50# steam is used for heating frozen water, in deaerators for removing air from feedwater, in trim heaters for heating recycled water, in tumblers for conversion into water, and for many other purpose. The system incorporates cokers (8-1 and 8-2) that are chemical reactors and utilize the 900# steam and hydrocarbons to produce bitumen. They also supply hot gases for the CO boilers.

1.2.3 Drum Level and Header Pressure Control

Figs. 1.5-1.6 (a simplified form is available in [61]) show methods to control the drum water level and the header pressure, respectively, in the plant. Drum water level is controlled by a three-element feedforward strategy using measurements of level, steam flow, and feedwater

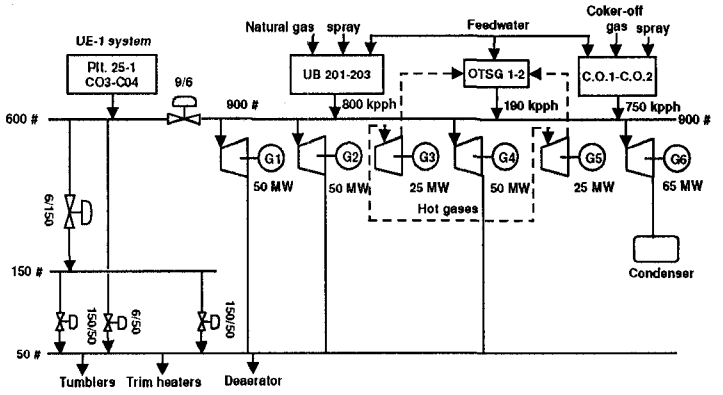

Figure 1.4: A part of the interconnected system at Syncrude.

flow. This method reduces the well-known swelling and shrinking problem. Without these loops, if the steam demand is suddenly increased, the pressure inside the drum will decrease causing the water level to rise (steam bubbles inside the water expand). Therefore, LIC-1 commands the valve LCV-1 to close, which is an opposite action because now more water is required due to an increase in load. With additional flow loops, the input to LIC-1 is $S' = S + k_1(f_s - f) - k_2(f_w - f')$, where S is the set point for the water level, f_s is the actual steam flow, f is the normal steady state flow, f_w is the actual feedwater flow, and f' is the steady state value of the feedwater. Hence, during high load conditions when additional steam is flowing out of the drum, the set point automatically increases, thereby avoiding the swelling problem. The gains k_1 and k_2 are conversion factors.

The 6.306 MPa header pressure control in Fig. 1.6 is based on the concept of a cross limiting system. For safe operation of the boiler, the furnace should function in an air rich condition. In a fuel affluent furnace there is a possibility that carbon monoxide, nitric oxide, and other explosive mixtures are formed, which is hazardous. This is overcome by a cross limiting system. The master control signal (output of PRC-1) is divided into two signals: fuel demand and air demand. A total air flow signal from the FD fan inlet (output of FT-1 and FT-2) is passed to a computing relay (k_1) to offer the required amount of fuel flow (excess air is always considered). This signal is compared with the fuel demand signal in a low selector relay (<), the output of which controls the fuel flow. Similarly, the output of the measured fuel flow is supplied to another computing relay (k_2) to provide the required amount of air for combustion. This signal is compared with the air demand signal from the master in a high selector relay (>), the output of which controls the air flow. In a cross limiting system an air rich condition is always maintained. As shown in Fig. 1.6, the

strategy is based on the notion of cascade control, where outputs of the selector relays act as set points of the loops that control the fuel valves and the FD fan vanes.

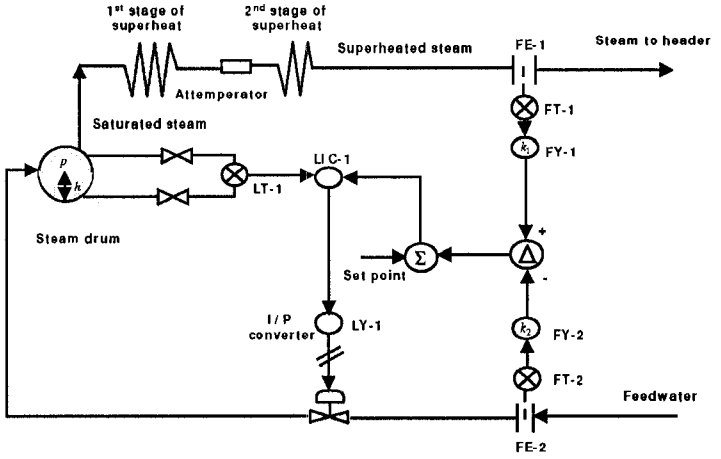

Figure 1.5: Drum level control.

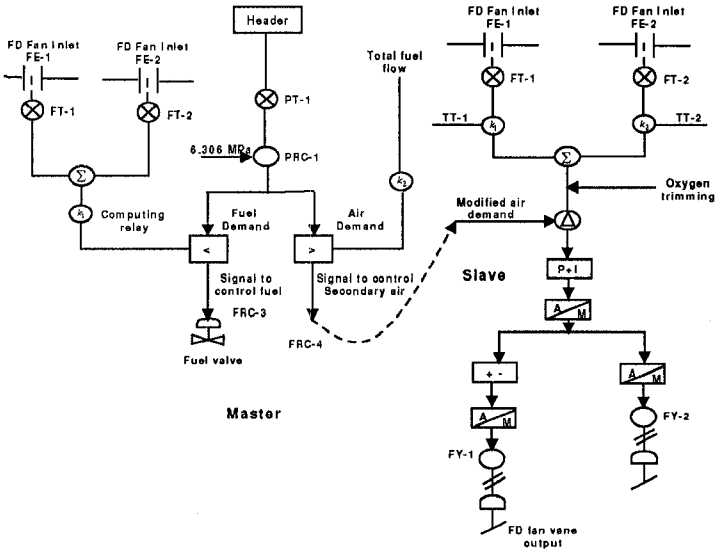

Figure 1.6: Header pressure control.

1.2.4 Design Strategy

In this work attention is focused on the control problem of the boilers and the header system in the Syncrude plant. The drum water level and pressure control loops are themselves

complex, but the addition of numerous other interacting loops in the turbines G1-G6, deaerators, in load levelling stations (let down stations), in superheaters (in addition to PID loops, burner tilts are utilized), in tumblers, and in many other sources–increases the complexity significantly. The decentralized PI controllers in the plant work well; however, the 6.306 MPa header pressure shows oscillatory behavior under load fluctuations that the controllers are incapable to damp out quickly. This happens due to nonlinearities and interactions from other subsystems. To take into account this issue, overlapping controllers are designed. Their performance under load fluctuations is then compared with the existing PI controllers in the plant. A best possible design strategy is proposed; it reveals that when the header pressure utilizes the extra measurement of the steam temperature, performance of the overall system significantly improves.

Finally, in chapter 5 the focus is on economic issues in the Syncrude plant. Sudden switching of the work towards the direction of MPC is due to several factors: a) the letter in [34] praised MPC algorithms over decentralized designs and claimed atleast 300 applications of this method in the HPIs, b) constraints on different process variables and manipulated variables as well as their rate of change can be easily incorporated in MPC; this is difficult in other methods, c) MPC algorithm development is possible even for a naive designer, and d) this method utilizes the Riccati approach, KKT conditions, and Hildreth's QP procedure rather than LMIs that use an interior point algorithm; this diversifies solution approaches used in this thesis. Shortcomings of the MPC method are that it requires a good process model and that the method is slow. Unlike other methods where the control output depends on the sensor measurements the controllers receive, MPC relies on the model for its control action [88]. Nevertheless, the operation of the boilers is sluggish with large settling times and constraints must be satisfied on the firing rate signal, fuel flow, air flow and spray flow, to mention just a few. Therefore, the application of MPC fits well in this context. In chapter 5 an efficient technique is presented to manipulate the firing rate of CO-type boilers (in addition to UBs) to control the header pressure. This set-up reduces the consumption of natural gases in UBs, leading to fuel economy. Emphasis is placed on modeling, programming, and writing S-functions to design the model predictive controller that involves online optimization, computation of the optimal control trajectory at each sampling instant, and implementation of the first sample while ignoring the rest (receding horizon control).

Each chapter includes a comprehensive literature survey relevant to the problem at hand. To improve the readability, most of the mathematical derivations have been moved to the

appendix and ideas are expressed verbally with numerical examples and figures.

1.3 Contributions

The contents of this thesis was presented in a number of international journals and conferences, as listed below:

- Chapter 2: A significant part of this chapter was published in Control Engineering Practice, 2007 [101], IEEE Transactions on Control Systems Technology, 2008 [103], American Control Conference, Minneapolis, 2006 [98] and American Control Conference, NewYork, 2007 [100].

- Chapter 3: The contents of this chapter were published in IEEE Conference on Decision and Control, New Orleans, 2007 [99] and accepted for publication in Control Engineering Practice [102].

- Chapter 4: The contents of this chapter were published in American Control Conference, Seattle, 2008 [104] and conditionally accepted (with minor revision) to International Journal of Robust and Nonlinear Control [105].

- Chapter 5: The central idea of this chapter is presented at the 2008 ECEGSA Graduate Research Symposium, Edmonton.

Chapter 2

Robust Stabilization of Nonlinear Interconnected Systems

This chapter presents a design algorithm for the decentralized output feedback control problem of large-scale interconnected systems. The subsystem consists of a LTI part, which may be unstable and the additive nonlinear function is assumed to be bounded by a quadratic inequality. Decentralized dynamic output feedback controllers and decentralized observer-based state feedback controllers are designed, based on LMIs. Sufficient conditions to achieve robust stabilization of the overall large-scale system are provided. A remarkable property of the proposed scheme is that it guarantees connective stability of the overall system, and requires no intersubsystem communication. The controller design is applied to a natural circulation drum boiler, and simulation results are presented to show the advantage of the design procedure.

2.1 Introduction

It is well known that the striking property of decentralized information structure, based on state feedback control vanishes when the states of subsystems are not available locally. Hence, there are many research attempts to design decentralized output feedback controllers using just measurements [87], or to design decentralized observer-based control that provides the estimated states for state feedback controller design [69, 82, 111]. However, these results are based on the fact that, all observers share their states to make use of the separation principle. The design is therefore unappealing, and can be prone to failure in communication links, delays and requires inter-subsystem communications. Moreover, as most of the ideas are devoted to linear systems, the controller may not assure good

performance under varying operating conditions.

The last decade has witnessed new results in the design of observer based control schemes for some specific class of nonlinear systems [2, 49, 70, 84, 125]. It is well researched that as the separation principle may not be valid to nonlinear systems [53, 67], the exponential stability of the observer that is designed separately from the controller does not lead to closed loop stability. Considering the challenge of designing decentralized observer-based controllers, [84] proposed a method of autonomous decentralized control design that requires no inter-subsystem communications and promise *connective* stability of the overall plant. The class of nonlinear systems is general, and the design exploits the LMI tools [14, 28]. However, the algorithm requires that the number of inputs of each subsystem must be equal to the number of the states (invertible input matrix), which is very restrictive. To resolve this issue, [70] presented some sufficient conditions of observer-based control design. The conditions used distance to uncontrollability (unobservability) of $(\mathbf{A}, \mathbf{B})((\mathbf{C}, \mathbf{A}))$ [24, 110], and the design is based on the positive definite solutions to AREs, if they exist (this leads to computation of the observers and controllers). Nevertheless, the controller design in [70] does not maximize the robustness against uncertainty in interconnections, which is important in practical scenarios like power systems and robotics. The method also requires trial and error selection of additional design parameters for each subsystem, so it may not be user friendly to engineers. In [125], a two-step design procedure was introduced to solve a non-convex optimization problem for the nonlinear system in [70, 84]. Interestingly, it provides a way to maximize the robustness; however, the optimization problem cannot give a global minimum because of non-convexity. The work in [95] also developed full order as well as reduced order decentralized observer-based control designs but the non-convexity of the optimization was not overcome.

In this chapter a design algorithm for decentralized observer-based controllers is proposed. It is shown that the restrictiveness of the design in [70, 84, 95, 125] can be resolved by providing additional degrees of freedom in the observer, and the design of decentralized observers and controllers boil down to solving a linear objective minimization problem in the LMI framework (convex optimization). The algorithm provides sufficient conditions for quadratic stability only; nevertheless, LMI-based design has advantages, namely, simplicity, grace of design, and ability to capture a variety of control problems [25, 80]. The method of this chapter also maximizes robustness against uncertain perturbations in interconnections, identifies the *matching* conditions and the control law

leads to connective stability.

An additional objective is to apply the LMI tools [14, 28] and the well known "change of controller variables method" [20] to design a robust decentralized dynamic output feedback control strategy (without any observer, and based on measurements only). The motivation for this work arose from scanning the literature of turbine/governor control [47, 48, 73, 85, 116], excitation control [16, 19, 37, 54, 118, 120], and both in power system applications [17]. A detailed description can be found in [85, 120]. The work of [73] utilized Lyapunov's direct method to design linear decentralized control laws (state feedback) that bring robustness against parameter changes, load fluctuations, and topology changes in the system. In [48] the same method was used to stabilize a power system nonlinear model against a range of disturbances (faults, line outages), which can occur anywhere in a system. For turbine-governor control, the authors in [116] calculated the decentralized state feedback gain of each generator by solving an ARE which takes into account the bounds in the values of the generator parameters. An elegant LMI approach for computing state feedback gains, which was simple to understand and applicable to a wide range of problems, was introduced in [85]. Regarding the excitation control, most of the current literature is based on the concept of feedback linearization [19, 37]. The results in [19] were applied to a 38-bus reduced model, and in [37] controllers were designed to cancel the nonlinearities and interactions between different subsystems. Based on Lyapunov stability, [17] developed algorithms for excitation control and power system stabilization. Finally in [118, 120], robust decentralized state feedback controllers were designed using LMI tools to improve transient stability in the face of load variations, short circuit faults, network topology changes, etc. Although an adaptive output feedback method was introduced in [47], and static and dynamic output feedback control designs for a class of nonlinear system were considered in [86, 121], it remained to design a decentralized output feedback controller in a convex optimization framework that can achieve a global minimum. This chapter deals with this problem.

An important difference of both algorithms from others are their capability to stabilize a system when all states are not available for feedback, and to achieve a global minimum. There is no assumption of matching conditions [59] in the perturbations or stability of the LTI part of the nonlinear model [55].

To show that the solutions are practical, the controller designs are applied to a nonlinear model of a power unit which describes the dynamics of the drum, risers, downcomers, and the turbine-generator set. The model of [5] is extended to accommodate governor,

turbine, and generator. Thus, interconnection terms between the steam generating unit and the electricity generating unit are identified. Throughout the modeling phase, SYNSIM is used. Experiments with SYNSIM reveal that the overall system is highly interacting and nonlinear. In addition to this, linearization of the developed nonlinear model gives two poles at the origin: one linked with water dynamics, and the other with generator dynamics. Considering these issues, the overall system is divided into two subsystems: a) drum-boiler, and b) governor, turbine, generator unit. Robust decentralized observer based controllers, which can maintain stability in the presence of load fluctuations are then designed. The performance of the controllers is tested for different initial conditions and load changes, and simulation results show the usefulness of the approach. The design algorithm described in this chapter can be applied to other practical systems like interconnected generators with control on the steam valve [85] and a two-link robot manipulator [33], to mention two.

The rest of this chapter is structured as follows. Section 2.2 deals with some background results where the control problem is motivated. In Section 2.3, decentralized observer based controllers are designed: sufficient conditions are provided to engender a global minimum. Dynamic output feedback control strategies are devised in Sections 2.4-2.5. The proposed techniques are applied to a utility boiler and a power unit in Sections 2.6-2.7 with particular attention to modeling and controller design. Finally, the chapter is summarized in Section 2.8.

2.2 Background

Consider an interconnected system [70, 84, 85, 87, 120, 125]

$$\dot{\mathbf{x}}_i = \mathbf{A}_i\mathbf{x}_i + \mathbf{B}_i\mathbf{u}_i + \mathbf{G}_i\mathbf{h}_i(\mathbf{x}), \;\; \mathbf{y}_i = \mathbf{C}_i\mathbf{x}_i, \;\; i = 1, 2, 3, \ldots, N \tag{2.1}$$

where $\mathbf{x}_i \in \Re^{n_i}$ are the states, $\mathbf{u}_i \in \Re^{m_i}$ are the inputs and $\mathbf{h}_i(\mathbf{x})$ are the interconnections. $\mathbf{A}_i$ is the state matrix, $\mathbf{B}_i$ is the input matrix, $\mathbf{C}_i$ is the output matrix, and $\mathbf{G}_i$ is a constant matrix with dimensions $n_i \times n_i$, $n_i \times m_i$, $p_i \times n_i$, and $n_i \times n_i$, respectively. It is assumed that $(\mathbf{A}_i, \mathbf{B}_i)$ is stabilizable, $(\mathbf{C}_i, \mathbf{A}_i)$ is detectable, and the uncertain nonlinear term $\mathbf{h}_i(\mathbf{x})$ is bounded by a quadratic inequality [70, 84, 85, 87, 120, 125]

$$\mathbf{h}_i^T(\mathbf{x})\mathbf{h}_i(\mathbf{x}) \leq \alpha_i^2\mathbf{x}^T\mathbf{H}_i^T\mathbf{H}_i\mathbf{x}, \tag{2.2}$$

where $\mathbf{x} = \begin{bmatrix} \mathbf{x}_1^T & \mathbf{x}_2^T & \ldots & \mathbf{x}_N^T \end{bmatrix}^T$, $\alpha_i > 0$ is an interconnection parameter and $\mathbf{H}_i$ is a known constant matrix for the i'th subsystem.

The overall system is given by

$$\begin{aligned} \dot{\mathbf{x}}(t) &= \mathbf{A}_D\mathbf{x}(t) + \mathbf{B}_D\mathbf{u}(t) + \mathbf{h}(\mathbf{x}), \\ \mathbf{y}(t) &= \mathbf{C}_D\mathbf{x}(t), \end{aligned} \tag{2.3}$$

where $\mathbf{A}_D = \text{diag}\,(\mathbf{A}_1, \ldots, \mathbf{A}_N)$, $\mathbf{B}_D = \text{diag}\,(\mathbf{B}_1, \ldots, \mathbf{B}_N)$, $\mathbf{C}_D = \text{diag}\,(\mathbf{C}_1, \ldots, \mathbf{C}_N)$ and the nonlinear function $\mathbf{h}(\mathbf{x})$ is bounded by

$$\mathbf{h}^T(\mathbf{x})\mathbf{h}(\mathbf{x}) \leq \mathbf{x}^T \left(\sum_{i=1}^{N} \alpha_i^2 \mathbf{H}_i^T \mathbf{H}_i \right) \mathbf{x}. \tag{2.4}$$

Here, $\mathbf{h}^T = \left[\mathbf{h}_1^T, \ldots, \mathbf{h}_N^T\right]$. For this class of interconnected system, three approaches were introduced in the past to guarantee closed loop stability:

1. Design static state feedback decentralized controllers by casting the design problem as an optimization problem [85–87, 120]. For the overall system in (2.3) the decentralized state feedback controllers can be expressed as

$$\mathbf{u}(t) = \mathbf{K}_D\mathbf{x}(t), \tag{2.5}$$

where $\mathbf{K}_D = \text{diag}\,(\mathbf{K}_1, \ldots, \mathbf{K}_N)$ is the controller static gain matrix and can be obtained from the following optimization problem, provided it is feasible

$$\begin{aligned} &\min \sum_{i=1}^{N} \gamma_i \\ &\text{subject to} \quad \mathbf{Y}_D > 0, \\ &\begin{bmatrix} \mathbf{A}_D\mathbf{Y}_D + \mathbf{Y}_D\mathbf{A}_D^T + \mathbf{B}_D\mathbf{L}_D + \mathbf{L}_D^T\mathbf{B}_D^T & \mathbf{G}_D & \mathbf{Y}_D\mathbf{H}_1^T & \cdots & \mathbf{Y}_D\mathbf{H}_N^T \\ \star & -\mathbf{I} & 0 & \cdots & 0 \\ \star & \star & -\gamma_1\mathbf{I} & \cdots & 0 \\ \vdots & \vdots & \vdots & \ddots & \vdots \\ \star & \star & \star & \cdots & -\gamma_N\mathbf{I} \end{bmatrix} < 0. \end{aligned} \tag{2.6}$$

Here, $\gamma_i = \frac{1}{\alpha_i^2}$ and $\mathbf{L}_D = \mathbf{K}_D\mathbf{Y}_D$. Under the assumption that (2.6) is feasible, the controller is calculated from $\mathbf{K}_D = \mathbf{L}_D\mathbf{Y}_D^{-1}$. This formulation is striking from an application point of view, since the decision variables are computed directly in one step and the optimization is maximizing α_i. However, the algorithm is restrictive because it is only applicable when all states are available for feedback. Furthermore, in many cases, achieving a (block) diagonal $\mathbf{Y}_D$ is a difficult task.

2. To overcome the problem associated with static state feedback controllers, [84] proposed a new method of decentralized observer-based control design. For the

system in (2.3) the decentralized observers and state feedback controllers can be expressed as

$$\begin{aligned} \mathbf{u}(t) &= \mathbf{K}_D\hat{\mathbf{x}}(t), \\ \dot{\hat{\mathbf{x}}}(t) &= \mathbf{A}_D\hat{\mathbf{x}}(t) + \mathbf{B}_D\mathbf{u}(t) + \mathbf{L}_D(\mathbf{y}(t) - \mathbf{C}_D\hat{\mathbf{x}}(t)), \end{aligned} \tag{2.7}$$

where $\mathbf{L}_D = \text{diag}\,(\mathbf{L}_1, \ldots, \mathbf{L}_N)$ is the observer gain matrix. The decision variables can be obtained from the following optimization problem, provided it is feasible

$$\min_{\tilde{\mathbf{P}}_1, \tilde{\mathbf{P}}_2, \mathbf{M}_D, \mathbf{N}_D, \gamma_i} \sum_{i=1}^{N} \gamma_i$$

$$\text{subject to} \quad \tilde{\mathbf{P}}_1 > 0, \tilde{\mathbf{P}}_2 > 0,$$

$$\begin{bmatrix} \mathbf{A}_D^T\tilde{\mathbf{P}}_1 + \tilde{\mathbf{P}}_1\mathbf{A}_D + \mathbf{M}_D^T + \mathbf{M}_D & -\mathbf{M}_D & \tilde{\mathbf{P}}_1 & \ldots & \mathbf{H}_N^T \\ \star & \mathbf{A}_D^T\tilde{\mathbf{P}}_2 + \tilde{\mathbf{P}}_2\mathbf{A}_D - \mathbf{C}_D^T\mathbf{N}_D^T - \mathbf{N}_D\mathbf{C}_D & \tilde{\mathbf{P}}_2 & \ldots & \mathbf{0} \\ \star & \star & -\mathbf{I} & \ldots & \mathbf{0} \\ \vdots & \vdots & \vdots & \ddots & \vdots \\ \star & \star & \star & \ldots & -\gamma_N\mathbf{I} \end{bmatrix} < 0,$$

where $\gamma_i \triangleq 1/\alpha_i^2$, $\tilde{\mathbf{P}}_1\mathbf{B}_D\mathbf{K}_D \triangleq \mathbf{M}_D$ and $\tilde{\mathbf{P}}_2\mathbf{L}_D \triangleq \mathbf{N}_D$. The gain matrices $\mathbf{K}_D$ and $\mathbf{L}_D$ are calculated from $\mathbf{K}_D = \mathbf{B}_D^{-1}\tilde{\mathbf{P}}_1^{-1}\mathbf{M}_D$ and $\mathbf{L}_D = \tilde{\mathbf{P}}_2^{-1}\mathbf{N}_D$, respectively. Hence, this method requires invertibility of the input matrix $\mathbf{B}_D$, which is restrictive and not practical.

3. The work in [70] criticized the above approach for its limitations and proposed a method, where designing an observer-based state feedback controller for the i'th subsystem requires symmetric positive definite solutions to the following two AREs, if they exist

$$\mathbf{A}_i^T\mathbf{P}_i + \mathbf{P}_i\mathbf{A}_i + 2\mathbf{P}_i(\mathbf{I} - \mathbf{B}_i(\mathbf{B}_i^T\mathbf{B}_i)^{-1}\mathbf{B}_i^T)\mathbf{P}_i + \gamma^2\mathbf{I} + \eta_i\mathbf{I} = \mathbf{0}, \tag{2.8}$$

$$\mathbf{A}_i^T\tilde{\mathbf{P}}_i + \tilde{\mathbf{P}}_i\mathbf{A}_i + \tilde{\mathbf{P}}_i\tilde{\mathbf{P}}_i + \tilde{\mathbf{Q}}_{i1} + \tilde{\eta}_i\mathbf{I} - \epsilon_i\mathbf{C}_i^T\mathbf{C}_i = 0. \tag{2.9}$$

Here, $\tilde{\mathbf{Q}}_{i1} \triangleq \mathbf{K}_i^T\mathbf{B}_i^T\mathbf{B}_i\mathbf{K}_i$ and $\gamma^2 \triangleq \sum_{i=1}^{N} 2\alpha_i^2\lambda_{max}(\mathbf{H}_i^T\mathbf{H}_i)$. The parameters $\alpha_i > 0$, $\epsilon_i > 0$, $\tilde{\eta}_i > 0$, and $\eta_i > 0$ are user defined. The sufficient conditions, such that the positive definite solutions to the AREs (2.8) and (2.9) exist are

$$\delta(\mathbf{A}_i, \sqrt{2(\gamma^2 + \eta_i)}(\mathbf{B}_i^T\mathbf{B}_i)^{-1/2}\mathbf{B}_i^T) > \sqrt{2(\gamma^2 + \eta_i)}, \tag{2.10}$$

$$\delta(\mathbf{A}_i, \epsilon_i^{1/2}\mathbf{C}_i) > \sqrt{\lambda_{max}(\tilde{\mathbf{Q}}_{i1}) + \tilde{\eta}_i}, \tag{2.11}$$

where

$$\delta(\mathbf{A}_i, \mathbf{C}_i) \triangleq \min_{\omega \in \Re} \underline{\sigma} \begin{bmatrix} j\omega\mathbf{I} - \mathbf{A}_i \\ \mathbf{C}_i \end{bmatrix}$$

represents the distance to unobservability of the pair $(\mathbf{A}_i, \mathbf{C}_i)$ [1, 74]. If solutions exist, then the controller and observer gain matrices are selected as

$$\mathbf{K}_i = -(\mathbf{B}_i^T\mathbf{B}_i)^{-1}\mathbf{B}_i^T\mathbf{P}_i, \quad \mathbf{L}_i = \epsilon\tilde{\mathbf{P}}_i^{-1}\mathbf{C}_i^T/2.$$

Here, $\mathbf{P}_i > 0$ is the symmetric positive definite solution of (2.8) and $\tilde{\mathbf{P}}_i$ is the solution of (2.9). This method, however, suffers from the following shortcomings:

- The designers have to choose the parameters ϵ_i, $\tilde{\eta}_i$, and η_i by trial and error until (2.10) and (2.11) are satisfied. There is no clear relationship between these parameters and the performance of overall closed loop system. How to tune them to achieve an acceptable performance is still a question.
- The computation of $\delta(\mathbf{A}_i, \mathbf{C}_i)$ depends on a bisection algorithm [1], which is approximate and also varies with different state space realizations [70].
- The method does not maximize the interconnection parameter α_i, which is important in practical fields like power systems, robotics, and space structures.

In the following, these restrictions are removed by converting the design problem into a convex optimization where the design parameters have clear physical meanings.

2.3 Decentralized Observer-Based Controllers in the LMI Framework

Consider a nonlinear autonomous process of the form [83, 85, 87]

$$\dot{\mathbf{x}}(t) = \mathbf{A}\mathbf{x}(t) + \mathbf{B}\mathbf{u}(t) + \mathbf{G}\mathbf{h}_r(\mathbf{x}), \quad \mathbf{y}(t) = \mathbf{C}\mathbf{x}(t), \tag{2.12}$$

where $\mathbf{x}(t) \in \Re^n$ is the state of the system, $\mathbf{u}(t) \in \Re^m$ is the input vector and $\mathbf{y}(t) \in \Re^p$ is the output vector. The matrices $\mathbf{A}$, $\mathbf{B}$, $\mathbf{C}$, and $\mathbf{G}$ are constant with dimensions $n \times n$, $n \times m$, $p \times n$, and $n \times n$, respectively. The term $\mathbf{h}_r(\mathbf{x})$ is an uncertain nonlinear function satisfying $\mathbf{h}_r(0) = 0$. This means that the origin is the equilibrium point of the unforced system. Assume that $(\mathbf{A}, \mathbf{B})$ is stabilizable, $(\mathbf{C}, \mathbf{A})$ is detectable and the uncertain term $\mathbf{h}_r(\mathbf{x})$ is bounded by an inequality [83, 85, 87]

$$\mathbf{h}_r^T(\mathbf{x})\mathbf{h}_r(\mathbf{x}) \leq \alpha^2\mathbf{x}^T\mathbf{H}_r^T\mathbf{H}_r\mathbf{x}, \tag{2.13}$$

where $\mathbf{H}_r$ is a known constant matrix and $\alpha > 0$ is a scalar parameter which can be termed as a degree of robustness. Maximization of α leads to an increased robustness of the closed

loop system (with controller) against uncertain nonlinear perturbations. Now, consider the following open loop dynamic observer

$$\dot{\hat{\mathbf{x}}}(t) = \mathbf{A}\hat{\mathbf{x}}(t) + \mathbf{B}\mathbf{u}(t) + \hat{\mathbf{u}}, \;\; \hat{\mathbf{y}}(t) = \mathbf{C}\hat{\mathbf{x}}(t). \tag{2.14}$$

Here $\hat{\mathbf{x}} \in \Re^n$ is the estimated state vector and $\hat{\mathbf{u}} \in \Re^n$ is an additional observer input. In this approach, a dynamic linear feedback of the following form is used

$$\dot{\mathbf{x}}_{obv} = \mathbf{A}_{obv}\mathbf{x}_{obv} + \mathbf{B}_{obv}\mathbf{C}(\mathbf{x} - \hat{\mathbf{x}}), \;\; \hat{\mathbf{u}} = \mathbf{C}_{obv}\mathbf{x}_{obv} + \mathbf{D}_{obv}\mathbf{C}(\mathbf{x} - \hat{\mathbf{x}}),$$

where $\hat{\mathbf{x}}_{obv} \in \Re^n$. With a static state feedback controller $\mathbf{u} = \mathbf{K}\hat{\mathbf{x}}$, the closed loop system takes the form

$$\begin{aligned} \dot{\mathbf{z}}(t) &= \begin{bmatrix} \mathbf{A}+\mathbf{B}\mathbf{K} & \mathbf{D}_{obv}\mathbf{C} & \mathbf{C}_{obv} \\ \mathbf{0} & \mathbf{A}-\mathbf{D}_{obv}\mathbf{C} & -\mathbf{C}_{obv} \\ \mathbf{0} & \mathbf{B}_{obv}\mathbf{C} & \mathbf{A}_{obv} \end{bmatrix} \mathbf{z}(t) + \begin{bmatrix} \mathbf{0} \\ \mathbf{G} \\ \mathbf{0} \end{bmatrix} \mathbf{w}(\mathbf{z}) \\ &= \hat{\mathbf{A}}\mathbf{z}(t) + \mathbf{G}_r\mathbf{w}(\mathbf{z}), \end{aligned} \tag{2.15}$$

where $\mathbf{z}(t) = \begin{bmatrix} \hat{\mathbf{x}}^T(t) & \mathbf{e}^T(t) & \mathbf{x}_{obv}^T(t) \end{bmatrix}^T$, the state estimation error $\mathbf{e} = (\mathbf{x} - \hat{\mathbf{x}})$, and the nonlinear function $\mathbf{h}_r(\mathbf{x})$ in terms of $\mathbf{z}$ is represented by $\mathbf{w}(\mathbf{z})$, which satisfies the following quadratic bound

$$\mathbf{w}^T(\mathbf{z})\mathbf{w}(\mathbf{z}) \leq \alpha^2\mathbf{z}^T \begin{bmatrix} \mathbf{H}_r^T\mathbf{H}_r & \mathbf{H}_r^T\mathbf{H}_r & \mathbf{0} \\ \mathbf{H}_r^T\mathbf{H}_r & \mathbf{H}_r^T\mathbf{H}_r & \mathbf{0} \\ \mathbf{0} & \mathbf{0} & \mathbf{0} \end{bmatrix} \mathbf{z} = \alpha^2\mathbf{z}^T(t)\mathbf{H}^T\mathbf{H}\mathbf{z}(t). \tag{2.16}$$

Next, for the i'th subsystem in (2.1), the closed loop is given by

$$\begin{aligned} \dot{\mathbf{z}}_{l_i} &= \begin{bmatrix} \mathbf{A}_i+\mathbf{B}_i\mathbf{K}_i & \mathbf{D}_{obv_i}\mathbf{C}_i & \mathbf{C}_{obv_i} \\ \mathbf{0} & \mathbf{A}_i-\mathbf{D}_{obv_i}\mathbf{C}_i & -\mathbf{C}_{obv_i} \\ \mathbf{0} & \mathbf{B}_{obv_i}\mathbf{C}_i & \mathbf{A}_{obv_i} \end{bmatrix} \mathbf{z}_{l_i} + \begin{bmatrix} \mathbf{0} \\ \mathbf{G}_i \\ \mathbf{0} \end{bmatrix} \mathbf{w}_i \\ &= \hat{\mathbf{A}}_{cl_i}\mathbf{z}_{l_i} + \mathbf{G}_{l_i}\mathbf{w}_i, \end{aligned} \tag{2.17}$$

where $\mathbf{z}_{l_i} = \begin{bmatrix} \hat{\mathbf{x}}_i^T & \mathbf{e}_i^T & \mathbf{x}_{obv_i}^T \end{bmatrix}^T$ and $\mathbf{x}_{obv_i}$ are the states of observer for the i'th subsystem. Defining $\mathbf{z}_N = \begin{bmatrix} \hat{\mathbf{x}}_1^T & \mathbf{e}_1^T & \mathbf{x}_{obv_1}^T & \cdots & \hat{\mathbf{x}}_N^T & \mathbf{e}_N^T & \mathbf{x}_{obv_N}^T \end{bmatrix}^T$, the overall system can be written as

$$\dot{\mathbf{z}}_N = \hat{\mathbf{A}}_D\mathbf{z}_N + \mathbf{G}_D\mathbf{w}(\mathbf{z}_N), \tag{2.18}$$

where $\hat{\mathbf{A}}_D = \text{diag}(\hat{\mathbf{A}}_{cl_1}, \ldots, \hat{\mathbf{A}}_{cl_N})$, $\mathbf{G}_D = \text{diag}(\mathbf{G}_{l_1}, \ldots, \mathbf{G}_{l_N})$ and $\mathbf{w} = [\mathbf{w}_1^T, \ldots, \mathbf{w}_N^T]^T$ satisfying

$$\mathbf{w}^T(\mathbf{z}_N)\mathbf{w}(\mathbf{z}_N) \leq \mathbf{z}_N^T \left(\sum_{i=1}^{N} \frac{1}{\gamma_i^2} \mathbf{H}_{i_l}^T \mathbf{H}_{i_l} \right) \mathbf{z}_N. \tag{2.19}$$

The elements of $\mathbf{H}_{i_l}$ corresponding to $\mathbf{x}_{obv_1}, \ldots, \mathbf{x}_{obv_N}$ are zero. In the following theorem, sufficient conditions for the design of decentralized controllers that can guarantee CL stability are provided.

Theorem 2.1 If the following optimization problem is feasible

$$\min \sum_{i=1}^{N} \gamma_i,$$

$$\text{subject to} \quad \mathbf{\Pi}_{2_D}^T \mathbf{Y}_D \mathbf{\Pi}_{2_D} > 0,$$

$$\begin{bmatrix} \mathbf{\Pi}_{2_D}^T \left(\hat{\mathbf{A}}_D \mathbf{Y}_D + \mathbf{Y}_D \hat{\mathbf{A}}_D^T\right) \mathbf{\Pi}_{2_D} & \mathbf{\Pi}_{2_D}^T \mathbf{G}_D & \mathbf{\Pi}_{2_D}^T \mathbf{Y}_D \mathbf{H}_{1_l}^T & \ldots & \mathbf{\Pi}_{2_D}^T \mathbf{Y}_D \mathbf{H}_{N_l}^T \\ \star & -\mathbf{I} & 0 & \ldots & 0 \\ \star & \star & -\gamma_1 \mathbf{I} & \ldots & 0 \\ \vdots & \vdots & \vdots & \ddots & \vdots \\ \star & \star & \star & \ldots & -\gamma_N \mathbf{I} \end{bmatrix} < 0,$$

where $\mathbf{Y}_D$ is a block diagonal Lyapunov function and $\mathbf{\Pi}_{2_D} = \text{diag}(\mathbf{\Pi}_{2_1}, \ldots, \mathbf{\Pi}_{2_N})$ is a transformation matrix, then the system in (2.18) is asymptotically stable for all nonlinearities satisfying the quadratic constraint in (2.19) ($\forall \mathbf{z}_N$ in $\mathbb{D}$; $\mathbb{D}$ is a disc close to the origin).

Proof: Please see Appendix A.

It is interesting to note that [125] proposed an algorithm of decentralized output feedback control design for the class of nonlinear system in (2.1). The method utilized the tools of LMI and the control design was devised as the following optimization problem [125]

$$\min \sum_{i=1}^{N} \gamma_i, \quad \text{subject to } \mathbf{Y} > \mathbf{0}, \ \mathbf{P}_0 > \mathbf{0} \text{ and } \begin{bmatrix} \mathbf{F}_c & \mathbf{S} \\ \star & \mathbf{F}_0 \end{bmatrix} < \mathbf{0}. \tag{2.20}$$

Here, $\mathbf{F}_c$ contains terms which are affine in decentralized controller parameters ($\mathbf{K}_D$) and $\mathbf{F}_o$ contains that of decentralized observer parameters ($\mathbf{L}_D$). The matrix $\mathbf{S}$ represents

$$\mathbf{S} = \begin{bmatrix} -\mathbf{B}_D \mathbf{K}_D & 0 & \ldots & 0 \\ \mathbf{I} & 0 & \ldots & 0 \end{bmatrix},$$

where $\mathbf{B}_D = \text{diag}\,(\mathbf{B}_1, \ldots, \mathbf{B}_N)$. Due to the presence of term $-\mathbf{B}_D \mathbf{K}_D$ in (2.20), this optimization problem is non-convex. Therefore, to apply the LMI tools, [125] proposed the following two step method:

1. Compute $\mathbf{K}_D$ by solving $\min \sum_{i=1}^{N} \gamma_i$ subject to $\mathbf{Y} > \mathbf{0}$ and $\mathbf{F}_c < \mathbf{0}$.
2. Using the $\mathbf{K}_D$ obtained from step 1, compute $\mathbf{L}_D$ by solving the following optimization problem

$$\min \sum_{i=1}^{N} \beta_i \text{ subject to } \mathbf{P}_0 > \mathbf{0}, \ \mathbf{\Lambda} > \mathbf{0}, \ \begin{bmatrix} \mathbf{\Lambda} \mathbf{F}_c & \mathbf{S} \\ \star & \mathbf{F}_0 \end{bmatrix} < \mathbf{0}, \tag{2.21}$$

where the parameter $\mathbf{\Lambda} = \text{diag}(\beta_1\mathbf{I}_1, \ldots, \beta_N\mathbf{I}_N, \beta_1\mathbf{I}_1, \ldots, \beta_N\mathbf{I}_N)$ was added to make the optimization problem in the second step feasible.

This method has some merit as it provides a way to handle a nonlinear optimization problem which the designer often encounter in many control problems. Moreover, maximization of the interconnection bounds and the introduction of parameter $\mathbf{\Lambda}$ are interesting. However, the approach of this thesis differs in the following way:

- The decentralized controller and observer design problem is formulated as a convex optimization problem using different congruence transformations, simplifications, new variable definitions (modified form of [20]) and the use of Schur's complement method. An important property of the linear objective minimization problem in Theorem 2.1 is that it yields a global minimum, if it exists.

- It should be noted that (2.20) and (2.21) are not theoretically equivalent. The constraint in (2.20) is equivalent to

$$\begin{bmatrix} \mathbf{\Lambda}^{1/2} & \mathbf{0} \\ \mathbf{0} & \mathbf{I} \end{bmatrix} \begin{bmatrix} \mathbf{F}_c & \mathbf{S} \\ \mathbf{S}^T & \mathbf{F}_0 \end{bmatrix} \begin{bmatrix} \mathbf{\Lambda}^{1/2} & \mathbf{0} \\ \mathbf{0} & \mathbf{I} \end{bmatrix} = \begin{bmatrix} \mathbf{\Lambda}\mathbf{F}_c & \mathbf{\Lambda}^{1/2}\mathbf{S} \\ \mathbf{S}^T\mathbf{\Lambda}^{1/2} & \mathbf{F}_0 \end{bmatrix} < \mathbf{0}.$$

  $\mathbf{\Lambda}$ in (2.21) has been introduced in a special way (only at (1,1) position) to make the optimization problem feasible. This is because, after substituting the designed controller $\mathbf{K}_D$ from step 1 in step 2 (to compute the observer parameters with $\mathbf{\Lambda} = \mathbf{I}$), there is no guarantee of the feasibility of optimization problem. However,

$$\begin{bmatrix} \mathbf{\Lambda}\mathbf{F}_c & \mathbf{S} \\ \mathbf{S}^T & \mathbf{F}_0 \end{bmatrix} < \mathbf{0} \Leftrightarrow$$

$$\begin{bmatrix} \mathbf{0} & \mathbf{I} \\ \mathbf{I} & \mathbf{0} \end{bmatrix} \begin{bmatrix} \mathbf{\Lambda}\mathbf{F}_c & \mathbf{S} \\ \mathbf{S}^T & \mathbf{F}_0 \end{bmatrix} \begin{bmatrix} \mathbf{0} & \mathbf{I} \\ \mathbf{I} & \mathbf{0} \end{bmatrix} < \mathbf{0} \Leftrightarrow \begin{bmatrix} \mathbf{F}_0 & \mathbf{S}^T \\ \mathbf{S} & \mathbf{\Lambda}\mathbf{F}_c \end{bmatrix} < \mathbf{0}. \qquad (2.22)$$

  Using Schur's complement method [14], (2.22) is equivalent to $\mathbf{F}_0 < 0$, $\mathbf{\Lambda}\mathbf{F}_c < 0$ and $\mathbf{F}_0 - \mathbf{S}^T(\mathbf{\Lambda}\mathbf{F}_c)^{-1}\mathbf{S} < 0$. Therefore, by choosing β's large enough, the feasibility of (2.22) can be assured. Although, this method works well in many cases, control engineers still demands an explicit solution to this design problem. In Theorem 2.1, the control design has been converted into a convex optimization problem which can be directly solved using the LMI toolbox in one step. Hence, it should be useful to both practitioners and theorists.

- It is worthwhile to note that due to the dynamic observer, the number of LMI decision variables are

$$\sum_{i=1}^{N} \left[n_{l_i} \times n_{l_i} + n_{l_i} \times p_i + n_i \times \left\{ n_{l_i} + m_i + p_i + \frac{3(n_i+1)}{2} \right\} \right].$$

In [125], the number of decision variables are only

$$\sum_{i=1}^{N} \left[n_i \times (n_i + 1) + n_i \times p_i + n_i \times m_i \right].$$

This causes an increase in the computational effort.

Remark 2.1 Theorem 2.1 does not place any constraint on the closed loop eigenvalues. This is required to fasten the observer dynamics, and to overcome very high feedback gain $\mathbf{K}_i$, which the LMI formulation may produce. Therefore, after applying some congruence transformations and simplifications on the pole placement objectives of [20], the following constraints are added to bound the minimum decay rate α_{min} (for speed of response), minimum damping ratio $\zeta = \cos\theta$ (for overshoot) and maximum undamped natural frequency ω_{nmax} (frequency of oscillations) for the control signal and the observation error dynamics, respectively.

$$\begin{aligned}
\mathbf{\Pi}_{2_i}^T \left(\hat{\mathbf{A}}_{cl_i} \mathbf{Y}_i + \mathbf{Y}_i \hat{\mathbf{A}}_{cl_i}^T \right) \mathbf{\Pi}_{2_i} + 2\alpha_{min_i} \mathbf{\Pi}_{2_i}^T \mathbf{Y}_i \mathbf{\Pi}_{2_i} &< \mathbf{0}, \\
\begin{bmatrix} -\omega_{nmax_i} \mathbf{\Pi}_{2_i}^T \mathbf{Y}_i \mathbf{\Pi}_{2_i} & \mathbf{\Pi}_{2_i}^T \hat{\mathbf{A}}_{cl_i} \mathbf{Y}_i \mathbf{\Pi}_{2_i} \\ \star & -\omega_{nmax_i} \mathbf{\Pi}_{2_i}^T \mathbf{Y}_i \mathbf{\Pi}_{2_i} \end{bmatrix} &< \mathbf{0}, \\
\begin{bmatrix} (\mathcal{D}_{11})_i & (\mathcal{D}_{12})_i \\ \star & (\mathcal{D}_{11})_i \end{bmatrix} &< \mathbf{0}.
\end{aligned}$$

Here,

$$\begin{aligned}
(\mathcal{D}_{11})_i &= (\sin\theta)_i \left(\mathbf{\Pi}_{2_i}^T \hat{\mathbf{A}}_{cl_i} \mathbf{Y}_i \mathbf{\Pi}_{2_i} + \mathbf{\Pi}_{2_i}^T \mathbf{Y}_i \hat{\mathbf{A}}_{cl_i}^T \mathbf{\Pi}_{2_i} \right), \\
(\mathcal{D}_{12})_i &= (\cos\theta)_i \left(\mathbf{\Pi}_{2_i}^T \hat{\mathbf{A}}_{cl_i} \mathbf{Y}_i \mathbf{\Pi}_{2_i} - \mathbf{\Pi}_{2_i}^T \mathbf{Y}_i \hat{\mathbf{A}}_{cl_i}^T \mathbf{\Pi}_{2_i} \right), \\
\alpha_{min_i} &= \text{diag}\left[2(\alpha_{min})_c, 2(\alpha_{min})_o, 2(\alpha_{min})_o \right]_i, \\
\omega_{nmax_i} &= \text{diag}\left[(\omega_{nmax})_c, (\omega_{nmax})_o, (\omega_{nmax})_o \right]_i, \\
(\sin\theta)_i &= \text{diag}\left[(\sin\theta)_c, (\sin\theta)_o, (\sin\theta)_o \right]_i, \\
(\cos\theta)_i &= \text{diag}\left[(\cos\theta)_c, (\cos\theta)_o, (\cos\theta)_o \right]_i.
\end{aligned}$$

Subscript c refers to the controller and o refers to the observer.

Remark 2.2 Consider the system in (2.12) with $\mathbf{G} = \mathbf{B}$ (the perturbation is entering the system through the same input matrix). This condition is referred as matching condition and it was proved that there always exist a stabilizing static state feedback controller in spite of the size of the perturbations in $\mathbf{h}_i(\mathbf{x})$ [83, 96]. It can be easily shown that the designed observer-based controller identifies this condition and a stabilizing observer-based

controller can *always* be calculated if this condition is satisfied. This is also true for the interconnected system in (2.1). The proof is shown in Appendix A.

Remark 2.3 Decentralized dynamic observer based controllers offer additional degrees of freedom in the design (compared to static ones). Moreover, the attractive feature of connective stability makes it appealing from an application point of view. To illustrate this point, consider the double pendulum example in [82–84]. It is composed of two inverted penduli connected by a sliding spring, where the location of the spring reflects the extent of coupling. The state space model for this interconnected system is represented by [83]

$$\begin{aligned}\dot{\mathbf{x}}_1 &= \begin{bmatrix} 0 & 1 \\ 1 & 0 \end{bmatrix}\mathbf{x}_1 + \begin{bmatrix} 0 \\ 1 \end{bmatrix}\mathbf{u}_1 + \begin{bmatrix} 0 & 0 & 0 & 0 \\ -1 & 0 & 1 & 0 \end{bmatrix}\mathbf{e}(\mathbf{x})\mathbf{x},\ y_1 = \begin{bmatrix} 1 & 0 \end{bmatrix}\mathbf{x}_1, \\ \dot{\mathbf{x}}_2 &= \begin{bmatrix} 0 & 1 \\ 1 & 0 \end{bmatrix}\mathbf{x}_2 + \begin{bmatrix} 0 \\ 1 \end{bmatrix}\mathbf{u}_2 + \begin{bmatrix} 0 & 0 & 0 & 0 \\ 1 & 0 & -1 & 0 \end{bmatrix}\mathbf{e}(\mathbf{x})\mathbf{x},\ y_2 = \begin{bmatrix} 1 & 0 \end{bmatrix}\mathbf{x}_2. \end{aligned} \tag{2.23}$$

Here, $\mathbf{x}_1 = \begin{bmatrix} x_{11}^T & x_{12}^T \end{bmatrix}^T$ represents the angular position and the angular velocity of the first pendulum and $\mathbf{x}_2$ is the state vector of the second pendulum. The normalized interconnection variable $\mathbf{e}(\mathbf{x}) : \Re^5 \rightarrow [0, 1]$ represents the amount of coupling and is useful to explore connective stability [83, 84] of the penduli under the influence of some external disturbances. The objective is to design decentralized control laws to keep the penduli in vertical position, bring robust stability for $\mathbf{e}(\mathbf{x}) \in [0, 1]$, and maximize the degree of robustness α_1 and α_2. It is clear that

$$\begin{aligned}\mathbf{h}_1^T(\mathbf{x})\mathbf{h}_1(\mathbf{x}) &\leq \mathbf{x}^T \begin{bmatrix} 1 & 0 & -1 & 0 \\ 0 & 0 & 0 & 0 \\ -1 & 0 & 1 & 0 \\ 0 & 0 & 0 & 0 \end{bmatrix}\mathbf{x}, \text{ and} \\ \mathbf{h}_2^T(\mathbf{x})\mathbf{h}_2(\mathbf{x}) &\leq \mathbf{x}^T \begin{bmatrix} 1 & 0 & -1 & 0 \\ 0 & 0 & 0 & 0 \\ -1 & 0 & 1 & 0 \\ 0 & 0 & 0 & 0 \end{bmatrix}\mathbf{x}. \end{aligned} \tag{2.24}$$

Since, $(\mathbf{A}_i, \mathbf{B}_i)$ is stabilizable and $(\mathbf{C}_i, \mathbf{A}_i)$ is detectable, the LMI formulation of Theorem 2.1 can be used to design decentralized observer based controllers. By appropriately selecting an admissibility region as (Fig. 2.1)

$$\begin{aligned}(\alpha_{min})_c &= 0.5,\ (\omega_{nmax})_c = 6.3,\ (\theta)_c = \frac{\pi}{4},\ (\alpha_{min})_0 = 2.5, \\ (\omega_{nmax})_o &= 10,\ (\theta)_o = \frac{\pi}{4}, \end{aligned} \tag{2.25}$$

for both subsystems and solving the linear objective minimization problem in Theorem 2.1,

the following design variables are obtained

$$\begin{aligned} \alpha_1 &= \alpha_2 = 0.581, \ \mathbf{K} = \begin{bmatrix} -30.60 & -9.23 & 0 & 0 \\ 0 & 0 & -30.60 & -9.23 \end{bmatrix}, \\ \mathbf{R}_{1_1} &= \mathbf{R}_{1_2} = \begin{bmatrix} 4.61 & -23.2 \\ -23.2 & 175.7 \end{bmatrix}, \ \mathbf{X}_{r_1} = \mathbf{X}_{r_2} = \begin{bmatrix} 1.47 & -4.12 \\ -4.12 & 20.58 \end{bmatrix}, \\ \mathbf{Y}_{r_1} &= \mathbf{Y}_{r_2} = \begin{bmatrix} 11.35 & -1.37 \\ -1.37 & 0.397 \end{bmatrix}. \end{aligned} \tag{2.26}$$

The parameters $\mathbf{R}_{1_1}(\mathbf{R}_{1_2})$, $\mathbf{X}_{r_1}(\mathbf{X}_{r_2})$, and $\mathbf{Y}_{r_1}(\mathbf{Y}_{r_2})$ determines the positive definite Lyapunov function $\mathbf{\Pi}_{2_D}^T \mathbf{Y}_D \mathbf{\Pi}_{2_D}$, which assures robust stability for $|\mathbf{e}(\mathbf{x})| \leq 0.581$. The admissibility region in (2.25) has been carefully selected to obtain a good transient characteristic. The eigenvalues of $\hat{\mathbf{A}}_{cl_1}$ and $\hat{\mathbf{A}}_{cl_2}$ are tabulated in Table 2.1. The first two eigenvalues are responsible for the controller dynamics, and the rest four for the observer dynamics. Clearly, the eigenvalues lie in the region specified by (2.25). For different initial conditions, Fig. 2.2 shows the dynamics of the states and the estimation errors, respectively, which shows that the controller in (2.26) stabilizes the overall interconnected system. However, the value of α's in (2.26) reveals that robust stability can be only guaranteed for $\mathbf{e}(\mathbf{x}) \in [0, 0.581]$. In [84], the model of this inverted penduli was also used and static observer based controllers were designed with $\mathbf{B}_i = \mathbf{I}_i$, where $\mathbf{I}_i$ is the $n_i \times n_i$ identity matrix. Therefore, the model was not realistic and the assumption that the number of control inputs are equal to the dimension of state was restrictive.

Table 2.1: Eigenvalues of the closed-loop system.

$-4.61 + j\,2.88$	$-5.7 + j\,3.24$	-2.86
$-4.61 - j\,2.88$	$-5.7 - j\,3.24$	-9.59

2.4 Dynamic Output Feedback Stabilization

Consider the nonlinear process in (2.12). If there exists a dynamic output feedback controller of the form

$$\dot{\mathbf{x}}_k(t) = \mathbf{A}_k \mathbf{x}_k(t) + \mathbf{B}_k \mathbf{y}(t), \ \ \mathbf{u}(t) = \mathbf{C}_k \mathbf{x}_k(t) + \mathbf{D}_k \mathbf{y}(t), \tag{2.27}$$

then the closed loop system can be represented as

$$\begin{aligned} \begin{bmatrix} \dot{\mathbf{x}}(t) \\ \dot{\mathbf{x}}_k(t) \end{bmatrix} &= \begin{bmatrix} \mathbf{A} + \mathbf{B}\mathbf{D}_k\mathbf{C} & \mathbf{B}\mathbf{C}_k \\ \mathbf{B}_k\mathbf{C} & \mathbf{A}_k \end{bmatrix} \begin{bmatrix} \mathbf{x}(t) \\ \mathbf{x}_k(t) \end{bmatrix} + \begin{bmatrix} \mathbf{G} \\ \mathbf{0} \end{bmatrix} \mathbf{h}(\tilde{\mathbf{x}}), \\ \mathbf{y}(t) &= \begin{bmatrix} \mathbf{C} & 0 \end{bmatrix} \begin{bmatrix} \mathbf{x}(t) \\ \mathbf{x}_k(t) \end{bmatrix}, \end{aligned} \tag{2.28}$$

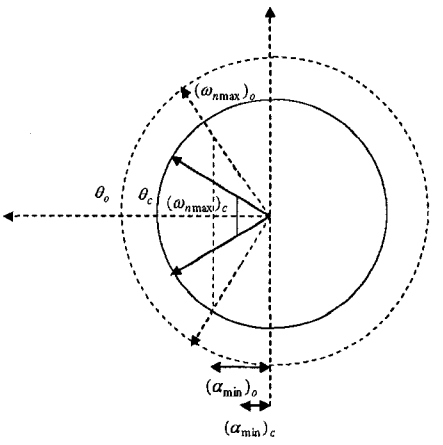

Figure 2.1: Admissibility region.

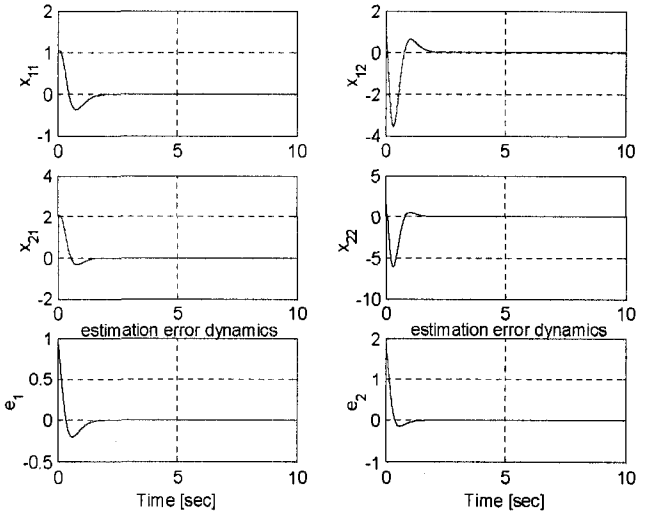

Figure 2.2: Stabilizing effect of the decentralized controller.

where $\tilde{\mathbf{x}}(t) = \left[\begin{array}{cc} \mathbf{x}^T(t) & \mathbf{x}_k^T(t) \end{array} \right]^T$. The function $\mathbf{h}(\tilde{\mathbf{x}})$ satisfies

$$\mathbf{h}^T(\tilde{\mathbf{x}})\mathbf{h}(\tilde{\mathbf{x}}) \leq \alpha^2 \tilde{\mathbf{x}}^T(t) \left[\begin{array}{cc} \mathbf{H}_r^T\mathbf{H}_r & \mathbf{0} \\ \mathbf{0} & \mathbf{0} \end{array} \right] \tilde{\mathbf{x}}(t) = \alpha^2 \tilde{\mathbf{x}}^T(t)\mathbf{H}_k^T\mathbf{H}_k\tilde{\mathbf{x}}, \qquad (2.29)$$

where $\mathbf{H}_k^T\mathbf{H}_k = \text{diag}\,(\mathbf{H}_r^T\mathbf{H}_r, \mathbf{0})$, and the closed loop system can be written as

$$\dot{\tilde{\mathbf{x}}}(t) = \hat{\mathbf{A}}_k\tilde{\mathbf{x}}(t) + \mathbf{G}_k\mathbf{h}(\tilde{\mathbf{x}}), \;\; \mathbf{y}(t) = \hat{\mathbf{C}}_k\tilde{\mathbf{x}}(t). \qquad (2.30)$$

Here,

$$\hat{\mathbf{A}}_k \triangleq \begin{bmatrix} \mathbf{A}+\mathbf{B}\mathbf{D}_k\mathbf{C} & \mathbf{B}\mathbf{C}_k \\ \mathbf{B}_k\mathbf{C} & \mathbf{A}_k \end{bmatrix}, \quad \hat{\mathbf{C}}_k \triangleq \begin{bmatrix} \mathbf{C} & \mathbf{0} \end{bmatrix}, \quad \mathbf{G}_k \triangleq \begin{bmatrix} \mathbf{G} \\ \mathbf{0} \end{bmatrix}.$$

In case, the quadratic constraint in (2.29) cannot be satisfied globally, but only in region $\tilde{\mathbf{x}} \in \Omega$, where $\Omega = \{\tilde{\mathbf{x}} : \ x_1 \in \Re \ , \ |x_2| \leq x_{2r}\}$ then Fig. 2.3 represents the region of attraction [53, 67, 120] (for a two dimensional case and with a Lyapunov function $v(\tilde{\mathbf{x}}) = x_1^2 + x_2^2$). In general, $\pi(r_0)$ can be viewed as an ellipsoidal approximation of the domain of attraction inside the set Ω.

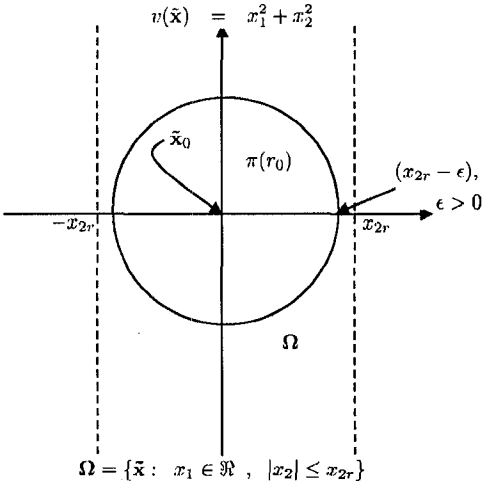

Figure 2.3: Region of attraction.

The following theorem provides sufficient conditions for the design of output feedback controller that can guarantee CL stability.

Theorem 2.2 If the following optimization problem is feasible

$$\min_{\mathbf{X}_1,\mathbf{Y}_1,\hat{\mathbf{A}}_1,\hat{\mathbf{B}}_1,\hat{\mathbf{C}}_1,\hat{\mathbf{D}}_1,\gamma} \gamma$$

$$\text{subject to} \quad \begin{bmatrix} \mathbf{X}_1 & \mathbf{I} \\ \star & \mathbf{Y}_1 \end{bmatrix} > \mathbf{0},$$

$$\begin{bmatrix} \mathbf{A}\mathbf{X}_1 + \mathbf{X}_1\mathbf{A}^T + \mathbf{B}\hat{\mathbf{C}}_1 + \left(\mathbf{B}\hat{\mathbf{C}}_1\right)^T & \mathbf{A} + \hat{\mathbf{A}}_1^T + \mathbf{B}\hat{\mathbf{D}}_1\mathbf{C} & \mathbf{G} & \mathbf{X}_1\mathbf{H}_1^T \\ \star & \mathbf{Y}_1\mathbf{A} + \hat{\mathbf{B}}_1\mathbf{C} + \mathbf{A}^T\mathbf{Y}_1 + \mathbf{C}^T\hat{\mathbf{B}}_1^T & \mathbf{Y}_1\mathbf{G} & \mathbf{H}_1^T \\ \star & \star & -\mathbf{I} & \mathbf{0} \\ \star & \star & \star & -\gamma\mathbf{I} \end{bmatrix} < \mathbf{0},$$

then the system in (2.30) is asymptotically stable for all nonlinearities satisfying the quadratic constraint in (2.29).

Proof: Please see Appendix A.

Corollary 2.1 As $v(\tilde{\mathbf{x}})$ is radially unbounded, if the quadratic constraint in (2.29) is valid $\forall\, \tilde{\mathbf{x}}$, then the CL system in (2.30) is globally asymptotically stable with the controller designed using Theorem 2.2.

Remark 2.4 It is clear that if a controller is strictly proper then the closed loop system has fast dynamics if the eigenvalues of $\hat{\mathbf{A}}_k$ lies far to the LHP. Therefore, similar to Section 2.3, constraints on the closed loop eigenvalues are imposed. Starting from the pole placement constraints of [20], some variable transformations and mathematical calculations lead to

$$\begin{bmatrix} \mathcal{F}_{11}+(2\alpha_{min})\mathbf{X}_1 & \mathcal{F}_{12}+(2\alpha_{min})\mathbf{I} \\ \star & \mathcal{F}_{22}+(2\alpha_{min})\mathbf{Y}_1 \end{bmatrix} < 0,$$

$$\begin{bmatrix} -\omega_{nmax}\mathbf{X}_1 & -\omega_{nmax}\mathbf{I} & \mathbf{A}\mathbf{X}_1+\mathbf{B}\hat{\mathbf{C}}_1 & \mathbf{A}+\mathbf{B}\hat{\mathbf{D}}_1\mathbf{C} \\ -\omega_{nmax}\mathbf{I} & -\omega_{nmax}\mathbf{Y}_1 & \hat{\mathbf{A}}_1 & \mathbf{Y}_1\mathbf{A}+\hat{\mathbf{B}}_1\mathbf{C} \\ \star & \star & -\omega_{nmax}\mathbf{X}_1 & -\omega_{nmax}\mathbf{I} \\ \star & \star & -\omega_{nmax}\mathbf{I} & -\omega_{nmax}\mathbf{Y}_1 \end{bmatrix} < 0,$$

$$\begin{bmatrix} \mathcal{D}_{11} & \mathcal{D}_{12} \\ \star & \mathcal{D}_{22} \end{bmatrix} < 0,$$

where

$$\mathcal{D}_{11} = \mathcal{D}_{22} \triangleq \begin{bmatrix} (\sin\theta)\mathcal{F}_{11} & (\sin\theta)\mathcal{F}_{12} \\ (\sin\theta)\mathcal{F}_{12}^T & (\sin\theta)\mathcal{F}_{22} \end{bmatrix},$$

$$\mathcal{D}_{12} \triangleq \cos\theta \begin{bmatrix} \mathbf{A}\mathbf{X}_1+\mathbf{B}\hat{\mathbf{C}}_1-\mathbf{X}_1\mathbf{A}^T-(\mathbf{B}\hat{\mathbf{C}}_1)^T & \mathbf{A}+\mathbf{B}\hat{\mathbf{D}}_1\mathbf{C}-\hat{\mathbf{A}}_1^T \\ \hat{\mathbf{A}}_1-\mathbf{A}^T-\mathbf{C}^T\hat{\mathbf{D}}_1^T\mathbf{B}^T & \mathbf{Y}_1\mathbf{A}+\hat{\mathbf{B}}_1\mathbf{C}-\mathbf{A}_1^T-\mathbf{C}^T\hat{\mathbf{B}}_1^T \end{bmatrix},$$

and $\mathcal{F}_{11}$, $\mathcal{F}_{12}$, $\mathcal{F}_{22}$ are defined in the Appendix (Eqn. (A-17)). These constraints define a specific region in the LHP [20]: a stability region $\mathrm{Re}(s) \leq \alpha_{min}$, a disc of radius ω_{nmax} and a sector $\mathcal{S}(0,0,\theta)$.

Remark 2.5 For static state feedback, the number of LMI decision variables are $n \times \left(\frac{n+1}{2}+m\right)$, while for the dynamic case this number increases to $n \times (2n+1+p+m)+m \times p$. In this sense, as far as stability is concerned, state feedback control offers low computational cost, provided all states are measurable.

Remark 2.6 Dynamic controllers offer additional degrees of freedom compared to the static case. If used appropriately, the additional freedom can lead to increased robustness properties. Consider the system [120]

$$\begin{aligned} \dot{x}_1 &= 3x_1+x_1x_2+x_2+u, \\ \dot{x}_2 &= -x_1+x_2^2+u. \end{aligned} \tag{2.31}$$

It has unstable equilibrium points at the origin, and at $\begin{bmatrix} 0.145 & -0.382 \end{bmatrix}^T$. As shown in Fig. 2.4, the system also possess one stable equilibrium point at $\begin{bmatrix} 6.853 & -2.618 \end{bmatrix}^T$. The nonlinear term $\mathbf{h}_r(\mathbf{x})$ in (2.31) satisfies

$$\mathbf{h}_r^T(\mathbf{x})\mathbf{h}_r(\mathbf{x}) = \mathbf{x}^T \begin{bmatrix} x_2^2 & 0 \\ 0 & x_2^2 \end{bmatrix} \mathbf{x}. \tag{2.32}$$

If a region is selected as [120]

$$\Omega_1 = \{\mathbf{x} : x_1 \in \Re, \quad |x_2| \leq 1\}, \tag{2.33}$$

then

$$\mathbf{h}_r^T(\mathbf{x})\mathbf{h}_r(\mathbf{x}) \leq \mathbf{x}^T\mathbf{x}, \quad \forall\, \mathbf{x} \in \Omega_1. \tag{2.34}$$

Solving Theorem 2.2 without pole placement constraints (using $\mathbf{H}_1 = \mathbf{I}$) gives $\alpha = 2.5$. This reflects the fact that the CL system is locally stable for the following bound in nonlinearity

$$\mathbf{h}_r^T(\mathbf{x})\mathbf{h}_r(\mathbf{x}) \leq \alpha^2\mathbf{x}^T\mathbf{H}_r^T\mathbf{H}_r\mathbf{x} = 6.25\mathbf{x}^T\mathbf{x}, \quad \forall\, \mathbf{x} \in \Omega_1. \tag{2.35}$$

Therefore, the system is significantly robust against nonlinear perturbations in $\mathbf{h}_r(\mathbf{x})$. However, this is obtained at the cost of very fast controller dynamics, which is undesirable. By choosing an admissible region $\mathbb{D}(4.45, 0.707, 6.3)$ of the closed loop eigenvalues, α is calculated to be 1.781 and the resulting eigenvalues are $-4.455 + j4.4545$, $-4.455 - j4.4545$, $-5.9167 + j0.5413$ and $-5.9167 - j0.5413$. For the same configuration, static state feedback control [120] produces $\alpha = 1.6$. This implies that the dynamic state feedback control is capable of bearing more uncertainty in $\mathbf{h}_r(\mathbf{x})$ than the static state feedback control strategy. Figs. 2.5-2.6 show the dynamics of states for full state and output feedback control designs. Hence, this framework can be applied to cases where all the states are not measurable, and fast controller dynamics can be prevented by choosing a suitable region in the left half of the complex plane.

Next, consider a larger region Ω_2 defined by

$$\Omega_2 = \{\mathbf{x} : x_1 \in \Re, \quad |x_2| \leq 1.6\}. \tag{2.36}$$

Here, $\mathbf{h}_r(\mathbf{x})$ satisfies

$$\mathbf{h}_r^T(\mathbf{x})\mathbf{h}_r(\mathbf{x}) \leq 2.56\mathbf{x}^T\mathbf{x}, \quad \forall\, \mathbf{x} \in \Omega_2. \tag{2.37}$$

With $\mathbf{H}_r = 1.6\,\mathbf{I}$, Theorem 2.2 yields $\alpha = 1$ and $\alpha = 1.14$ for static state and dynamic state feedback control designs, respectively. Since the Lyapunov's theorem is a

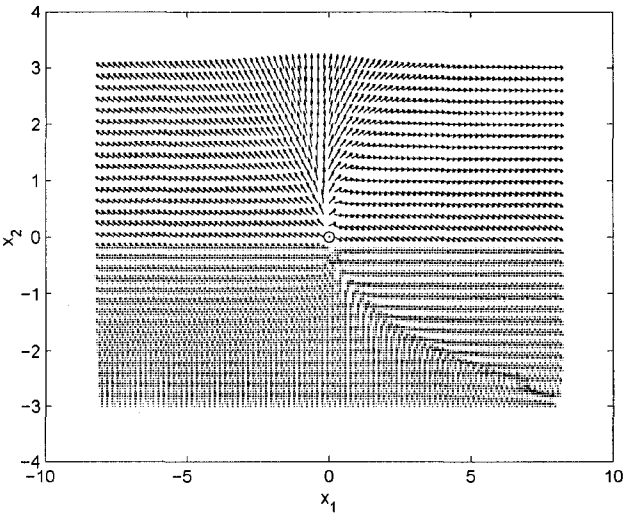

Figure 2.4: System trajectory.

sufficient condition, one can achieve a larger region of attraction by changing this Lyapunov function. The number of LMI decision variables for the static state feedback controller is $2\times\left(\frac{3}{2}+1\right)=5$. For the dynamic controller, this is increased to $2\times(5+2+1)+1\times 2=18$ for full state feedback and $2\times(5+1+1)+1\times 1=15$ for dynamic output feedback (assuming that x_1 is measured). Dynamic controllers have computational complexity, but they offer more physical insight because the transient behavior of the overall system is affected considerably by a dynamic controller. Moreover, in real time implementation, the dynamics of the controller filters the measurement noise.

2.5 Generalization to Multiple Subsystems

Following the discussions of the previous section, the closed loop system for the i'th subsystem (as in (2.30)) can be written as

$$\dot{\tilde{\mathbf{x}}}_{k_i}=\hat{\mathbf{A}}_{k_i}\tilde{\mathbf{x}}_{k_i}+\mathbf{G}_{k_i}\mathbf{h}_i,\qquad i=1,2,\ldots,n \tag{2.38}$$

where $\tilde{\mathbf{x}}_{k_i}=\left[\begin{array}{cc}\mathbf{x}_i^T & \mathbf{x}_{k_i}^T\end{array}\right]^T$, $\mathbf{x}_{k_i}$ represent controller states for the i'th subsystem and

$$\hat{\mathbf{A}}_{k_i}\triangleq\left[\begin{array}{cc}\mathbf{A}_i+\mathbf{B}_i\mathbf{D}_{k_i}\mathbf{C}_i & \mathbf{B}_i\mathbf{C}_{k_i}\\ \mathbf{B}_{k_i}\mathbf{C}_i & \mathbf{A}_{k_i}\end{array}\right],\quad \mathbf{G}_{k_i}\triangleq\left[\begin{array}{c}\mathbf{G}_i\\ \mathbf{0}\end{array}\right]. \tag{2.39}$$

The state space matrices $\mathbf{A}_{k_i}$, $\mathbf{B}_{k_i}$, $\mathbf{C}_{k_i}$ and $\mathbf{D}_{k_i}$ defines the controller for the i'th subsystem. With $\tilde{\mathbf{x}}_N=\left[\begin{array}{cccccccc}\mathbf{x}_1^T & \mathbf{x}_{k_1}^T & \mathbf{x}_2^T & \mathbf{x}_{k_2}^T & \ldots & \mathbf{x}_N^T & \mathbf{x}_{k_N}^T\end{array}\right]^T$, the quadratic

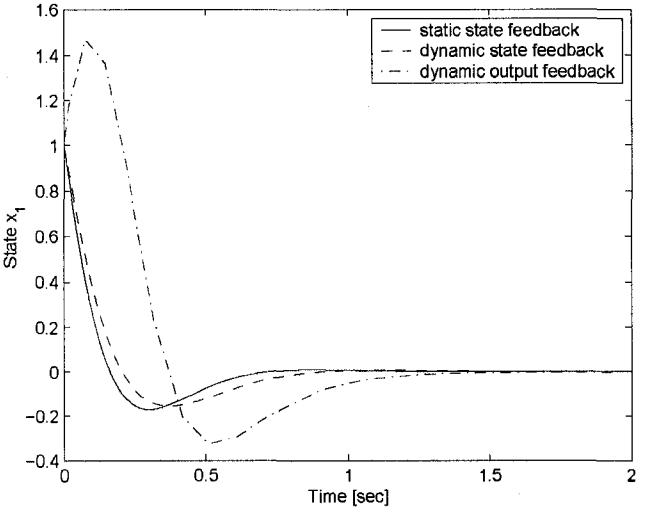

Figure 2.5: State x_1 of the system.

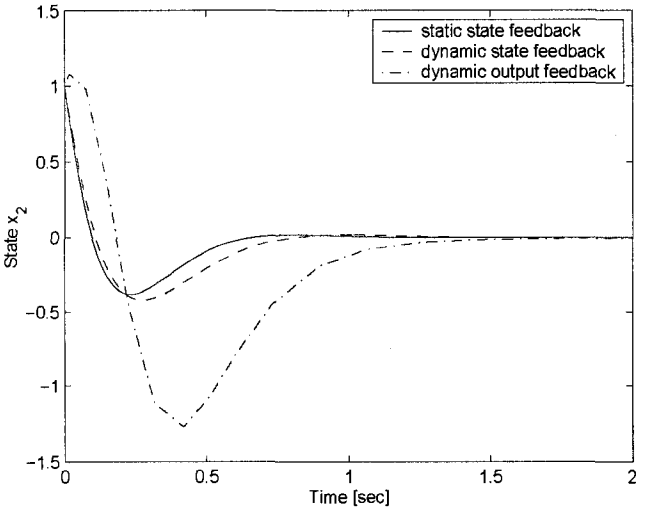

Figure 2.6: State x_2 of the system.

inequality of the i'th subsystem (as in (2.29)) is given by

$$\mathbf{h}_i^T(\mathbf{x})\mathbf{h}_i(\mathbf{x}) \leq \alpha_i^2 \mathbf{x}^T \mathbf{H}_i^T \mathbf{H}_i \mathbf{x} = \alpha_i^2 \tilde{\mathbf{x}}_N^T \mathbf{H}_{i_k}^T \mathbf{H}_{i_k} \tilde{\mathbf{x}}_N, \tag{2.40}$$

where the elements of $\mathbf{H}_{i_k}$ corresponding to $\mathbf{x}_{k_1}$, $\mathbf{x}_{k_2}$, ..., $\mathbf{x}_{k_N}$ are zero. The overall interconnected system can be written as

$$\dot{\tilde{\mathbf{x}}}_N = \hat{\mathbf{A}}_{D_k} \tilde{\mathbf{x}}_N + \mathbf{G}_{D_k} \mathbf{h}(\tilde{\mathbf{x}}_N), \tag{2.41}$$

where $\hat{\mathbf{A}}_{D_k} = \text{diag}(\hat{\mathbf{A}}_{k_1}, \hat{\mathbf{A}}_{k_2}, \ldots, \hat{\mathbf{A}}_{k_N})$, $\mathbf{G}_{D_k} = \text{diag}(\mathbf{G}_{k_1}, \mathbf{G}_{k_2}, \ldots, \mathbf{G}_{k_N})$ and $\mathbf{h} = \begin{bmatrix} \mathbf{h}_1^T & \mathbf{h}_2^T & \ldots & \mathbf{h}_N^T \end{bmatrix}^T$. The nonlinear function $\mathbf{h}(\tilde{\mathbf{x}}_N)$ is bounded by a quadratic

inequality

$$\mathbf{h}^T(\tilde{\mathbf{x}}_N)\mathbf{h}(\tilde{\mathbf{x}}_N) \leq \tilde{\mathbf{x}}_N^T\left(\sum_{i=1}^{N}\alpha_i^2\mathbf{H}_{i_k}^T\mathbf{H}_{i_k}\right)\tilde{\mathbf{x}}_N = \tilde{\mathbf{x}}_N^T\left(\sum_{i=1}^{N}\frac{1}{\gamma_i^2}\mathbf{H}_{i_k}^T\mathbf{H}_{i_k}\right)\tilde{\mathbf{x}}_N. \tag{2.42}$$

The following algorithm provides sufficient conditions for the design of decentralized controllers that can guarantee CL stability.

Theorem 2.3 If the following optimization problem is feasible

$$\begin{aligned}
&\min \sum_{i=1}^{N}\gamma_i, \\
&\text{subject to} \quad \boldsymbol{\Pi}_{2_D}^T\mathbf{Y}_D\boldsymbol{\Pi}_{2_D} > \mathbf{0}, \\
&\begin{bmatrix}
\boldsymbol{\Pi}_{2_D}^T(\hat{\mathbf{A}}_{D_k}\mathbf{Y}_D + \mathbf{Y}_D\hat{\mathbf{A}}_{D_k}^T)\boldsymbol{\Pi}_{2_D} & \boldsymbol{\Pi}_{2_D}^T\mathbf{G}_{D_k} & \boldsymbol{\Pi}_{2_D}^T\mathbf{Y}_D\mathbf{H}_{1_k}^T & \cdots & \boldsymbol{\Pi}_{2_D}^T\mathbf{Y}_D\mathbf{H}_{N_k}^T \\
\star & -\mathbf{I} & \mathbf{0} & \cdots & \mathbf{0} \\
\star & \star & -\gamma_1\mathbf{I} & \cdots & \mathbf{0} \\
\vdots & \vdots & \vdots & \ddots & \vdots \\
\star & \star & \star & \cdots & -\gamma_N\mathbf{I}
\end{bmatrix} < \mathbf{0}, \\
&\boldsymbol{\Pi}_{2_D}^T(\hat{\mathbf{A}}_{D_k}\mathbf{Y}_D + \mathbf{Y}_D\mathbf{A}_{D_k}^T)\boldsymbol{\Pi}_{2_D} + 2\alpha_{min_D}\boldsymbol{\Pi}_{2_D}^T\mathbf{Y}_D\boldsymbol{\Pi}_{2_D} < \mathbf{0}, \\
&\begin{bmatrix}
-\omega_{nmax_i}\boldsymbol{\Pi}_{2_i}^T\mathbf{Y}_i\boldsymbol{\Pi}_{2_i} & \boldsymbol{\Pi}_{2_i}^T\hat{\mathbf{A}}_{k_i}\mathbf{Y}_i\boldsymbol{\Pi}_{2_i} \\
\star & -\omega_{nmax_i}\boldsymbol{\Pi}_{2_i}^T\mathbf{Y}_i\boldsymbol{\Pi}_{2_i}
\end{bmatrix} < \mathbf{0}, \\
&\begin{bmatrix}
\mathcal{D}_{11_i} & \mathcal{D}_{12_i} \\
\star & \mathcal{D}_{22_i}
\end{bmatrix} < \mathbf{0},
\end{aligned}$$

where

$$\begin{aligned}
\alpha_{min_D} &\triangleq \text{diag}\,(\alpha_{min_1}, \alpha_{min_2}, \ldots, \alpha_{min_N}), \\
\mathcal{D}_{11_i} &= \mathcal{D}_{22_i} \triangleq \sin\theta_i \begin{bmatrix} (\mathcal{F}_{11})_i & (\mathcal{F}_{12})_i \\ (\mathcal{F}_{21})_i & (\mathcal{F}_{22})_i \end{bmatrix}, \\
\mathcal{D}_{12_i} &\triangleq \cos\theta_i(\boldsymbol{\Pi}_{2_i}^T\hat{\mathbf{A}}_{k_i}\mathbf{Y}_i\boldsymbol{\Pi}_{2_i} - \boldsymbol{\Pi}_{2_i}^T\mathbf{Y}_i\hat{\mathbf{A}}_{k_i}^T\boldsymbol{\Pi}_{2_i}),
\end{aligned}$$

then the interconnected system in (2.41) is asymptotically stable for all nonlinearities satisfying the quadratic constraint in (2.42).

Proof: Please see Appendix A.

Remark 2.7 It is worthwhile to note that a trade-off always subsist between the range of the region of attraction ($\pi(r_0)$) and the degree of robustness (α_i) of the CL system [120]. If Ω is large, then the LMI optimization yields a small value of α_i. On the other hand, if Ω is small then α_i is large. Remark 2.6 clearly illustrates this effect.

Remark 2.8 In the proposed method, stability can be retained when the subsystems are disconnected and again connected during maintenance and other operational jobs of the

plant [82–84]. This is due to the fact that bounds on the constraint accommodates the case when any of them have $\mathbf{h}_i(\mathbf{x}) \equiv 0$. Thus, the CL system in (2.41) is connectively stable [82, 83], because $\mathbf{h}_i(\mathbf{x}) \equiv 0$ implies that the i'th subsystem is disconnected, but (2.42) is still satisfied and the controller designed based on Theorem 2.3 (or, Theorem 2.1) guarantees overall closed loop stability.

Remark 2.9 Due to the requirement of a (block) diagonal Lyapunov function in decentralized design, there may be problems of infeasibility and loss of robustness of the closed loop system. Moreover, the interior point algorithm, which solves the linear objective minimization problem in MATLAB cannot be used for more than 20 matrix variables. Hence, it is necessary to write new codes if the order of the system is high.

Remark 2.10 Usually, controllers designed using Theorem 2.3 are for a normal load operating condition. However, as α_i is maximized, the same controller can be used for an array of operating regions. If, in some cases, this leads to a poor performance then it is better to compute different controllers for different operating regions and switch them using bumpless transfer algorithms or gain scheduling methods.

2.6 Application to an Utility Boiler

To illustrate how the proposed LMI approach can be applied to a boiler system, this section exploits a nonlinear dynamic model for natural circulation drum-boiler [5]. It will be shown that the nonlinearity in the drum-boiler model can be bounded in the form of (2.13).

2.6.1 Physical Model

Since boilers are very common in literature, the past few decades have seen a number of modeling and control efforts. Recently, a new scheme on advanced combustion control, based on MPC strategy has been developed in [38]. The method deals with fire side of the boiler and the effort was placed on boiler pressure control by simultaneously managing the ratio of air and fuel flow. This approach leads to an increase in boiler efficiency and reduces the emission of NO_X that may cause global warming. There are other results available in literature, which deals with a tool called bond graph modeling [13]. This is in fact one way to symbolize model configurations and their control system instrumentation. They are widely used for detecting faults and for recognizing redundancies in the hardware. There are also black box models that work in a particular operating region [60]; nevertheless, there

is always a demand of good nonlinear process model that is valid for an array of operating conditions.

This chapter deals with designing a robust control strategy for the water side of the boiler. In the following, the symbols q_f, Q and q_s reflects the feed water, heat delivered to risers and saturated steam, respectively. The boilers use ID fan and FD fan, where the function of ID fan is to remove the flue gas and FD fan is used to supply excess air for fuel combustion.

Let V be the volume, ρ the specific density, u the specific internal energy, h the specific enthalpy, t the temperature, p the drum pressure, q the mass flow rate, m_t the total mass of the tubes and drum, and C_p the specific heat of the metal. Moreover, subscripts s, w, f, t, d, r, and m symbolize steam, water, feedwater, total steam, drum, riser and metal, respectively [5].

The global mass and energy balances are given by [5]

$$\frac{d}{dt}[\rho_s V_{st} + \rho_w V_{wt}] = q_f - q_s, \tag{2.43}$$

$$\frac{d}{dt}[\rho_s h_s V_{st} + \rho_w h_w V_{wt} - pV_t + m_t C_p t_m] = Q + q_f h_f - q_s h_s, \tag{2.44}$$

where V_{st} and V_{wt} characterize the total steam volume and the total water volume, respectively. Therefore, the total volume of the boiler drum, downcomers and risers is $V_t = V_{st} + V_{wt}$.

Riser Dynamics [5]: The global mass balance for the riser can be written as [5]

$$\frac{d}{dt}[\rho_s \bar{\alpha}_v V_r + \rho_w (1 - \bar{\alpha}_v) V_r] = q_{dc} - q_r, \tag{2.45}$$

where q_{dc} is the downcomer flow rate, q_r is flow rate out of the risers, V_r represent the riser volume and the total steam in the risers is denoted by the average volume fraction [5]

$$\bar{\alpha}_v = \frac{1}{\alpha_r}\int_0^{\alpha_r} f(\xi)d\xi = \frac{\rho_w}{\rho_w - \rho_s} \times \left[1 - \frac{\rho_s}{(\rho_w - \rho_s)\alpha_r} \ln\left(1 + \frac{\rho_w - \rho_s}{\rho_s}\alpha_r\right)\right], \tag{2.46}$$

where α_r is the steam mass fraction. Finally, the global energy balance for the risers is given by [5]

$$\frac{d}{dt}[\rho_s h_s \bar{\alpha}_v V_r + \rho_w h_w (1 - \bar{\alpha}_v) V_r - pV_r + m_r C_p t_s] = Q + q_{dc} h_w - (\alpha_r h_c + h_w) q_r. \tag{2.47}$$

Drum Dynamics [5]: The mass balance for the steam below the liquid level is governed by [5]

$$\frac{d}{dt}(\rho_s V_{sd}) = \alpha_r q_r - q_{sd} - q_{cd}, \tag{2.48}$$

where V_{sd} is the volume of the steam under the liquid level, q_{sd} is the steam flow rate passing through the liquid surface in the drum and q_{cd} is the condensation flow, which can be expressed as [5]

$$q_{cd} = \frac{h_w - h_f}{h_c} q_f + \frac{1}{h_c}\left(\rho_s V_{sd}\frac{dh_s}{dt} + \rho_w V_{wd}\frac{dh_w}{dt} - (V_{sd} + V_{wd})\frac{dp}{dt} + m_d C_p \frac{dt_s}{dt}\right).$$

The term V_{wd} represent the volume of water under the liquid level and the empirical model of q_{sd} is given by [5]

$$q_{sd} = \frac{\rho_s}{T_d}(V_{sd} - V_{sd}^0) + \alpha_r q_{dc} + \alpha_r \beta (q_{dc} - q_r), \tag{2.49}$$

where V_{sd}^0 is the volume of the steam when there is no condensation in the drum, T_d is the residence time of the steam, and the constant β is user defined that is approximately 0.3.

2.6.2 Simplification of the Nonlinear Model to Standard Form

In this section, the conversion of the nonlinear model given by (2.43), (2.44), (2.45), (2.47), and (2.48) to the form in (2.12) has been carried out. The state variables of the system are: total water volume ($V_{wt} = x_1$), drum pressure ($p = x_2$), steam-mass fraction in the riser ($\alpha_r = x_3$) and steam volume in the drum ($V_{sd} = x_4$). The control variables are: feedwater flow rate ($q_f = u_1$), steam flow rate ($q_s = u_2$), and heat supplied to the risers ($Q = u_3$). From (2.43), straightforward calculation shows that

$$\begin{aligned}
\frac{d}{dt}\left[\rho_s(V_t - x_1) + \rho_w x_1\right] &= u_1 - u_2, \\
(\rho_w - \rho_s)\frac{dx_1}{dt} + \left[(V_t - x_1)\frac{\partial \rho_s}{\partial x_2}\right]\frac{dx_2}{dt} &= u_1 - u_2, \\
e_{11}\frac{dx_1}{dt} + e_{12}\frac{dx_2}{dt} &= u_1 - u_2,
\end{aligned} \tag{2.50}$$

where $e_{11} = \rho_w - \rho_s$ and $e_{12} = x_1 \frac{\partial \rho_w}{\partial x_2} + (V_t - x_1)\frac{\partial \rho_s}{\partial x_2}$. Similarly, from (2.44)

$$\begin{aligned}
&\frac{d}{dt}\left[\rho_s h_s(V_t - x_1) + \rho_w h_w x_1 - x_2 V_t + m_t C_p t_m\right] = u_3 + u_1 h_f - u_2 h_s, \\
&(\rho_w h_w - \rho_s h_s)\frac{dx_1}{dt} + \left[(V_t - x_1)h_s\frac{\partial \rho_s}{\partial x_2} + (V_t - x_1)\rho_s\frac{\partial h_s}{\partial x_2}\right]\frac{dx_2}{dt} \\
&+ x_1\left[h_w\frac{\partial \rho_w}{\partial x_2} + \rho_w\frac{\partial h_w}{\partial x_2}\right]\frac{dx_2}{dt} - V_t\frac{dx_2}{dt} + m_t C_p\frac{\partial t_m}{\partial x_2}\frac{dx_2}{dt} \\
&= u_3 + u_1 h_f - u_2 h_s, \\
&e_{21}\frac{dx_1}{dt} + e_{22}\frac{dx_2}{dt} = u_3 + u_1 h_f - u_2 h_s,
\end{aligned} \tag{2.51}$$

where $e_{21} = \rho_w h_w - \rho_s h_s$ and $e_{22} = x_1 \left(h_w \frac{\partial \rho_w}{\partial x_2} + \rho_w \frac{\partial h_w}{\partial x_2} \right) - V_t + m_t C_p \frac{\partial t_m}{\partial x_2} + (V_t - x_1) \left(h_s \frac{\partial \rho_s}{\partial x_2} + \rho_s \frac{\partial h_s}{\partial x_2} \right)$. Following along the same lines, multiplying (2.45) by $(x_3 h_c + h_w)$ and subtracting (2.47) from (2.45)

$$e_{32} \frac{dx_2}{dt} + e_{33} \frac{dx_3}{dt} = u_3 - x_3 h_c q_{dc}, \tag{2.52}$$

where

$$\begin{aligned} e_{32} &= \left(\rho_w \frac{\partial h_w}{\partial x_2} - x_3 h_c \frac{\partial \rho_w}{\partial x_2} \right) (1 - \bar{\alpha}_v) V_r - V_r \\ &\quad + \left((1 - x_3) h_c \frac{\partial \rho_s}{\partial x_2} + \rho_s \frac{\partial h_s}{\partial x_2} \right) \bar{\alpha}_v V_r + m_r C_p \frac{\partial t_s}{\partial x_2}, \\ e_{33} &= ((1 - x_3)\rho_s + x_3 \rho_w) h_c V_r \frac{\partial \bar{\alpha}_v}{\partial x_3}. \end{aligned} \tag{2.53}$$

Finally, the drum dynamics is governed by

$$e_{43} \frac{dx_3}{dt} + e_{44} \frac{dx_4}{dt} = \frac{\rho_s}{T_d}(x_4^0 - x_4) + \frac{h_f - h_w}{h_c} u_1, \tag{2.54}$$

where $h_c = h_s - h_w$, $e_{44} = \rho_s$, and $e_{43} = 1.3\, x_3 (\rho_s - \rho_w) V_r \frac{\partial \bar{\alpha}_v}{\partial x_3}$. Starting from the nonlinear equations (2.50), (2.51), (2.52), and (2.54), linear algebra and simplifications give

$$\begin{aligned} \dot{x}_1 &= \frac{(e_{22} - e_{12} h_f) u_1 + (e_{12} h_s - e_{22}) u_2 - e_{12} u_3}{e_{11} e_{22} - e_{12} e_{21}}, \\ \dot{x}_2 &= \frac{(e_{11} h_f - e_{21}) u_1 + (e_{21} - e_{11} h_s) u_2 + e_{11} u_3}{e_{11} e_{22} - e_{12} e_{21}}, \\ \dot{x}_3 &= -\frac{h_c q_{dc} x_3}{e_{33}} + \frac{e_{21} e_{32} - e_{11} e_{32} h_f}{e_{11} e_{22} e_{33} - e_{12} e_{21} e_{33}} u_1 \\ &\quad + \frac{(e_{11} e_{32} h_s - e_{21} e_{32}) u_2 + (e_{11} e_{22} - e_{12} e_{21}) u_3}{e_{11} e_{22} e_{33} - e_{12} e_{21} e_{33}}, \\ \dot{x}_4 &= \frac{e_{43} h_c q_{dc} x_3}{e_{33} e_{44}} - \frac{\rho_s x_4}{T_d e_{44}} + \frac{\rho_s x_4^0}{e_{44} T_d} + \frac{e_{21} e_{32} e_{43} u_2}{(e_{11} e_{22} - e_{12} e_{21}) e_{33} e_{44}} - \frac{e_{43} u_3}{e_{33} e_{44}} \\ &\quad + \frac{(h_f - h_w)(e_{11} e_{22} - e_{12} e_{21}) e_{33} - e_{21} e_{32} e_{43} h_c}{(e_{11} e_{22} - e_{12} e_{21}) e_{33} e_{44} h_c} u_1. \end{aligned} \tag{2.55}$$

Some parameters of this nonlinear model are obtained from steam table at a saturation pressure of 7018.6 kPa, shown in Table 2.2. The term $\frac{\partial h_s}{\partial x_2}$ is obtained by first plotting h_s vs x_2 (in MPa) and then approximating it by a quadratic function, which on subsequent differentiation yields the corresponding value. Similarly, other parameters are obtained. In Table 2.2, the terms h_s and h_w are in KJ/kg and t_s is in °C; therefore, they should be converted into J/kg and kelvin (K) while calculating e_{11}, e_{12}, ..., e_{43}. Other parameters of the nonlinear model can be obtained from [5] and [77]. At steady state, $u_1 = u_2 = 58$ in pu, $u_3 = 84$ in pu, $x_1 = V_{wt} = 57.5\ \text{m}^3$, $x_2 = p = 7018\ \text{kPa}$, $x_3 = \alpha_r = 0.05$, $x_4 = V_{sd} = 5\ \text{m}^3$ and total volume of water and steam $V_t = 85\ \text{m}^3$.

Table 2.2: Parameters of the nonlinear model at a saturation pressure of 7018.6 kPa.

t_s	h_w	h_s	ρ_w	ρ_s	$\frac{\partial h_w}{\partial x_2}$	$\frac{\partial h_s}{\partial x_2}$	$\frac{\partial \rho_w}{\partial x_2}$	$\frac{\partial \rho_s}{\partial x_2}$	$\frac{\partial t_s}{\partial x_2}$
285.9	1267.8	2772.3	739.9	36.6	51.9	−13.3	−18.1	5.9	11.53

The terms e_{11}, e_{12}, ..., e_{43} are functions of states $x_1, \ldots, x_4$, and properties of steam and water, namely, specific enthalpy, specific density, etc. However, they are not functions of u_1, u_2, and u_3. This provides an advantage in bringing the nonlinear model to the form in (2.12). The following Taylor series expansion is used

$$\begin{aligned}\dot{\mathbf{x}} &= [\mathbf{f}(\mathbf{x},\mathbf{u})]_{X_0} + \left[\frac{\partial \mathbf{f}}{\partial \mathbf{x}}\right]_{X_0}(\mathbf{x}-\mathbf{x_0}) + \frac{1}{2!}\left[\frac{\partial^2 \mathbf{f}}{\partial \mathbf{x}^2}\right]_{X_0}(\mathbf{x}-\mathbf{x_0})^2 + \ldots \\ &\quad + \left[\frac{\partial \mathbf{f}}{\partial \mathbf{u}}\right]_{X_0}(\mathbf{u}-\mathbf{u_0}) + \frac{1}{2!}\left[\frac{\partial^2 \mathbf{f}}{\partial \mathbf{u}^2}\right]_{X_0}(\mathbf{u}-\mathbf{u_0})^2 + \ldots, \end{aligned} \tag{2.56}$$

where X_0 represent the equilibrium values, $\mathbf{x}^T = [x_1^T\ x_2^T\ x_3^T\ x_4^T]$, and $\mathbf{u}^T = [u_1^T\ u_2^T\ u_3^T]$. The expansion in (2.56) gives the input matrix $\mathbf{B} =$

$$\begin{bmatrix} \left[\frac{e_{22}-e_{12}h_f}{e_{11}e_{22}-e_{12}e_{21}}\right]_{X_0} & \left[\frac{e_{12}h_s-e_{22}}{e_{11}e_{22}-e_{12}e_{21}}\right]_{X_0} & \left[-\frac{e_{12}}{e_{11}e_{22}-e_{12}e_{21}}\right]_{X_0} \\ \left[\frac{e_{11}h_f-e_{21}}{e_{11}e_{22}-e_{12}e_{21}}\right]_{X_0} & \left[\frac{e_{21}-e_{11}h_s}{e_{11}e_{22}-e_{12}e_{21}}\right]_{X_0} & \left[\frac{e_{11}}{e_{11}e_{22}-e_{12}e_{21}}\right]_{X_0} \\ \left[\frac{e_{21}e_{32}-e_{11}e_{32}h_f}{(e_{11}e_{22}-e_{12}e_{21})e_{33}}\right]_{X_0} & \left[\frac{e_{11}e_{32}h_s-e_{21}e_{32}}{(e_{11}e_{22}-e_{12}e_{21})e_{33}}\right]_{X_0} & \left[\frac{e_{11}e_{22}-e_{12}e_{21}}{(e_{11}e_{22}-e_{12}e_{21})e_{33}}\right]_{X_0} \\ \left[\frac{(h_f-h_w)(e_{11}e_{22}-e_{12}e_{21})e_{33}-e_{21}e_{32}e_{43}h_c}{(e_{11}e_{22}-e_{12}e_{21})e_{33}e_{44}h_c}\right]_{X_0} & \left[\frac{e_{21}e_{32}e_{43}}{(e_{11}e_{22}-e_{12}e_{21})e_{33}e_{44}}\right]_{X_0} & \left[-\frac{e_{43}}{e_{33}e_{44}}\right]_{X_0} \end{bmatrix},$$

which is calculated from $\left[\frac{\partial \mathbf{f}}{\partial \mathbf{u}}\right]_{X_0}$. Moreover, as none of e_{11}, e_{12}, ..., e_{43} are functions of u_1, u_2, and u_3, $\left[\frac{\partial^2 \mathbf{f}}{\partial \mathbf{u}^2}\right]_{X_0} = \left[\frac{\partial^3 \mathbf{f}}{\partial \mathbf{u}^3}\right]_{X_0} = \ldots = 0$. Similarly, the state matrix A in (2.12) can be calculated from $\left[\frac{\partial \mathbf{f}}{\partial \mathbf{x}}\right]_{X_0}$. With $\Delta\mathbf{x} = (\mathbf{x}-\mathbf{x}_0)$, (2.56) can be expressed as

$$\begin{aligned}\Delta\dot{\mathbf{x}} &= \underbrace{\left[\frac{\partial \mathbf{f}}{\partial \mathbf{x}}\right]_{X_0}}_{\mathbf{A}}\Delta\mathbf{x} + \underbrace{\left[\frac{\partial \mathbf{f}}{\partial \mathbf{u}}\right]_{X_0}}_{\mathbf{B}}\Delta\mathbf{u} \\ &\quad + \underbrace{\frac{1}{2!}\left[\frac{\partial^2 \mathbf{f}}{\partial \mathbf{x}^2}\right]_{X_0}\Delta\mathbf{x}^2 + \frac{1}{3!}\left[\frac{\partial^2 \mathbf{f}}{\partial \mathbf{x}^3}\right]_{X_0}\Delta\mathbf{x}^3 + \ldots}_{\mathbf{h_r(\Delta x)}}, \end{aligned}$$

where

$$\left[\frac{\partial \mathbf{f}}{\partial \mathbf{x}}\right]_{X_0} = \mathbf{A} = \begin{bmatrix} 0 & 0 & 0 & 0 \\ 0 & 0 & 0 & 0 \\ 0 & 0 & -\frac{h_c q_{dc}}{e_{33}} & 0 \\ 0 & 0 & \frac{e_{43}h_c q_{dc}}{e_{33}e_{44}} & -\frac{\rho_s}{T_d e_{44}} \end{bmatrix}.$$

After substituting the following parameters

$$\begin{aligned} e_{11} &= 666, \quad e_{12} = 9.078e-004, \quad e_{21} = 830e+006, \quad e_{22} = 4795, \\ e_{32} &= 1616.34, \quad e_{33} = 3.7e+0010, \quad e_{43} = -14.36e+003, \quad e_{44} = 46.134, \end{aligned}$$

the state and input matrices are given by

$$\mathbf{A} = \begin{bmatrix} 0 & 0 & 0 & 0 \\ 0 & 0 & 0 & 0 \\ 0 & 0 & -0.045 & 0 \\ 0 & 0 & -22.23 & -0.083 \end{bmatrix}, \quad \mathbf{B} = \begin{bmatrix} 0.001465 & -0.000943 & -3.71e-10 \\ 26.68 & -410 & 0.000272 \\ -1.165e-6 & 1.791e-5 & 1.508e-11 \\ 0.000555 & 0.00557 & 4.717e-9 \end{bmatrix},$$

and $\mathbf{G}$ is an identity matrix. Starting from (2.46), some calculations show that

$$\frac{\partial \bar{\alpha}_v}{\partial x_3} = \frac{\rho_w}{2\rho_s}\left[\frac{(1+x_3)\rho_s - \rho_w x_3}{(1-x_3)\rho_s + \rho_w x_3}\right]. \tag{2.57}$$

Hence, from (2.55)

$$\begin{aligned} -\frac{h_c q_{dc} x_3}{e_{33}} &= -\frac{2\rho_s q_{dc} x_3}{V_r \rho_w [\rho_s + x_3(\rho_s - \rho_w)]} \\ &= -\left[\frac{2\rho_s q_{dc} x_3}{V_r \rho_w [\rho_s + x_3(\rho_s - \rho_w)]}\right]_{X_0} - \left[\frac{2\rho_s q_{dc}}{V_r \rho_w [\rho_s + x_3(\rho_s - \rho_w)]} \right. \\ &\quad \left. + \frac{2\rho_s x_3 q_{dc}(\rho_s - \rho_w)}{V_r \rho_w [\rho_s + x_3(\rho_s - \rho_w)]^2}\right]_{X_0} \triangle x_3 \\ &\quad + \left[\frac{2\rho_s q_{dc}(\rho_s - \rho_w)}{V_r \rho_w [\rho_s + x_3(\rho_s - \rho_w)]^2}\left\{1 - \frac{x_3(\rho_s - \rho_w)}{[\rho_s + x_3(\rho_s - \rho_w)]}\right\}\right]_{X_0} \\ &\quad \times \triangle x_3^2. \end{aligned} \tag{2.58}$$

Moreover, $-\frac{\rho_s x_4}{T_d e_{44}} = -\frac{x_4}{T_d}$ and

$$\begin{aligned} \frac{e_{43} h_c q_{dc} x_3}{e_{33} e_{44}} &= \frac{q_{dc} x_3}{\rho_s}\left[\frac{1.3(\rho_s - \rho_w)x_3}{[\rho_s + x_3(\rho_s - \rho_w)]}\right] \\ &= \left[\frac{q_{dc} x_3}{\rho_s}\left\{\frac{1.3(\rho_s - \rho_w)x_3}{[\rho_s + x_3(\rho_s - \rho_w)]}\right\}\right]_{X_0} \\ &\quad + \left[\frac{q_{dc} x_3^2}{\rho_s}\left\{\frac{1.3(\rho_s - \rho_w)^2}{[\rho_s + x_3(\rho_s - \rho_w)]^2}\right\}\right. \\ &\quad \left. + \frac{q_{dc} x_3}{\rho_s}\left\{\frac{2.6(\rho_s - \rho_w)}{[\rho_s + x_3(\rho_s - \rho_w)]}\right\}\right]_{X_0} \triangle x_3 \\ &\quad + \left[\frac{1.3(\rho_s - \rho_w) q_{dc}}{\rho_s[(1-x_3)\rho_s + x_3\rho_w]}\right. \\ &\quad \left.\left\{1 + \frac{x_3(\rho_s - \rho_w)}{[(1-x_3)\rho_s + x_3\rho_w]} + \frac{x_3^2(\rho_s - \rho_w)^2}{[(1-x_3)\rho_s + x_3\rho_w]^2}\right\}\right]_{X_0} \\ &\quad \times \triangle x_3^2. \end{aligned} \tag{2.59}$$

The higher order terms can be neglected as the variation of the steam mass fraction from normal operating point is 5% to 6%. In real time application, the drum level is measured, where its deviation from the normal operating point is given by [5]

$$y_{level} = (V_{wd} + V_{sd})/A_d = l_w + l_s. \tag{2.60}$$

Here, l_w and l_s denotes the effect caused by the water and the steam in the drum, respectively. The water volume in the drum V_{wd} is governed by [5]

$$V_{wd} = V_{wt} - V_{dc} - (1 - \bar{\alpha}_v)V_r, \tag{2.61}$$

where V_{dc} is the downcomer volume. With some simplifications, the drum level can be expressed as

$$y_{level} = \left[\frac{1}{A_d} \quad 0 \quad \frac{1}{A_d}\left\{\frac{\rho_w}{2\rho_s}\left(\frac{(1+x_3)\rho_s - \rho_w x_3}{(1-x_3)\rho_s + \rho_w x_3}\right)\right\}_{X_0} \quad \frac{1}{A_d} \right] \begin{bmatrix} \Delta x_1 \\ \Delta x_2 \\ \Delta x_3 \\ \Delta x_4 \end{bmatrix}.$$

The drum pressure in the boiler is measured by a differential pressure transmitter, and, in some cases (for small boilers), the total volume of the water is measured. This is obtained based on the water supplied by the boiler feed pump and from other measurements.

2.6.3 Computation of Quadratic Bounds for the Nonlinearities

The PZ map of the linearized system is shown in Fig. 2.7. It has two poles at the origin and it contains a RHP zero at 0.021. These are sources of interaction, bandwidth limitation and instability. It has been found that other nonlinear terms obtained by Taylor's expansion of (2.55) are very small compared to (2.58) and (2.59). Therefore, they are neglected while computing the quadratic bounds for nonlinearities. As the steam mass fraction is always less than 100 %, a region Ω is defined as

$$\Omega = \{\mathbf{x} : x_1, x_2, x_4 \in \Re, \quad |x_3| \leq 1\}. \tag{2.62}$$

Using (2.62), (2.58) and (2.59), it can be verified that the nonlinear function $\mathbf{h}_r(\mathbf{x})$ is bounded by

$$\begin{aligned} \mathbf{h}_r^T(\mathbf{x})\mathbf{h}_r(\mathbf{x}) \leq & \left[\frac{1.3(\rho_s - \rho_w)q_{dc}}{\rho_s[(1-x_3)\rho_s + x_3\rho_w]}\left\{1 + \frac{x_3(\rho_s - \rho_w)}{[(1-x_3)\rho_s + x_3\rho_w]}\right.\right. \\ & \left.\left. + \frac{x_3^2(\rho_s - \rho_w)^2}{[(1-x_3)\rho_s + x_3\rho_w]^2}\right\}\right]_{X_0}^2 \Delta x_3^2 \\ & + \left[\frac{2\rho_s q_{dc}(\rho_s - \rho_w)}{V_r\rho_w[\rho_s + x_3(\rho_s - \rho_w)]^2}\right. \\ & \left. \times \left\{1 - \frac{x_3(\rho_s - \rho_w)}{[\rho_s + x_3(\rho_s - \rho_w)]}\right\}\right]_{X_0}^2 \Delta x_3^2. \end{aligned} \tag{2.63}$$

Since, the bound in (2.63) is based on nominal operating conditions, the target of the proposed control scheme is to maximize the parameter α such that

$$\mathbf{h}_r^T(\mathbf{x})\mathbf{h}_r(\mathbf{x}) \leq \alpha^2 \mathbf{x}^T \mathbf{H}_r^T \mathbf{H}_r \mathbf{x}, \tag{2.64}$$

is satisfied for a range of operating points and load variations. The physical interpretation of this inequality is shown in Fig. 2.8 for one dimensional case and for a nominal load condition. The shaded region ($-\alpha \mathbf{H}_r \mathbf{x} \leq \mathbf{h}_r(\mathbf{x}) \leq \alpha \mathbf{H}_r \mathbf{x}$) increases as α is maximized.

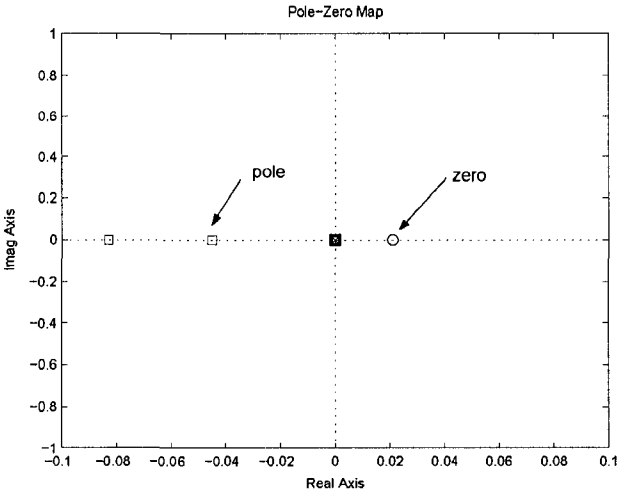

Figure 2.7: PZ map of the linearized model.

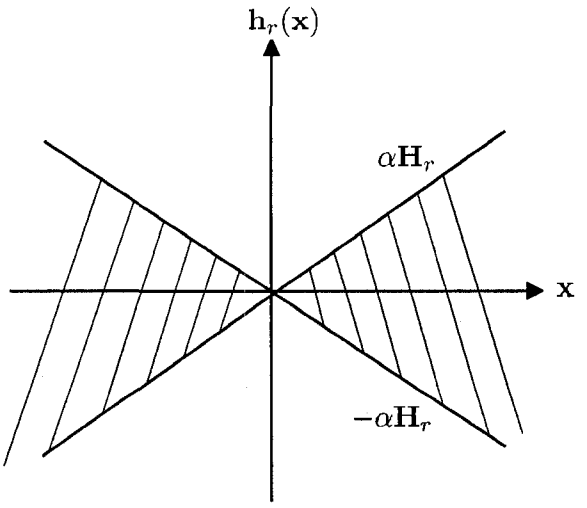

Figure 2.8: Physical interpretation of the quadratic inequality.

2.6.4 Simulation Results

The controllers are designed by solving the linear objective minimization problem of Theorem 2.2. The static state feedback controller is given by

$$\mathbf{K} = \begin{bmatrix} -85.52 & -10.48 & -6545.83 & -10.67 \\ -5.46 & -0.69 & -451.73 & -0.71 \\ -155584 & -31182.5 & -44640510 & -30267.5 \end{bmatrix},$$

with closed loop eigenvalues -2.7933, -0.1422, -0.0741, and -0.0450 and the dynamic control law has the form

$$\mathbf{A}_k = \begin{bmatrix} -167 & 5.594 & 1.361e-005 & -17.13 \\ 74.07 & -150.6 & -0.0006258 & -92.44 \\ -0.0009433 & -0.0002375 & -104.4 & 0.001007 \\ -2.706 & -27.74 & 0.0002953 & -121.6 \end{bmatrix},$$

$$\mathbf{B}_k = \begin{bmatrix} 1.364 & -2.761e-005 & 96.94 & -3.038 \\ -4.874 & 0.0001103 & 520.9 & 2.318 \\ 0.0001085 & 2.54 & 0.002707 & 1.358e-005 \\ 1.298 & 7.644e-006 & 517.7 & 1.308 \end{bmatrix},$$

$$\mathbf{C}_k = \begin{bmatrix} -875000 & -356600 & 23.24 & 1092000 \\ -56940 & -23210 & -1.064 & 71060 \\ 143600 & 109500 & -0.1619 & -4704000 \end{bmatrix},$$

$$\mathbf{D}_k = \begin{bmatrix} -63120 & -0.6657 & -6151000 & -39720 \\ -4107 & 0.3118 & -400300 & -2585 \\ -313 & -0.0364 & -1001000 & 479.9 \end{bmatrix}.$$

The original system has two poles at the origin, related to water dynamics and pressure dynamics. For output feedback, the admissibility region is assumed to be $\mathbb{D}$ ($\alpha_{min} = 0.01$, $\zeta = 0.707$, $\omega_{nmax} = 30$) and the stabilizing effect of three different types of controllers: static state feedback, dynamic state feedback and dynamic output feedback are shown in Figs. 2.9-2.10. Fig. 2.11 shows the disturbance rejection capability of the output feedback controller. Due to sudden decrease in load, the pressure in the drum rises, which increases the volume of water due to condensation. The steam quality α_r also increases due to strong interactions between different state variables, and the volume of the steam V_{sd} decreases due to the condensation of the steam. The time scale reveals the effect of RHP zero which limits the closed loop bandwidth. The controller also lessens the effect of sudden increase in load. Pole placement constraints help to reduce the initial peaking caused by load variations.

It should be noted that the control design does not consider uncertainties in the $\mathbf{A}$ matrix, namely, $(\mathbf{A} + \Delta\mathbf{A})$, and the nominal controller is obtained with residence time of steam in the drum $T_d = 12$ sec. Therefore, additional set of simulations to study the robustness of the controller are performed with $10 \leq T_d \leq 15$. The responses are shown in Fig. 2.12, which are caused by sudden load variations.

As shown by examples, this LMI-based design along with pole placement constraints to avoid fast controller dynamics is useful in many cases. However, it should be stressed

that to achieve a good performance, the choice of an appropriate α_{min} stability region, $\mathrm{Re}(s) \leq \alpha_{min}$, a disc of radius ω_{nmax}, and the conic sector $\mathcal{S}(0,0,\theta)$ has to be done carefully and several attempts are needed if the exact region of the closed loop eigenvalues are not known a priori.

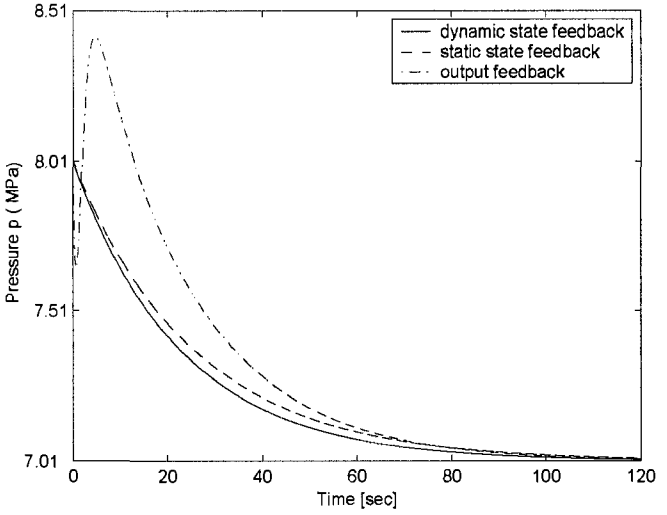

Figure 2.9: Stabilizing effect of decentralized controllers.

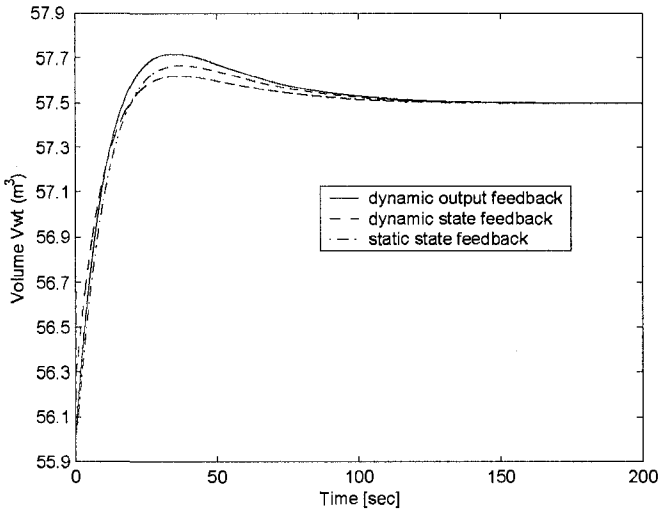

Figure 2.10: Stabilizing effect of the controllers.

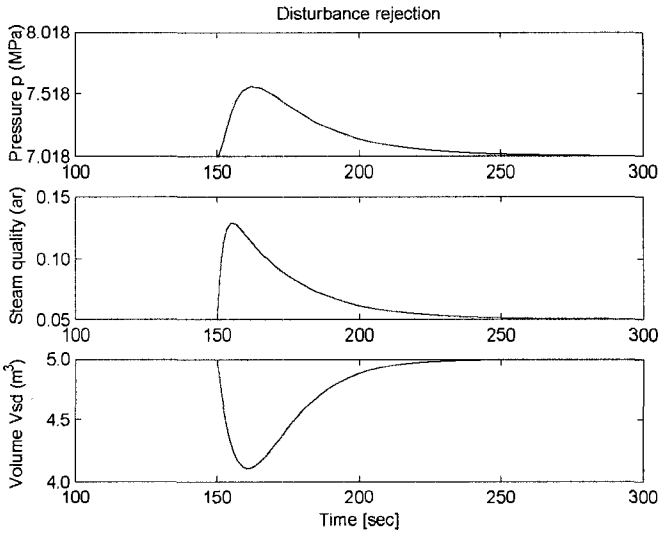

Figure 2.11: Effect of load variation.

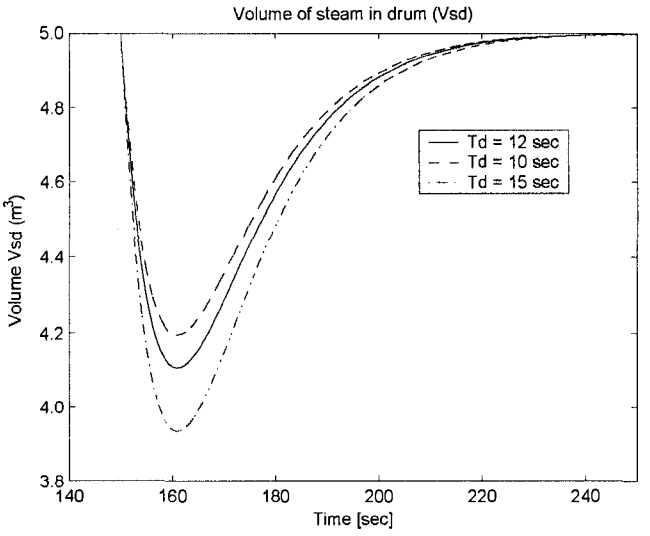

Figure 2.12: Volume of steam in the drum for three randomly chosen set of T_d.

2.7 Observer-Based Controllers for Boiler Systems

In this section, the nonlinear model of [5] is extended to include the dynamics of the governor, turbine, and the generator unit. Some simplifications of (2.55) lead to

$$\begin{aligned}\dot{x}_1 &= \frac{(e_{22}-e_{12}h_f)u_1+(e_{12}h_s-e_{22})u_2-e_{12}u_3/h_m}{e_{11}e_{22}-e_{12}e_{21}},\\ \dot{x}_2 &= \frac{(e_{11}h_f-e_{21})u_1+(e_{21}-e_{11}h_s)u_2+e_{11}u_3/h_m}{e_{11}e_{22}-e_{12}e_{21}},\end{aligned}$$

$$\begin{aligned}
\dot{x}_3 &= -\frac{h_c q_{dc} x_3}{e_{33}} + \frac{e_{21}e_{32} - e_{11}e_{32}h_f}{e_{11}e_{22}e_{33} - e_{12}e_{21}e_{33}}u_1 \\
&\quad + \frac{(e_{11}e_{32}h_s - e_{21}e_{32})u_2 + (e_{11}e_{22} - e_{12}e_{21})u_3/h_m}{e_{11}e_{22}e_{33} - e_{12}e_{21}e_{33}}, \\
\dot{x}_4 &= \frac{e_{43}h_c q_{dc} x_3}{e_{33}e_{44}} - \frac{\rho_s x_4}{T_d e_{44}} + \frac{\rho_s x_4^0}{e_{44}T_d} + \frac{e_{21}e_{32}e_{43}u_2}{(e_{11}e_{22} - e_{12}e_{21})e_{33}e_{44}} - \frac{e_{43}u_3/h_m}{e_{33}e_{44}}.
\end{aligned} \tag{2.65}$$

In the following, a governor, turbine, and a generator is connected to the boiler drum (Fig. 2.13) to move the pole coupled with the pressure dynamics to the LHP.

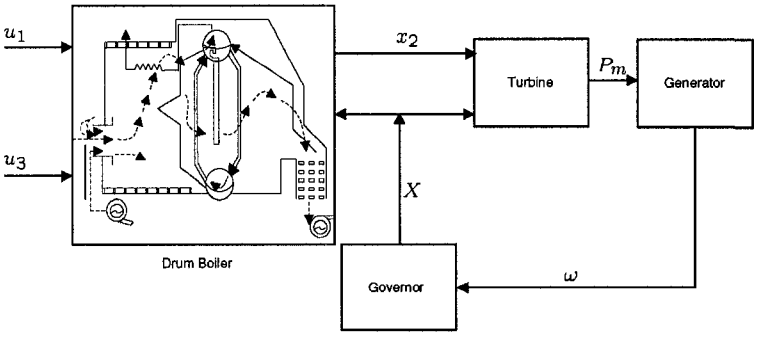

Figure 2.13: Schematic of the boiler, governor and turbine unit.

By utilizing ideas from [5, 6], some experiments are done that is required for modeling. In the experiment, the feedwater flow, fuel flow and control valve position (X) are the inputs, and the drum level, drum pressure, steam flow, and active power (P_m) are the outputs. It has been found that the response of the drum pressure is similar when perturbations are introduced in fuel flow and control valve opening. However, P_m reacts very fast when a change is introduced in the control valve setting. Furthermore, the drum pressure decreases with the increase in valve opening. Nevertheless, these variations are not consistent with the corresponding change in inputs. The characteristics are shown in Figs. 2.14-2.15. Many other experiments also reveal that the system is highly *interacting* and *nonlinear*. Under the assumptions [6] that the content (by mass) of the drum is constant, and the energy distribution in iron, water and steam does not vary significantly during transients, the stored energy of water and steam can be expressed in terms of drum pressure as $E = ax_2 + b$. Hence, $\frac{dE}{dt} = a\frac{dx_2}{dt} = P_i - P_m$, where P_i is the input power (in terms of feedwater and fuel flow) and P_m is the output power of the boiler-turbine unit.

As the output power P_m is a function of control valve position and the pressure at the

turbine, it can be written as [6]

$$P_m = r_1 u_2 \Delta h + r_2. \tag{2.66}$$

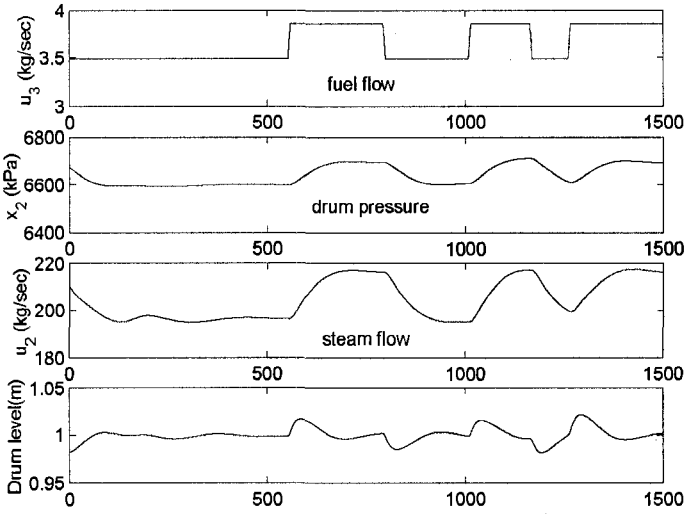

Figure 2.14: Responses due to change in fuel flow.

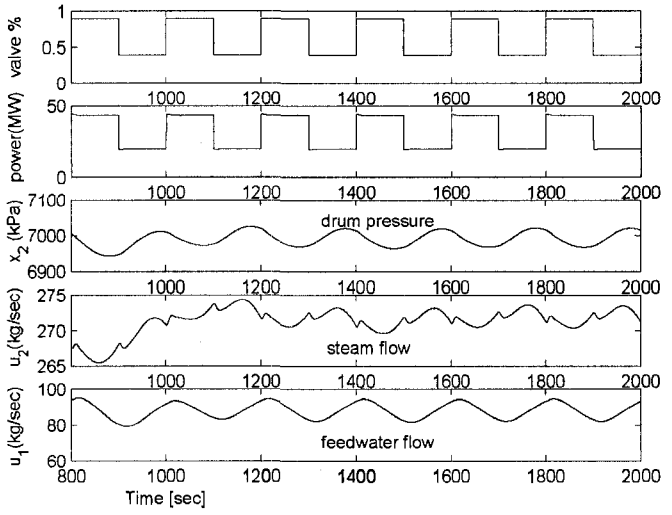

Figure 2.15: Responses due to change in control valve position.

Here, Δh is the enthalpy drop across the turbine, and r_2 is added to consider losses in the flow. Moreover, as the input power is a function of feedwater flow and fuel flow rate,

P_i is given by $P_i = a_1u_3 - a_2u_1$. From the curve of steam flow u_2 versus drum pressure x_2, $u_2 = 0.0904 \times 10^{-3}Xx_2 - 538.9242$ is obtained, where x_2 is in Pascal (Fig. 2.16). In power generating systems, significant part of power (70%) is generated by the IP and LP turbines. Therefore, the enthalpy drop in the pressure range of 1 MPa to 4 MPa (Fig. 2.16) is taken into account, which gives $\Delta h \approx 103.99x_2^{1/8}$. Combining all, (2.66) reduces to $P_m = \alpha_4\left(Xx_2^{9/8} - \alpha_5\right)$, and

$$\frac{1}{a}\frac{dE}{dt} = \frac{dx_2}{dt} = \alpha_2u_3 - \alpha_3u_1 - \alpha_1\left(Xx_2^{9/8} - \alpha_5\right), \tag{2.67}$$

where $\alpha_1 = \frac{\alpha_4}{a}$, $\alpha_2 = \frac{a_1}{a}$, $\alpha_3 = \frac{a_2}{a}$. Fig. 2.17 shows the dynamics of drum pressure, when small perturbations are done on steam valve opening and feedwater flow. Keeping u_1 and u_3 constant, a change $\Delta\dot{x}_2$ of $\frac{dx_2}{dt}$ at time t_1 caused by a change ΔX of X is given by $\Delta\dot{x}_2(t_1) = -\alpha_1x_2^{9/8}(t_1)\Delta X(t_1)$. From the figure, $\alpha_1 = 2.876 \times 10^{-6}$ is calculated. To compute α_3, small perturbations are done on the feedwater flow (Fig. 2.17) and $\alpha_3 = 26.75$ Pa/kg is achieved. Similar arguments give $\alpha_2 = 1019$, and $\alpha_5 = -9.16$. After calculating the parameters and substituting u_2 (in terms of x_2 and X), (2.65) and (2.67) clearly reveals that the pole has moved to the left half of the complex plane.

Similar to Section 2.6.2, a Taylor series expansion of (2.65) is done to bring it in the standard form. Defining a region:

$$\Omega = \{\mathbf{x} : x_1, x_4 \in \Re,\ |x_3| \leq 1,\ x_2 \leq 7.1 \text{ MPa}, |X| \leq 0.5\},$$

and denoting $\mathbf{x}_0$ as the operating point, the quadratic bound on the nonlinearity is given by

$$\begin{aligned}\mathbf{h}_1^T(\mathbf{x})\mathbf{h}_1(\mathbf{x}) \leq\ & \left[\frac{1.3(\rho_s - \rho_w)q_{dc}}{\rho_s[(1-x_3)\rho_s + x_3\rho_w]}\left\{1 + \frac{x_3(\rho_s - \rho_w)}{[(1-x_3)\rho_s + x_3\rho_w]}\right.\right. \\ & \left.\left. + \frac{x_3^2(\rho_s - \rho_w)^2}{[(1-x_3)\rho_s + x_3\rho_w]^2}\right\}\right]_{\mathbf{x}_0}^2 \Delta x_3^2 + \left[\frac{2\rho_s q_{dc}(\rho_s - \rho_w)}{V_r\rho_w[\rho_s - x_3\rho_w]^2}\right. \\ & \left.\times\left\{1 + \frac{x_3\rho_w}{[\rho_s - x_3\rho_w]}\right\}\right]_{\mathbf{x}_0}^2 \Delta x_3^2 + 1.4641\Delta X^2,\ \forall x \in \Omega.\end{aligned}$$

The physical model of the governor, turbine and generator is governed by

$$\begin{aligned}\dot{\delta}_g &= \omega_g,\ \dot{\omega}_g = -\frac{\omega_g}{T_p} + \frac{K_p}{T_p}[P_m = 0.3(P_{m_h} + P_{m_L}) + 0.4P_{m_I}], \\ 0.35\dot{P}_{m_h} &= -P_{m_h} + 3.12Xx_2^{9/8},\ \dot{P}_{m_I} = -\frac{P_{m_I}}{7} + \frac{P_{m_h}}{7}, \\ \dot{P}_{m_L} &= -\frac{P_{m_L}}{0.5} + \frac{P_{m_I}}{0.5},\ T_E\dot{X} = -X - \frac{\omega_g}{R} + P_m^0 + u,\end{aligned}$$

where P_{m_h}, P_{m_I}, and P_{m_L} are mechanical power outputs of the HP turbine, IP turbine, and the LP turbine, respectively. The parameter R is the regulation constant, T_E and T_p are time

constants, K_P is the power system gain, u is the control input, δ_g is the power angle, ω_g is the angular speed and P_m is the total mechanical power output.

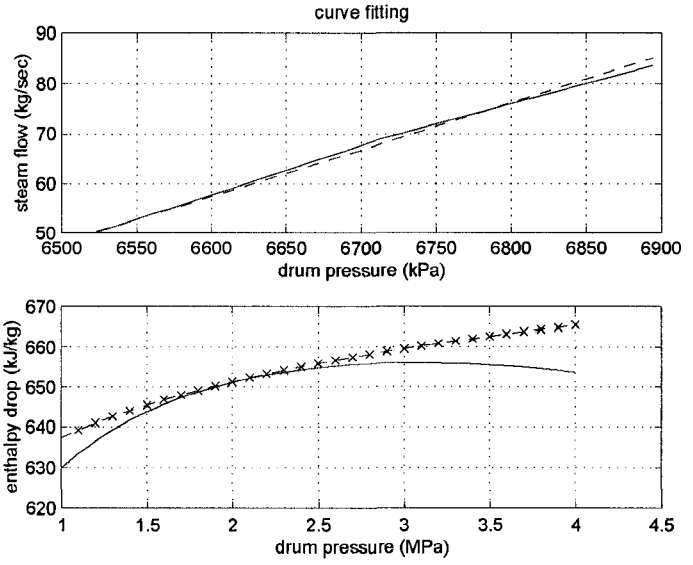

Figure 2.16: Curve fitting.

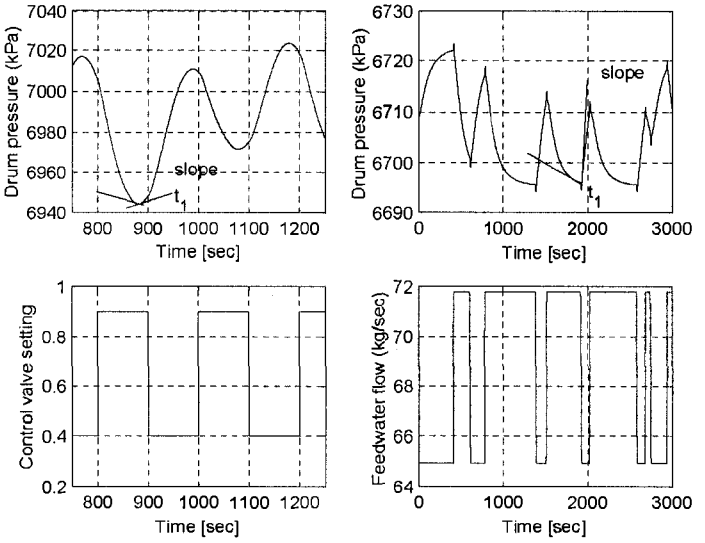

Figure 2.17: Computation of parameter α_1 and α_3.

It is important to note that $X = 0$ corresponds to 50% valve opening. Hence, -0.5 reveals a fully closed valve and +0.5 a fully opened valve. The utility boilers usually work in three

different load conditions (low load, normal load, high load), and the drum pressure always remain less than 7.1 MPa. Therefore, although the nonlinear model of the steam generating and the electricity generating unit contains quadratic nonlinearities ($x_2^{9/8}$, x_3^4, etc.), it is possible to bound the nonlinear functions as in (2.2) after some linear algebra. Moreover, even if the quadratic bounds are computed locally (limits of X, x_3 and x_2), in reality, the physical limits of these state variables lie in this range and the presented method can work well under different load conditions.

2.7.1 Controller Design and Simulation Results

After completing the modeling part, the plant is decomposed into two subsystems: a) boiler, and b) governor, turbine, generator unit. They are interconnected as in Fig. 2.13. The linearized system possess two poles at the origin: linked with water dynamics and generator dynamics. Moreover, the electrical unit has eigenvalues at $0.9359 \pm 8.0259i$. The stabilizing decentralized controllers are designed by solving the linear objective minimization problem of Theorem 2.1. They are given by

$$\mathbf{K}_{turbine} = \begin{bmatrix} -0.2671 & -0.4325 & -1.0595 & -1.7186 & -1.0506 & -4.4705 \end{bmatrix},$$

$$\mathbf{K}_{boiler} = \begin{bmatrix} -119.48 & 0.000253 & -7391.596 & -152.91 \\ -3.136 & -0.0121 & -194.039 & -4.0141 \end{bmatrix}.$$

The stabilizing effect of controllers are shown in Fig. 2.18. It can be seen that the dynamics of electricity generating unit is much faster than the drum-boiler dynamics. The term '0' on the y-axis represent steady state values ($X^0 = 0.5$, $P_m^0 = 48$MW, etc.). Fig. 2.19 shows the dynamics of estimation errors, where $(e_1)_{boiler}$, $(e_2)_{boiler}$ and $(e_3)_{boiler}$ are $x_1 - \hat{x}_1$, $x_2 - \hat{x}_2$, and $x_4 - \hat{x}_4$, respectively. The other estimation errors are for the turbine-generator unit (δ_g, ω_g and P_m).

Similar to Fig. 2.11, Fig. 2.20 shows the disturbance rejection potential of the boiler controller caused by load fluctuations in the system. Due to sudden decrease in load, the steam valve opening reduces and the pressure in the drum rises. This increases the volume of water due to condensation, which is caused by a decrease in the volume of the steam.

2.8 Chapter Summary

An algorithm for decentralized observer-based control design, which guarantees robust stabilization of the overall interconnected system is proposed. The approach alleviates the necessity of having invertible input matrix $\mathbf{B}_i$ [84], choice of parameters by trial and error [70], or any two step approach [125]. The design makes use of LMI tools

that can incorporate matching conditions, separate regions of controller and observer eigenvalues and bounds on the interconnections. The presented LMI conditions maximizes the interconnection parameter, thereby increasing the robustness of CL system against uncertain perturbations. In addition to this contribution, decentralized dynamic output feedback controllers are designed.

The developed theoretical frameworks are then applied to a power unit. The model of [5] is extended to incorporate the dynamics of governor, turbine, and generator. Simulation results show the benefits of the proposed technique.

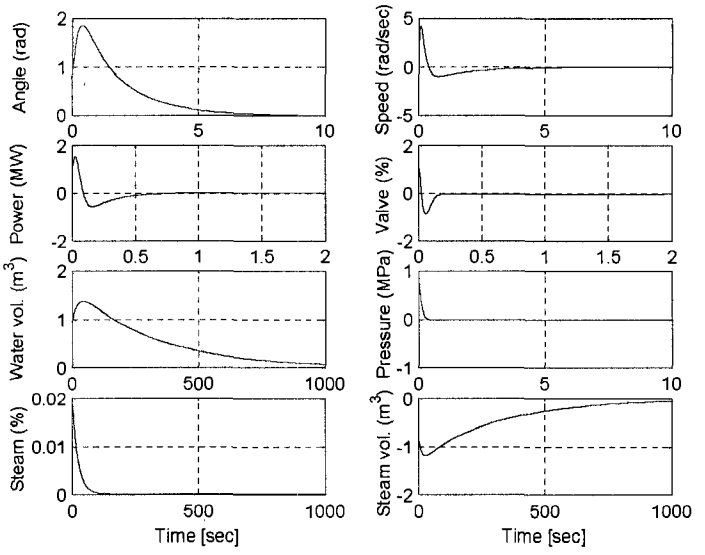

Figure 2.18: Stabilizing effect of decentralized controllers.

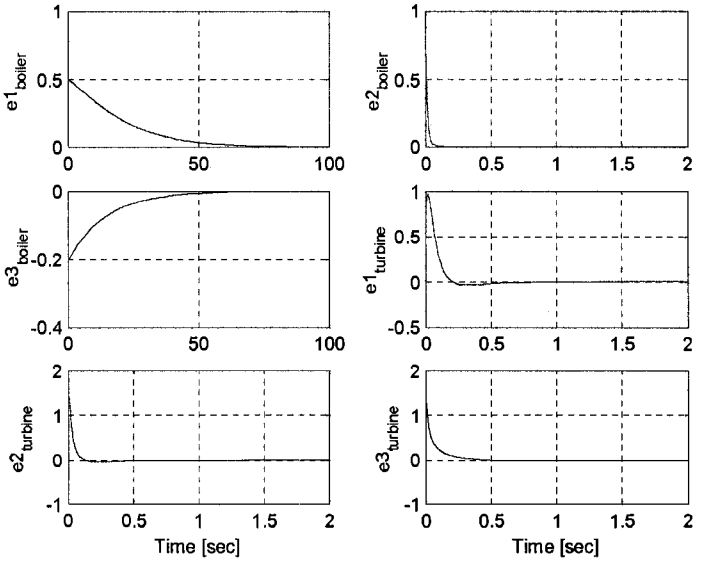

Figure 2.19: Estimation error dynamics.

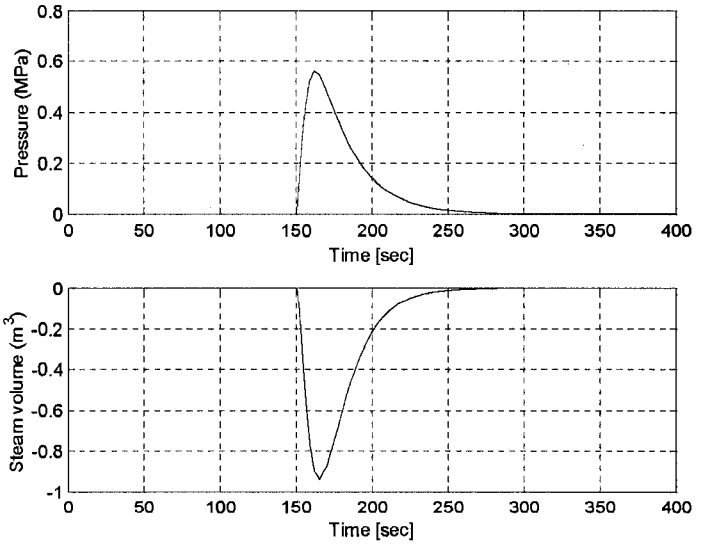

Figure 2.20: Disturbance rejection.

Chapter 3

A New Framework for Overlapping Control Design

This chapter presents a new practical framework for output feedback control design with overlapping structure. In comparison to the earlier work, the presented scheme removes some restrictions in the control design algorithm by utilizing congruence transformations, simplifications, and the reciprocal variant of the projection lemma. This results in a less conservative solution than previous design methods because the choice of some design parameters by trial and error is eliminated. Moreover, in some cases the structural constraint of having a diagonal Lyapunov function in LMIs is removed. The method is extended to capture a more general scenario of output feedback control design for nonlinear interconnected systems, and the approach is applied to an industrial utility boiler and to a multi-area power system. Simulation experiments using SYNSIM reveal that the design strategy overcomes control problems in the present plant and maintains stability in the presence of sudden load variations. Furthermore, the performance of the overlapping controllers is found to be better than existing PI controllers in the plant.

3.1 Introduction

It is well known that if some information is shared between subsystems, the concept of overlapping control arises [82, 87, 122]. Local controllers use these extra states to improve the stability and performance of the overall closed loop system. Practical scenarios where this kind of situation arises include platooning vehicles, power systems, web handling systems, and traffic light control systems [11, 87, 92, 94, 122]. However, in many cases, finding an *explicit* solution to overlapping control design is still a problem.

In the past, expansion and inclusion principles were generally used for designing overlapping control laws [45, 82, 93]. In the expansion principle, systems are stretched out such that they seem to be decoupled. The control design can then be viewed as a decentralized control problem in the expanded region. Using the inclusion principle, the control laws are then converted into the original form for the application purpose. One important problem, which may crop up while using this approach is that the method is not appropriate if some subsystem ($\mathbf{A}_{22}$) is unstable [122], because the eigenvalues of this subsystem reflects fixed modes of the expansion space and restrict the practical appeal of this algorithm. In [87, 122], an approach in the direction of reducing this weakness was shown. Their method solves static state feedback problems for both Type I and Type II overlapping (Fig. 1.1), where the input matrix and the control law have the form in (1.1). The method blends LMIs [14] and expansion principle to overcome the aforementioned problem, which is elegant and meritorious. However, in the Type II overlapping case, the selection of some parameters in the optimization problem remains an open question. The parameters are generally selected on a trial and error basis to convert the nonlinear optimization problem into LMIs. Moreover, for both Type I and Type II overlapping, the algorithm requires a Lyapunov function with some special structural constraint and, in some cases, a diagonal version of Lyapunov functions. This may cause infeasibility and reduction in robustness [123]; hence, it may not be user friendly to control engineers.

In this chapter two different techniques to solve the foregoing problems are proposed. Different congruence transformations, some simplifications, change of controller variables [20], and the reciprocal variant of the projection lemma [4] are used to obtain less conservative solutions. This is possible because the use of diagonal Lyapunov functions and choice of parameters by trial and error are not required in this approach. The method is extended to capture a general scenario of *output feedback* control design and the results are generalized to include large-scale nonlinear interconnected systems. Some interesting observations of the algorithm, which are a source of attraction to both theorists and practitioners, are as follows:

1. Method I: A general algorithm which deals with both Type I and Type II overlapping has been developed for linear as well as nonlinear systems. The method can handle static state feedback, static output feedback, full order, and reduced order dynamic output feedback control designs. There is no need to select parameters by trial and error or to use structured Lyapunov functions. The overlapping control design problem is converted into an optimization problem that involves LMIs and *only* one

equality constraint of the form: $\mathbf{Q} = \mathbf{M^T M}$. This constraint is then relaxed as:

$$\begin{bmatrix} \mathbf{Q} & \mathbf{M}^T \\ \star & \mathbf{I} \end{bmatrix} \geq 0, \tag{3.1}$$

and an iterative algorithm is used to compute controller parameters. The objective function value strictly decreases in each step, proving the convergence of this algorithm. It should be noted that $\mathbf{Q} = \mathbf{M^T M}$ reflects the boundary of the convex sets in (3.1). As the optimization involves only one equality constraint, *few* iterations are required for the control design. Moreover, in every step LMIs (feasibility problem, eigenvalue problem) are solved and there is no requirement for an initial guess. Generalization of the results to N nonlinear interconnected systems is straightforward. The algorithm can also deal with many other structures of the controllers, namely, decentralized design, or control design when information are shared by a number of subsystems and bordered block diagonal (BBD) structure [87]. This makes the results general and increases the applicability of the algorithm to a number of practical systems.

2. Method II: The control design problem for Type II overlapping is converted into a sequential two-part optimization problem using different congruence transformations, simplifications, and change of controller variables. A two step method, similar to that employed by [125], is used for computing controller parameters. The advantage of this approach is that no iteration is required and the control law can be obtained in two steps. However, this method requires block diagonal Lyapunov functions and cannot handle static output feedback control designs (additional non-convex rank constraints are needed).

To show that the approach is practical, two engineering problems are considered. In the first case, an overlapping load frequency control law for a two-area power system (a benchmark example) is designed. The areas are the subsystems and the tie lines are the overlapping divisions. It is shown that the scenario corresponds to a Type II overlapping case and the designed controller overcomes the frequency deviations in the presence of changing load conditions. The stability is studied in the presence of GRC and the results are compared with results from the decentralized design. In the second case the control problem of the Syncrude Canada integrated energy facility is considered. To bring overall stability under load variations, a nonlinear interconnected model of utility boilers and the 6.306 MPa header is first identified. The pressure equation is obtained by data fitting and the drum

water level is obtained on the basis of physical laws. Inputs to the model are feedwater flow rate, firing rate (to control air and fuel flow), and attemperator spray flow rate; the outputs are drum level, header pressure, and steam temperature. Different overlapping controllers are designed and their performance under load variations are compared with the existing PI controllers in SYNSIM. The controllers are linear, so they can be easily implemented.

The rest of this chapter is ordered as follows. Some instrumental tools are introduced in Section 3.2. A solution to Type I and Type II overlapping control is given in Section 3.3, which involves the use of a Lyapunov function without any structural constraint. Different cases are considered under which the extension to output feedback control design and to overlapping control laws for nonlinear interconnected systems are noteworthy. In Section 3.4, a sequential two-part optimization procedure to solve control problems in Type II framework is introduced. Section 3.5 deals with the application of the proposed design strategy to two-area power system and to an industrial utility boiler. Finally, Section 3.6 presents the summary of this chapter.

3.2 Instrumental Tools

Throughout this chapter, the following instrumental tool is used.

Lemma 3.1 Reciprocal Projection Lemma [4]: Let $\mathbf{X}$ denote any given positive-definite matrix. The following conditions are equivalent:

1. $\Psi + \mathbf{S} + \mathbf{S}^{\mathbf{T}} < 0$.
2. The LMI problem
$$\begin{bmatrix} \Psi + \mathbf{X} - (\mathbf{W} + \mathbf{W}^{\mathrm{T}}) & \mathbf{S}^{\mathrm{T}} + \mathbf{W}^{\mathrm{T}} \\ \star & -\mathbf{X} \end{bmatrix} < 0$$
is feasible w.r.t $\mathbf{W}$.

Here, $\mathbf{S}$ is a square matrix of size compatible with Ψ (a symmetric matrix), which appears in the control design algorithm. The matrices Ψ and $\mathbf{S}$ can contain elements that are affine/nonaffine in the controller parameters. The slack variable $\mathbf{W}$ gives an additional degree of freedom in a variety of problems. In Section 3.3, it will be shown that this additional variable plays an important role in the design of overlapping controller.

3.3 A Solution to Overlapping Control Design

In the following, an algorithm to design overlapping controllers for the Type I and Type II case is developed.

3.3.1 Design

Consider a nonlinear process of the form [120, 122]

$$\dot{\mathbf{x}}(t) = \mathbf{A}\mathbf{x}(t) + \mathbf{B}\mathbf{u}(t) + \mathbf{h}_r(\mathbf{x}), \quad \mathbf{y}(t) = \mathbf{C}\mathbf{x}(t), \tag{3.2}$$

where $\mathbf{x}(t) \in \Re^n$ is the state, $\mathbf{u}(t) \in \Re^m$ is the control input, $\mathbf{y}(t) \in \Re^p$ is the output, $\mathbf{C} = \text{diag}\,(\mathbf{C}_1, \mathbf{C}_2, \mathbf{C}_3)$ and

$$\mathbf{A} = \begin{bmatrix} \mathbf{A}_{11} & \mathbf{A}_{12} & \mathbf{A}_{13} \\ \mathbf{A}_{21} & \mathbf{A}_{22} & \mathbf{A}_{23} \\ \mathbf{A}_{31} & \mathbf{A}_{32} & \mathbf{A}_{33} \end{bmatrix}, \quad \mathbf{B} = \begin{bmatrix} \mathbf{B}_{11} & 0 \\ \mathbf{B}_{21} & \mathbf{B}_{22} \\ 0 & \mathbf{B}_{32} \end{bmatrix},$$

with $\mathbf{B}_{21} = \mathbf{B}_{22} = 0$ for Type II and $\mathbf{C} = \mathbf{I}$ for full state feedback. The uncertain nonlinear function $\mathbf{h_r}(\mathbf{x})$ is bounded by [120, 122]

$$\mathbf{h}_r^T(\mathbf{x})\mathbf{h}_r(\mathbf{x}) \leq \alpha^2 \mathbf{x}^T \mathbf{H}_r^T \mathbf{H}_r \mathbf{x}.$$

Consider a static output feedback overlapping controller of form $\mathbf{u} = \mathbf{K}\mathbf{y}$ ($\mathbf{K}$ in (1.1)), and a dynamic output feedback overlapping control law

$$\begin{aligned} \dot{\mathbf{x}}_{k_1} &= \mathbf{A}_{k_1}\mathbf{x}_{k_1} + \mathbf{B}_{k_{11}}\mathbf{C}_1\mathbf{x}_1 + \mathbf{B}_{k_{12}}\mathbf{C}_2\mathbf{x}_2, \ \mathbf{u}_1 = \mathbf{C}_{k_1}\mathbf{x}_{k_1} + \mathbf{D}_{k_{11}}\mathbf{C}_1\mathbf{x}_1 + \mathbf{D}_{k_{12}}\mathbf{C}_2\mathbf{x}_2, \\ \dot{\mathbf{x}}_{k_2} &= \mathbf{A}_{k_2}\mathbf{x}_{k_2} + \mathbf{B}_{k_{21}}\mathbf{C}_2\mathbf{x}_2 + \mathbf{B}_{k_{22}}\mathbf{C}_3\mathbf{x}_3, \mathbf{u}_2 = \mathbf{C}_{k_2}\mathbf{x}_{k_2} + \mathbf{D}_{k_{21}}\mathbf{C}_2\mathbf{x}_2 + \mathbf{D}_{k_{22}}\mathbf{C}_3\mathbf{x}_3. \end{aligned} \tag{3.3}$$

In both cases, the closed loop system is given by

$$\dot{\mathbf{x}}_{cl} = (\mathbf{A}_0 + \bar{\mathbf{B}}\mathbf{K}_d\bar{\mathbf{C}})\mathbf{x}_{cl} + \mathbf{h}_r(\mathbf{x}_{cl}) = \hat{\mathbf{A}}_D\mathbf{x}_{cl} + \mathbf{h}_r(\mathbf{x}_{cl}), \tag{3.4}$$

where, for static case: $\mathbf{A}_0 = \mathbf{A}$, $\bar{\mathbf{B}} = \mathbf{B}$, $\mathbf{K}_d = \mathbf{K}$, $\bar{\mathbf{C}} = \mathbf{C}$, $\mathbf{x}_{cl} = \mathbf{x}$ and $\mathbf{h}_r(\mathbf{x}_{cl}) = \mathbf{h}_r(\mathbf{x})$ is bounded by

$$\mathbf{h}_r^T(\mathbf{x}_{cl})\mathbf{h}_r(\mathbf{x}_{cl}) \leq \alpha^2 \mathbf{x}_{cl}^T \mathbf{H}_r^T \mathbf{H}_r \mathbf{x}_{cl} = \alpha^2 \mathbf{x}_{cl}^T \mathbf{H}_l^T \mathbf{H}_l \mathbf{x}_{cl}. \tag{3.5}$$

However, for the case of dynamic output feedback with $\mathbf{x}_{cl}^T = [\ \mathbf{x}_1^T \ \ \mathbf{x}_2^T \ \ \mathbf{x}_3^T \ \ \mathbf{x}_{k_1}^T \ \ \mathbf{x}_{k_2}^T\ ]$,

$$\begin{aligned} \hat{\mathbf{A}}_D &= \begin{bmatrix} \mathbf{A}_{11} & \mathbf{A}_{12} & \mathbf{A}_{13} & 0 & 0 \\ \mathbf{A}_{21} & \mathbf{A}_{22} & \mathbf{A}_{23} & 0 & 0 \\ \mathbf{A}_{31} & \mathbf{A}_{32} & \mathbf{A}_{33} & 0 & 0 \\ 0 & 0 & 0 & 0 & 0 \\ 0 & 0 & 0 & 0 & 0 \end{bmatrix} + \begin{bmatrix} 0 & 0 & \mathbf{B}_{11} & 0 \\ 0 & 0 & \mathbf{B}_{21} & \mathbf{B}_{22} \\ 0 & 0 & 0 & \mathbf{B}_{32} \\ \mathbf{I} & 0 & 0 & 0 \\ 0 & \mathbf{I} & 0 & 0 \end{bmatrix} \\ &\quad \times \begin{bmatrix} \mathbf{A}_{k_1} & 0 & \mathbf{B}_{k_{11}} & \mathbf{B}_{k_{12}} & 0 \\ 0 & \mathbf{A}_{k_2} & 0 & \mathbf{B}_{k_{21}} & \mathbf{B}_{k_{22}} \\ \mathbf{C}_{k_1} & 0 & \mathbf{D}_{k_{11}} & \mathbf{D}_{k_{12}} & 0 \\ 0 & \mathbf{C}_{k_2} & 0 & \mathbf{D}_{k_{21}} & \mathbf{D}_{k_{22}} \end{bmatrix} \begin{bmatrix} 0 & 0 & 0 & \mathbf{I} & 0 \\ 0 & 0 & 0 & 0 & \mathbf{I} \\ \mathbf{C}_1 & 0 & 0 & 0 & 0 \\ 0 & \mathbf{C}_2 & 0 & 0 & 0 \\ 0 & 0 & \mathbf{C}_3 & 0 & 0 \end{bmatrix} \\ &= \mathbf{A}_0 + \bar{\mathbf{B}}\mathbf{K}_d\bar{\mathbf{C}}, \end{aligned} \tag{3.6}$$

$$\text{and } \mathbf{h}_r^T(\mathbf{x}_{cl})\mathbf{h}_r(\mathbf{x}_{cl}) \leq \alpha^2\mathbf{x}_{cl}^T\begin{bmatrix}\mathbf{H}_r^T\mathbf{H}_r & 0 & 0\\ 0 & 0 & 0\\ 0 & 0 & 0\end{bmatrix}\mathbf{x}_{cl} = \alpha^2\mathbf{x}_{cl}^T\mathbf{H}_l^T\mathbf{H}_l\mathbf{x}_{cl}. \quad (3.7)$$

In the following theorem, sufficient conditions are provided to design overlapping control laws for the nonlinear system in (3.4) that can guarantee CL stability. It is assumed that $(\mathbf{A}, \mathbf{B})$ is stabilizable, $(\mathbf{C}, \mathbf{A})$ is detectable and the system has no unstable fixed modes for the control structure in (1.1).

Theorem 3.1 If there exists a controller $\mathbf{K}_d$ such that the following optimization is feasible

$$\min \ \gamma$$

$$\text{subject to} \quad \mathbf{X}_P > 0, \quad (3.8)$$

$$\begin{bmatrix} -\mathbf{Q} & \mathbf{A}_0^T + \bar{\mathbf{C}}^T\mathbf{K}_d^T\bar{\mathbf{B}}^T + \mathbf{M}^T & \mathbf{X}_P & \mathbf{H}_l^T & \mathbf{X}_P - \mathbf{M}^T \\ \star & -\mathbf{I} & 0 & 0 & 0 \\ \star & \star & -\mathbf{I} & 0 & 0 \\ \star & \star & \star & -\gamma\mathbf{I} & 0 \\ \star & \star & \star & \star & -\mathbf{I} \end{bmatrix} < 0, \quad (3.9)$$

$$\mathbf{Q} = \mathbf{M}^{\mathbf{T}}\mathbf{M},$$

then the system in (3.4) is asymptotically stable for nonlinearities satisfying the quadratic constraint in (3.5) or (3.7).

Proof: Please see Appendix A.

Corroborated by many simulations, it has been found that by replacing $\mathbf{X}$ with $r\mathbf{I}$ (where $r > 0$ is a tuning parameter) instead of $\mathbf{I}$ gives faster convergence speed. This is because, the inequality in (A-27) is then equivalent to

$$-\mathbf{X} < 0,$$

$$\mathbf{I} + \frac{1}{\gamma}\mathbf{Y}\mathbf{H}_l^T\mathbf{H}_l\mathbf{Y} + r\mathbf{I} - (\mathbf{W} + \mathbf{W}^T) < 0, \quad (3.10)$$

$$\mathbf{I} + \frac{1}{\gamma}\mathbf{Y}\mathbf{H}_l^T\mathbf{H}_l\mathbf{Y} + r\mathbf{I} - (\mathbf{W} + \mathbf{W}^T) + \frac{1}{r}(\mathbf{Y}\hat{\mathbf{A}}_D^T + \mathbf{W}^T)(\hat{\mathbf{A}}_D\mathbf{Y} + \mathbf{W}) < 0. \quad (3.11)$$

It is clear that (3.10) is negative definite and $\frac{1}{r}(\mathbf{Y}\hat{\mathbf{A}}_D^T + \mathbf{W}^T)(\hat{\mathbf{A}}_D\mathbf{Y} + \mathbf{W})$ is positive definite (or positive semi-definite). Therefore, in most cases, (3.11) can be easily satisfied by increasing r, since it decreases the positive contribution of $[\frac{1}{r}(\mathbf{Y}\hat{\mathbf{A}}_D^T + \mathbf{W}^T)(\hat{\mathbf{A}}_D\mathbf{Y} + \mathbf{W})]$ (Fig. 3.1), and this decrease is much more pronounced compared to the decrease of negative definiteness in $\mathbf{I} + \frac{1}{\gamma}\mathbf{Y}\mathbf{H}_l^T\mathbf{H}_l\mathbf{Y} + r\mathbf{I} - (\mathbf{W} + \mathbf{W}^T)$. This makes the optimization problem feasible and leads to faster convergence speed. The equality constraint can also be reduced to the form: $\mathbf{Q} = (\mathbf{X}_P + \mathbf{M})^T(\mathbf{X}_P + \mathbf{M})$, which is useful in some applications due to extra degree of freedom provided by $\mathbf{X}_P$.

A linear system is a special case of (3.2) with $\mathbf{h}_r(\mathbf{x}) = 0$, hence, the optimization problem becomes

$$\mathbf{X}_P > 0, \ \mathbf{Q} = \mathbf{M}^T\mathbf{M}, \begin{bmatrix} -\mathbf{Q} & \mathbf{A}_0^T + \bar{\mathbf{C}}^T\mathbf{K}_d^T\bar{\mathbf{B}}^T + \mathbf{M}^T & \mathbf{X}_P - \mathbf{M}^T \\ \star & -\mathbf{I} & \mathbf{0} \\ \star & \star & -\mathbf{I} \end{bmatrix} < 0.$$

In Theorem 3.1, the positive definite matrix $\mathbf{X}_P$ (which has no structural constraint) is decoupled from the controller $\mathbf{K}_d$. This is an important advantage, because other structures of $\mathbf{K}_d$ (decentralized design, control design when $\mathbf{x}_2$ in Fig. 1.1 is reachable from $\mathbf{u}_1$ or $\mathbf{u}_2$ only, etc.) can be assigned. Moreover, it is possible to design reduced order dynamic controllers, because different orders of $\mathbf{A}_{k_1}$ and $\mathbf{A}_{k_2}$ in (3.6) can be imposed.

In some cases, Theorem 3.1 yields a controller with fast dynamics. Therefore, additional pole placement constraints (similar to [20]) should be added.

Remark 3.1 Consider an interconnected system of the form

$$\dot{\mathbf{x}} = \mathbf{A}\mathbf{x} + \mathbf{B}\mathbf{u} + \mathbf{h}_{int}(\mathbf{x}), \ \ \mathbf{y} = \mathbf{C}\mathbf{x}, \tag{3.12}$$

where $\mathbf{h}_{int}(\mathbf{x}) = [\ \mathbf{h}_1^T(\mathbf{x}) \quad \mathbf{h}_2^T(\mathbf{x}) \quad \mathbf{h}_3^T(\mathbf{x})\ ]^T$. The functions $\mathbf{h}_i(\mathbf{x})$ (for $i = 1, 2, 3$) contain the nonlinearities in subsystems and in the interconnections. They are assumed to be bounded by a quadratic inequality [85]

$$\mathbf{h}_i^T(\mathbf{x})\mathbf{h}_i(\mathbf{x}) \leq \alpha_i^2\mathbf{x}^T\mathbf{H}_i^T\mathbf{H}_i\mathbf{x}, \ \ i = 1, 2, 3 \tag{3.13}$$

where α_i's are the interconnection parameters. Here, with static output feedback control law

$$\mathbf{h}_{int}^T(\mathbf{x}_{cl})\mathbf{h}_{int}(\mathbf{x}_{cl}) \leq \mathbf{x}_{cl}^T\left(\sum_{i=1}^{3}\alpha_i^2\mathbf{H}_i^T\mathbf{H}_i\right)\mathbf{x}_{cl} = \mathbf{x}_{cl}^T\left(\sum_{i=1}^{3}\alpha_i^2\mathbf{H}_{i_l}^T\mathbf{H}_{i_l}\right)\mathbf{x}_{cl},$$

and with dynamic output feedback control law

$$\mathbf{h}_i^T(\mathbf{x}_{cl})\mathbf{h}_i(\mathbf{x}_{cl}) \leq \alpha_i^2\mathbf{x}_{cl}^T\underbrace{\begin{bmatrix} \mathbf{H}_i^T\mathbf{H}_i & 0 & 0 \\ 0 & 0 & 0 \\ 0 & 0 & 0 \end{bmatrix}}_{\mathbf{H}_{i_l}^T\mathbf{H}_{i_l}}\mathbf{x}_{cl}.$$

For large-scale interconnected systems, where the nonlinearities in the i'th subsystem satisfy the constraint in (2.2) the following optimization problem should be solved for the

controller parameters

$$\min \ \gamma_1 + \gamma_2 + \ldots + \gamma_N$$

$$\text{subject to} \quad \mathbf{X}_P > 0,$$

$$\begin{bmatrix} -\mathbf{Q} & \mathbf{A}_0^T + \bar{\mathbf{C}}^T\mathbf{K}_d^T\bar{\mathbf{B}}^T + \mathbf{M}^T & \mathbf{X}_P & \mathbf{H}_{1_l}^T & \ldots & \mathbf{H}_{N_l}^T & \mathbf{X}_P - \mathbf{M}^T \\ \star & -\mathbf{I} & \mathbf{0} & \mathbf{0} & \ldots & \mathbf{0} & \mathbf{0} \\ \star & \star & -\mathbf{I} & \mathbf{0} & \ldots & \mathbf{0} & \mathbf{0} \\ \star & \star & \star & -\gamma_1\mathbf{I} & \ldots & \mathbf{0} & \mathbf{0} \\ \vdots & \vdots & \vdots & \vdots & \ddots & \vdots & \vdots \\ \star & \star & \star & \star & \star & -\gamma_N\mathbf{I} & \mathbf{0} \\ \star & \star & \star & \star & \star & \star & -\mathbf{I} \end{bmatrix} < 0,$$

$$\mathbf{Q} = \mathbf{M}^T\mathbf{M}.$$

Hence, the generalization of the result here is very straightforward. Since, (3.13) is a special case of (2.2), the optimization follows along the same lines.

Remark 3.2 For solving the optimization problem using the available numerical software, a key idea is to relax the equality constraint as

$$\begin{bmatrix} \mathbf{Q} & \mathbf{M}^T \\ \star & \mathbf{I} \end{bmatrix} \geq 0, \tag{3.14}$$

and then apply a CCL algorithm [27] for computing the controller parameters. The following algorithm shows a modified version of the CCL method.

3.3.2 Computational Method

As the equality constraint $\mathbf{Q} = \mathbf{M}^T\mathbf{M}$ lies in the boundary of the convex set in (3.14), let

$\mathbb{H}_r \triangleq \{\mathbf{X}_P, \mathbf{K}_d, \mathbf{Q}, \mathbf{M};$ (3.8), (3.9) and (3.14) are satisfied, where $\mathbb{H}_r$ is a convex set$\}$.

Algorithm OC (overlapping control):

1. Find the feasible set $(\mathbf{X}_P^0, \mathbf{K}_d^0, \mathbf{Q}^0, \mathbf{M}^0) \in \mathbb{H}_r$. Let $k := 0$.

2. Solve the following convex optimization problem:

$$\min_{\mathbb{H}_r} \ \text{trace}\left[\mathbf{Q} - (\mathbf{M}^k)^T\mathbf{M} - \mathbf{M}^T\mathbf{M}^k\right]$$
subject to (3.8), (3.9) and (3.14).

3. Substitute the values of $(\mathbf{X}_P, \mathbf{K}_d, \mathbf{M})$ in (A-28). If the condition is satisfied then output the feasible solutions $(\mathbf{X}_P, \mathbf{K}_d, \mathbf{Q}, \mathbf{M})$. EXIT.

4. Set $k = k + 1$, $(\mathbf{X}_P^k, \mathbf{K}_d^k, \mathbf{Q}^k, \mathbf{M}^k) = (\mathbf{X}_P, \mathbf{K}_d, \mathbf{Q}, \mathbf{M})$, and go to step 2.

Remark 3.3 It is important to note that the optimization problem in the k'th step, $\tilde{J}^{k*} = \min \tilde{J}^k = \min [\mathrm{tr}\,(\mathbf{Q}^k + \mathbf{Q} - (\mathbf{M}^k)^T\mathbf{M} - \mathbf{M}^T\mathbf{M}^k)]$, subject to (3.8), (3.9), (3.14) and the step 2 in algorithm OC are equivalent. This is because $\mathbf{Q}^k$ is a constant matrix; therefore, both of them output the same solution. Using ideas from literatures (Theorem 3.2 of [108]; [107]), it can be easily derived that $\tilde{J}^{k*} \geq 0$ and the sequence $\{\tilde{J}^{1*}, \tilde{J}^{2*}, \ldots\}$ strictly decreases in each step, thereby revealing the convergence of this algorithm. Moreover, another way to solve the algorithm OC is to expand the set to include the equality constraint by substituting $-\mathbf{Q}$ with $-\mathbf{Q} + z\mathbf{I}$ ($z > 0$, say), and to stop the iterative algorithm to output the feasible solution if $[\mathbf{Q}^k - (\mathbf{M}^k)^T\mathbf{M}^k] < z\mathbf{I}$. This is due to the fact that the equality constraint lies in the boundary of (3.14), whereas the LMI solver works in a fashion to achieve a solution in the interior of this set (strict inequalities). Consequently, the parameter z is introduced to expand the set such that the periphery appears inside and (3.8) as well as (3.9) are satisfied (Fig. 3.1) under these situations [108].

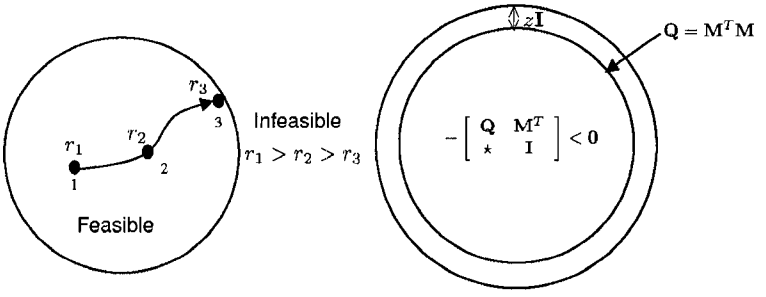

Figure 3.1: Physical meaning of parameters r and z.

Remark 3.4 It is apparent that the conditions in Theorem 3.1 are not convex owing to a matrix equality $\mathbf{Q} = \mathbf{M}^T\mathbf{M}$. In this regard, one question may be fascinating to many control engineers: how to achieve convex conditions? To answer this question, if the condition (3.9) in Theorem 3.1 is substituted by

$$\begin{bmatrix} -(\mathbf{M}+\mathbf{M}^T)+\mathbf{I} & \mathbf{A}_0^T + \bar{\mathbf{C}}^T\mathbf{K}_d^T\bar{\mathbf{B}}^T + \mathbf{M}^T & \mathbf{X}_P & \mathbf{H}_l^T & \mathbf{X}_P - \mathbf{M}^T \\ \star & -\mathbf{I} & \mathbf{0} & \mathbf{0} & \mathbf{0} \\ \star & \star & -\mathbf{I} & \mathbf{0} & \mathbf{0} \\ \star & \star & \star & -\gamma\mathbf{I} & \mathbf{0} \\ \star & \star & \star & \star & -\mathbf{I} \end{bmatrix} < 0,$$

on the basis that $(\mathbf{M}-\mathbf{I})^T(\mathbf{M}-\mathbf{I}) \geq 0$ (which yields $-\mathbf{M}^T\mathbf{M} \leq -(\mathbf{M}+\mathbf{M}^T)+\mathbf{I}$), then the controller design conditions can be treated as convex.

Remark 3.5 It is interesting to note that in power systems the state information is shared by a number of subsystems. Under this situation, the algorithms presented in this paper can be easily used, because the optimization problem involves $\hat{\mathbf{A}}_D$ which is affine in controller parameters $\hat{\mathbf{A}}_D = \mathbf{A}_0 + \bar{\mathbf{B}}\mathbf{K}_d\bar{\mathbf{C}}$. Therefore, different structures for $\mathbf{K}_d$ and $\bar{\mathbf{B}}$ can be assigned (different control laws and different overlapping). For a three area power system, $\mathbf{K}_d$ has the structure

$$\mathbf{K}_d = \begin{bmatrix} \mathbf{K}_{11} & \mathbf{K}_{12} & 0 & \mathbf{K}_{14} & 0 & 0 \\ 0 & \mathbf{K}_{22} & \mathbf{K}_{23} & 0 & \mathbf{K}_{24} & 0 \\ 0 & 0 & 0 & \mathbf{K}_{34} & \mathbf{K}_{35} & \mathbf{K}_{36} \end{bmatrix}.$$

Example 3.1 Consider the system in [122]

$$\dot{\mathbf{x}} = \begin{bmatrix} 1 & 4 & 0 \\ 1 & 2 & 2 \\ 0 & -2 & 3 \end{bmatrix} \mathbf{x} + \begin{bmatrix} 1 & 0 \\ 0 & 0 \\ 0 & 1 \end{bmatrix} \mathbf{u}.$$

Here, the open loop system has eigenvalues at $\lambda = -0.166,\ 3.08 \pm j1.58$, and the goal is to stabilize the system with an overlapping control law. In [122], system expansion and LMIs (with some parameters selected by trial and error) was used to obtain $\mathbf{K} = \begin{bmatrix} -4.06 & -12.8 & 0 \\ 0 & -3.27 & -11.6 \end{bmatrix}$. Using the algorithm OC, the stabilizing static controller in (1.1) and the dynamic controller in (3.6) are given by

$$\mathbf{K}_{static} = \begin{bmatrix} -5.65 & -5.99 & 0 \\ 0 & -1.79 & -7.34 \end{bmatrix},$$

$$\mathbf{K}_{dynamic} = \begin{bmatrix} -9.4929 & 0 & 0.0069 & -0.1184 & 0 \\ 0 & -9.4873 & 0 & -0.1756 & 0.0676 \\ 1 & 0 & -9.9991 & -7.3232 & 0 \\ 0 & 1 & 0 & -4.8233 & -10.8633 \end{bmatrix}.$$

The number of iterations is 5 for the static controller and 7 for the dynamic controller. The optimum value of the objective function is $\tilde{J}^*$ = 7.8435e-005 for static control, and the $\mathbf{Q}$ and $\mathbf{M}$ matrices are given by

$$\mathbf{Q} = \begin{bmatrix} 27.09 & 8.35 & -4.05 \\ 8.35 & 20.13 & 16.70 \\ -4.05 & 16.70 & 20.69 \end{bmatrix}, \quad \mathbf{M} = \begin{bmatrix} 5.1865 & 1.8787 & -0.4225 \\ 0.1339 & 1.5256 & 0.2728 \\ -0.4208 & 3.7788 & 4.5218 \end{bmatrix},$$

which satisfy $\mathbf{Q} = \mathbf{M}^{\mathbf{T}}\mathbf{M}$.

3.4 Two-Step Optimization Method for Overlapping Control Design

The advantage of this approach is that no iteration is required and the overlapping control law for Type II can be obtained in two steps only.

The idea behind this approach is straightforward. For linear as well as nonlinear systems, if the asymptotic stability condition is given by

$$\mathbf{F} = \begin{bmatrix} \mathbf{F}_{11} & \mathcal{F}_{12} \\ \star & \mathcal{F}_{22} \end{bmatrix} < 0, \tag{3.15}$$

where $\mathcal{F}_{22}$ and $\mathbf{F}_{11}$ are affine in controller parameters and the bilinear terms appear in $\mathcal{F}_{12}$, then

1. Solve the feasibility problem $\mathcal{F}_{22} < 0$ to calculate some of the controller parameters.
2. Define $\xi = \text{diag}(\xi_1\mathbf{I}, \xi_2\mathbf{I}, \ldots) > 0$. Substitute the variables from step 1 and solve the optimization [125]

$$\min \ \xi_1 + \xi_2 + \ldots, \quad \text{subject to} \quad \mathbf{F}_\xi = \begin{bmatrix} \mathbf{F}_{11} & \mathcal{F}_{12} \\ \star & \xi\mathcal{F}_{22} \end{bmatrix} < 0,$$

where ξ can be considered as a tuning variable to guarantee a feasible solution in the second step. In the following, a dynamic output feedback overlapping control design problem for a nonlinear interconnected system is converted into the form of (3.15), using different transformations, simplifications, and new variable definitions. It helps to utilize the two-step approach.

3.4.1 Dynamic Output Feedback Overlapping Control Design

Consider the nonlinear interconnected system in (3.12), where a dynamic output feedback overlapping controller has to be designed. With the control law in (3.3), the closed loop system is given by

$$\begin{bmatrix} \dot{\mathbf{x}}_1 \\ \dot{\mathbf{x}}_{k_1} \\ \dot{\mathbf{x}}_2 \\ \dot{\mathbf{x}}_3 \\ \dot{\mathbf{x}}_{k_2} \end{bmatrix} = \dot{\mathbf{x}}_{cl} = \underbrace{\begin{bmatrix} \mathbf{A}_{11} + \mathbf{B}_{11}\mathbf{D}_{k_{11}}\mathbf{C}_1 & \mathbf{B}_{11}\mathbf{C}_{k_1} & \mathbf{A}_{12r} + \mathbf{B}_{11}\mathbf{D}_{k_{12r}}\mathbf{C}_{2r} & 0 \\ \mathbf{B}_{k_{11}}\mathbf{C}_1 & \mathbf{A}_{k_1} & \mathbf{B}_{k_{12r}}\mathbf{C}_{2r} & 0 \\ \mathbf{A}_{21r} & 0 & \mathbf{A}_{22r} + \mathbf{B}_{32r}\mathbf{D}_{k_{2r}}\mathbf{C}_r & \mathbf{B}_{32r}\mathbf{C}_{k_2} \\ 0 & 0 & \mathbf{B}_{k_{2r}}\mathbf{C}_r & \mathbf{A}_{k_2} \end{bmatrix}}_{\hat{\mathbf{A}}_D}$$

$$\times \mathbf{x}_{cl} + \underbrace{\begin{bmatrix} \mathbf{I} & 0 & 0 \\ 0 & 0 & 0 \\ 0 & \mathbf{I} & 0 \\ 0 & 0 & \mathbf{I} \\ 0 & 0 & 0 \end{bmatrix}}_{\mathbf{G}} \underbrace{\begin{bmatrix} \mathbf{h}_1(\mathbf{x}) \\ \mathbf{h}_2(\mathbf{x}) \\ \mathbf{h}_3(\mathbf{x}) \end{bmatrix}}_{\mathbf{h}_{int}(\mathbf{x})}. \tag{3.16}$$

Here,

$$\begin{aligned}
\mathbf{A}_{12r} &= \begin{bmatrix} \mathbf{A}_{12} & \mathbf{A}_{13} \end{bmatrix}, \mathbf{B}_{k_{12r}} = \begin{bmatrix} \mathbf{B}_{k_{12}} & 0 \end{bmatrix}, \mathbf{C}_{2r} = \mathrm{diag}(\mathbf{C}_2, 0), \\
\mathbf{D}_{k_{2r}} &= \begin{bmatrix} \mathbf{D}_{k_{21}} & \mathbf{D}_{k_{22}} \end{bmatrix}, \mathbf{C}_r = \mathrm{diag}(\mathbf{C}_2, \mathbf{C}_3), \mathbf{D}_{k_{12r}} = \begin{bmatrix} \mathbf{D}_{k_{12}} & 0 \end{bmatrix}, \\
\mathbf{B}_{k_{2r}} &= \begin{bmatrix} \mathbf{B}_{k_{21}} & \mathbf{B}_{k_{22}} \end{bmatrix}, \mathbf{A}_{22r} = \begin{bmatrix} \mathbf{A}_{22} & \mathbf{A}_{23} \\ \mathbf{A}_{32} & \mathbf{A}_{33} \end{bmatrix}, \mathbf{B}_{32r} = \begin{bmatrix} 0 \\ \mathbf{B}_{32} \end{bmatrix}, \\
\mathbf{A}_{21r} &= \begin{bmatrix} \mathbf{A}_{21} \\ \mathbf{A}_{31} \end{bmatrix}. \qquad (3.17)
\end{aligned}$$

After using a quadratic Lyapunov function, different congruence transformations, and change of controller variables method [20], the asymptotic stability conditions for the closed loop system are given by the following optimization problem:

$$\min \ \gamma_1 + \gamma_2 + \gamma_3$$

$$\text{subject to } \mathrm{diag}\left(\begin{bmatrix} \mathbf{X}_1 & \mathbf{I} \\ \star & \mathbf{Y}_1 \end{bmatrix}, \begin{bmatrix} \mathbf{X}_2 & \mathbf{I} \\ \star & \mathbf{Y}_2 \end{bmatrix}\right) > 0,$$

$$\begin{bmatrix}
\begin{bmatrix} \mathbf{F}_{11} & \mathbf{F}_{12} \\ \star & \mathbf{F}_{22} \end{bmatrix} & \begin{bmatrix} \mathbf{G}_1 & 0 \\ 0 & \mathbf{G}_2 \end{bmatrix} & \begin{bmatrix} \mathbf{T}^1_{1_l} \\ \mathbf{T}^2_{1_l} \end{bmatrix} & \begin{bmatrix} \mathbf{T}^1_{2_l} \\ \mathbf{T}^2_{2_l} \end{bmatrix} & \begin{bmatrix} \mathbf{T}^1_{3_l} \\ \mathbf{T}^2_{3_l} \end{bmatrix} \\
\star & -\mathbf{I} & 0 & 0 & 0 \\
\star & \star & -\gamma_1 \mathbf{I} & 0 & 0 \\
\star & \star & \star & -\gamma_2 \mathbf{I} & 0 \\
\star & \star & \star & \star & -\gamma_3 \mathbf{I}
\end{bmatrix} < 0,$$

where

$$\begin{bmatrix} \mathbf{F}_{11} & \mathbf{F}_{12} \\ \star & \mathbf{F}_{22} \end{bmatrix} = \mathbf{R}_1 + \mathbf{R}_1^T, \ \mathbf{G}_1 = \begin{bmatrix} \mathbf{I} \\ \mathbf{Y}_1 \end{bmatrix}, \ \mathbf{G}_2 = \begin{bmatrix} \mathbf{I} \\ \mathbf{Y}_2 \end{bmatrix},$$

$$\begin{bmatrix} \mathbf{T}^1_{1_l} \\ \mathbf{T}^2_{1_l} \end{bmatrix} = \begin{bmatrix} \mathbf{X}_1 \mathbf{h}_{11_1} & 0 & \mathbf{X}_1 \mathbf{h}_{12r_1} & 0 \\ \mathbf{h}_{11_1} & 0 & \mathbf{h}_{12r_1} & 0 \\ \mathbf{X}_2 \mathbf{h}^T_{12r_1} & 0 & \mathbf{X}_2 \mathbf{h}_{22r_1} & 0 \\ \mathbf{h}^T_{12r_1} & 0 & \mathbf{h}_{22r_1} & 0 \end{bmatrix},$$

$$\mathbf{R}_1 = \begin{bmatrix} \mathbf{A}_{11}\mathbf{X}_1 + \mathbf{B}_{11}\hat{\mathbf{C}}_1 & \mathbf{A}_{11} + \mathbf{B}_{11}\hat{\mathbf{D}}_1\mathbf{C}_1 & \mathbf{A}_{12r}\mathbf{X}_2 + \mathbf{B}_{11}\hat{\mathbf{D}}_{k_{12}}\mathbf{C}_{2r}\mathbf{X}_2 & \mathbf{A}_{12r} + \mathbf{B}_{11}\hat{\mathbf{D}}_{k_{12}}\mathbf{C}_{2r} \\ \hat{\mathbf{A}}_1 & \mathbf{Y}_1\mathbf{A}_{11} + \hat{\mathbf{B}}_1\mathbf{C}_1 & \mathbf{Y}_1\mathbf{A}_{12r}\mathbf{X}_2 + \hat{\mathbf{B}}_{k_{12}}\mathbf{C}_{2r}\mathbf{X}_2 & \mathbf{Y}_1\mathbf{A}_{12r} + \hat{\mathbf{B}}_{k_{12}}\mathbf{C}_{2r} \\ \mathbf{A}_{21r}\mathbf{X}_1 & \mathbf{A}_{21r} & \mathbf{A}_{22r}\mathbf{X}_2 + \mathbf{B}_{32r}\hat{\mathbf{C}}_2 & \mathbf{A}_{22r} + \mathbf{B}_{32r}\hat{\mathbf{D}}_2\mathbf{C}_r \\ \mathbf{Y}_2\mathbf{A}_{21r}\mathbf{X}_1 & \mathbf{Y}_2\mathbf{A}_{21r} & \hat{\mathbf{A}}_2 & \mathbf{Y}_2\mathbf{A}_{22r} + \hat{\mathbf{B}}_2\mathbf{C}_r \end{bmatrix}. \qquad (3.18)$$

The terms $\mathbf{h}_{11_1}$, $\mathbf{h}_{12r_1}$, $\mathbf{h}_{22r_1}$ are the elements of the matrix $\mathbf{H}^T_{1_l}$. Similar expressions exist for $\mathbf{T}^1_{2_l}$, $\mathbf{T}^2_{2_l}$, $\mathbf{T}^1_{3_l}$ and $\mathbf{T}^2_{3_l}$ in terms of elements in $\mathbf{H}^T_{2_l}$ and $\mathbf{H}^T_{3_l}$, respectively:

$$\begin{bmatrix} \mathbf{T}^1_{2_l} \\ \mathbf{T}^2_{2_l} \end{bmatrix} = \begin{bmatrix} \mathbf{X}_1 \mathbf{h}_{11_2} & 0 & \mathbf{X}_1 \mathbf{h}_{12r_2} & 0 \\ \mathbf{h}_{11_2} & 0 & \mathbf{h}_{12r_2} & 0 \\ \mathbf{X}_2 \mathbf{h}^T_{12r_2} & 0 & \mathbf{X}_2 \mathbf{h}_{22r_2} & 0 \\ \mathbf{h}^T_{12r_2} & 0 & \mathbf{h}_{22r_2} & 0 \end{bmatrix}, \begin{bmatrix} \mathbf{T}^1_{3_l} \\ \mathbf{T}^2_{3_l} \end{bmatrix} = \begin{bmatrix} \mathbf{X}_1 \mathbf{h}_{11_3} & 0 & \mathbf{X}_1 \mathbf{h}_{12r_3} & 0 \\ \mathbf{h}_{11_3} & 0 & \mathbf{h}_{12r_3} & 0 \\ \mathbf{X}_2 \mathbf{h}^T_{12r_3} & 0 & \mathbf{X}_2 \mathbf{h}_{22r_3} & 0 \\ \mathbf{h}^T_{12r_3} & 0 & \mathbf{h}_{22r_3} & 0 \end{bmatrix}.$$

In (3.18),

$$\begin{aligned}
\hat{\mathbf{A}}_1 &= \mathbf{Y}_1\mathbf{A}_{11}\mathbf{X}_1 + \hat{\mathbf{B}}_1\mathbf{C}_1\mathbf{X}_1 + \mathbf{Y}_1\mathbf{B}_{11}\mathbf{C}_{k_1}\mathbf{M}_1^T + \mathbf{N}_1\mathbf{A}_{k_1}\mathbf{M}_1^T,\\
\hat{\mathbf{A}}_2 &= \mathbf{Y}_2\mathbf{A}_{22r}\mathbf{X}_2 + \hat{\mathbf{B}}_2\mathbf{C}_r\mathbf{X}_2 + \mathbf{Y}_2\mathbf{B}_{32r}\mathbf{C}_{k_2}\mathbf{M}_2^T + \mathbf{N}_2\mathbf{A}_{k_2}\mathbf{M}_2^T,\\
\hat{\mathbf{B}}_1 &= \mathbf{Y}_1\mathbf{B}_{11}\mathbf{D}_{k_{11}} + \mathbf{N}_1\mathbf{B}_{k_{11}},\ \hat{\mathbf{B}}_2 = \mathbf{Y}_2\mathbf{B}_{32r}\mathbf{D}_{k_{2r}} + \mathbf{N}_2\mathbf{B}_{k_{2r}},\\
\hat{\mathbf{C}}_1 &= \mathbf{D}_{k_{11}}\mathbf{C}_1\mathbf{X}_1 + \mathbf{C}_{k_1}\mathbf{M}_1^T,\ \hat{\mathbf{C}}_2 = \mathbf{D}_{k_{2r}}\mathbf{C}_r\mathbf{X}_2 + \mathbf{C}_{k_2}\mathbf{M}_2^T,\\
\hat{\mathbf{B}}_{k_{12}} &= \mathbf{Y}_1\mathbf{B}_{11}\mathbf{D}_{k_{12r}} + \mathbf{N}_1\mathbf{B}_{k_{12r}},\ \hat{\mathbf{D}}_1 = \mathbf{D}_{k_{11}},\ \hat{\mathbf{D}}_{k_{12}} = \mathbf{D}_{k_{12r}},\ \hat{\mathbf{D}}_2 = \mathbf{D}_{k_{2r}}.
\end{aligned} \tag{3.19}$$

According to the two-step method, the following steps should be used for computing the controller parameters.

Step 1: Maximize the interconnection bounds $\alpha_1, \ldots, \alpha_3$ ($\alpha_i^2 = \frac{1}{\gamma_i}$) by solving the following optimization problem

$$\min\ \gamma_1 + \gamma_2 + \gamma_3$$
$$\text{subject to} \begin{bmatrix} \mathbf{X}_2 & \mathbf{I} \\ \star & \mathbf{Y}_2 \end{bmatrix} > \mathbf{0},$$
$$\mathcal{F}_{22} = \begin{bmatrix} \mathbf{F}_{22} & \begin{bmatrix} \mathbf{0} & \mathbf{G}_2 \end{bmatrix} & \mathbf{T}_{1_l}^2 & \mathbf{T}_{2_l}^2 & \mathbf{T}_{3_l}^2 \\ \star & -\mathbf{I} & \mathbf{0} & \mathbf{0} & \mathbf{0} \\ \star & \star & -\gamma_1\mathbf{I} & \mathbf{0} & \mathbf{0} \\ \star & \star & \star & -\gamma_2\mathbf{I} & \mathbf{0} \\ \star & \star & \star & \star & -\gamma_3\mathbf{I} \end{bmatrix} < \mathbf{0}.$$

This gives $\mathbf{X}_2$, $\mathbf{Y}_2$, $\hat{\mathbf{A}}_2$, $\hat{\mathbf{B}}_2$, $\hat{\mathbf{C}}_2$ and $\hat{\mathbf{D}}_2$. Now, compute $\mathbf{N}_2$, $\mathbf{M}_2$ square and invertible from $\mathbf{N}_2\mathbf{M}_2^T = \mathbf{U}_2\mathbf{S}_2\mathbf{V}_2^T = \text{svd}(\mathbf{I} - \mathbf{Y}_2\mathbf{X}_2)$, which yields $\mathbf{N}_2 = \mathbf{U}_2\mathbf{S}_2^{1/2}$ and $\mathbf{M}_2 = \mathbf{V}_2\mathbf{S}_2^{1/2}$. Next, the controller parameters are calculated from

$$\begin{aligned}
\mathbf{C}_{k_2} &= (\hat{\mathbf{C}}_2 - \mathbf{D}_{k_{2r}}\mathbf{C}_r\mathbf{X}_2)(\mathbf{M}_2^T)^{-1},\ \mathbf{B}_{k_{2r}} = \mathbf{N}_2^{-1}(\hat{\mathbf{B}}_2 - \mathbf{Y}_2\mathbf{B}_{32r}\mathbf{D}_{k_{2r}}),\\
\mathbf{A}_{k_2} &= \mathbf{N}_2^{-1}(\hat{\mathbf{A}}_2 - \mathbf{Y}_2\mathbf{A}_{22r}\mathbf{X}_2 - \hat{\mathbf{B}}_2\mathbf{C}_r\mathbf{X}_2 - \mathbf{Y}_2\mathbf{B}_{32r}\mathbf{C}_{k_2}\mathbf{M}_2^T)(\mathbf{M}_2^T)^{-1},\\
\mathbf{D}_{k_{2r}} &= \hat{\mathbf{D}}_2.
\end{aligned}$$

Step 2: Define the tuning parameter $\xi = \text{diag}\,(\text{diag}\,(\xi_2\mathbf{I}, \xi_3\mathbf{I}), \xi_4\mathbf{I}, \xi_1\mathbf{I}, \xi_2\mathbf{I}, \xi_3\mathbf{I})$. Using $\mathbf{X}_2$, $\mathbf{Y}_2$ and other parameters from step 1, solve

$$\min\ \xi_1 + \xi_2 + \xi_3 + \xi_4$$
$$\text{subject to} \quad \begin{bmatrix} \mathbf{X}_1 & \mathbf{I} \\ \star & \mathbf{Y}_1 \end{bmatrix} > 0,\ \xi > 0,\ \begin{bmatrix} \mathbf{F}_{11} & \mathcal{F}_{12} \\ \star & \xi\mathcal{F}_{22} \end{bmatrix} < 0,$$

where $\mathcal{F}_{12} = \begin{bmatrix} \mathbf{F}_{12} & \begin{bmatrix} \mathbf{G}_1 & \mathbf{0} \end{bmatrix} & \mathbf{T}_{1_l}^1 & \mathbf{T}_{2_l}^1 & \mathbf{T}_{3_l}^1 \end{bmatrix}$. This gives $\mathbf{X}_1$, $\mathbf{Y}_1$, $\hat{\mathbf{A}}_1$, $\hat{\mathbf{B}}_1$, $\hat{\mathbf{C}}_1$, $\hat{\mathbf{D}}_1$, $\hat{\mathbf{B}}_{k_{12}}$ and $\hat{\mathbf{D}}_{k_{12}}$. Hence, other parameters of the controller in (3.19) can be computed in the same way as in step 1 using $\mathbf{N}_1\mathbf{M}_1^T = \text{svd}(\mathbf{I} - \mathbf{Y}_1\mathbf{X}_1)$.

Remark 3.6 In this section, the problem formulation falls within the framework of BMIs. There are many algorithms available in the literature to solve BMI problems. The work in [39] is now widely accepted because of the software tool PENBMI (available at www.penopt.com). This software can deal with matrices, and (exterior) penalty, (interior) barrier, and augmented Lagrangian methods are blended to come up with a solution to BMIs. The technique starts with an initial guess, iterates based on the penalty function, and converges when a local optimum value is obtained. Some results utilize a nonlinear spectral semidefinite programming method to solve BMIs [109]. This approach is also a kind of augmented Lagrangian method and the BMIs are approximated by several unconstrained optimization problems. It requires an initial guess of the decision variables, and the penalty and Lagrangian multipliers are updated in each iteration. Both of these routines can deal with a number of examples in feedback control theory and application. Nevertheless, due to the complexity of the algorithm, when dealing with matrix variables it very difficult to trace out the reason for infeasibility, if it arises.

The authors in [30] utilize the "Method of Centers" for solving BMI problems; this method assures convergence to a local minimum. Other work [29] provides a branch and bound global optimization algorithm that can achieve a global minimum within some tolerance bounds. Both methods are interesting but it is difficult to apply them to systems with more than two scalar variables. It is not clear whether they can deal with matrices.

The work in [40, 41] utilizes the fact that BMIs become LMIs if one of the decision parameters is kept fixed. Therefore, the authors used an approximation method called LMI relaxations (LMIRs). The technique starts with an initial guess, solve the LMIs (LMIR 1-LMIR 4) in each step, and iterates until the desired objective is attained. There are, however, more than two steps involved in these algorithms. The sequential two-step optimization procedure presented in this chapter is distinguished from other results by the following properties:

- The main advantage of this algorithm is its simplicity. The transformations and other steps in the derivations are easy to follow and the final asymptotic stability conditions are easily programmable using the LMI toolbox in MATLAB. It should be useful to practitioners.
- LMIs are solved in only two sequential steps; there is no requirement for an initial guess. The method can easily deal with matrices of arbitrary size.
- The parameter ξ that appears in the second step acts as a tuning variable and

guarantees feasibility of the optimization problem, because $\mathbf{F}_{11} - \mathcal{F}_{12}(\xi\mathcal{F}_{22})^{-1}\mathcal{F}_{12}^T$ can always be made negative definite by selecting ξ large enough. This gives us some insight into the feasibility of the optimization as shown in Figs. 3.2-3.3. Other BMI algorithms do not favor visualization and many iterations are involved.

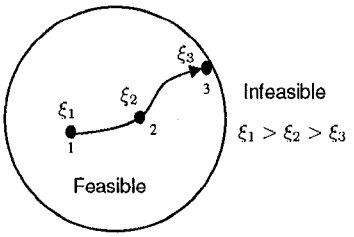

Figure 3.2: Effect on feasibility

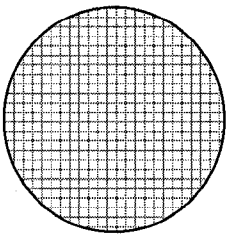

Figure 3.3: Feasibility set

One shortcoming of this approach is that the order of the dynamic controller (k) should be no less than the order of the corresponding subsystem (n). For designing reduced order controllers with orders $k_1 < n_1$ and $k_2 < n_2$, additional non-convex constraints [80]: $\text{rank}(\mathbf{I} - \mathbf{Y}_1\mathbf{X}_1) = k_1$ and $\text{rank}(\mathbf{I} - \mathbf{Y}_2\mathbf{X}_2) = k_2$ must be satisfied.

3.5 Applications to a Two-Area Power System and an Industrial Utility Boiler

The algorithms developed in Sections 3.3-3.4 are applied to a power system and utility boilers.

3.5.1 Two-Area Power System

In the two-area power system shown in Fig. 3.4, the numerical values of the parameters are obtained from [119]. The controllers are designed to share the overlapping state (ΔP_{tie}) to improve the performance of the overall CL system. They minimize the frequency deviations Δf_1 in area 1 as well as Δf_2 in area 2 under the influence of the load disturbances P_{D1} and P_{D2}.

The overall system is of ninth order and the output measurements (frequency deviations) as well as the system input matrix $\mathbf{B}$ are given by:

$$\mathbf{y} = \begin{bmatrix} \Delta f_1 & \Delta f_2 \end{bmatrix}^T, \quad \mathbf{B} = \begin{bmatrix} 0 & 0 & T_{g1} & 0 & 0 & 0 & 0 & 0 & 0 \\ 0 & 0 & 0 & 0 & 0 & 0 & 0 & T_{g2} & 0 \end{bmatrix}^T,$$

which reveals Type II overlapping (Fig. 3.5).

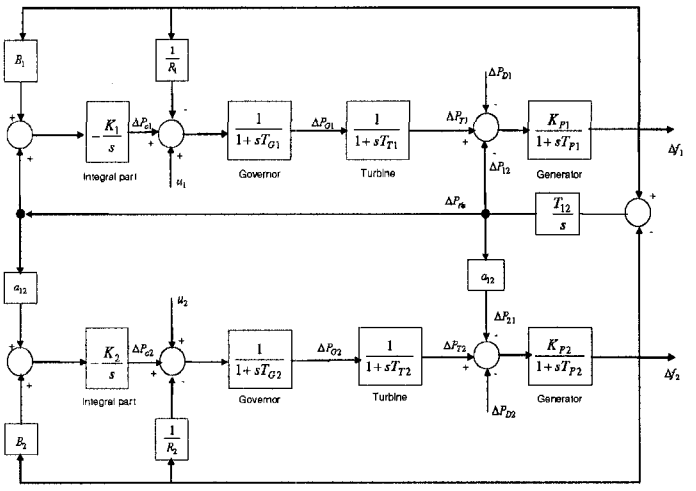

Figure 3.4: Two area power system [119].

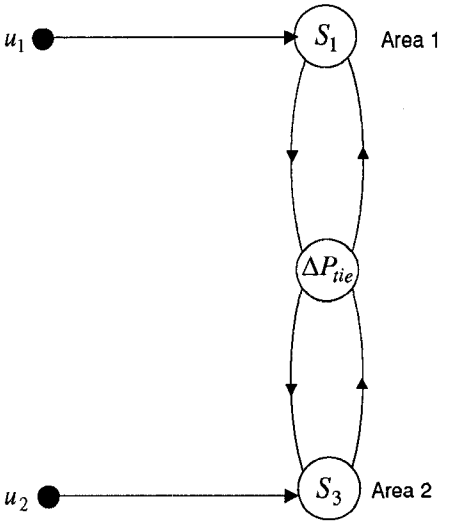

Figure 3.5: Overlapping scenario of the two area power system.

In Figs. 3.6-3.7, the frequency deviations in the two areas due to the disturbance of ΔP_{D1} = 0.01 pu in area 1 are shown (by dotted lines, without controller). This and the Nyquist array with the column Gershgorin circles (Fig. 3.8, first row) on g_{11} show that the system is highly interacting. Gershgorin circles for the first subsystem (g_{11} and g_{12}) only are drawn because the transfer functions of both subsystems are the same. The responses in Figs. 3.6-3.7 also show that local controllers should be designed to minimize the oscillations.

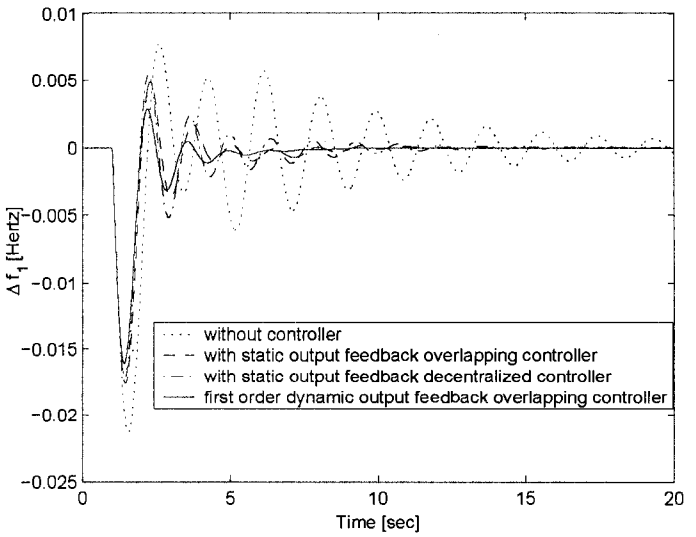

Figure 3.6: Frequency deviation of the first area with output feedback controllers.

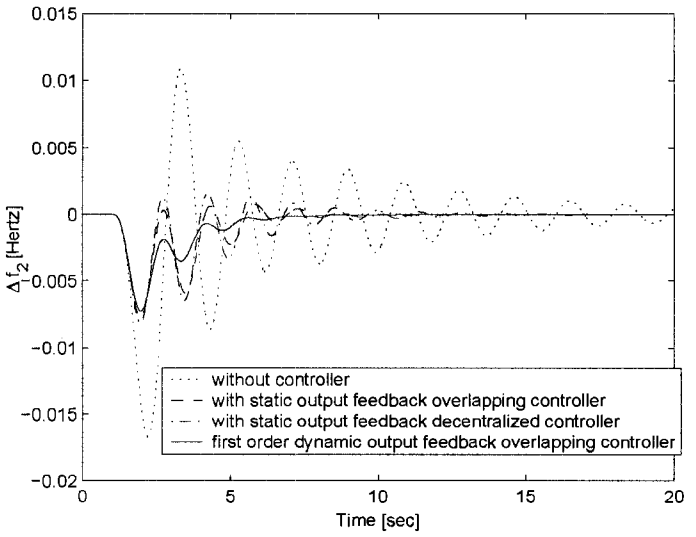

Figure 3.7: Frequency deviation of the second area with output feedback controllers.

By using the algorithm OC for a linear system in Section 3.3, output feedback (static and dynamic) decentralized and overlapping controllers are designed. They have the following

forms:

$$\begin{bmatrix} -0.4638 & 0 \\ 0 & -0.4638 \end{bmatrix}, \begin{bmatrix} -0.4098 & 0.2778 & 0 \\ 0 & -0.2778 & -0.4098 \end{bmatrix},$$
$$\begin{bmatrix} -5.1443 & 0 & 1.9535 & -2.8866 & 0 \\ 0 & -5.1443 & 0 & 2.8866 & 1.9535 \\ 1 & 0 & -0.7943 & 0.3099 & 0 \\ 0 & 1 & 0 & -0.3099 & -0.7943 \end{bmatrix}.$$

From Figs. 3.6-3.7, it can be seen that the controllers are capable of attenuating most of the oscillations. The performance of the first order dynamic controller is better than the static overlapping control law, which in turn shows a better response than static decentralized control. For performance assessment, an ITAE criteria is used [119]:

$$J_{fre} = \int_0^{20} t|\Delta f_1(t)|\mathrm{d}t.$$

Table 3.1 shows the values of J_{fre} for different controllers, which verifies that a dynamic overlapping controller is better. The control signals in Fig. 3.9 give some idea of economic issues. It is clear that it takes more effort to control the system and there are more transients with a static output feedback decentralized controller than with an overlapping controller. Hence, the overlapping control law may lead to less wear and tear of the control valve and requires less steam, which in turn reduces fuel consumption.

Table 3.1: J_{fre} values with static and first order dynamic overlapping controller.

no control	static decentralized	static overlapping	dynamic overlapping
28.3728	6.2166	4.3148	3.0808

The second row of Fig. 3.8 shows the Gershgorin circles of the closed loop system with a static output feedback decentralized controller. It is noticeable that some circles enclose the origin only at low frequencies, whereas at medium and high frequencies the system is diagonal dominant. With the first order dynamic output feedback decentralized controller in the third row of Fig. 3.8, the radii of circles at medium frequencies are very small compared to those in the second row. Hence, this controller is capable of minimizing the effects of interactions between different loops and has better performance. To overcome the oscillations completely, state feedback controllers for which all the local states are available for measurement are then designed. Responses with the static state feedback overlapping controller, decentralized controller, and the controller designed based on the two-step approach are shown in Figs. 3.10-3.11. The controllers are now capable of attenuating the oscillations completely. The response with the decentralized controller has some transients,

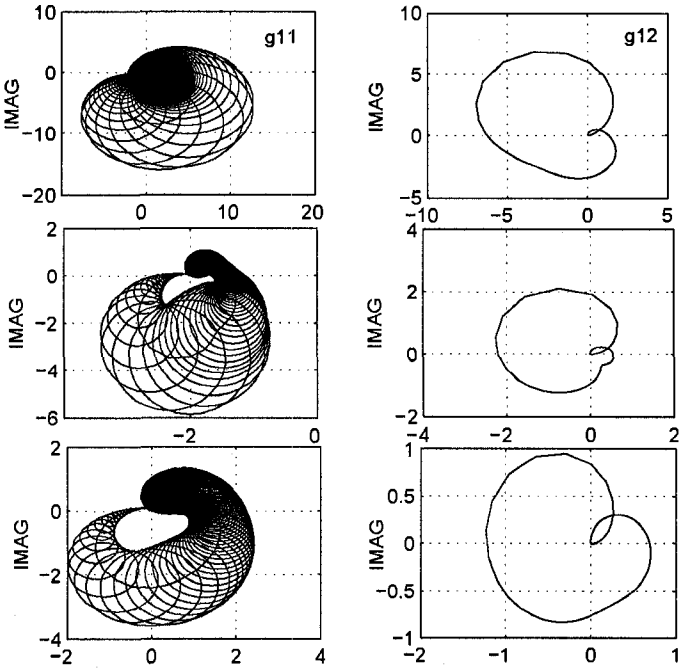

Figure 3.8: Nyquist array with column Gershgorin circles of the first area: without controller (first row), with static output feedback controller (second row), with dynamic output feedback controller (third row).

but with the overlapping controller the response is very smooth. It should be noted that using the two-step approach, the frequency deviations have less undershoot, but the response is slow. Extension of these results to multi-area power systems is straightforward.

3.5.2 Industrial Utility Boiler

Here, the work is concentrated on redesigning the control system of the utility boilers, whose job is to regulate the 900# header pressure and to maintain the drum water level and the steam temperature at their set points (1 m and 500°C, respectively). To this end, a nonlinear model of the utility boiler and the 900# header is first developed. Inputs to this system are feedwater flow rate, firing rate (output of which is then fanned out into fuel demand and air demand), and attemperator spray flow rate; the outputs are drum water level, header pressure, and steam temperature.

As shown in Fig. 3.12, application of Bernoulli's law gives:

$$x_2 = k_s\sqrt{y_{drum}^2 - y_{header}^2} = 30\sqrt{y_{drum}^2 - y_{header}^2}, \tag{3.20}$$

where x_2 is the steam flow rate (in kg/sec), and y_{header} and y_{drum} are header and drum

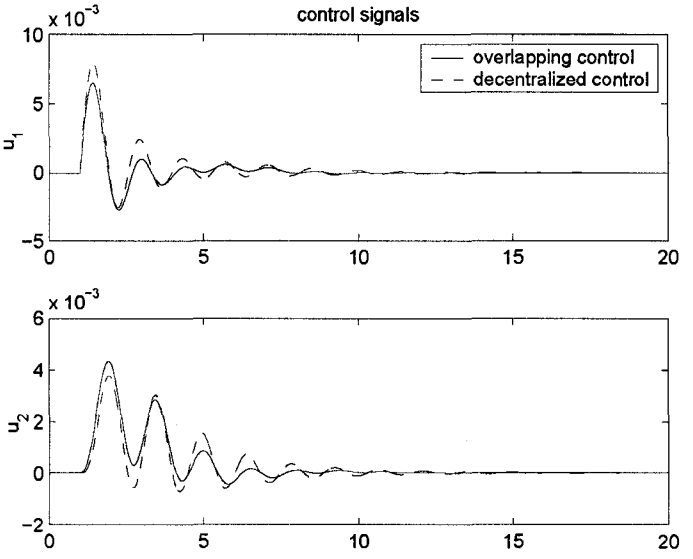

Figure 3.9: Control signals with static output feedback controllers.

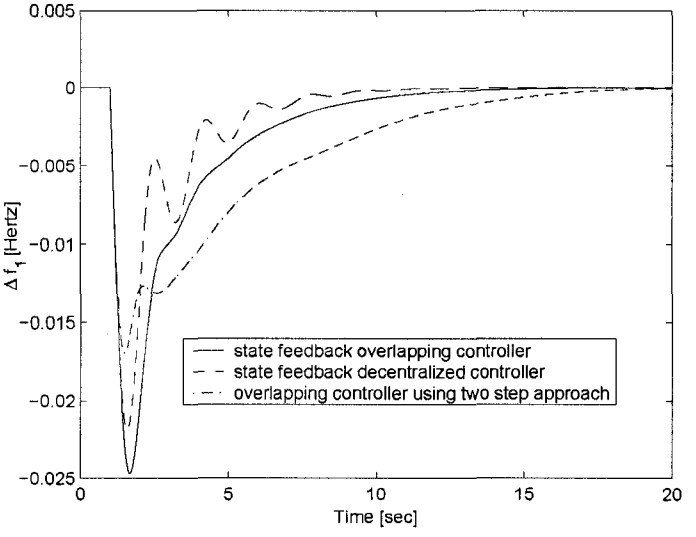

Figure 3.10: Frequency deviation of the first area with state feedback controllers.

pressures (in kPa), respectively. The master control block in Fig. 3.12 contains a complex logic (high/low select, rate limit, PI loops), therefore, at first, a linear model at normal operating point (using the MATLAB identification toolbox) was developed from the firing rate (u_2) to the fuel flow (x_5), which is governed by:

$$\dot{x}_5 = x_6 + 0.1758u_2, \quad \dot{x}_6 = -0.001833x_5 - 0.1731x_6 - 0.0177u_2.$$

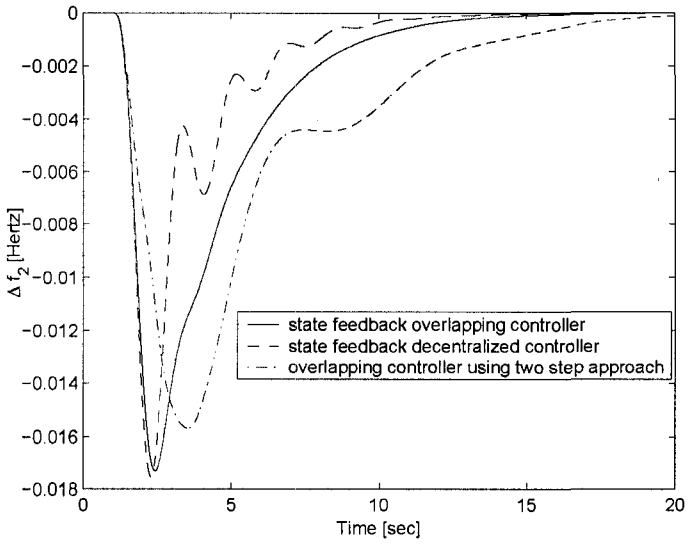

Figure 3.11: Frequency deviation of the second area with state feedback controllers.

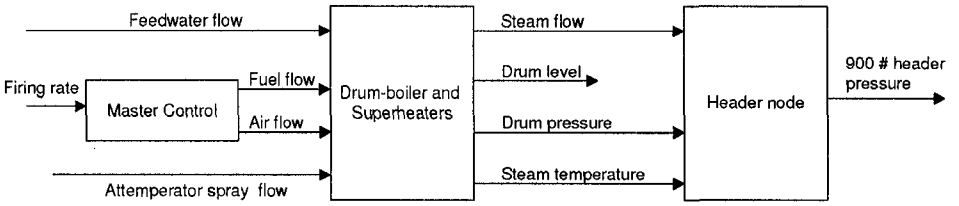

Figure 3.12: Modeling of the utility boiler and the header.

The air flow usually bears a constant relationship with the fuel flow, i.e., air flow=$18.8x_5$, hence, it is not separately identified. Similarly, the differential equation for the steam flow rate (x_2) is given by:

$$\begin{aligned}\dot{x}_2 &= x_3 + 0.009151u_1 + 0.02988x_5 + 0.2239u_3,\\ \dot{x}_3 &= -0.001864x_2 - 0.1533x_3 - 0.001987u_1 + 0.03634x_5 - 0.03288u_3,\end{aligned}$$

where u_1 represents the feedwater flow rate and u_3 is the attemperator spray flow rate (in kg/sec). The intermediate variables x_3 and x_6 affect the dynamics of the steam flow rate and the fuel flow rate, respectively. To model the drum water level, the physical relations

developed in [8–10, 71] were used:

$$\begin{aligned} \dot{x}_7 &= \frac{u_1 - x_2}{V_T} = \frac{u_1 - x_2}{155.1411}, \\ q_e &= \frac{1}{1+K}[k_b e_f + r u_1] + \frac{K}{1+K} x_2, \\ y_{level} &= \frac{1}{A_d}[v_w V_T x_7 + k_1 \alpha_r + T_s q_e]. \end{aligned}$$

Here, x_7 is the fluid density (mixture of steam and water in the system) and V_T is the total volume of the drum, the downcomers and the risers (=155.1411 m^3). The constant K is a measure of the change in mass of steam generated in the boiler per unit mass lost from the steam space, e_f is the energy flow rate (which depends linearly on the fuel flow x_5 and can be obtained from measured data), A_d is drum area, v_w is the specific volume of water, T_s is the increase in water volume per unit increase in evaporation rate, $k_b = \frac{1}{h_{fg}}$ and $r = \frac{h_w - h_f}{h_{fg}}$. Here, h_{fg} is the latent heat of evaporation, h_f is the enthalpy of saturated water, and h_w is the enthalpy of feedwater. After some calculations and substituting values from the steam table at a saturation pressure, the value of q_e is obtained. The expression for the quality of the steam (α_r) in the system, based on volume, is determined by curve fitting with the data from SYNSIM (which gives a relation in terms of x_2, x_5, u_1). Finally, after substituting the construction parameters and steam table data and making some adjustments, the model for the drum water level (deviation about mean) is given by:

$$\Delta y_{level} = 0.01028 x_7 + 0.0044963 x_2 + 0.035154 x_5 - 5.71107 u_{w1} - 7.2741,$$

where an additional feedthrough term $u_{w1} = 10^{-5} u_1$ is added to obtain a good match between the model and the process data.

Following the models of the pressure equation in [8–10] and incorporating some heuristic knowledge of boiler behavior (to accommodate the data from SYNSIM), the effect of the fuel flow rate (x_5) and the feedwater flow rate (u_1) on the drum pressure is formulated as:

$$\dot{x}_1 = -r_1 x_1 + (r_2 x_5 + r_5) c_v + r_3 x_5 - r_4 u_1, \tag{3.21}$$

where c_v is referred to as an imaginary control valve position from drum to header $\left(c_v = \sqrt{1 - \frac{y_{header}^2}{y_{drum}^2}} \right)$. It should be noted that (3.21) does not consider the effects of attemperator spray flow rate (u_3) on drum pressure. Therefore, an identification test was carried out that gives $\dot{x}_4 = -0.08 x_4 + 0.0006 u_3$. It is clear that $y_{drum} = x_1 + x_4$ and the steam flow out of the boiler drum is related to the drum pressure by $x_2 = 30 c_v y_{drum}$ (from (3.20)), which yields: $c_v = \frac{x_2}{30(x_1 + x_4)}$. The parameters r_1 to r_5 are obtained through a curve

fit to the data from SYNSIM and some specifications of the plant. Finally, the nonlinear differential equation for the drum pressure is governed by:

$$\begin{aligned}\dot{x}_1 &= -0.0157x_1 + \left[1.866\left\{\frac{10^{-4}x_2}{(x_1+x_4)}\right\} + 0.00157\right]x_5 - 0.0000395u_1 \\ &\quad -3.545\left\{\frac{10^{-4}x_2}{x_1+x_4}\right\} + 0.099333, \\ \dot{x}_4 &= -0.08x_4 + 0.0006u_3, \quad y_{drum} = x_1 + x_4. \end{aligned} \tag{3.22}$$

To obtain the parameters r_1 to r_5, symbolic linearization or nonlinear regression techniques can also be used. From (3.20) and (3.22), the 900# header pressure can be expressed as:

$$y_{header} = \sqrt{x_1^2 + x_4^2 + 2x_1x_4 - \frac{x_2^2}{900}}.$$

The overall nonlinear model and the fourth order linear model for steam temperature dynamics have shown good fit with the data from SYNSIM. This is shown in Figs. 3.13-3.16 and the fitness in other operating regions is also good. The model for the steam temperature dynamics is governed by:

$$\begin{aligned}\dot{x}_8 &= x_9 - 0.002324u_1 + 0.5772x_5 + 2.194u_3, \ \dot{x}_9 = x_{10} + 0.002323u_1 - \\ &\quad 0.08838x_5 - 1.859u_3, \ \dot{x}_{10} = x_{11} - 0.001799u_1 + 0.06898x_5 \\ &\quad +1.436u_3, \\ \dot{x}_{11} &= -(2.35)10^{-6}x_8 - 0.000531x_9 - 0.0346x_{10} - 0.8159x_{11} + 0.001391u_1 \\ &\quad -0.05352x_5 - 1.108u_3, \quad y_{steam} = x_8. \end{aligned}$$

Linearization of the overall model at the normal operating point has one pole at the origin (linked with water dynamics) and one RHP zero at 0.0619, which reveals nonminimum phase characteristics. Next, based on the algorithm of Section 3.3, the following stabilizing overlapping controllers were designed:

$$\mathbf{K}_{full} = \begin{bmatrix} \frac{-11.98s-12.92}{s+1.122} & \frac{5.318s+3.154}{s+1.122} & 0 \\ 0 & \frac{27.61s+33.76}{s+1.227} & \frac{-113.4s-139.2}{s+1.227} \\ 0 & 0 & \frac{-3.797s-6.5}{s+1.908} \end{bmatrix},$$

$$\mathbf{K}_{partial} = \begin{bmatrix} \frac{-11.97s-13.05}{s+1.134} & 0 & 0 \\ 0 & \frac{61.08s+74.81}{s+1.227} & \frac{-113.5s-139.3}{s+1.227} \\ 0 & 0 & \frac{-3.797s-6.506}{s+1.91} \end{bmatrix}.$$

In the first case (full overlapping), the feedwater controller uses the extra measurement of header pressure (in addition to drum level) and the firing rate controller utilizes the extra measurement of steam temperature (in addition to header pressure) to control the header pressure. In the second case (partial overlapping), only the firing rate controller shares the

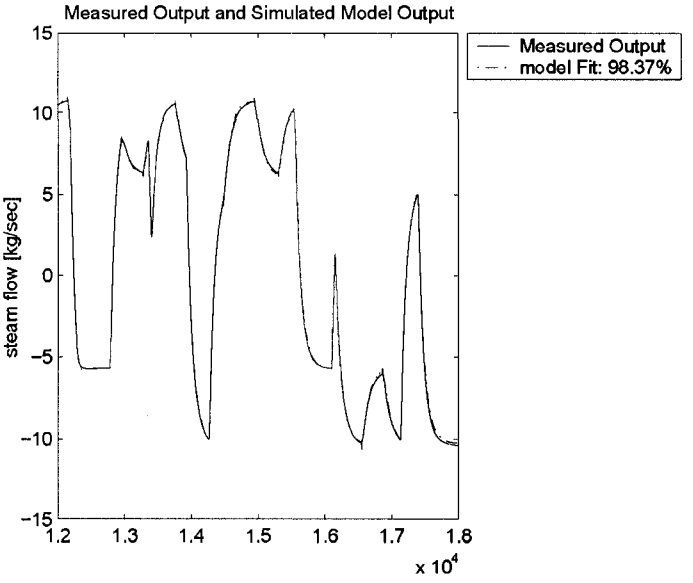

Figure 3.13: Validation of the steam flow.

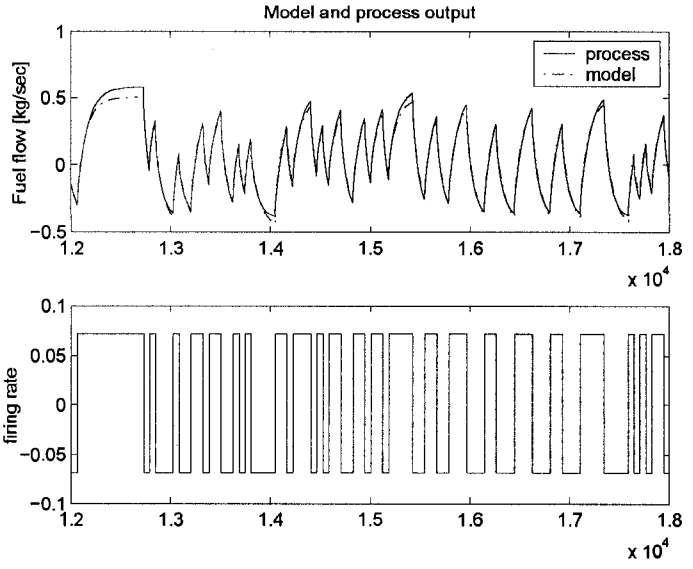

Figure 3.14: Validation of the firing rate.

measurement of steam temperature. The simulations were done under several perturbed conditions and the designed controllers were implemented in SYNSIM. These simulations took into account interactions from other subsystems, namely, CO boilers, OTSGs, tie lines, and turbine-generator units G1-G6 (Fig. 1.4). Fig. 3.17 shows the stabilizing effect of the

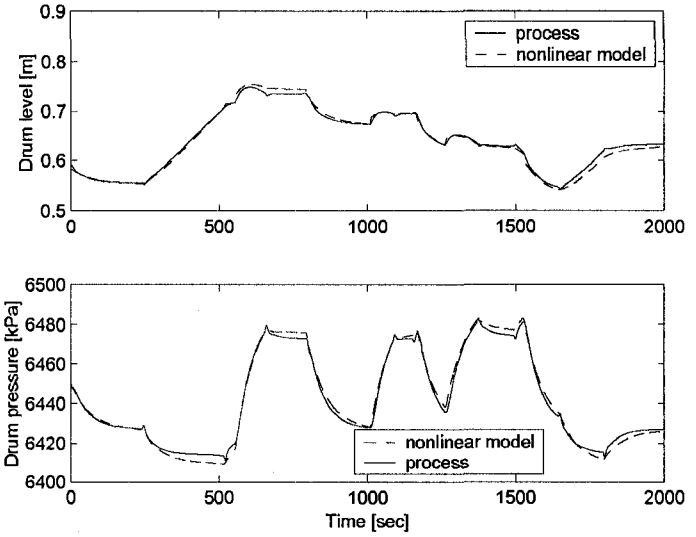

Figure 3.15: Fitness of the model.

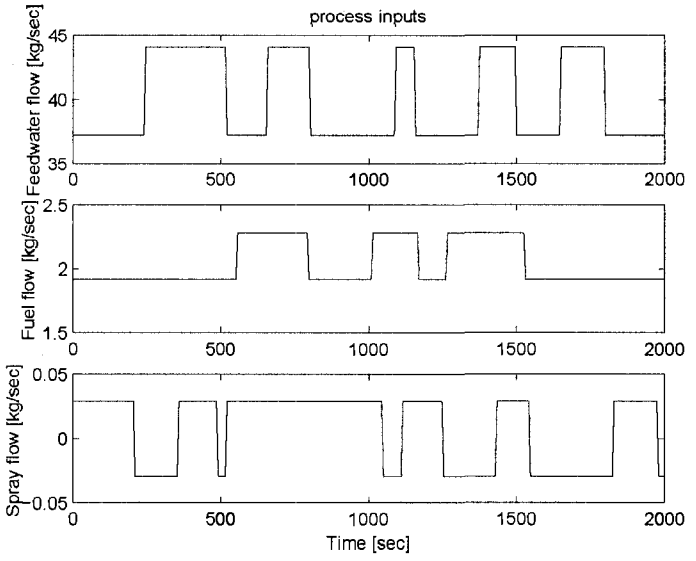

Figure 3.16: Inputs to the process.

overlapping controllers revealing good regulation under high load conditions. Figs. 3.18-3.19 show responses caused by a load change in the 50# (50 pound) header and Figs. 3.20-3.21 show responses of different process variables due to a load change of 30 kpph on the 900# header. In both cases, plots of total steam flow rate, 900# steam temperature, and 50# header pressure show non-oscillatory behavior. Responses with overlapping controllers are

better than those of the existing PI controllers and there is also suppression in amplitude. The improvement in the 50# header steam pressure shown in Fig. 3.20 could lead to an enhancement in power production, because the 50# header pressure is the back pressure of the turbines (G1, G2, and G4). There are slight deviations in drum level (1%) and header pressure (0.09% for partial overlapping) from steady state values due to lack of integrators in the overlapping controllers. However, response of the partial overlapping controller is within range (very less offset) and is acceptable in the present plant. Moreover, this limitation is compensated by improvement in the 900# header steam pressure, which shows no oscillations, the main concern in practice. Fig. 3.17 reveals the robustness of controllers, since they are designed at normal load conditions and are operated under high load conditions.

It is clear that the partial overlapping controller $\mathbf{K}_{partial}$, where only the firing rate controller is using the extra measurement of steam temperature, provides a better result than the full overlapping controller and the decentralized PI controllers of the plant. Since this controller is linear and of only third order, it is simple to implement. Intuitively, the performance of $\mathbf{K}_{full}$ should be better than $\mathbf{K}_{partial}$; however, it is sometime difficult to trace out the exact reason due to high nonlinearities and couplings in the simulation package (SYNSIM) where the controller is implemented. The result suggests that it is not proper to use the measurement of header pressure to control the drum level as it may lead to a negative impact in the response of different process variables.

3.6 Chapter Summary

Two different approaches to solving the overlapping control design problem are introduced. In the first case, an iterative algorithm is used to obtain the controller parameters. This method is applicable to a vast array of overlapping control problems including static state feedback, static output feedback, full order, and reduced order dynamic output feedback control designs. The method eliminates the necessity to choose parameters by trial and error and removes the structural constraint on the Lyapunov function. In the second case, a two-step approach is employed that requires no iteration. However, the first approach is found to be superior to the second in several aspects.

Simulation results in SYNSIM show that the performance of the designed controllers is good under different load conditions. Moreover, when only the firing rate controller (which controls header pressure) is utilizing the extra measurement of steam temperature, the performance of the closed loop system is better (no header oscillations, minimum

offset) than in the case of full overlapping. The presented algorithm can also capture other overlapping cases in addition to Type I and Type II.

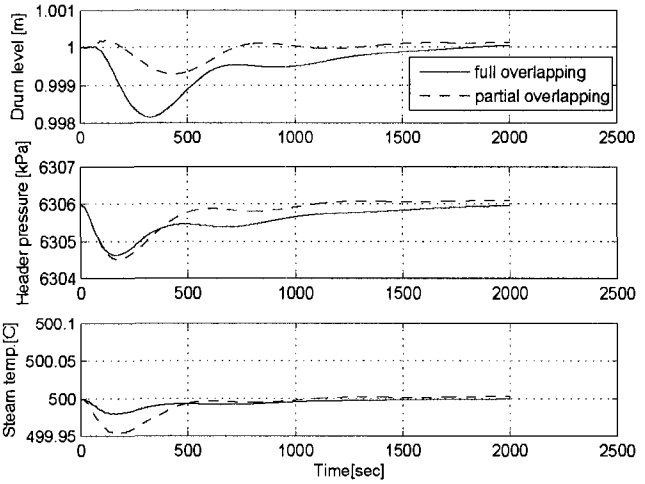

Figure 3.17: Performance of the overlapping controllers under high load conditions.

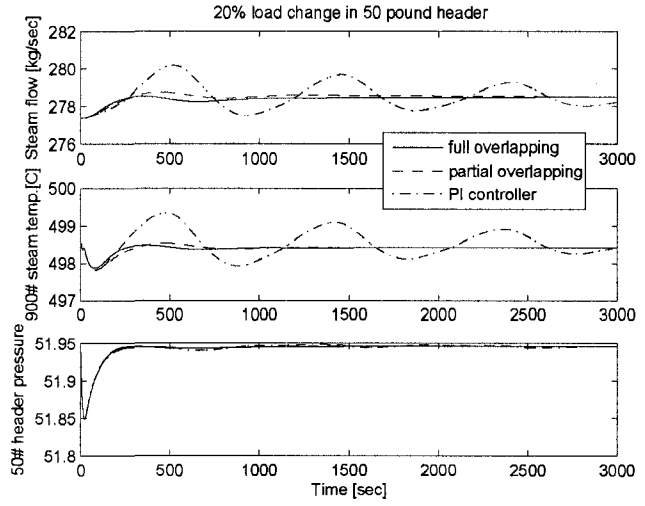

Figure 3.18: Sudden load change in the 50# header.

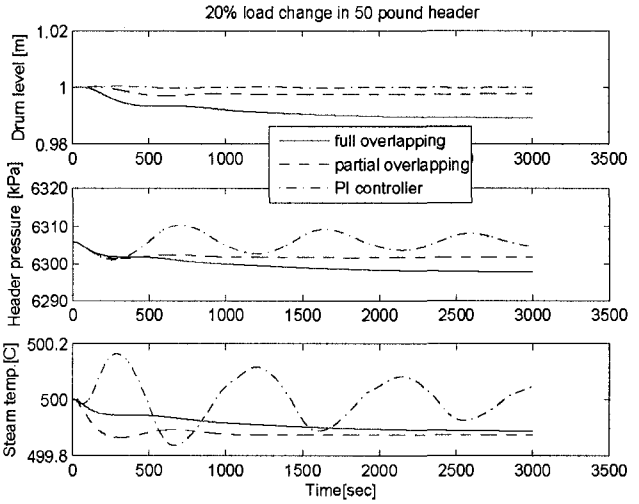

Figure 3.19: Responses during load change in the 50# header.

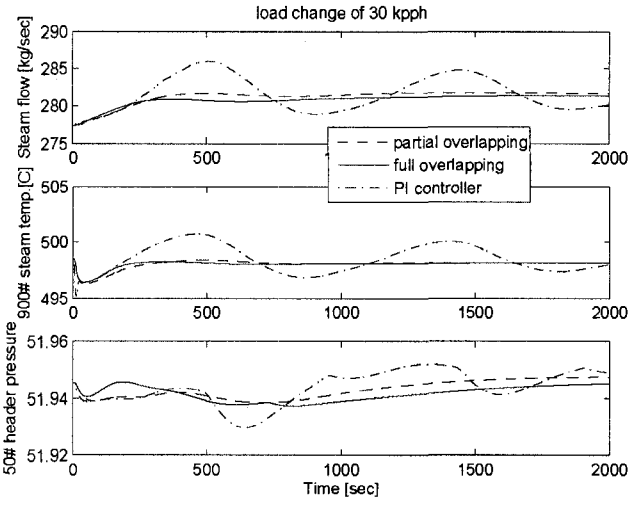

Figure 3.20: Stabilizing effect of the overlapping controllers.

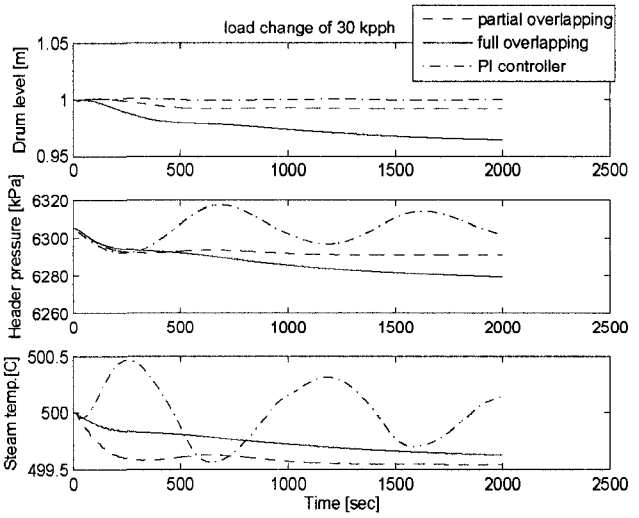

Figure 3.21: Header pressure response during sudden load change.

Chapter 4

Multiloop Control Synthesis Based on μ Interaction Measure

This chapter presents a new practical framework for multiloop controller design in which controllers are designed independently, i.e., a controller in one loop is designed without using information of other controllers. The method is based on the (block) diagonal approximation of a system. The focus of this work is on unstable plants and the approximated systems are obtained by minimizing an upper bound of a scaled $\mathcal{L}_\infty$ norm for the error systems. This extends the validity of the μ-interaction measure to a more general scenario. Numerical simulations are performed and the method is applied to an industrial boiler simulation package to show the advantage of the proposed approach.

4.1 Introduction

In this chapter, the work is focussed on control by independent designs. Though simpler than other design techniques, one practically important question may always attract the attention of many engineers: "How much is the performance loss of the overall CL system caused by *disregarding* the off-diagonal system blocks, and what should be the upper bound on the interactions such that overall closed loop stability can be maintained?" To answer these questions, a number of interaction measures are available in the literature, which points out different conditions under which the stability of (block) diagonal parts lead to stability of the overall closed loop system. They also help in tuning controllers, predicting closed-loop stability and quantifying the performance loss due to the use of different structures in controllers (decentralized, block decentralized, BBD) [36].

Among the different interaction measures available so far, namely, Rijnsdrop's

interaction measure [76], RGA [15], μ-interaction measure (μ-IM) [35, 36] and DNA [78], the μ-IM is noteworthy. This is because, it offers a dynamic measure of interactions, and is also applicable to high order systems. Due to its applicability to block pairings and other elegant properties, it has attracted the attention of many researchers in the field of decentralized control [35, 51, 52, 57, 63, 64, 89]. Based on μ-IM, the method proposed by [35] utilizes an independent design approach. Sufficient conditions are provided under which the controllers can maintain nominal stability of the overall closed loop system. This approach, however, suffers from the shortcoming that it requires that the system and its diagonal version to possess the same number of RHP poles. Since this criterion is not general, and in most of the cases cannot be satisfied, it restricts the approach to *only* open loop stable systems.

In spite of these restrictions, [89] generalized the results of [35] by providing sufficient conditions to guarantee robust performance of the overall CL system. Pairing rules for unstable plants, based on μ-IM are then introduced in [43] and their relationship with RGA and NI are explicated. In [57], phase stability conditions are presented which claimed to remove some conservativeness associated with the μ-IM (since it constrains only the magnitude of each SISO loop). An independent robust decentralized control design approach for unstable as well as non-square systems was carried out in [64] and [63], respectively. Several examples in chemical industry where this method can be of practical use are highlighted, e.g., in exothermic reactions there is a need of control strategy for retaining operation at unstable steady state [64]. Many other ideas also came into picture and subsequently improved, some were really interesting and innovative, but finding a (block) diagonal approximated system that possesses the same number of unstable poles as the system itself still remains an open question. In [50–52], a step towards solving this approximation problem for unstable systems was carried out. The method is interesting because it extended the validity of μ-IM to unstable systems and the outcome of numerical example given in the paper is also good. However, the algorithm bears some complexity and includes approximations, iterations in the frequency-wise approximation step as well as in the parametric identification step, which have no guarantee of convergence. This open problem, which remains almost unsolved during the last twenty years, constitutes the motivation of development in this chapter.

In this chapter, Smith-McMillan decompositions, properties of norms, congruence transformations and reciprocal variant of the projection lemma are utilized to provide an easily understandable and programmable approach of obtaining (block) diagonal

approximated systems. By using a constant scaling matrix ($\mathbf{D}_r$), the design algorithm is converted into an optimization problem, which can be directly solved by the available numerical software. There is no trial and error or approximations involved and, in some cases, the optimization problem involves LMIs and *only* one semidefinite constraint. This quasi-convex optimization can be readily solved using YALMIP [62], which is a parser, namely, the interface between different solvers (including LMILab) and MATLAB. An upper bound on the performance due to the decentralized architecture is derived and special attention is paid on the effect of non-minimum phase transmission zeros. It is well known that in multiloop control systems, because of the interactions between different loops, closing one loop propels the transmission zeros of other loops to move across the imaginary axis [15, 22]. This is possible even if the subsystems are minimum phase, and it reflects the restrictions imposed on the CL performance due to decentralized controllers [22]. They are responsible for sensitivity peak as well as bandwidth limitation of the resulting closed loop system. To overcome this problem, some conditions are developed, such that these zero crossings can be prevented.

The foregoing method is applied to a numerical example and to a simulated industrial utility boiler. Different cases are considered under which the failure tolerance of the remaining loops when a lower level loop fails is of interest (this is an important property of control by *independent* designs). Simulations in SYNSIM under different perturbed conditions reveal the advantage of the proposed scheme.

The rest of this chapter is aranged as follows. Section 4.3 deals with some background results and open problems in the independent control design approach. In Section 4.4, an algorithm for obtaining a (block) diagonal approximated system is first developed. This is followed by an independent design method for each controller based on a skewed-μ condition. Some discussions on the CL performance is done and, in Section 4.5, a sufficient condition is derived under which the zero crossings can be prevented. Section 4.6 provides a numerical example and the design strategy is applied to a steam generating unit. Finally, Section 4.7 summarizes this chapter.

4.2 Definitions and Instrumental Tools

1. Structured singular value (μ) [23, 50, 91]: Let $\mathbf{\Delta} = \{\text{diag}(\mathbf{\Delta}_i)\}$ represents complex matrices with a given structure, where some of the elements are repeated or may be

real. The structured singular value of a matrix $\mathbf{M}$ is defined by

$$\mu_{\mathbf{\Delta}}(\mathbf{M}) = \frac{1}{\min\{\bar{\sigma}(\mathbf{\Delta}) : \det(\mathbf{I} - \mathbf{M}\mathbf{\Delta}) = 0\}}.$$

If there does not exist a structured $\mathbf{\Delta}$, then $\mu_{\mathbf{\Delta}}(\mathbf{M}) = 0$. If some of the $\mathbf{\Delta}_i$'s are fixed and the interest is on finding one particular $\mathbf{\Delta}_i$ which can make $\det(\mathbf{I} - \mathbf{M}\mathbf{\Delta}) = 0$, then this value is represented as $1/\mu^s$, where μ^s is called skewed-μ. Hence, it can be viewed as a simplification of $\mu_{\mathbf{\Delta}}(\mathbf{M})$.

2. For matrices $\mathbf{M} \in \Re^{m\times n}$ and $\mathbf{N} \in \Re^{n\times m}$, $\det(\mathbf{I} + \mathbf{MN}) = \det(\mathbf{I} + \mathbf{NM})$.

3. For a partitioned matrix $\mathbf{M}$, with $\mathbf{M}_{22}$ square and nonsingular [91]

$$\det\left(\begin{bmatrix} \mathbf{M}_{11} & \mathbf{M}_{12} \\ \mathbf{M}_{21} & \mathbf{M}_{22} \end{bmatrix}\right) = \det(\mathbf{M}_{22}).\det(\mathbf{M}_{11} - \mathbf{M}_{12}\mathbf{M}_{22}^{-1}\mathbf{M}_{21}).$$

4. For stable transfer matrices $\mathbf{G}_1(s)$ and $\mathbf{G}_2(s)$ [91]

$$\|\mathbf{G}_1(s) + \mathbf{G}_2(s)\|_\infty \leq \|\mathbf{G}_1(s)\|_\infty + \|\mathbf{G}_2(s)\|_\infty.$$

4.3 Background

Consider an open loop system $\mathbf{G}(s)$, which is expressed as $\mathbf{G}(s) = (\mathbf{I} + \mathbf{E}(s))\tilde{\mathbf{G}}(s)$ (Fig. 4.1). Here, $\tilde{\mathbf{G}}(s)$ denotes the (block) diagonal parts of $\mathbf{G}(s)$, and it is assumed that the number of RHP poles of $\mathbf{G}(s)$ and $\tilde{\mathbf{G}}(s)$ are the same [35]. The term $\mathbf{E}(s) = (\mathbf{G}(s) - \tilde{\mathbf{G}}(s))\tilde{\mathbf{G}}^{-1}(s)$ represents the relative error and let the (block) diagonal controller $\mathbf{K}(s)$ is designed to stabilize the transfer matrix $\tilde{\mathbf{H}}(s)$, where $\tilde{\mathbf{H}}(s) = \tilde{\mathbf{G}}\mathbf{K}(s)(\mathbf{I} + \tilde{\mathbf{G}}\mathbf{K}(s))^{-1}$.

The following lemma reflects the condition under which the aforementioned designed $\mathbf{K}(s)$ also stabilize the unstable system $\mathbf{G}(s)$.

Lemma 4.1 [35]: Assume that $\tilde{\mathbf{H}}(s)$ is stable. With this assumption, the closed loop system $\mathbf{H}(s) = \mathbf{G}\mathbf{K}(s)(\mathbf{I} + \mathbf{G}\mathbf{K}(s))^{-1}$ is stable iff the following condition hold

$$N(0, \det(\mathbf{I} + \mathbf{E}\tilde{\mathbf{H}}(s))) = 0.$$

Here, $N(k, \mathbf{F}(s))$ is the net number of clockwise encirclements of the point $(k, 0)$ by the image of Nyquist D contour under $\mathbf{F}(s)$ [36, 50].

Based on this lemma, the following μ-IM condition was derived.

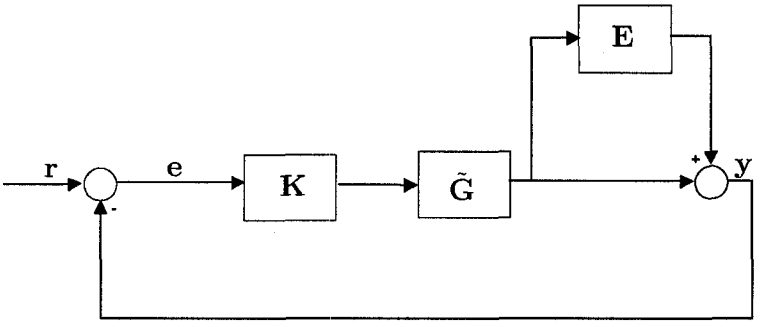

Figure 4.1: A general closed loop system.

Theorem 4.1 [35]: With the assumption of Lemma 4.1, $\mathbf{H}(s)$ is stable if

$$|\tilde{h}_i(j\omega)| < \mu^{-1}(\mathbf{E}(j\omega)), \ \forall\omega \tag{4.1}$$

where $\mu(.)$ is the structured singular value w.r.t the structure of $\tilde{\mathbf{H}}(s)$ [23], and $\tilde{h}_i(s)$ is the closed loop transfer matrix of each individual loop. For a triangular plant, this is a necessary and sufficient condition for stability.

Although the result is influential, the requirement that $\mathbf{G}(s)$ and $\tilde{\mathbf{G}}(s)$ possess the same number of RHP poles restrict its validity to only stable plants. The initiative to solve this problem was taken by [50–52], in which the μ-IM condition was expressed in terms of control sensitivity function.

Proposition 4.1 [50, 51]: Denote $\mathbf{G}(s)$ as $\mathbf{G}(s) = \tilde{\mathbf{G}}(s) + \mathbf{G}_I(s)$, where it is assumed that the number of RHP poles of $\tilde{\mathbf{G}}(s)$ and $\mathbf{G}(s)$ are the same. Then, the stabilizing decentralized controller $\mathbf{K}(s)$ of $\tilde{\mathbf{G}}(s)$ can also stabilize $\mathbf{G}(s)$ if

$$\bar{\sigma}(\mathbf{K}\tilde{\mathbf{S}}(j\omega)) < \mu^{-1}(\mathbf{G}_I(j\omega)), \ \forall\,\omega \in \mathbb{R} \tag{4.2}$$

where $\tilde{\mathbf{S}}(s) = (I + \tilde{\mathbf{G}}\mathbf{K}(s))^{-1}$ is the sensitivity function and $\mathbf{G}_I(s) = \mathbf{G}(s) - \tilde{\mathbf{G}}(s)$ represents the interactions.

Since $\mathbf{G}_I(s)$ is independent of $\mathbf{K}(s)$, the design proceeds to finding $\tilde{\mathbf{G}}(s)$ that has the same number of unstable poles as $\mathbf{G}(s)$, such that $\mu(\mathbf{G}_I(s))$ is minimized. Then, the controller was designed by using the relation in (4.2).

4.4 A Solution to (Block) Diagonal Approximation and Controller Design

In this section, an algorithm is developed, which finds (block) diagonal approximation $\tilde{\mathbf{G}}(s)$ by minimizing an upper bound of the following scaled $\mathcal{L}_\infty$-norm

$$\min_{\tilde{\mathbf{G}}(j\omega)} \bar{\sigma}[\mathbf{D}_r(\mathbf{G}(j\omega) - \tilde{\mathbf{G}}(j\omega))\mathbf{D}_r^{-1}], \ \forall \omega \in \mathbb{R} \tag{4.3}$$

where $\mathbf{D}_r$ is a constant scaling matrix.

4.4.1 (Block) Diagonal Approximation

Clearly, as $\mathbf{G}(s)$ contains both stable and unstable poles, achieving an optimal solution to this problem is a very difficult task. However, an acceptable solution can be obtained by proceeding in the following way:

1. Separate the stable and antistable part of $\mathbf{G}(s)$ by

$$\begin{aligned}\mathbf{G}(s) = \mathbf{G}_1(s) + \mathbf{G}_2(s) &= \mathbf{L}^{-1}(s)\,[\mathbf{G}^{sm}]_s\,\mathbf{R}^{-1}(s) + \\ &\quad \mathbf{L}^{-1}(s)\,[\mathbf{G}^{sm}]_{as}\,\mathbf{R}^{-1}(s),\end{aligned}$$

   where $\mathbf{G}^{sm}(s)$ is the Smith-McMillan form [91] of $\mathbf{G}(s)$, and $\mathbf{L}(s)$ and $\mathbf{R}(s)$ are unimodular matrices. $[\mathbf{G}^{sm}]_s$ and $[\mathbf{G}^{sm}]_{as}$ contain stable and unstable poles of $\mathbf{G}(s)$, respectively. Note that Smith McMillan decomposition is just one way to separate the stable and anti-stable part of $\mathbf{G}(s)$. One can use other methods, for example, *sdecomp* command in MATLAB decomposes a system matrix as the sum of stable and unstable systems. It utilizes Schur's decomposition and orthogonal-triangular decomposition for this operation. Another useful function is *stabsep*.

2. Now, $\mathbf{G}_2^T(-s)$, $\mathbf{G}_1(s) \in \mathcal{RH}_\infty$, and $\tilde{\mathbf{G}}(s)$ can be parameterized as $\tilde{\mathbf{G}}(s) = \tilde{\mathbf{G}}_1(s) + \tilde{\mathbf{G}}_2(s)$, which gives

$$\begin{aligned}\|\mathbf{D}_r[\mathbf{G}(s) - \tilde{\mathbf{G}}(s)]\mathbf{D}_r^{-1}\|_{\mathcal{L}_\infty} \ \leq \ &(\|\mathbf{D}_r[\mathbf{G}_1(s) - \tilde{\mathbf{G}}_1(s)]\mathbf{D}_r^{-1}\|_\infty) \\ &+(\|(\mathbf{D}_r^{-1})^T[\mathbf{G}_2^T(-s) - \tilde{\mathbf{G}}_2^T(-s)]\mathbf{D}_r^T\|_\infty),\end{aligned} \tag{4.4}$$

   since $\|\mathbf{D}_r[\mathbf{G}_2(s) - \tilde{\mathbf{G}}_2(s)]\mathbf{D}_r^{-1}\|_{\mathcal{L}_\infty} = \|(\mathbf{D}_r^{-1})^T[\mathbf{G}_2^T(-s) - \tilde{\mathbf{G}}_2^T(-s)]\mathbf{D}_r^T\|_\infty$ (Nehari extension problem [91]).

3. Solve the following optimization problem for decision variables γ, $\mathbf{X}_P$, $\mathbf{K}_d$, $\mathbf{M}$, $\mathbf{H}$ and $\mathbf{Q}$:

$$\min \ \gamma$$

$$\text{subject to } \mathbf{X}_P > 0, \tag{4.5}$$

$$\begin{bmatrix} -\mathbf{Q} & \mathbf{A}_{cl}^T + \mathbf{M}^T & 0 & \mathbf{C}_{cl,h}^T & \sqrt{2}\mathbf{X}_P & \mathbf{M}^T \\ \star & -\mathbf{I} & \mathbf{B}_{cl} & \mathbf{0} & \mathbf{0} & \mathbf{0} \\ \star & \star & -\gamma\mathbf{H} & \mathbf{D}_{cl,h}^T & \mathbf{0} & \mathbf{0} \\ \star & \star & \star & -\gamma\mathbf{H} & \mathbf{0} & \mathbf{0} \\ \star & \star & \star & \star & -\mathbf{I} & \mathbf{0} \\ \star & \star & \star & \star & \star & -\mathbf{I} \end{bmatrix} < 0, \tag{4.6}$$

$$\begin{bmatrix} -\gamma\mathbf{H} & \mathbf{D}_{cl,h}^T \\ \star & -\gamma\mathbf{H} \end{bmatrix} < 0, \begin{bmatrix} \mathbf{Q} & \mathbf{X}_P + \mathbf{M}^T \\ \star & \mathbf{I} \end{bmatrix} \geq 0, \tag{4.7}$$

where

$$\begin{aligned}
\mathbf{A}_{cl} &= \begin{bmatrix} \mathbf{A} & 0 \\ 0 & 0 \end{bmatrix} + \begin{bmatrix} 0 & 0 \\ \mathbf{I} & 0 \end{bmatrix} \begin{bmatrix} \mathbf{A}_d & \mathbf{B}_d \\ \mathbf{C}_d & \mathbf{D}_d \end{bmatrix} \begin{bmatrix} 0 & \mathbf{I} \\ 0 & 0 \end{bmatrix} = \mathbf{A}_0 + \bar{\mathbf{B}}\mathbf{K}_d\bar{\mathbf{C}}, \\
\mathbf{B}_{cl} &= \begin{bmatrix} \mathbf{B} \\ 0 \end{bmatrix} + \begin{bmatrix} 0 & 0 \\ \mathbf{I} & 0 \end{bmatrix} \begin{bmatrix} \mathbf{A}_d & \mathbf{B}_d \\ \mathbf{C}_d & \mathbf{D}_d \end{bmatrix} \begin{bmatrix} 0 \\ \mathbf{I} \end{bmatrix} = \mathbf{B}_0 + \bar{\mathbf{B}}\mathbf{K}_d\bar{\mathbf{D}}_{21}, \\
\mathbf{C}_{cl} &= \begin{bmatrix} \mathbf{C} & 0 \end{bmatrix} + \begin{bmatrix} 0 & -\mathbf{I} \end{bmatrix} \begin{bmatrix} \mathbf{A}_d & \mathbf{B}_d \\ \mathbf{C}_d & \mathbf{D}_d \end{bmatrix} \begin{bmatrix} 0 & \mathbf{I} \\ 0 & 0 \end{bmatrix} = \mathbf{C}_0 + \bar{\mathbf{D}}_{12}\mathbf{K}_d\bar{\mathbf{C}}, \\
\mathbf{D}_{cl} &= \mathbf{D} + \begin{bmatrix} 0 & -\mathbf{I} \end{bmatrix} \begin{bmatrix} \mathbf{A}_d & \mathbf{B}_d \\ \mathbf{C}_d & \mathbf{D}_d \end{bmatrix} \begin{bmatrix} 0 \\ \mathbf{I} \end{bmatrix} = \mathbf{D} + \bar{\mathbf{D}}_{12}\mathbf{K}_d\bar{\mathbf{D}}_{21}, \\
\mathbf{C}_{cl,h}^T &= \mathbf{C}_{cl}^T\mathbf{H}, \ \mathbf{D}_{cl,h}^T = \mathbf{D}_{cl}^T\mathbf{H}, \ \mathbf{H} = \mathbf{D}_r^T\mathbf{D}_r.
\end{aligned}$$

Here, $(\mathbf{A}, \mathbf{B}, \mathbf{C}, \mathbf{D})$ is a minimal state space realization of $\mathbf{G}_1(s)$ and $(\mathbf{A}_d, \mathbf{B}_d, \mathbf{C}_d, \mathbf{D}_d)$ is the state space realization of $\tilde{\mathbf{G}}_1(s)$. This optimization problem, which minimizes the scaled $\mathcal{H}_\infty$ norm of the error system should also be solved to obtain structured $\tilde{\mathbf{G}}_2^T(-s)$ from $\mathbf{G}_2^T(-s)$ (except that $\mathbf{H}$ is now $\mathbf{H} = \mathbf{D}_{r_{inv}}^T\mathbf{D}_{r_{inv}}$, where $\mathbf{D}_{r_{inv}} = (\mathbf{D}_r^{-1})^T$).

Proof: Please see Appendix A.

Compared to (A-30), $\mathbf{A}_{cl}$ and $\mathbf{B}_{cl}$ are now completely decoupled from the Lyapunov matrix $\mathbf{P}$. Hence, the terms are now affine in the design parameters $(\mathbf{A}_d, \mathbf{B}_d, \mathbf{C}_d, \mathbf{D}_d)$ and can be easily computed. However, in (4.6) and (4.7) there is one bilinear term $\gamma\mathbf{H}$. Therefore, by fixing γ to a small value or by selecting $\mathbf{D}_r$ equal to identity matrix (which works in many practical problems), the conditions are LMIs with only one semidefinite constraint (A-38). Since $\mathbf{Q} = (\mathbf{X}_P + \mathbf{M})^T(\mathbf{X}_P + \mathbf{M})$ represents the boundary of convex sets in (A-38), the solution of the optimization problem in (4.5), (4.6) and (4.7) using the parser YALMIP or the CCL approach [27] always yields $\mathbf{Q} = (\mathbf{X}_P + \mathbf{M})^T(\mathbf{X}_P + \mathbf{M})$.

Remark 4.1 It should be noted that the triangular inequality in (4.4) has introduced some conservativeness in the design algorithm. The total number of decision variables in the (block) diagonal approximation algorithm is $n \times (2n+1) + n \times (2n+1) + 2n \times 2n + p \times n + (n+p) \times (n+m) = n \times (9n + m + p + 2) + 2p \times m$, where n is the order, m is the number of inputs and p is the number of outputs of $\mathbf{G}(s)$.

4.4.2 Controller Design

Here, an algorithm of designing $\mathbf{K}(s)$ is presented, which satisfies the μ-IM condition [35, 36].

The closed loop system $\mathbf{H}(s)$ is stable (all loops are closed) if

$$\bar{\sigma}\left(\frac{1}{c_H}\tilde{\mathbf{H}}(j\omega)\right) \leq 1, \ \forall \omega \in \mathbb{R}. \tag{4.8}$$

where at each frequency c_H solves

$$\mu_{\hat{\mathbf{\Delta}}}\begin{bmatrix} 0 & (\mathbf{G}(j\omega) - \tilde{\mathbf{G}}(j\omega))\tilde{\mathbf{G}}^{-1}(j\omega) \\ c_H\mathbf{I} & 0 \end{bmatrix} = 1. \tag{4.9}$$

Here, μ is computed w.r.t the structure $\hat{\mathbf{\Delta}} = \text{diag}(\tilde{\mathbf{H}}(j\omega), \tilde{\mathbf{H}}(j\omega))$. It should be noted that (4.8) and (4.9) can be easily derived by using the μ-IM condition and properties of singular values in [89, 91] (see Theorem 1 of [89]). The advantage is that it is easy to program. One can calculate c_H from (4.9) and design the controller for each loop independently using (4.8). The only shortcoming is that c_H provides equal partiality to all loops, however, if some roll offs in $\tilde{h}_i(s)$ is not required then they can be overcome by incorporating some weighting matrix $\mathbf{W}(s)$ whose structure coincides with the structure of $\tilde{\mathbf{H}}(s)$.

Remark 4.2 It is interesting to note that condition (4.9) is equivalent to

$$\det\left(\mathbf{I} - \begin{bmatrix} 0 & (\mathbf{G}(j\omega) - \tilde{\mathbf{G}}(j\omega))\tilde{\mathbf{G}}^{-1}(j\omega) \\ c_H\mathbf{I} & 0 \end{bmatrix}\begin{bmatrix} \mathbf{\Delta}_1 & 0 \\ 0 & \mathbf{\Delta}_2 \end{bmatrix}\right) = 0,$$

which can be written as $\det[\mathbf{I} - (\mathbf{G}(j\omega) - \tilde{\mathbf{G}}(j\omega))\tilde{\mathbf{G}}^{-1}\mathbf{\Delta}_2(j\omega) \times c_H\mathbf{\Delta}_1(j\omega)] = 0$. Therefore, if the interactions are large at low frequencies, namely, $\mu[(\mathbf{G}(j\omega) - \tilde{\mathbf{G}}(j\omega))\tilde{\mathbf{G}}^{-1}(j\omega)]$, then c_H has to be small to satisfy this condition. This can lead to a poor performance, because $\tilde{\mathbf{H}}(j\omega)$ in (4.8) has to be small to satisfy the nominal stability condition. Using the inequality [91]

$$\mu_{\text{diag }(\mathbf{\Delta}_1,\mathbf{\Delta}_2)}\begin{bmatrix} \mathbf{N}_{11} & \mathbf{N}_{12} \\ \mathbf{N}_{21} & \mathbf{N}_{22} \end{bmatrix} \geq \max[\mu_{\mathbf{\Delta}_1}(\mathbf{N}_{11}), \mu_{\mathbf{\Delta}_2}(\mathbf{N}_{22})], \tag{4.10}$$

it can be interpreted that it is possible to satisfy the condition in (4.9) at all frequencies by appropriate choice of $c_H > 0$.

The following proposition reveals that the condition in (4.1) (which is equivalent to (4.2)) leads to minimization of an upper bound of the CL performance. Similar condition in terms of control sensitivity function was also derived in [50, 51].

Proposition 4.2 Under the assumption that $\mathbf{G}(s)$ and $\tilde{\mathbf{G}}(s)$ have the same number of RHP poles and (4.1) holds

$$\bar{\sigma}(\mathbf{H}(j\omega)) \leq \frac{\kappa(\mathbf{D}(\omega))\,\bar{\sigma}(\mathbf{G}\tilde{\mathbf{G}}^{-1}(j\omega))}{\bar{\sigma}^{-1}(\tilde{\mathbf{H}}(j\omega)) - \mu(\mathbf{E}(j\omega))}, \forall \omega \in \mathbb{R}$$

where $\kappa(\mathbf{D}(\omega))$ is the Euclidean condition number, $\mathbf{D}(\omega)$ is the frequency dependent scaling matrix, and $\mathbf{E}(j\omega) = (\mathbf{G}(j\omega) - \tilde{\mathbf{G}}(j\omega))\tilde{\mathbf{G}}^{-1}(j\omega)$ is the relative error.

Proof: It is clear that

$$\begin{aligned}(\mathbf{I} + \mathbf{GK}(s))\mathbf{K}^{-1}(s)\tilde{\mathbf{G}}^{-1}(s) &= (\mathbf{I} + \tilde{\mathbf{G}}\mathbf{K}(s))\mathbf{K}^{-1}(s)\tilde{\mathbf{G}}^{-1}(s) + (\mathbf{G}(s) - \tilde{\mathbf{G}}(s)) \\ &\quad \times \tilde{\mathbf{G}}^{-1}(s) = \tilde{\mathbf{S}}^{-1}(s)\mathbf{K}^{-1}(s)\tilde{\mathbf{G}}^{-1}(s) + \mathbf{E}(s),\end{aligned}$$

where $\tilde{\mathbf{S}}(s) = (\mathbf{I} + \tilde{\mathbf{G}}\mathbf{K}(s))^{-1}$ is the sensitivity function of the approximated system $\tilde{\mathbf{G}}(s)$. Pre- and post- multiplying by $\mathbf{D}(\omega)$ and $\mathbf{D}^{-1}(\omega)$, respectively and using the properties of the singular values [50, 91]

$$\begin{aligned}\underline{\sigma}\left(\mathbf{D}(\omega)\mathbf{S}^{-1}\mathbf{K}^{-1}\tilde{\mathbf{G}}^{-1}(j\omega)\mathbf{D}^{-1}(\omega)\right) &\geq \underline{\sigma}(\mathbf{D}(\omega)\tilde{\mathbf{H}}^{-1}(j\omega)\mathbf{D}^{-1}(\omega)) - \\ &\quad \overline{\sigma}\left(\mathbf{D}(\omega)\mathbf{E}(j\omega)\mathbf{D}^{-1}(\omega)\right), \qquad (4.11)\end{aligned}$$

where $\mathbf{S}(s) = (\mathbf{I} + \mathbf{GK}(s))^{-1}$ is the sensitivity function of the overall closed loop system and $\tilde{\mathbf{H}}^{-1}(j\omega) = \tilde{\mathbf{S}}^{-1}\mathbf{K}^{-1}\tilde{\mathbf{G}}^{-1}(j\omega)$. Now,

$$\begin{aligned}\mathbf{D}(\omega)\mathbf{S}^{-1}\mathbf{K}^{-1}\tilde{\mathbf{G}}^{-1}(j\omega)\mathbf{D}^{-1}(\omega) &= \mathbf{D}(\omega)\mathbf{S}^{-1}\mathbf{K}^{-1}\mathbf{G}^{-1}\mathbf{G}\tilde{\mathbf{G}}^{-1}(j\omega)\mathbf{D}^{-1}(\omega) \\ &= \mathbf{D}\mathbf{H}^{-1}(j\omega)(\mathbf{I} + \mathbf{E}(j\omega))\mathbf{D}^{-1}(\omega),\end{aligned}$$

where $\mathbf{H}(s)$ is the closed loop transfer matrix and

$$\begin{aligned}\underline{\sigma}[\mathbf{D}(\omega)\mathbf{H}^{-1}(j\omega)(\mathbf{I} + \mathbf{E}(j\omega))\mathbf{D}^{-1}(\omega)] &\leq \overline{\sigma}(\mathbf{D}(\omega))\underline{\sigma}[\mathbf{H}^{-1}(j\omega)(\mathbf{I} + \mathbf{E}(j\omega))\mathbf{D}^{-1}(\omega)] \\ &\leq \overline{\sigma}(\mathbf{D}(\omega))\underline{\sigma}(\mathbf{H}^{-1}(j\omega))\overline{\sigma}(\mathbf{I} + \mathbf{E}(j\omega)) \\ &\quad \times \overline{\sigma}(\mathbf{D}^{-1}(\omega)) \\ &= \kappa(\mathbf{D}(\omega))\overline{\sigma}(\mathbf{I} + \mathbf{E}(j\omega))\underline{\sigma}(\mathbf{H}^{-1}(j\omega)). \qquad (4.12)\end{aligned}$$

Here, $\kappa(\mathbf{D}(\omega)) = \overline{\sigma}(\mathbf{D}(\omega))\overline{\sigma}(\mathbf{D}^{-1}(\omega))$ is the Euclidean condition number. Since, $\mathbf{D}(\omega)\tilde{\mathbf{H}}^{-1}(j\omega)\mathbf{D}^{-1}(\omega) = \tilde{\mathbf{H}}^{-1}(j\omega)$, and suppose that $\mathbf{D}(\omega)$ is selected to minimize $\overline{\sigma}\left(\mathbf{D}(\omega)\mathbf{E}(j\omega)\mathbf{D}^{-1}(j\omega)\right)$, then from (4.11) and (4.12)

$$\kappa(\mathbf{D}(\omega))\overline{\sigma}(\mathbf{I} + \mathbf{E}(j\omega))\underline{\sigma}(\mathbf{H}^{-1}(j\omega)) \geq \underline{\sigma}(\tilde{\mathbf{H}}^{-1}(j\omega)) - \mu(\mathbf{E}),$$

$$\text{which gives, } \overline{\sigma}(\mathbf{H}(j\omega)) \leq \frac{\kappa(\mathbf{D}(\omega))\overline{\sigma}(\mathbf{I}+\mathbf{E}(j\omega))}{\overline{\sigma}^{-1}(\tilde{\mathbf{H}}(j\omega)) - \mu(\mathbf{E}(j\omega))}.$$

■

Hence, stabilization of the closed loop system satisfying (4.8) and (4.9) leads to minimization of an upper bound (loose) of the CL performance. The inequality also reflects the robustness of the system against output multiplicative uncertainty.

4.5 Performance Limitations due to RHP Zero Crossings

In the following, a method of multiloop controller design is presented, which can prevent the movement of the zeros of open loop subsystems across the imaginary axis (when some other loops are closed). The main concern is to find an upper bound for the interactions, such that zero crossings can be prevented. For sake of brevity, a stable open loop system is considered.

Theorem 4.2 Assume that $\mathbf{G}(s)$ is divided into two blocks and the subsystems $\mathbf{G}_{11}(s)$ and $\mathbf{G}_{22}(s)$ are minimum phase. When the first loop is closed with a (block) decentralized controller $\mathbf{K}_1(s)$, such that $\tilde{\mathbf{H}}_1(s) = \mathbf{G}_{11}\mathbf{K}_1(s)(\mathbf{I}+\mathbf{G}_{11}\mathbf{K}_1(s))^{-1}$ is stable, then the transmission zeros of the other subsystem will not cross the imaginary axis, if

$$\bar{\sigma}(\tilde{\mathbf{H}}_1(j\omega)) < \mu^{-1}\left[\mathbf{G}_{12}\mathbf{G}_{22}^{-1}\mathbf{G}_{21}\mathbf{G}_{11}^{-1}(j\omega)\right],\ \forall\omega\in\mathbb{R}$$

Proof: Consider the following system

$$\mathbf{y}_1 = \mathbf{G}_{11}(s)\mathbf{u}_1 + \mathbf{G}_{12}(s)\mathbf{u}_2,\ \mathbf{y}_2 = \mathbf{G}_{21}(s)\mathbf{u}_1 + \mathbf{G}_{22}(s)\mathbf{u}_2.$$

When a negative feedback $\mathbf{u}_1 = -\mathbf{K}_1(s)\mathbf{y}_1$ is introduced around the first subsystem $\mathbf{G}_{11}(s)$, then the other subsystem $\hat{\mathbf{G}}_{22}(s)$ is represented by $\hat{\mathbf{G}}_{22}(s) = \mathbf{G}_{22}(s) - \mathbf{G}_{21}(s)(\mathbf{I}+\mathbf{G}_{11}\mathbf{K}_1(s))^{-1}\mathbf{K}_1\mathbf{G}_{12}(s) = \mathbf{G}_{22}(s)\left[\mathbf{I}-\mathbf{G}_{22}^{-1}\mathbf{G}_{21}(s)(\mathbf{I}+\mathbf{G}_{11}\mathbf{K}_1(s))^{-1}\mathbf{K}_1\mathbf{G}_{12}(s)\right]$. Now,

$$\begin{aligned}
\det(\hat{\mathbf{G}}_{22}(s)) &= \det(\mathbf{G}_{22}(s))\det\left[\mathbf{I}-\mathbf{G}_{22}^{-1}\mathbf{G}_{21}\mathbf{G}_{11}^{-1}\mathbf{G}_{11}(s)\mathbf{K}_1(s)\right.\\
&\quad \left.\times(\mathbf{I}+\mathbf{G}_{11}\mathbf{K}_1(s))^{-1}\mathbf{G}_{12}(s)\right]\\
&= \det(\mathbf{G}_{22}(s))\det\left[\mathbf{I}-\mathbf{G}_{22}^{-1}\mathbf{G}_{21}\mathbf{G}_{11}^{-1}\tilde{\mathbf{H}}_1\mathbf{G}_{12}(s)\right]\\
&= \det(\mathbf{G}_{22}(s))\det\left[\mathbf{I}-\tilde{\mathbf{H}}_1\mathbf{G}_{12}\mathbf{G}_{22}^{-1}\mathbf{G}_{21}\mathbf{G}_{11}^{-1}(s)\right].
\end{aligned}$$

Therefore, if the overall system is stable, then the zeros of the second subsystem will not cross the imaginary axis if and only if the nyquist plot of $\det\left[\mathbf{I}-\tilde{\mathbf{H}}_1\mathbf{G}_{12}\mathbf{G}_{22}^{-1}\mathbf{G}_{21}\mathbf{G}_{11}^{-1}(j\omega)\right]$, $\forall\omega \in \mathbb{R}$ does not encircle the origin. Using the spectral radius stability condition [91], the zero crossing can be prevented if $\rho\left[\tilde{\mathbf{H}}_1\mathbf{G}_{12}\mathbf{G}_{22}^{-1}\mathbf{G}_{21}\mathbf{G}_{11}^{-1}(j\omega)\right] < 1, \forall\,\omega \in \mathbb{R}$. Since, $\tilde{\mathbf{H}}_1(j\omega)$ has a structure and $\rho[\tilde{\mathbf{H}}_1\mathbf{G}_{12}\mathbf{G}_{22}^{-1}\mathbf{G}_{21}\mathbf{G}_{11}^{-1}(j\omega)] \leq \mu[\tilde{\mathbf{H}}_1\mathbf{G}_{12}\mathbf{G}_{22}^{-1}\mathbf{G}_{21}\mathbf{G}_{11}^{-1}(j\omega)]$, $\forall\omega \in \mathbb{R}$, the sufficient condition is given by

$$\bar{\sigma}(\tilde{\mathbf{H}}_1(j\omega)) < \mu^{-1}\left[\mathbf{G}_{12}\mathbf{G}_{22}^{-1}\mathbf{G}_{21}\mathbf{G}_{11}^{-1}(j\omega)\right],\ \forall\omega\in\mathbb{R}. \tag{4.13}$$

This derivation utilizes the fact that $\mu_{\mathbf{\Delta}}(\mathbf{AB}) \leq \mu_{\mathbf{\Delta}}(\mathbf{A})\bar{\sigma}(\mathbf{B})$ and μ is computed w.r.t the structure of $\tilde{\mathbf{H}}_1(j\omega)$.

■

Remark 4.3 For a 2×2 system with scalar loops, Theorem 4.2 boils down to $\bar{\sigma}(\tilde{h}_1(j\omega)) < \mu^{-2}(\mathbf{E}(j\omega)),\ \forall\omega\in\mathbb{R}$. In general, for controllers designed independently

$$\bar{\sigma}(\tilde{\mathbf{H}}_1(j\omega)) < \min\left(\mu^{-1}(\mathbf{E}(j\omega)), \mu^{-1}\left[\mathbf{G}_{12}\mathbf{G}_{22}^{-1}\mathbf{G}_{21}\mathbf{G}_{11}^{-1}(j\omega)\right]\right), \tag{4.14}$$

$$\text{and } \bar{\sigma}(\tilde{\mathbf{H}}_2(j\omega)) < \mu^{-1}(\mathbf{E}(j\omega)), \forall\omega\in\mathbb{R} \tag{4.15}$$

guarantee overall closed loop stability and also prevent the movement of transmission zeros in $\mathbf{G}_{22}(s)$ across the imaginary axis, when the first loop is closed. This has an important impact on the CL system performance. For scalar loops, (4.14) can be represented by $\bar{\sigma}(\tilde{h}_1(j\omega)) < \min\left[\mu^{-1}(\mathbf{E}(j\omega)), \mu^{-2}(\mathbf{E}(j\omega))\right],\ \forall\,\omega$. If interactions are large, then designing controller based on (4.14) and (4.15) leads to performance loss in the low frequency region of the first channel. This is because, $\bar{\sigma}(\tilde{\mathbf{H}}_1(j\omega))$ has to be reduced at low frequencies ($\mu^{-1}\left[\mathbf{G}_{12}\mathbf{G}_{22}^{-1}\mathbf{G}_{21}\mathbf{G}_{11}^{-1}(j\omega)\right] < \mu^{-1}(\mathbf{E}(j\omega)) < 1$). For systems with integral action in all channels, the upper bound of the interaction is given by

$$\max\left(\mu(\mathbf{E}(0)),\ \mu\left[\mathbf{G}_{12}\mathbf{G}_{22}^{-1}\mathbf{G}_{21}\mathbf{G}_{11}^{-1}(0)\right]\right) < 1, \tag{4.16}$$

since $\tilde{\mathbf{H}}_1(0) = \tilde{\mathbf{H}}_2(0) = \mathbf{I}$. This result also gives some idea of pairing, because the loops should atleast be paired in such a way that $\mu(\mathbf{E}(0)) < 1$ is satisfied for closed loop stability. Since this condition depends on the steady state gain information, it can be easily verified by some experiments. Moreover, it is also a sufficient condition for decentralized integral controllability (closed loop stability can be maintained when the loops are detuned arbitrarily) [124]. For loops that have no integral action, the designer should keep in mind

that $\bar{\sigma}(\tilde{\mathbf{T}}) \approx 1$ at low frequencies, ≥ 1 in the bandwidth region and ≤ 1 at high frequencies. Therefore, pairings should be such that $\mu(\mathbf{E}(j\omega)) < 1$ is satisfied in the low frequency region (based on the μ-IM condition).

Remark 4.4 For stable plants, the μ-IM condition guarantees stability under controller failures (implying actuator saturation). For a 3×3 system with $\mathbf{E} = (\mathbf{G} - \tilde{\mathbf{G}})\tilde{\mathbf{G}}^{-1}$, when the first controller k_1 fails, the stability of the remaining system is judged by

$$\det\left[\begin{pmatrix}1&0&0\\0&1&0\\0&0&1\end{pmatrix}+\begin{pmatrix}g_{11}&g_{12}&g_{13}\\g_{21}&g_{22}&g_{23}\\g_{31}&g_{32}&g_{33}\end{pmatrix}\begin{pmatrix}0&0&0\\0&k_2&0\\0&0&k_3\end{pmatrix}\right] = \det\left[\begin{pmatrix}1&0\\0&1\end{pmatrix}+\begin{pmatrix}g_{22}&g_{23}\\g_{32}&g_{33}\end{pmatrix}\begin{pmatrix}k_2&0\\0&k_3\end{pmatrix}\right].$$

Now, from (4.10),

$$\mu(\mathbf{E}) = \mu\begin{bmatrix}0&\frac{g_{12}}{g_{22}}&\frac{g_{13}}{g_{33}}\\\frac{g_{21}}{g_{11}}&0&\frac{g_{23}}{g_{33}}\\\frac{g_{31}}{g_{11}}&\frac{g_{32}}{g_{22}}&0\end{bmatrix} \geq \max\left[0, \mu\begin{pmatrix}0&\frac{g_{23}}{g_{33}}\\\frac{g_{32}}{g_{33}}&0\end{pmatrix}\right] = \max\left[0, \mu(\mathbf{E}_1)\right].$$

Therefore, the μ-IM condition for the remaining loops is still satisfied, since $\mu(\mathbf{E}_1) \leq \mu(\mathbf{E})$. When the second loop fails, the condition $\mu(\mathbf{E}) = \mu\left(\mathbf{D}\mathbf{E}\mathbf{D}^{-1}\right)$ can be utilized to prove stability, where the scaling matrix is given by

$$\mathbf{D} = \begin{bmatrix}1&0&0\\0&0&1\\0&1&0\end{bmatrix}.$$

4.6 Simulation Results

Consider the following system [51]

$$\mathbf{G}(s) = \left[\begin{array}{cccc|ccc}1&0&0&0&1&0.5&0.5\\0&2&0&0&0.5&1&0.5\\0&0&3&0&0.5&0.5&1\\0&0&0&-4&1&0.4&0.4\\\hline1&0.1&0.1&1&0&0&0\\0.1&1&0.1&0.6&0&0&0\\0.1&0.1&1&0.6&0&0&0\end{array}\right].$$

The system has unstable poles at 1, 2 and 3. Application of the (block) diagonal approximation algorithm gives

$$\tilde{\mathbf{G}}(s) = \begin{bmatrix}\frac{0.7923s-6.009}{s^2-7.179s-37.82}&0&0\\0&\frac{0.6135s-0.05103}{s^2-1.402s-27.43}&0\\0&0&\frac{0.7911s+0.9201}{s^2-0.8216s-24.77}\end{bmatrix},$$

which has poles at 10.71, -3.53, 5.98, -4.58, 5.40 and -4.58, i.e., the same number of unstable poles as the original system $\mathbf{G}(s)$. The singular values of the error system

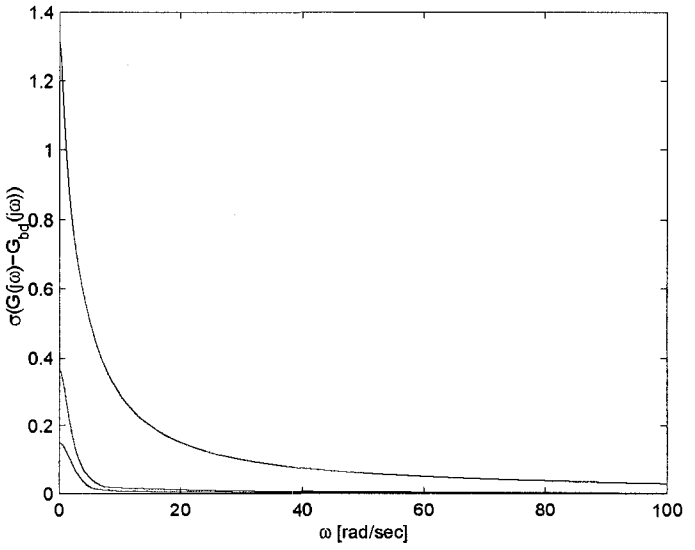

Figure 4.2: Singular values of the error system.

$\mathbf{G}(j\omega) - \mathbf{G}_{bd}(j\omega)$, where $\mathbf{G}_{bd}(j\omega) = \tilde{\mathbf{G}}(j\omega)$ are shown in Fig. 4.2. The optimum γ is 1.3.

Next, consider the controller design. Since, $\mathbf{E}(s) = (\mathbf{G}(s) - \tilde{\mathbf{G}}(s))\tilde{\mathbf{G}}^{-1}(s)$ is improper, the algorithm in (4.8) and (4.9) is slightly modified to $\bar{\sigma}\left(\frac{1}{c_H}\tilde{\mathbf{R}}(j\omega)\right) \leq 1$, $\forall \omega \in \mathbb{R}$ where at each frequency c_H solves

$$\mu_{\hat{\mathbf{\Delta}}}\begin{bmatrix} 0 & (\mathbf{G}(j\omega) - \tilde{\mathbf{G}}(j\omega)) \\ c_H\mathbf{I} & 0 \end{bmatrix} = 1.$$

Here, $\tilde{\mathbf{R}}(j\omega) = \mathbf{K}(j\omega)(\mathbf{I} + \tilde{\mathbf{G}}\mathbf{K}(j\omega))^{-1}$ is the control sensitivity function and μ is computed w.r.t the structure $\hat{\mathbf{\Delta}} = \text{diag}(\tilde{\mathbf{H}}(j\omega), \tilde{\mathbf{R}}(j\omega))$. Application of this algorithm gives $c_H = 0.8026$ and the decentralized controller

$$\mathbf{K}(s) = \text{diag}\left(\frac{123.2s + 435}{s - 72.64}, \frac{34.94s + 160.1}{s - 4.881}, \frac{20.78s + 95.24}{s - 1.046}\right). \tag{4.17}$$

The stabilizing effect of this controller for simultaneous reference step inputs of amplitude 1 (at $t = 1$ sec) and unit step disturbances occurring at $t = 3$ is shown in Fig. 4.3.

Hence, the design procedure here is very straightforward. When the unstable poles in the LMI optimization are kept fixed, the approximated system is given by

$$\tilde{\mathbf{G}}(s) = \text{diag}\left(\frac{1.067s + 0.9654}{s^2 + 2.531s - 3.531}, \frac{0.9054s + 2.366}{s^2 + 2.583s - 9.167}, \frac{0.9953s + 2.508}{s^2 + 1.583s - 13.75}\right),$$

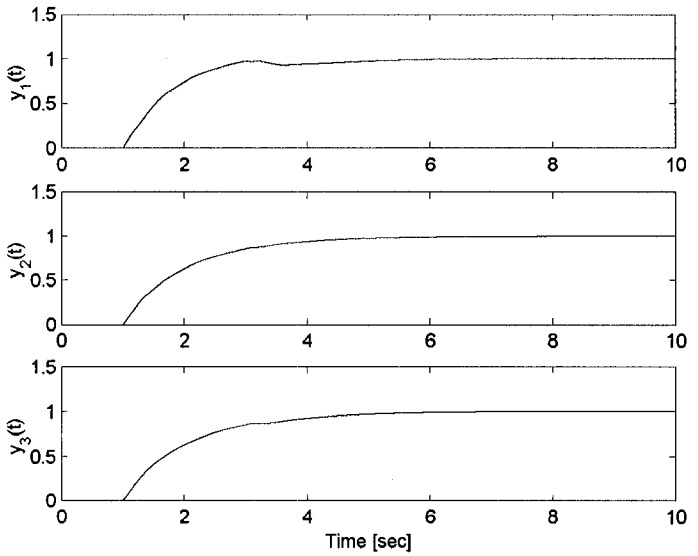

Figure 4.3: Outputs of the plant.

with $\gamma = 0.9$. Application of the design algorithm to this system gives $c_H = 1.1233$ and the stabilizing controller

$$\mathbf{K}(s) = \text{diag}\left(\frac{4.459s + 15.75}{s + 0.7735}, \frac{6.304s + 28.89}{s + 2.876}, \frac{8.283s + 37.96}{s + 2.34}\right).$$

4.6.1 Utility Boilers

Here, the nonlinear model of the utility boilers (UB 201-203) and the 6.306 MPa header (developed in chapter 3) is used. The linearized model has one pole at the origin and one RHP zero at 0.0619. The block diagonal approximation gives $\gamma = 0.28$ and for implementation the controller is then discretized with a sampling period of 6 seconds. It has the following form:

$$\mathbf{K}(z) = \text{diag}[K_{11}(z), K_{22}(z), K_{33}(z)], \tag{4.18}$$

where

$$\begin{aligned}
K_{11}(z) &= \frac{60.64z^3 - 41.41z^2 - 91.75z + 72.96}{z^3 - 1.875z^2 + 0.8786z}, \\
K_{22}(z) &= \frac{0.0003238z^3 - 0.0009514z^2 + 0.0009314 - 0.0003039}{z^3 - 2.97z^2 + 2.941z - 0.9708}, \\
K_{33}(z) &= \frac{-0.02555z^3 - 0.006817z^2 - 0.01441z + 2.1 \times 10^{-4}}{z^3 - 0.008143z^2 + 0.001135z}.
\end{aligned}$$

With this controller, the condition in (4.2) can be satisfied at all frequencies (Fig. 4.4) and RHP zero crossings can be prevented (conditions (4.14) and (4.15) are satisfied). Figs 4.5-4.8 shows the response of the system under perturbed conditions. Fig. 4.5 represents the measurements during a sudden load change of 100 kpph in the 6.306 MPa steam header. Fig. 4.6 shows the inputs that are required to overcome the load variations.

The interesting feature of Fig. 4.7 is that when the plant is controlled by a multivariable controller and if the firing rate master controller fails, then the overall system becomes unstable. However, the decentralized controller in (4.18) is capable of maintaining the stability. This is an important property of control by *independent designs*. Fig. 4.8 shows the system response for a step change in steam temperature from high to normal load condition. Hence, the controller can also track the reference input change and works well in different load conditions.

4.7 Chapter Summary

This chapter develops an algorithm to apply the concept of μ-IM to unstable systems. It is shown that the (block) diagonal approximation can be obtained by solving a quasi-convex optimization problem. In addition to this, other results of decentralized control design are presented, which includes: a) derivation of an upper bound of the performance, and b) sufficient conditions to prevent zero crossings across the imaginary axis. The results are validated with SYNSIM.

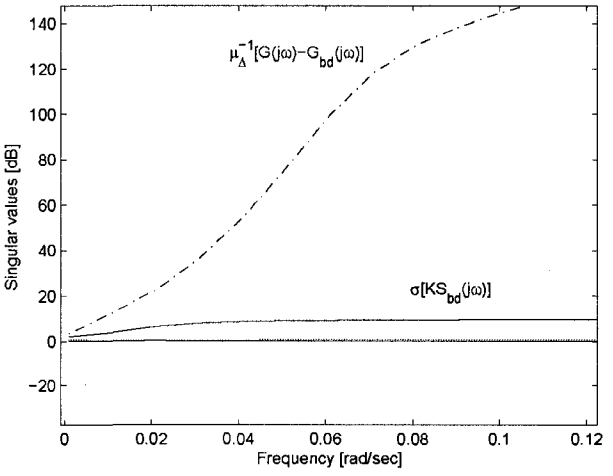

Figure 4.4: Verification of condition in (4.2). In figure, $\mathbf{S}_{bd}(j\omega) = \tilde{\mathbf{S}}(j\omega)$.

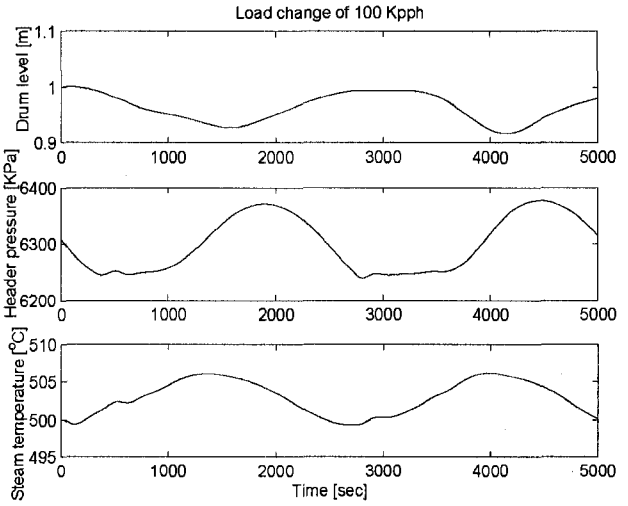

Figure 4.5: Controlled variables during load change.

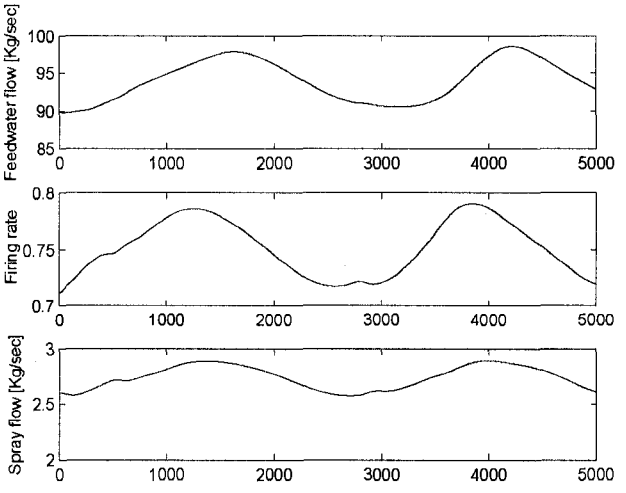

Figure 4.6: Inputs during load change.

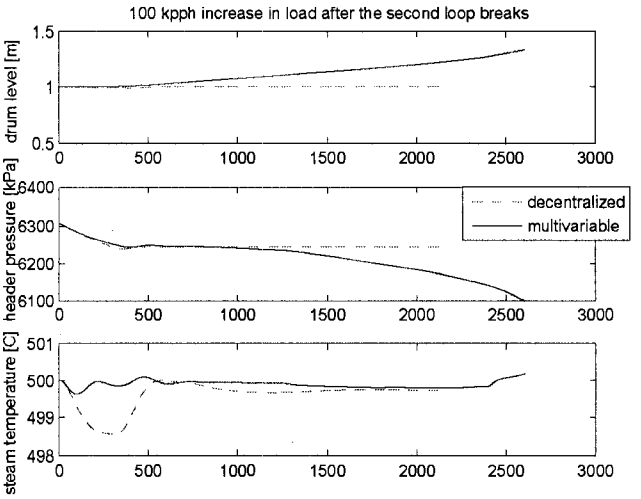

Figure 4.7: System response during loop failure.

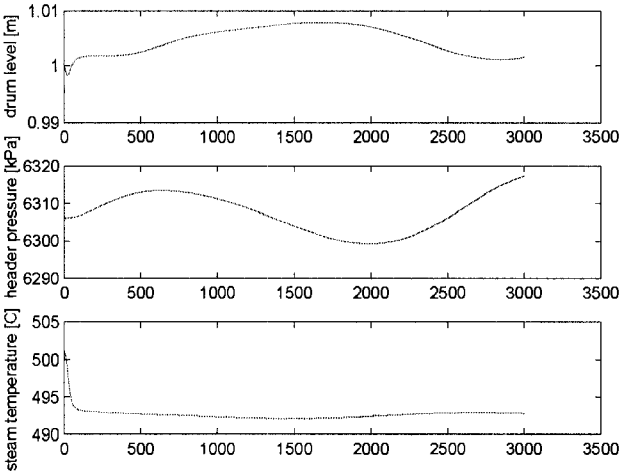

Figure 4.8: Step change in steam temperature.

Chapter 5

Model Predictive Control Strategy

This chapter utilizes the MPC design, based on discrete time laguerre functions to achieve fuel economy for the the Syncrude Canada Ltd. integrated energy facility. The firing rate of CO boilers are controlled in addition to the firing rate of UBs to meet the load demand. This method utilizes the fact that CO boilers exploit the exhaust gas (coker-off gas) of cokers, therefore, if they respond in addition to the UBs during load fluctuations then the fuel (natural gas) consumption in the UBs will be reduced. The use of MPC technique is to incorporate the practical limits of the control signal and its rate of change; this is difficult in other methods.

5.1 Introduction

In chemical process industry, namely, HPIs, which includes refining, petrochemical and gas processing plants, the last few decades have seen increasing research interest in the design of MPC strategies [34]. Motivations include a) straightforward application to non-square systems, and b) the control signal and its rate of change can be optimized at each sampling instant, to mention just a few [34]. Another important aspect is simplicity in the design phase, which is a source of attraction to a naive designer.

The traditional approach of the MPC strategy involves expressing the control signal using forward shift operators and solving a quadratic optimization problem online. However, if the dynamics of the process is complex involving large interactions, fast sampling rate, instability, the control signal needs to be expressed by large number of forward shift operators to obtain a satisfactory and reliable closed loop control [114]. This leads to substantial online computation effort and ill conditioned solutions. To overcome this

problem, [113, 114] presented an approach of MPC design using Laguerre functions. In [114], the difference of the control trajectory was modeled using the discrete orthogonal laguerre functions and it was shown that the decision variables in the online optimization problem could be reduced by a significant number.

In this work, the aforementioned theory is applied to achieve fuel economy of the Syncrude Canada Ltd. integrated energy facility. As mentioned earlier, due to different time constants of the boilers, whenever there is a load change in the 900-pound header, the utility boilers respond to this change and try to regulate the header pressure. On the other hand, the CO type boilers and once through steam generators always produce steam at a constant rate of 750 kpph and 190 kpph, respectively. They have their self loops to control the steam flow rates of CO boilers and superheated steam temperature for the OTSGs (Fig. 5.1). This leads to consumption of the natural gas (used to generate steam in the utility boilers) by a significant amount. To overcome this problem, the present work involves designing a firing rate master controller of the CO type boilers that along with UBs can react to the load fluctations leading to less fuel (non-renewable energy source) utilization in the UBs.

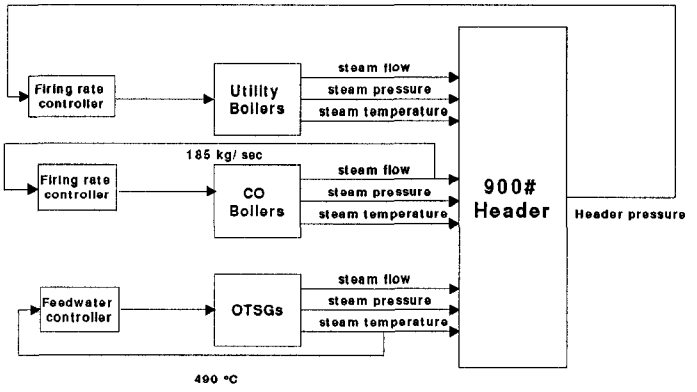

Figure 5.1: A part of the boilers, once through steam generators and header system [106].

In this chapter, a model predictive control law is designed where constraints on the manipulated variable and its rate of change are imposed. Particular emphasis is placed on maintaining overall closed loop stability and improving the performance of the present plant. In SYNSIM, the MPC is implemented as a S-function block that involves online optimization of the objective function and generation of the control trajectory at each sampling instant. It is shown that the proposed design approach can achieve considerable fuel economy.

The rest of this chapter is as follows. Section 5.2 deals with the design, which is followed by results with SYNSIM in Section 5.3. Finally, Section 5.4 provides a brief summary of this chapter.

5.2 Design of Control Strategy

Advanced control ideas lingered to be a source of attraction to different vendors of electrical power plants. In Japan (1987), Kyushu Electric Power Company developed a LQR control design for OTSGs. Other examples include [75]: a) ROC steam temperature control and a plant master controller design using the ARMAX model by Honeywell, b) superheater steam temperature controller using state variable feedback, decoupling controllers for once through systems and digital technology for condenser throttling by Siemens and c) neural network for reducing NO_X emissions and fuzzy logic controller for drum level control. In this sense, the adoption of advanced technology is just an exception rather than a statute [75].

To achieve fuel economy, UBs and CO-type boilers are used to control the 900# header pressure, shown in Fig. 5.2. The motivation of MPC strategy to solve the economy problem arose due to constraints on the firing rate ($0.25 \leq u \leq 1$) and its rate of change ($-0.16/60 \leq \Delta u \leq 0.16/60$), which are difficult to accommodate in the design by other techniques.

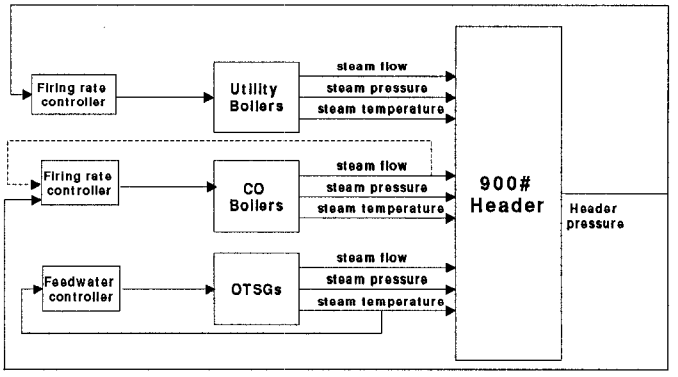

Figure 5.2: Schematic to achieve fuel economy.

In the following, emphasis is placed on optimizing the future incremental control variable. This treatment can lead to inclusion of the integral action in the loop, which in turn provides good tracking and disturbance rejection capabilities. The required steps for this aim are [114, 115]:

1. Augment the model

$$\underbrace{\begin{bmatrix}\Delta\mathbf{x}_n(k+1)\\ \mathbf{y}(k+1)\end{bmatrix}}_{\mathbf{x}(k+1)} = \underbrace{\begin{bmatrix}\mathbf{A}_n & \mathbf{0}\\ \mathbf{C}_n\mathbf{A}_n & \mathbf{I}_p\end{bmatrix}}_{\mathbf{A}}\underbrace{\begin{bmatrix}\Delta\mathbf{x}_n(k)\\ \mathbf{y}(k)\end{bmatrix}}_{\mathbf{x}(k)} + \underbrace{\begin{bmatrix}\mathbf{B}_n\\ \mathbf{C}_n\mathbf{B}_n\end{bmatrix}}_{\mathbf{B}} \times\Delta\mathbf{u}(k)$$

$$\mathbf{y}(k) = \underbrace{\begin{bmatrix}\mathbf{0} & \mathbf{I}_p\end{bmatrix}}_{\mathbf{C}}\begin{bmatrix}\Delta\mathbf{x}_m(k)\\ \mathbf{y}(k)\end{bmatrix},$$

where $\mathbf{x}_n$ are the states of the plant with $\mathbf{A}_n$, $\mathbf{B}_n$, $\mathbf{C}_n$ as state, input and output matrices, respectively. The augmented system contains p eigenvalues on the unit circle, in addition to the eigenvalues of the original system, given by $(\lambda-1)^p\det(\lambda\mathbf{I}-\mathbf{A}_m)$. It is detectable and stabilizable provided that the original system is detectable and stabilizable and possess no transmission zeros on the unit circle.

2. Define the following look ahead prediction

$$\begin{aligned}\mathbf{x}_p &= \begin{bmatrix}\mathbf{x}^T(k_i+1|k_i) & \mathbf{x}^T(k_i+2|k_i) & \dots & \mathbf{x}^T(k_i+N_p|k_i)\end{bmatrix}^T,\\ \Delta\mathbf{u}_p &= \begin{bmatrix}\Delta\mathbf{u}^T(k_i) & \Delta\mathbf{u}^T(k_i+1) & \dots & \Delta\mathbf{u}^T(k_i+N_c-1)\end{bmatrix}^T,\\ \mathbf{y}_p &= \begin{bmatrix}\mathbf{y}^T(k_i+1|k_i) & \mathbf{y}^T(k_i+3|k_i) & \dots & \mathbf{y}^T(k_i+N_p|k_i)\end{bmatrix}^T,\end{aligned}$$

which yields the following prediction equations

$$\begin{aligned}\mathbf{x}_p &= \mathbf{F}\mathbf{x}(k_i)+\Phi\Delta\mathbf{u}_p,\\ \mathbf{y}_p &= \bar{\mathbf{C}}\mathbf{x}_p = \bar{\mathbf{C}}\mathbf{F}\mathbf{x}(k_i)+\bar{\mathbf{C}}\Phi\Delta\mathbf{u}_p,\end{aligned}$$

where

$$\mathbf{F}=\begin{bmatrix}\mathbf{A}\\ \mathbf{A}^2\\ \mathbf{A}^3\\ \vdots\\ \mathbf{A}^{N_p}\end{bmatrix},\quad \Phi=\begin{bmatrix}\mathbf{B} & \mathbf{0} & \mathbf{0} & \dots & \mathbf{0}\\ \mathbf{AB} & \mathbf{B} & \mathbf{0} & \dots & \mathbf{0}\\ \mathbf{A}^2\mathbf{B} & \mathbf{AB} & \mathbf{B} & \dots & \mathbf{0}\\ \vdots & \vdots & \vdots & \vdots & \vdots\\ \mathbf{A}^{N_p-1}\mathbf{B} & \mathbf{A}^{N_p-2}\mathbf{B} & \mathbf{A}^{N_p-3}\mathbf{B} & \dots & \mathbf{A}^{N_p-N_c-1}\mathbf{B}\end{bmatrix}.$$

Here, N_p and N_c are the prediction horizon and the control horizon, respectively (Fig. 5.3 [115]). For an unconstrained case with the objective function $J=(\mathbf{s}_p-\mathbf{y}_p)^T\bar{\mathbf{Q}}(\mathbf{s}_p-\mathbf{y}_p)+\Delta\mathbf{u}_p^T\bar{\mathbf{R}}\Delta\mathbf{u}_p$, where $\mathbf{s}_p$ contains the vectors of the set points and $\bar{\mathbf{Q}}$, $\bar{\mathbf{R}}$ are the weighting matrices, the optimal solution attained by minimizing J is given by

$$\Delta\mathbf{u}_p=-(\Phi^T\bar{\mathbf{C}}^T\bar{\mathbf{Q}}\bar{\mathbf{C}}\Phi+\bar{\mathbf{R}})^{-1}\Phi^T\bar{\mathbf{C}}^T\bar{\mathbf{Q}}(\bar{\mathbf{C}}\mathbf{F}\mathbf{x}(k_i)-\mathbf{s}_p). \tag{5.1}$$

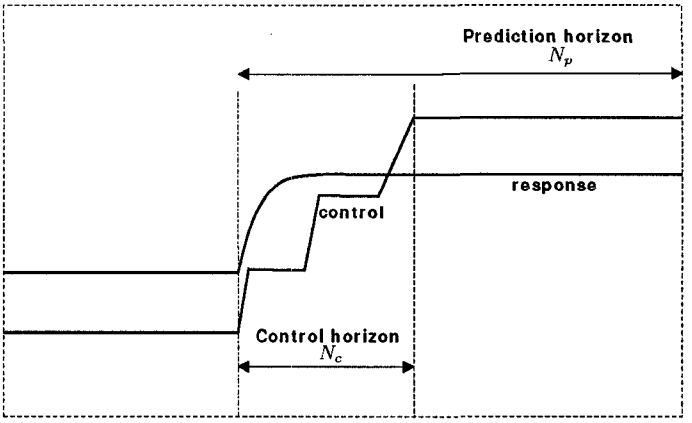

Figure 5.3: Model predictive control strategy.

3. With the following additional constraints on the control signal and its rate of change:
$\mathbf{\Delta u}_p \leq \mathbf{\Delta u}_{pmax}$, $-\mathbf{\Delta u}_p \leq -\mathbf{\Delta u}_{pmin}$,

$$\mathbf{u}_{pmin} \leq \begin{bmatrix} \mathbf{u}(k_i) \\ \mathbf{u}(k_i+1) \\ \mathbf{u}(k_i+2) \\ \cdots \\ \mathbf{u}(k_i+N_c-1) \end{bmatrix} = \begin{bmatrix} \mathbf{I} \\ \mathbf{I} \\ \mathbf{I} \\ \vdots \\ \mathbf{I} \end{bmatrix} \mathbf{u}(k_i-1) + \begin{bmatrix} \mathbf{I} & \mathbf{0} & \mathbf{0} & \ldots & \mathbf{0} \\ \mathbf{I} & \mathbf{I} & \mathbf{0} & \ldots & \mathbf{0} \\ \mathbf{I} & \mathbf{I} & \mathbf{I} & \ldots & \mathbf{0} \\ \vdots & \vdots & \vdots & \vdots & \vdots \\ \mathbf{I} & \mathbf{I} & \ldots & \mathbf{I} & \mathbf{I} \end{bmatrix} \times \begin{bmatrix} \mathbf{\Delta u}(k_i) \\ \mathbf{\Delta u}(k_i+1) \\ \mathbf{\Delta u}(k_i+2) \\ \vdots \\ \mathbf{\Delta u}(k_i+N_c-1) \end{bmatrix} \leq \mathbf{u}_{pmax},$$

which gives

$$\begin{aligned} -(\mathbf{C}_1\mathbf{u}(k_i-1) + \mathbf{C}_2\mathbf{\Delta u}_p) &\leq -\mathbf{u}_{pmin}, \\ (\mathbf{C}_1\mathbf{u}(k_i-1) + \mathbf{C}_2\mathbf{\Delta u}_p) &\leq \mathbf{u}_{pmax}, \end{aligned}$$

the constrained optimization problem can be written as

$$\begin{aligned} \min \quad & [\mathbf{\Delta u}_p^T(\mathbf{\Phi}^T\bar{\mathbf{C}}^T\bar{\mathbf{Q}}\bar{\mathbf{C}}\mathbf{\Phi} + \bar{\mathbf{R}})\mathbf{\Delta u}_p + 2\mathbf{\Delta u}_p^T\mathbf{\Phi}^T\bar{\mathbf{C}}^T\bar{\mathbf{Q}} \\ & \times(\bar{\mathbf{C}}\mathbf{F}\mathbf{x}(k_i) - \mathbf{s}_p) + \text{constant}], \\ \text{subject to} \quad & \begin{bmatrix} \mathbf{M}_1 \\ \mathbf{M}_2 \\ \mathbf{M}_3 \end{bmatrix} \mathbf{\Delta u}_p \leq \begin{bmatrix} \mathbf{n}_1 \\ \mathbf{n}_2 \\ \mathbf{n}_3 \end{bmatrix}, \end{aligned}$$

where the third constraint is reflecting the limits on the states. This is in the form of $\min\left[J = \frac{1}{2}\mathbf{\Delta u}_p^T\mathbf{E}\mathbf{\Delta u}_p + \mathbf{\Delta u}_p^T\mathbf{F}\right]$, subject to $\mathbf{M}\mathbf{\Delta u}_p \leq \mathbf{n}$. To solve this quadratic

optimization, a number of techniques are available in the literature, namely, primal methods, dual methods, penalty and barrier methods, lagrange methods as well as specially tailored interior-point methods. It is solvable provided the number of active constraints are less than the number of decision variables and the constraints are linearly independent.

Using primal-dual methods, assuming feasibility (there exists an $\mathbf{\Delta u}_p$ such that $\mathbf{M\Delta u}_p \leq \mathbf{n}$), the KKT conditions are comparable to

$$\max_{\lambda \geq 0} \min_{\mathbf{\Delta u}_p} \left[\frac{1}{2} \mathbf{\Delta u}_p^T \mathbf{E} \mathbf{\Delta u}_p + \mathbf{\Delta u}_p^T \mathbf{F} + \lambda^T \left(\mathbf{M\Delta u}_p - \mathbf{n} \right) \right].$$

Minimization of this function over $\mathbf{\Delta u}_p$ gives $\mathbf{\Delta u}_p = -\mathbf{E}^{-1} \left(\mathbf{F} + \mathbf{M}^T \lambda \right)$ that contains the unconstrained solution $-\mathbf{E}^{-1}\mathbf{F}$ (similar to (5.1)). Substitution of this value gives the following dual problem

$$\max_{\lambda \geq 0} \left[-\frac{1}{2} \lambda^T \mathbf{H} \lambda - \lambda^T \mathbf{K} - \frac{1}{2} \mathbf{F}^T \mathbf{E}^{-1} \mathbf{F} \right] = \min_{\lambda \geq 0} \left[\frac{1}{2} \lambda^T \mathbf{H} \lambda + \lambda^T \mathbf{K} + \frac{1}{2} \mathbf{F}^T \mathbf{E}^{-1} \mathbf{F} \right],$$

where $\mathbf{H} = \mathbf{M}\mathbf{E}^{-1}\mathbf{M}^T$ and $\mathbf{K} = \mathbf{n} + \mathbf{M}\mathbf{E}^{-1}\mathbf{F}$. Since, the constraint is now much straightforward ($\lambda \geq 0$), it can be readily solved using the Hildreth's QP procedure.

4. It is clear that by using the aforementioned method, it is sometime difficult to compute the control signal due to the presence of an inversion in (5.1) that needs to be calculated online. To overcome this problem, the control signal is modeled using a series of orthogonal laguerre functions. For SISO case, it can be expressed as $\Delta u(k_i + m) = \sum_{i=1}^{N} l_i(m) c_i = \mathbf{l}(m)^T \eta$, shown in Fig. 5.4. The tuning parameters are now scaling factor (a) and the number of laguerre terms (N). These functions satisfy the following difference equation:

$$\mathbf{l}(k+1) = \mathbf{A}_l \mathbf{l}(k), \tag{5.2}$$

where

$$\begin{aligned}
\mathbf{l}(k) &= \begin{bmatrix} l_1(k) & l_2(k) & \dots & l_N(k) \end{bmatrix}^T, \\
\mathbf{A}_l &= \begin{bmatrix} a & 0 & 0 & \dots & 0 \\ \beta & a & 0 & \dots & 0 \\ -a\beta & \beta & a & \dots & 0 \\ \vdots & \vdots & \vdots & \vdots & \vdots \\ (-1)^{N-2} a^{N-2} \beta & (-1)^{N-3} a^{N-3} \beta & \dots & \beta & a \end{bmatrix}, \\
\beta &= 1 - a^2, \ \mathbf{l}(0)^T = \sqrt{(1-a^2)} \begin{bmatrix} 1 & -a & a^2 & \dots & (-a)^N \end{bmatrix}.
\end{aligned}$$

Corroborated by numerous simulations, it has been found that realization of a control signal can be done much more easily and efficiently by proper choice of parameter a and a small value of N rather than a large number of forward shift operators (large control horizon N_c). They are easy to understand by programmers and also deals with MIMO systems. Based on this control law, the overall system can be written as

$$\mathbf{x}(k_i+m|k_i) = \mathbf{A}^m\mathbf{x}(k_i) + \underbrace{\sum_{i=0}^{m-1}\mathbf{A}^{m-i-1}\mathbf{B}\mathbf{l}(i)^T}_{\mathbf{\Phi}^T(m)}\eta.$$

Hence, minimization of the cost function $J = \sum_{m=1}^{N_p}\mathbf{x}^T(k_i+m|k_i)\bar{\mathbf{Q}}\mathbf{x}(k_i+m|k_i)+\eta^T\mathbf{R}_L\eta$ leads to

$$\eta = -(\sum_{m=1}^{N_p}\mathbf{\Phi}(m)\bar{\mathbf{Q}}\mathbf{\Phi}^T(m)+\mathbf{R}_L)^{-1}(\sum_{m=1}^{N_p}\mathbf{\Phi}(m)\bar{\mathbf{Q}}\mathbf{A}^m)\mathbf{x}(k_i). \tag{5.3}$$

This solution is also in the form of $\eta = -\mathbf{E}^{-1}\mathbf{F}$, but the invertibility of (5.3) can be computed online in a more efficient manner than in (5.1). For the constrained part, the foregoing Hildreth's QP procedure can be directly employed.

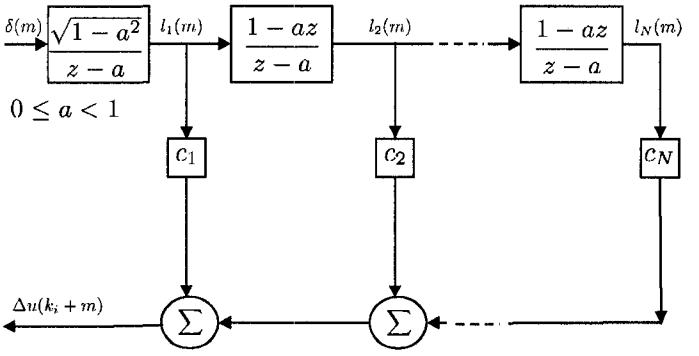

Figure 5.4: Discrete time laguerre functions [115].

5.3 Simulation Results

At first, system identification technique is used in the open loop system (Fig. 5.5) to obtain a 8^{th} order CO boiler model, which is given by the following SS matrices: $\mathbf{A}_n =$

$$\begin{bmatrix}
0.001565 & -0.01279 & 3.8\times10^{-5} & -9.1\times10^{-5} & -1.5\times10^{-4} & -2\times10^{-4} & 3.2\times10^{-4} & 7.5\times10^{-4} \\
0.01659 & 0.0003517 & -0.04369 & -0.01035 & -0.02172 & -0.02769 & 0.04743 & 0.1112 \\
0.00224 & 0.04532 & 0.1913 & -0.5485 & -0.7207 & -1.25 & 1.794 & 3.994 \\
4.1\times10^{-4} & -0.007854 & 0.5049 & -0.5644 & -0.4656 & -1.568 & 2.633 & 6.175 \\
-0.001702 & 0.01162 & -0.5883 & 0.2672 & 2.246 & 4.147 & -5.657 & -12.11 \\
2.3\times10^{-4} & -0.01077 & 0.6157 & -0.8413 & -2.563 & -3.027 & 4.715 & 9.812 \\
-0.002681 & 0.005376 & -0.3486 & 0.4431 & 1.453 & 1.597 & -2.688 & -5.98 \\
-1.8\times10^{-4} & -5.3\times10^{-5} & -0.001301 & 0.0008194 & 0.006315 & 0.003494 & -0.02842 & -0.3808
\end{bmatrix},$$

$$\mathbf{B}_n = \begin{bmatrix} -0.0001449 \\ -0.01647 \\ -1.18 \\ -3.232 \\ 5.379 \\ -3.078 \\ 1.99 \\ 0.1092 \end{bmatrix},$$

$$\mathbf{C}_n = \begin{bmatrix} 3.4 \times 10^{-3} & -2.2 \times 10^{-5} & 5.4 \times 10^{-7} & -6.8 \times 10^{-8} & 1 \times 10^{-8} & -6.2 \times 10^{-8} & 8.4 \times 10^{-9} \\ -2.7 \times 10^{-8} \end{bmatrix}. \quad (5.4)$$

By selecting $a = 0.7$, $N = 50$, $N_p = 100$, $\bar{\mathbf{R}} = 0.3$, $\bar{\mathbf{Q}} = \mathbf{C}_n'\mathbf{C}_n$ and online solving a constrained quadratic optimization problem, the controller is implemented. Fig. 5.6 shows the steam flow rate of CO-type boilers with MPC (top one) and the existing PI controllers of the plant (bottom). Due to an increase in load, the additional demand is met by increasing the firing rate of these boilers (Fig. 5.7). Fig. 5.8 shows the firing rate master signal of the utility boilers, where the dotted one corresponds to the PI case. In concert with Fig. 5.9, it clearly reveals that the proposed strategy can achieve significant reduction in the consumption of the fuel flow (natural gas), i.e., fuel economy of 11.5% is achieved. Figs. 5.10-5.12 shows the dynamics of different process variables with the MPC and the PI controllers, respectively. The MPC strategy leads to an initial peaking of the 900# header pressure, but the oscillations die out faster than the existing PI controllers of the plant. An initial decrease of the header pressure is due to an increase in the load change of 100 kpph in the header. Pressure rises afterwards because the firing rate of CO boilers and UBs increases abruptly to meet the load demand. The responses of the drum level and the steam temperature with the PI controllers appear to be better than the MPC (less undershoot and overshoot), since two controllers are acting simultaneously leading to a very fast control action.

Remark 5.1 For tuning, if interest lies in long N_c value then choose a large value of a; this will require smaller number of laguerre terms N. In some cases, it may not be possible to satisfy the constraint on $\mathbf{u}_p$ and $\Delta\mathbf{u}_p$ simultaneously. Therefore, one of them should be restricted by a function block (similar situation arose with firing rate of CO boilers which was constrained in SYNSIM by a function block).

5.4 Chapter Summary

This chapter introduces some basic concepts of MPC and finds an efficient technique that can be applicable to an industrial system. The method is then applied to achieve fuel economy by controlling the firing rate of CO-type boilers. Simulation results in SYNSIM show that the requirement of the natural gas consumption in the present plant can be reduced

by 11.5% using this method.

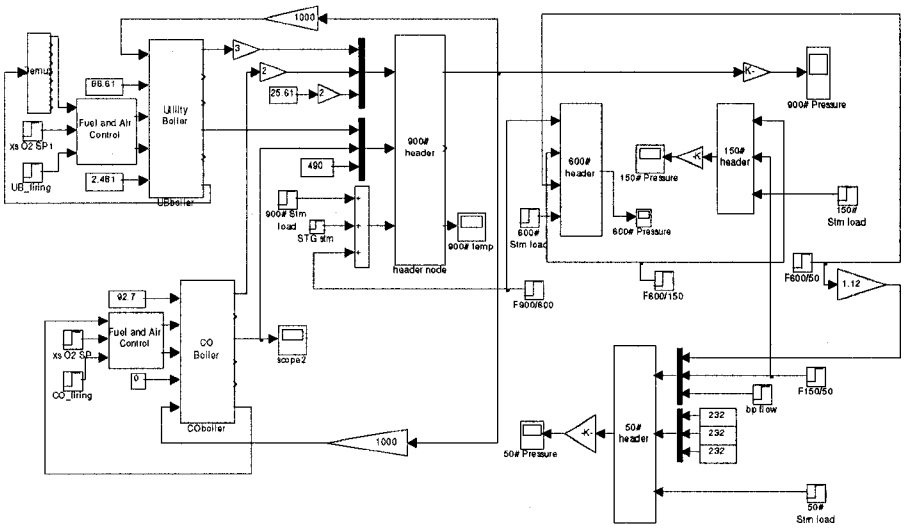

Figure 5.5: Open loop model of UBs, headers and OTSGs.

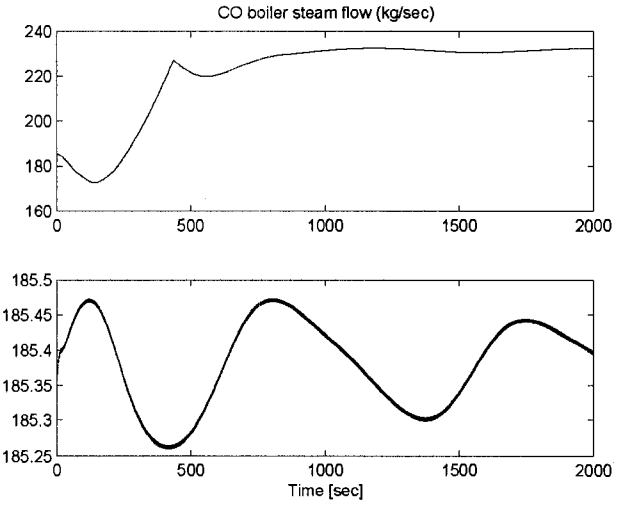

Figure 5.6: Steam flow out of the CO type boilers.

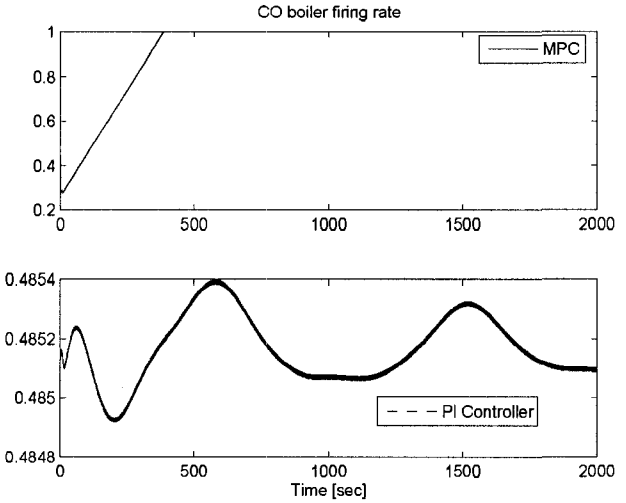

Figure 5.7: Firing rate of the CO type boilers.

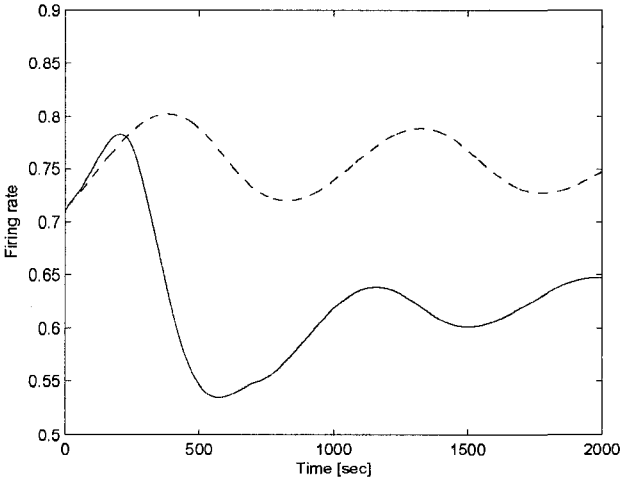

Figure 5.8: Firing rate of the utility boilers.

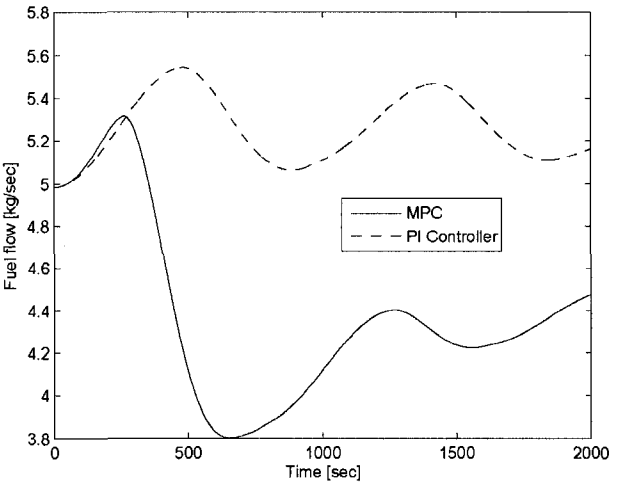

Figure 5.9: Fuel flow rate for steam production in the utility boilers.

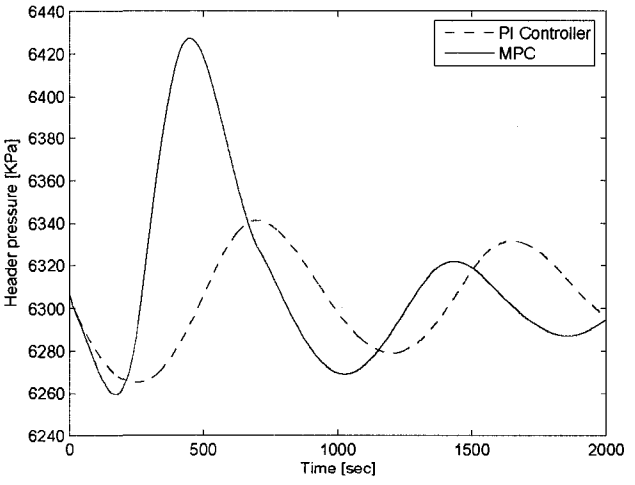

Figure 5.10: Header pressure response.

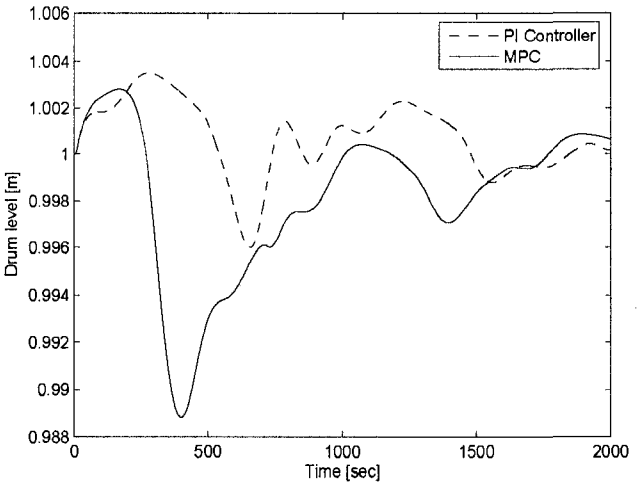

Figure 5.11: Drum level of the utility boilers.

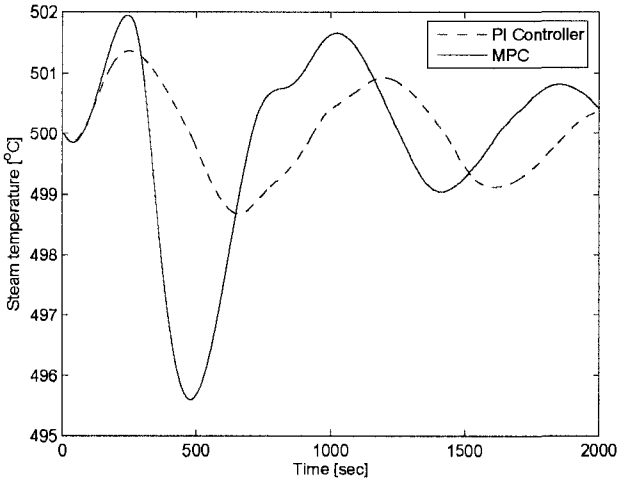

Figure 5.12: Superheater steam temperature.

Chapter 6

Conclusions and Recommendations

6.1 Conclusions

In this thesis, different algorithms are developed for decentralized as well as overlapping control designs of linear as well as nonlinear interconnected systems. The major contributions are:

1. Design of observer-based decentralized controllers and dynamic output feedback control laws for N nonlinear interconnected systems are casted into a convex optimization problem. With these results a global minimum can be achieved, *if* it exists.

2. A general algorithm has been developed that provides a solution to a number of NP-hard problems in overlapping control design. In every case, the results are generalized to large scale systems.

3. A new approach of obtaining a (block) diagonal approximated system that possesses the same number of unstable poles as the plant is presented. This helps to extend the theory of μ-interaction measure to unstable plants. The results of [89] that is concerned with robust stability and robust performance of stable systems are now capable of dealing with unstable systems.

4. The aforementioned theoretical algorithms are all applied to SYNSIM for overcoming different control problems of the present plant. A detailed analysis is carried out to judge the performance of controllers under several perturbed conditions: load fluctuations in different headers, tripping of boilers, and loop failures. In addition to this, a thorough literature survey has been carried out to get into a deep understanding of the drum-boiler modeling and a physical model for the

UBs at Syncrude is then developed. Therefore, they should be a source of attraction to both theorists and practitioners.

5. Efforts are laid on modeling and programming to develop a MPC strategy for achieving fuel economy of Syncrude Canada Ltd.

6.2 Future Work

In the following, some future directions for extending and improving the results of this thesis are provided.

1. It will be interesting to extend the results of chapters 2-3 to consider the following class of nonlinear interconnected discrete time systems [97]

$$\mathbf{x}_i(k+1) = \mathbf{A}_i\mathbf{x}_i(k) + \mathbf{B}_i\mathbf{u}_i(k) + \mathbf{h}_i(\mathbf{x}(k)), \quad i = 1, 2, \ldots, N$$

where the interconnections satisfy

$$\mathbf{h}_i^T(\mathbf{x}(k))\mathbf{h}_i(\mathbf{x}(k)) \leq \alpha_i^2\mathbf{x}^T\mathbf{H}_i^T\mathbf{H}_i\mathbf{x}.$$

Static state feedback decentralized control design for this class of system was considered in [97], however, due to complexity, the design was restricted to subsystems with only single input. Moreover, some restrictive constraints on the structure of the Lyapunov matrix was imposed. In addition to rectifying this problem, it would be certainly useful to develop decentralized output feedback and overlapping control laws.

2. In chapter 4, a constant scaling matrix was employed that introduced some conservativeness in the algorithm. Therefore, it is useful to solve the optimization problem using a frequency dependent scaling matrix $\mathbf{D}(j\omega)$, which can give a better solution due to extra degrees of freedom provided by $\mathbf{D}(j\omega)$. This is a NP-hard problem, but following the ideas of chapter 4, there is a possibility to obtain some numerical solution.

   In many cases, when interactions in the plant are large, designing a decentralized controller using the results of chapter 4 may be a problem. Therefore, one may consider finding a (block) diagonal approximation of $\mathbf{G}(s)$ that possess same number of RHP *zeros* as the system itself [72]. An analytical solution to this problem is still an open area of research.

In the present work, some conditions are derived under which when one loop is closed then due to interactions the transmission zeros of other subsystems does not cross the imaginary axis. Nevertheless, they are only restricted to *stable* plants and generalization of the results to include more than two subsystems and their applicability to unstable systems are still unclear.

It would also be remarkable to develop results on the achievable decentralized performance using independent designs. This problem was not considered in the past and using the results of chapter 4 there is an opportunity to derive some conditions, possibly an upper bound. The outcome of [32] seems to offer a good initiative in this direction.

3. This thesis deals with MPC design, concerning fuel economy. An interesting approach would be to develop decentralized MPC law for the nonlinear interconnected systems in (2.1). On the way to solve this problem, ideas from [66] can be utilized. Moreover, while applying the MPC approach, it is useful to consider environmental factors as well, namely, reducing the production of NO_x, SO_x, etc., which leads to acid rain and global warming. They should be lessened by redesigning the firing rate controllers of UBs.

   In industry, the operators usually prefer PI, PID controllers because they are easy to understand and tune. If some advanced technique is required then they demand that it should not alter much the present control system working in the plant. To take into account this issue, a scheme of conditioning only the reference signal could be used. Similar to [26], the ideas of "sliding mode" and "reference conditioning" can to be combined to provide limits on the loop interactions that can be decided by the designer in advance. This approach appears to be effective for reducing the oscillations in the 900# header without redesigning the PI controllers of Syncrude Canada Ltd.

4. In chapter 4, some minor discussion on pairings and DIC is introduced. When the loops (with integral action) are paired in such a way that overall closed loop stability can be maintained *if* any of them are detuned arbitrarily, then the system is said to be DIC [58]. Hence, the concept of DIC is useful for eliminating impracticable pairings and, in many cases, can be easily verified using the steady state gain information of the plant. In the past, various necessary and sufficient conditions for checking DIC was developed [18, 58, 90]. Nonetheless, finding a necessary and sufficient

condition is still an open area of research. The result in [58] offer one such solution, however, it requires computing a series of real structured singular values and is based on pure integral controllers $\left(\frac{K_i}{s}\right)$. Therefore, new methods should be investigated. Furthermore, it would be interesting to derive DIC conditions in the presence of model uncertainty. In particular, one can ask the following questions:

- When interactions in a plant are large, systems are not DIC. What is the worst case interaction with a norm bounded uncertainty, $\overline{\sigma}(\mathbf{\Delta}(j\omega)) \leq 1$?
- For a nominal plant $\mathbf{G}(s)$ that is DIC, what is the size of minimum perturbation such that the system loses the DIC property?

Bibliography

[1] C. Aboky, G. Sallet, and J. C. Vivalda. Observers for Lipschitz Nonlinear Systems. *International Journal of Control*, 75(3):204–212, 2002.

[2] M. Aldeen and J. F. Marsh. Decentralized Observer-Based Control Scheme for Interconnected Dynamical Systems with Unknown Inputs. *IEE Proceedings-Control Theory and Applications*, 146:349–358, 1999.

[3] ANSI/ISA-S5.1. *Instrumentation Symbols and Identification*. Instrument Society of America, Research Triangle Park, North Carolina, USA, 1992.

[4] P. Apkarian, H. D. Tuan, and J. Bernussou. Continuous-Time Analysis, Eigenstructure Assignment, and $\mathcal{H}_2$ Synthesis with Enhanced Linear Matrix Inequalities (LMI) Characterizations. *IEEE Transactions on Automatic Control*, 46: 1941–1946, 2001.

[5] K. J. Astrom and R. D. Bell. Drum-Boiler Dynamics. *Automatica*, 36(3):363–378, 2000.

[6] K. J. Astrom and K. Eklund. A Simplified Non-Linear Model of a Drum Boiler-Turbine Unit. *International Journal of Control*, 16(1):145–169, 1972.

[7] J. Bao, J. F. Forbes, and P. J. McLellan. Robust Multiloop PID Controller Design: A Successive Semidefinite Programming Approach. *Industrial & Engineering Chemistry Research*, 38:3407–3419, 1999.

[8] R. D. Bell and K. J. Astrom. A Low-order Nonlinear Dynamic Model for Drum Boiler-Turbine-Alternator Units. *Technical Report TFRT-7162, Lund Institute of Technology*, pages 1–39, 1979.

[9] R. D. Bell and K. J. Astrom. Dynamic Models for Boiler-Turbine-Alternator Units: Data Logs and Parameter Estimation for a 160 MW Unit. *Technical Report TFRT-3192, Lund Institute of Technology*, pages 1–137, 1987.

[10] R. D. Bell and K. J. Astrom. Simplified Models for Boiler-Turbine Units. *Technical Report TFRT-3191, Lund Institute of Technology*, pages 1–52, 1987.

[11] A. Benlatreche, D. Knittel, and E. Ostertag. Robust Decenteralized Control Strategies for Large-Scale Web Handling Systems. *Control Engineering Practice*, 16(6):736–750, 2008.

[12] V. Blondel and J. N. Tsitsiklis. A Survey of Computational Complexity Results in Systems and Control. *Automatica*, 36:1249–1274, 2000.

[13] B. O. Bouamama, K. Medjaher, A. K. Samantaray, and M. Staroswiecki. Supervision of an Industrial Steam Generator. Part I: Bond Graph Modelling. *Control Engineering Practice*, 14(1):71–83, 2006.

[14] S. Boyd, L. El. Ghaoui, E. Feron, and V. Balakrishnan. *LMIs in System and Control Theory*. SIAM, Philadelphia, 1994.

[15] E. H. Bristol. On a New Measure of Interaction for Multivariable Process Control. *IEEE Tranactions on Automatic Control*, 11:133–134, 1966.

[16] H. Cai, Z. Qu, and J. Dorsey. Robust Decentralized Excitation Control for Large Scale Power Systems. In *Proceedings of* 13^{th} *IFAC Congress*, volume 3, pages 217–222, San Fransisco, 1996.

[17] H. Cai, Z. Qu, D. Gan, and J. Dorsey. A Comparison and Simulation Study of Nonlinearily Designed Robust Controllers for Power System Transient Stability. *International Journal of Electrical Power & Energy Systems*, 22(1):15–28, 2000.

[18] P. J. Campo and M. Morari. Achievable Closed-Loop Properties of Systems under Decentralized Control: Conditions Involving the Steady-State Gain. *IEEE Transactions on Automatic Control*, 39:932–943, 1994.

[19] J. Chapman, M. Ilic, D. King, C. Eng, and H. Kaufman. Stabilizing a Multimachine Power System via Decentralized Feedback Linearizing Excitation Control. *IEEE Transcations on Power System*, 8(3):830–839, 1993.

[20] M. Chilali and P. Gahinet. $\mathcal{H}_\infty$ Design with Pole Placement Constraints: An LMI Approach. *IEEE Transactions on Automatic Control*, 41(3):358–367, 1996.

[21] M. S. Chiu and Y. Arkun. A Methodology for Sequential Design of Robust Decentralized Control Systems. *Automatica*, 28:997–1001, 1992.

[22] H. Cui and E. W. Jacobsen. Performance Limitations in Decentralized Control. *Journal of Process Control*, 12:485–494, 2002.

[23] J. C. Doyle, J. E. Wall, and G. Stein. Performance and Robustness Analysis for Structured Uncertainty. In *IEEE Conference on Decision and Control*, volume 21, pages 629–636, Orlando, Florida, USA, 1982.

[24] R. Eising. Between Controllable and Uncontrollable. *Systems and Control Letters*, 4:263–264, 1984.

[25] P. Gahinet. Explicit Controller Formulas for LMI-based $\mathcal{H}_\infty$ Synthesis. *Automatica*, 32(7):1007–1014, 1996.

[26] F. Garelli, R. J. Mantz, and H. De Battista. Limiting Interactions in Decentralized Control of MIMO Systems. *Journal of Process Control*, 16(5):473–483, 2006.

[27] L. E. Ghaoui, F. Oustry, and M. A. Rami. A Cone Complementary Linearization Algorithm for Static Output Feedback and Related Problems. *IEEE Transactions on Automatic Control*, 42:1171–1176, 1997.

[28] L. El. Ghaoui and S. Niculesu. *Advances in Linear Matrix Matrix Inequalities Methods in Control*. SIAM, Philadelphia, 2000.

[29] K. C. Goh, M. G. Safonov, and G. P. Papavassilopoulos. A Global Optimization Approach for the BMI Problem. In *Proceedings of the* 33^{rd} *Conference on Decision and Contro*, pages 2009–2014, Lake Buena Vista, FL, 1994.

[30] K. C. Goh, L. Turan, M. G. Safonov, G. P. Papavassilopoulos, and J. H. Ly. Biaffine Matrix Inequality Properties and Computational Methods. In *Proceedings of American Control Conference*, pages 850–855, Baltimore, Maryland, 1994.

[31] Z. Gong. Decentralized Robust Control of Uncertain Interconnected Systems with Prescribed Degree of Exponential Convergence. *IEEE Transactions on Automatic Control*, 40:704–707, 1995.

[32] G. C. Goodwin, M. E. Salgado, and E. I. Silva. Time-Domain Performance Limitations Arising from Decentralized Architectures and their Relationship to the RGA. *International Journal of Control*, 78(13):1045–1062, 2005.

[33] A. Green and J. Z. Sasiadek. Dynamics and Trajectory Tracking Control of a Two-Link Robot Manipulator. *Journal of Vibration and Control*, 10(10):1415–1440, 2004.

[34] P. Grosdidier. Letter. *Journal of Process Control*, 5(6):399, 1995.

[35] P. Grosdidier and M Morari. Interaction Measures for Systems Under Decentralized Control. *Automatica*, 22:309–319, 1986.

[36] P. Grosdidier and M Morari. The μ Interaction Measure. *Industrial & Engineering Chemistry Research*, 26:1193–1202, 1987.

[37] G. Guo, Y. Wang, and D. Hill. Nonlinear Output Stabilization Control for Multimachine Power Systems-Part I. *IEEE Transactions on Circuits and Systems*, 47(1):46–53, 2000.

[38] V. Havlena and J. Findejs. Application of Model Predictive Control to Advanced Combustion Control. *Control Engineering Practice*, 13(6):671–680, 2005.

[39] D. Henrion, J. Loefberg, M. Kočvara, and M. Stingl. Solving polynomial static output feedback problems with PENBMI. In 44^{th} *IEEE Conference on Decision and Control, and the European Control Conference*, pages 7581–7586, Seville, Spain, 2005.

[40] D. Henrion and S. Tarbouriech. LMI Relaxations for Robust Stability of Linear Systems with Saturating Controls. *Automatica*, 35:1599–1604, 1999.

[41] D. Henrion, S. Tarbouriech, and G. Garcia. Output Feedback Robust Stabilization of Uncertain Linear Systems with Saturating Controls: An LMI Approach. *IEEE Transactions on Automatic Control*, 44(11):2230–2237, 1999.

[42] M. Hovd and S. Skogestad. Improved Independent Design of Robust Decentralized Controllers. *Journal of Process Control*, 3(1):43–51, 1993.

[43] M. Hovd and S. Skogestad. Pairing Criteria for Decentralized Control of Unstable Plants. *Industrial & Engineering Chemistry Research*, 33, 1994.

[44] M. Ikeda. *Decentralized Control of Large Scale Systems*. Springer-Verlag, New York, 1989.

[45] M. Ikeda, D. D. Siljak, and D. E. White. An Inclusion Principle for Dynamic Systems. *IEEE Transactions on Automatic Control*, 43:1040–1055, 1984.

[46] M. Illic and J. Zaborszky. *Dynamics and Control of Large Electric Power Systems*. Wiley, New York, 2000.

[47] S. Jain and F. Khorrami. Robust Decentralized Control of Power System Utilizing only Swing Angle Measurements. *International Journal of Control*, 66(4):581–601, 1997.

[48] H. Jiang, H. Chai, J. Dorsey, and Z. Qu. Toward a Globally Robust Decentralized Control for Large Scale Power Systems. *IEEE Transactions on Control Systems Technology*, 5(3):309–319, 1997.

[49] Z. P. Jiang. Decentralized and Adaptive Nonlinear Tracking of Large-Scale Systems via Output Feedback. *IEEE Transactions on Automatic Control*, 45:2122–2128, 2000.

[50] V. Kariwala. *Multiloop Controller Synthesis and Performance Analysis, PhD Dissertation*. University of Alberta, 2005.

[51] V. Kariwala, F. Forbes, and S. Skogestad. μ-Interaction Measure for Unstable Systems. *International Journal of Automation and Control*, 1(4):295–313, 2007.

[52] V. Kariwala, S. Skogestad, J. F. Forbes, and E. S. Meadows. Input Performance Limitations of Feedback Control. In *American Control Conference*, volume 3, pages 2063–2068, Boston, MA, 2004.

[53] H. K. Khalil. *Nonlinear Systems*. Prentice Hall, 2002.

[54] C. King, J. Chapman, and M. Ilic. Feedback Linearizing Excitation Control on a Full-Scale Power System Model. *IEEE Transcations on Power System*, 9(2):1102–1109, 1994.

[55] P. Kokotovic and M. Arcak. Constructive Nonlinear Control: Progress in the 90s. In *Proceedings of 14th IFAC World Congress*, pages 49–77, Beijing, P. R. China, 1999.

[56] P. Kundur. *Power System Stability and Control*. McGraw-Hill, New York, 1994.

[57] J. Lee and T. F. Edgar. Phase Conditions for Stability of Multi-Loop Control Systems. *Computers and Chemical Engineering*, 23:1623–1630, 2000.

[58] J. Lee and T. F. Edgar. Conditions for Decentralized Integral Controllability. *Journal of Process Control*, 12:797–805, 2002.

[59] G. Leitmann. On One Approach to the Control of Uncertain Systems. *Journal of Dynamic Systems, Measurement and Control*, 115:373–380, 1993.

[60] D. Li, T. Chen, H. J. Marquez, and R. K. Gooden. Life Extending Control of Boiler-Turbine Systems via Model Predictive Methods. *Control Engineering Practice*, 14 (4):319–326, 2006.

[61] D. Lindsley. *Power-Plant Control and Instrumentation.* The Institute of Electrical Engineers, London, United Kingdom, 2000.

[62] J. Loefberg. YALMIP: A Toolbox for Modeling and Optimization in MATLAB. In *IEEE International Symposium on Computer Aided Control Systems Design*, pages 284–289, Taipei, Taiwan, 2004.

[63] K. P. Loh and M. S. Chiu. Robust Decentralized Control of Non-Square Systems. *Chemical Engineering Communications*, 158:157–180, 1997.

[64] K. P. Loh and M. S. Chiu. Robust Decentralized Controller Design for Unstable Systems. *Chemical Engineering Science*, 52(14):2299–2311, 1997.

[65] W. L. Luyben. Simple Method for tuning SISO Controllers in Multivariable Systems. *Industrial Engineering & Chemical Process Design Development*, 25:654–660, 1986.

[66] L. Magni and R. Scattolini. Stabilizing Decentralized Model Predictive Control of Nonlinear Systems. *Automatica*, 42:1231–1236, 2006.

[67] H. J. Marquez. *Nonlinear Control Systems: Analysis and Design.* Wiley-Interscience, Canada, 2003.

[68] D. Q. Mayne. The Design of Linear Multivariable Systems. *Automatica*, 9:201–207, 1976.

[69] P. R. Pagilla, E. O. King, L. H. Drienhoefer, and S. S. Garimella. Robust Observer-Based Control of an Aluminium Strip Processing Line. *IEEE Transactions on Industry Applications*, 36:865–870, 2000.

[70] P. R. Pagilla and Y. Zhu. A Decentralized Output Feedback Controller for a Class of Large-Scale Interconnected Nonlinear Systems. *ASME Journal of Dynamic Systems, Measurement, and Control*, 127:167–172, 2005.

[71] G. Pellegrinetti and J. Bentsman. Nonlinear Control Oriented Modeling- A Benchmark Problem for Controller Design. *IEEE Transactions on Control Systems Technology*, 4(1):57–64, 1996.

[72] I. Postlethwaite and Y. K. Foo. Robustness with Simultaneous Pole and Zero Movement Across the $j\omega$ Axis. *Automatica*, 21(4):433–443, 1985.

[73] Z. Qu, J. Dorsey, J. Bond, and J. Mc.Calley. Application of Robust Control to Sustained Oscillations in Power Systems. *IEEE Transactions on Circuits and Systems-I: Fundamental Theory and Applications*, 39(6):470–476, 1992.

[74] R. Rajamani. Observers for Lipschitz Nonlinear Systems. *IEEE Transactions on Automatic Control*, 43(3):397–401, 1998.

[75] N. W. Rees and C. X. Lu. Some Thoughts on the Advanced Control of Electric Power Plants. *Transactions of the Institute of Measurement and Control*, 24(2):87–106, 2002.

[76] J. E. Rijnsdorp. Interaction in Two-Variable Control Systems for Distillation Columns-I. *Automatica*, 1:15–28, 1965.

[77] R. Rink, D. White, and K. Gooden. SYNSIM: A Computer Simulation Model for the Mildred Lake Steam/Electrical System of Syncrude Canada Ltd. *Technical Report, University of Alberta*, 2005.

[78] H. H. Rosenbrock. *Computer-Aided Control System Design.* Academic Press, London, 1974.

[79] M. Rotkowitz and S. Lall. A Characterization of Convex Problems in Decentralized Control. *IEEE Transactions on Automatic Control*, 51:274–286, 2006.

[80] C. Scherer, P. Gahinet, and M. Chilali. Multiobjective Output Feedback Control via LMI Optimization. *IEEE Transactions on Automatic Control*, 42:896–911, 1997.

[81] D. D. Siljak. *Large-Scale Dynamic Systems: Stability and Structure.* NewYork: North Holland, NewYork, 1978.

[82] D. D. Siljak. *Decentralized Control of Complex Systems*. Academic Publisher, Boston, 1991.

[83] D. D. Siljak and D. M. Stipanovic. Robust Stabilization of Nonlinear Systems: The LMI approach. *Mathematical Problems in Engineering*, 6:461–493, 2000.

[84] D. D. Siljak and D. M. Stipanovic. Autonomous Decentralized Control. In *ASME International Mechanical Engineering Congress and Exposition*, volume 70, pages 761–765, New York, 2001.

[85] D. D. Siljak, D. M. Stipanovic, and A. I. Zecevic. Robust Decentralized Turbine/Governor Control using Linear Matrix Inequalities. *IEEE Transactions on Power Systems*, 17(3):715–722, 2002.

[86] D. D. Siljak and A. I. Zecevic. Control of Large-Scale Systems: Beyond Decentralized Feedback. In 10^{th} *IFAC Symposium on Large Scale Systems*, pages 1–10, Osaka, Japan, 2004.

[87] D. D. Siljak and A. I. Zecevic. Control of Large-Scale Systems: Beyond Decentralized Feedback. *Annual Reviews in Control*, 29:169–179, 2005.

[88] S. Skogestad and M. Hovd. Letter. *Journal of Process Control*, 5(6):399–400, 1995.

[89] S. Skogestad and M. Morari. Robust Performance of Decentralized Control Systems by Independent Designs. *Automatica*, 25:119–125, 1989.

[90] S. Skogestad and M. Morari. Variable Selection for Decentralized Control. *Modeling, Identification and Control*, 13:113–125, 1992.

[91] S. Skogestad and I. Postlethwaite. *Multivariable Feedback Control: Analysis and Design*. John Wiley and Sons, 2005.

[92] S. S. Stankovic, X. B. Chen, M. R. Matausek, and D. D. Siljak. Stochastic Inclusion Principle Applied to Decentralized Automatic Generation Control. *International Journal of Control*, 72:276–288, 1999.

[93] S. S. Stankovic and D. D. Siljak. Contractibility of Overlapping Decentralized Control. *Systems and Control Letters*, 44:189–199, 2001.

[94] S. S. Stankovic, M. J. Stanojevic, and D. D. Siljak. Decentralized Overlapping Control of a Platoon of Vehicles. *IEEE Transactions on Control System Technology*, 8:816–832, 2000.

[95] S. S. Stankovic, D. M. Stipanovic, and D. D. Siljak. Decentralized Dynamic Output Feedback for Robust Stabilization of a Class of Nonlinear Interconnected Systems. *Automatica*, 43:861–867, 2007.

[96] D. M. Stipanović. *Stability and Stabilization of Nonlinear Discontinuous Systems, PhD Dissertation.* School of Engineering, Santa Clara University, 2000.

[97] D. M. Stipanovic and D. D. Siljak. Robust Stability and Stabilization of Discrete-Time Non-Linear Systems: The LMI Approach. *International Journal of Control*, 74(9):873–879, 2001.

[98] A. Swarnakar, H. J. Marquez, and T. Chen. Robust Output Feedback Stabilization of Nonlinear Interconnected Systems with Application to an Industrial Utility Boiler. In *Proceedings of the 2006 American Control Conference*, pages 857–862, Minneapolis, Minnesota, USA, 2006.

[99] A. Swarnakar, H. J. Marquez, and T. Chen. A Design Framework for Overlapping Controllers and its Application. In *Proceedings of the 46th IEEE Conference on Decision and Control*, pages 2809–2814, New Orleans, LA, USA, 2007.

[100] A. Swarnakar, H. J. Marquez, and T. Chen. A New Scheme on Robust Observer Based Control Design for Nonlinear Interconnected Systems with Application to an Industrial Utility Boiler. In *Proceedings of the 2007 American Control Conference*, pages 5601–5606, New York, USA, 2007.

[101] A. Swarnakar, H. J. Marquez, and T. Chen. Robust Stabilization of Nonlinear Interconnected Systems with Application to an Industrial Utility Boiler. *Control Engineering Practice*, 15(6):639–654, 2007.

[102] A. Swarnakar, H. J. Marquez, and T. Chen. A Design Framework for Overlapping Control Design and its Industrial Application. *Control Engineering Practice, doi: 10.1016/j.conengprac.2008.05.009*, 2008.

[103] A. Swarnakar, H. J. Marquez, and T. Chen. A New Scheme on Robust Observer Based Control Design for Interconnected Systems with Application to an Industrial Utility Boiler. *IEEE Transactions on Control Systems Technology*, 16(3), 2008.

[104] A. Swarnakar, H. J. Marquez, and T. Chen. Frequency Domain Multiloop Control Synthesis for Unstable Systems: an Approach Based on μ Interaction Measure. In

Proceedings of the 2008 American Control Conference, pages 3595–3600, Seattle, Washington, USA, 2008.

[105] A. Swarnakar, H. J. Marquez, and T. Chen. Frequency Domain Multiloop Control Synthesis for Unstable Systems and its Application: An Approach Based on μ Interaction Measure. *International Journal of Robust and Nonlinear Control (conditionally accepted with minor revision)*, 2008.

[106] W. Tan, H. J. Marquez, and T. Chen. Stabilizer Design for Industrial Co-generation Systems. *Control Engineering Practice*, 10:615–624, 2002.

[107] F. Tao. *Stochastic Fault Tolerant Control: Analysis and Synthesis, PhD Dissertation.* University of Alberta, 2007.

[108] F. Tao and Q. Zhao. Design of Stochastic Fault Tolerant Control for $\mathcal{H}_2$ Performance. *International Journal of Robust and Nonlinear Control*, 17:1–24, 2007.

[109] J. P. Thevenet, D. Noll, and P. Apkarian. *Nonlinear Spectral SDP Method for BMI-Constrained Problems: Applications to Control Design*. Springer, Netherlands, 2006.

[110] A. F. Vaz and E. J. Davison. On the Quantitative Characterization of Approximate Decentralized Fixed Modes using Transmission Zeros. *Mathematics of Control Signals and Systems*, 2(3):287–302, 1989.

[111] N. Viswanadham and A. Ramakrishna. Decentralized Estimation and Control of Interconnected Systems. *Large Scale Systems*, 3:255–266, 1982.

[112] N. Viswanadham and J. H. Taylor. Sequential Design of Large-Scale Decentralized Control Systems. *International Journal of Control*, 47:257–279, 1988.

[113] L. Wang. Continuous Time Model Predictive Control using Orthonormal Functions. *International Journal of Control*, 74:1588–1600, 2001.

[114] L. Wang. Discrete Model Predictive Controller Design using Laguerre Functions. *Journal of Process Control*, 14:131–142, 2004.

[115] L. Wang and J. A. Rossiter. Tutorial Workshop on Model Predictive Control. In *2007 American Control Conference Workshop*, New York, USA, 2007.

[116] Y. Wang, D. Hill, and G. Guo. Robust Decentralized Control for Multimachine Power Systems. *IEEE Transactions on Circuits and Systems-I: Fundamental Theory and Applications*, 45(3):271–279, 1998.

[117] Wikipedia. Rankine Cycle. *http://en.wikipedia.org/wiki/Rankine_cycle*, April 6, 2008.

[118] S. Xie, L. Xie, Y. Wang, and G. Guo. Decentralized Control of Multimachine Power Systems with Guarenteed Performance. *IEE Proceedings Control Theory and Applications*, 147(3):355–365, 2000.

[119] T. C. Yang, Z. T. Ding, and H. Yu. Decentralized Power System Load Frequency Control Beyond the Limit of Diagonal Dominance. *Electrical power and Energy Systems*, 24:173–184, 2002.

[120] A. I. Zecevic, G. Neskovic, and D. D. Siljak. Robust Decentralized Exciter Control with Linear Feedback. *IEEE Transactions on Power Systems*, 19(2):1096–1103, 2004.

[121] A. I. Zecevic and D. D. Siljak. Design of Robust Static Output Feedback for Large-Scale Systems. *IEEE Transactions on Automatic Control*, 49(11):2040–2044, 2004.

[122] A. I. Zecevic and D. D. Siljak. A New Approach to Control Design with Overlapping Information Structure Constraints. *Automatica*, 41:265–272, 2005.

[123] A. I. Zecevic and D. D. Siljak. Global Low-Rank Enhancement of Decentralized Control for Large-Scale Systems. *IEEE Transactions on Automatic Control*, 50: 740–744, 2005.

[124] W. Z. Zhang, J. Bao, and P. L. Lee. Control Structure Selection Based on Block-Decentralized Integral Controllability. *Industrial & Enginering Chemistry Research*, 42:5152–5156, 2003.

[125] Y. Zhu and P. R. Pagilla. Decentralized Output Feedback Control of a Class of Large-Scale Interconnected Systems. *IMA Journal of Mathematical Control and Information*, 24:57–69, 2007.

Appendix A

Proofs of Theorems

A.1 Proof of Theorem 2.1

Here, a control design algorithm for the autonomous system in (2.12) is first developed, which is then generalized to multiple subsystems in (2.1). Consider a Lyapunov function $v = \mathbf{z}^T\mathbf{P}\mathbf{z}$ [67], where $\mathbf{P}$ is a symmetric positive definite matrix ($\mathbf{P} > \mathbf{0}$). The sufficient conditions for asymptotic stability of the closed loop system in (2.15) are

$$\mathbf{P} > 0,\ \ \mathbf{z}^T\hat{\mathbf{A}}^T\mathbf{P}\mathbf{z} + \mathbf{w}^T\mathbf{G}_r^T\mathbf{P}\mathbf{z} + \mathbf{z}^T\mathbf{P}\hat{\mathbf{A}}\mathbf{z} + \mathbf{z}^T\mathbf{P}\mathbf{G}_r\mathbf{w} < \mathbf{0}.$$

According to the S-procedure [14], when (2.16) is satisfied, the above condition is equivalent to the existence of matrix $\mathbf{P}$ and a number $\tau > 0$ such that $\mathbf{P} > \mathbf{0}$ and

$$\begin{bmatrix} \hat{\mathbf{A}}^T\mathbf{P} + \mathbf{P}\hat{\mathbf{A}} + \tau\alpha^2\mathbf{H}^T\mathbf{H} & \mathbf{P}\mathbf{G}_r \\ \mathbf{G}_r^T\mathbf{P} & -\tau\mathbf{I} \end{bmatrix} < \mathbf{0}. \tag{A-1}$$

Using the Schur's complement this is equivalent to the existence of matrix $\mathbf{Y} > \mathbf{0}$, and

$$\begin{bmatrix} \hat{\mathbf{A}}\mathbf{Y} + \mathbf{Y}\hat{\mathbf{A}}^T & \mathbf{G}_r & \mathbf{Y}\mathbf{H}^T \\ \mathbf{G}_r^T & -\mathbf{I} & 0 \\ \mathbf{H}\mathbf{Y} & 0 & -\gamma\mathbf{I} \end{bmatrix} < \mathbf{0}, \tag{A-2}$$

where $\mathbf{Y} = \tau\mathbf{P}^{-1}$ and $\gamma = \frac{1}{\alpha^2}$. This LMI cannot be used to find the observer-based controller because it is not affine on observer parameters $\mathbf{A}_{obv}$, $\mathbf{B}_{obv}$, $\mathbf{C}_{obv}$ and $\mathbf{D}_{obv}$, which are constant $n \times n$, $n \times p$, $n \times n$, and $n \times p$ matrices, respectively. Hence, a variable transformation is necessary. Partition $\mathbf{Y}$ and $\mathbf{Y}^{-1}$ as

$$\mathbf{Y} = \begin{bmatrix} \mathbf{R}_1 & 0 & 0 \\ 0 & \mathbf{X}_r & \mathbf{M}_r \\ 0 & \mathbf{M}_r^T & \mathbf{V}_r \end{bmatrix},\ \ \mathbf{Y}^{-1} = \begin{bmatrix} \mathbf{R}_2 & 0 & 0 \\ 0 & \mathbf{Y}_r & \mathbf{N}_r \\ 0 & \mathbf{N}_r^T & \mathbf{U}_r \end{bmatrix},$$

where $\mathbf{R}_1$, $\mathbf{R}_2$, $\mathbf{X}_r$ and $\mathbf{Y}_r$ are $n \times n$ and symmetric, $\mathbf{M}_r$ and $\mathbf{N}_r$ are $n \times n_r$ and $\mathbf{Y} > \mathbf{0}$ implies $\mathbf{R}_1 > \mathbf{0}$, $\mathbf{X}_r > \mathbf{0}$, and $\mathbf{Y}_r > \mathbf{0}$. From $\mathbf{Y}^{-1}\mathbf{Y} = \mathbf{I}$, it can be derived that

$\mathbf{Y}^{-1}\left[\begin{array}{ccc}\mathbf{R}_1^T & \mathbf{X}_r^T & \mathbf{M}_r\end{array}\right]^T = \left[\begin{array}{ccc}\mathbf{I} & \mathbf{I} & 0\end{array}\right]^T$, which leads to $\mathbf{Y}^{-1}\mathbf{\Pi}_1 = \mathbf{\Pi}_2$, where,

$$\mathbf{\Pi}_1 \triangleq \begin{bmatrix} \mathbf{R}_1 & 0 & 0 \\ 0 & \mathbf{X}_r & \mathbf{I} \\ 0 & \mathbf{M}_r^T & 0 \end{bmatrix}, \quad \mathbf{\Pi}_2 \triangleq \begin{bmatrix} \mathbf{I} & 0 & 0 \\ 0 & \mathbf{I} & \mathbf{Y}_r \\ 0 & 0 & \mathbf{N}_r^T \end{bmatrix}. \tag{A-3}$$

Pre-and post-multiplying $\mathbf{Y} > 0$ by $\mathbf{\Pi}_2^T$ and $\mathbf{\Pi}_2$, respectively and (A-2) by diag $(\mathbf{\Pi}_2^T, \mathbf{I}, \mathbf{I})$ and diag $(\mathbf{\Pi}_2, \mathbf{I}, \mathbf{I})$, respectively, the conditions are $\mathbf{\Pi}_2^T\mathbf{Y}\mathbf{\Pi}_2 > 0$ and

$$\begin{bmatrix} \mathbf{\Pi}_2^T\hat{\mathbf{A}}\mathbf{Y}\mathbf{\Pi}_2 + \mathbf{\Pi}_2^T\mathbf{Y}\hat{\mathbf{A}}^T\mathbf{\Pi}_2 & \mathbf{\Pi}_2^T\mathbf{G}_r & \mathbf{\Pi}_2^T\mathbf{Y}\mathbf{H}^T \\ \mathbf{G}_r^T\mathbf{\Pi}_2 & -\mathbf{I} & 0 \\ \mathbf{H}\mathbf{Y}\mathbf{\Pi}_2 & 0 & -\gamma\mathbf{I} \end{bmatrix} < \mathbf{0}. \tag{A-4}$$

Some linear algebra shows that

$$\mathbf{\Pi}_2^T\mathbf{Y}\mathbf{\Pi}_2 = \begin{bmatrix} \mathbf{R}_1 & 0 & 0 \\ 0 & \mathbf{X}_r & \mathbf{I} \\ 0 & \mathbf{I} & \mathbf{Y}_r \end{bmatrix} \text{ and}$$

$$\mathbf{\Pi}_2^T\hat{\mathbf{A}}\mathbf{Y}\mathbf{\Pi}_2 = \begin{bmatrix} \mathbf{A}\mathbf{R}_1 + \mathbf{B}\mathbf{L}_1 & \hat{\mathbf{C}}_r & \hat{\mathbf{D}}_r\mathbf{C} \\ 0 & \mathbf{A}\mathbf{X}_r - \hat{\mathbf{C}}_r & \mathbf{A} - \hat{\mathbf{D}}_r\mathbf{C} \\ 0 & \hat{\mathbf{A}}_r & \mathbf{Y}_r\mathbf{A} + \hat{\mathbf{B}}_r\mathbf{C} \end{bmatrix},$$

where $\mathbf{L}_1 \triangleq \mathbf{K}\mathbf{R}_1$,

$$\begin{aligned} \hat{\mathbf{A}}_r &\triangleq \mathbf{Y}_r^T(\mathbf{A} - \mathbf{D}_{obv}\mathbf{C})\mathbf{X}_r + \mathbf{N}_r\mathbf{B}_{obv}\mathbf{C}\mathbf{X}_r - \mathbf{Y}_r^T\mathbf{C}_{obv}\mathbf{M}_r^T + \mathbf{N}_r\mathbf{A}_{obv}\mathbf{M}_r^T, \\ \hat{\mathbf{B}}_r &\triangleq -\mathbf{Y}_r\mathbf{D}_{obv} + \mathbf{N}_r\mathbf{B}_{obv}, \ \hat{\mathbf{C}}_r \triangleq \mathbf{D}_{obv}\mathbf{C}\mathbf{X}_r + \mathbf{C}_{obv}\mathbf{M}_r^T, \ \hat{\mathbf{D}}_r \triangleq \mathbf{D}_{obv}. \end{aligned} \tag{A-5}$$

Moreover,

$$\mathbf{\Pi}_2^T\hat{\mathbf{A}}\mathbf{Y}\mathbf{\Pi}_2 + \mathbf{\Pi}_2^T\mathbf{Y}\hat{\mathbf{A}}^T\mathbf{\Pi}_2 = \begin{bmatrix} \mathcal{F}_{11} & \hat{\mathbf{C}}_r & \hat{\mathbf{D}}_r\mathbf{C} \\ \hat{\mathbf{C}}_r^T & \mathcal{F}_{22} & \mathcal{F}_{23} \\ \mathbf{C}^T\hat{\mathbf{D}}_r^T & \mathcal{F}_{23}^T & \mathcal{F}_{33} \end{bmatrix}, \ \mathbf{\Pi}_2^T\mathbf{G}_r = \begin{bmatrix} 0 \\ \mathbf{G} \\ \mathbf{Y}_r\mathbf{G} \end{bmatrix},$$

$$\text{and } \mathbf{\Pi}_2^T\mathbf{Y}\mathbf{H}^T = \begin{bmatrix} \mathbf{R}_1\mathbf{H}_r^T \\ \mathbf{X}_r\mathbf{H}_r^T \\ \mathbf{H}_r^T \end{bmatrix},$$

where

$$\begin{aligned} \mathcal{F}_{11} &\triangleq \mathbf{A}\mathbf{R}_1 + \mathbf{B}\mathbf{L}_1 + \mathbf{R}_1\mathbf{A}^T + \mathbf{L}_1^T\mathbf{B}^T, \ \mathcal{F}_{22} \triangleq \mathbf{A}\mathbf{X}_r + \mathbf{X}_r\mathbf{A}^T - \hat{\mathbf{C}}_r - \hat{\mathbf{C}}_r^T, \\ \mathcal{F}_{23} &\triangleq \mathbf{A} + \hat{\mathbf{A}}_r^T - \hat{\mathbf{D}}_r\mathbf{C}, \ \mathcal{F}_{33} \triangleq \mathbf{Y}_r\mathbf{A} + \hat{\mathbf{B}}_r\mathbf{C} + \mathbf{A}^T\mathbf{Y}_r + \mathbf{C}^T\hat{\mathbf{B}}_r^T. \end{aligned}$$

This makes the LMIs in (A-4) affine in controller and observer parameters. A linear objective minimization problem ($\min\gamma$) subject to the convex constraints in (A-4) can be easily applied to compute them.

Since $\mathbf{X}_r$ and $\mathbf{Y}_r$ are symmetric matrices, $\mathbf{N}_r$ and $\mathbf{M}_r$ can be chosen square and non-singular such that $\mathbf{N}_r\mathbf{M}_r^T = \mathbf{I} - \mathbf{Y}_r\mathbf{X}_r$. Using singular value decomposition, $[\mathbf{\Sigma}\mathbf{\Lambda}\mathbf{\Omega}^T] =$

svd $(\mathbf{I} - \mathbf{Y}_r\mathbf{X}_r)$. This gives, $\mathbf{N}_r\mathbf{M}_r^T = \mathbf{\Sigma\Lambda\Omega}^T$, $\mathbf{N}_r = \mathbf{\Sigma\Lambda}^{\frac{1}{2}}$, $\mathbf{M}_r = \mathbf{\Omega\Lambda}^{\frac{1}{2}}$. Hence, from (A-5), the parameters $\mathbf{K}$, $\mathbf{A}_{obv}$, $\mathbf{B}_{obv}$, $\mathbf{C}_{obv}$ and $\mathbf{D}_{obv}$ can be easily calculated:

$$\begin{aligned}
\mathbf{A}_{obv} &= \mathbf{N}_r^{-1}(\hat{\mathbf{A}}_r - \mathbf{Y}_r^T\mathbf{A}\mathbf{X}_r + \mathbf{Y}_r^T\mathbf{D}_{obv}\mathbf{C}\mathbf{X}_r - \mathbf{N}_r\mathbf{B}_{obv}\mathbf{C}\mathbf{X}_r + \mathbf{Y}_r^T\mathbf{C}_{obv}\mathbf{M}_r^T)\mathbf{M}_r^{T^{-1}}, \\
\mathbf{K} &= \mathbf{L}_1\mathbf{R}_1^{-1}, \quad \mathbf{D}_{obv} = \hat{\mathbf{D}}_r, \quad \mathbf{C}_{obv} = (\hat{\mathbf{C}}_r - \mathbf{D}_{obv}\mathbf{C}\mathbf{X}_r)(\mathbf{M}_r^T)^{-1}, \\
\mathbf{B}_{obv} &= \mathbf{N}_r^{-1}(\hat{\mathbf{B}}_r + \mathbf{Y}_r\mathbf{D}_{obv}).
\end{aligned}$$

This method does not require that the input matrix $\mathbf{B}$ to be invertible [84], or choice of any parameters by trial and error [70]. Hence, the critical restriction is removed. One can easily verify that when $\mathbf{A}_{obv} = \mathbf{B}_{obv} = \mathbf{C}_{obv} = \mathbf{0}$ (static observer gain), then $\hat{\mathbf{A}}_r = \mathbf{Y}_r^T(\mathbf{A} - \mathbf{D}_{obv}\mathbf{C})\mathbf{X}_r$, $\hat{\mathbf{B}}_r = -\mathbf{Y}_r\mathbf{D}_{obv}$, $\hat{\mathbf{C}}_r = \mathbf{D}_{obv}\mathbf{C}\mathbf{X}_r$ and $\hat{\mathbf{D}}_r = \mathbf{D}_{obv}$. Therefore, the parameters become non affine.

Now, the decentralized control design for the system in (2.1) is quite straightforward with block diagonal Lyapunov function $\mathbf{Y}_D = \text{diag}(\mathbf{Y}_1, \ldots, \mathbf{Y}_N)$ and transformation matrix $\mathbf{\Pi}_{2_D} = \text{diag}(\mathbf{\Pi}_{2_1}, \ldots, \mathbf{\Pi}_{2_N})$. Similar to (A-2), it is easy to verify that the sufficient conditions of the closed loop system in (2.18) to be asymptotically stable under the constraint in (2.19) are $\mathbf{Y}_D > 0$, and

$$\begin{bmatrix}
\hat{\mathbf{A}}_D\mathbf{Y}_D + \mathbf{Y}_D\hat{\mathbf{A}}_D^T & \mathbf{G}_D & \mathbf{Y}_D\mathbf{H}_{1_l}^T & \ldots & \mathbf{Y}_D\mathbf{H}_{N_l}^T \\
\star & -\mathbf{I} & 0 & \ldots & 0 \\
\star & \star & -\gamma_1\mathbf{I} & \ldots & 0 \\
\star & \star & \star & \ddots & \vdots \\
\star & \star & \star & \star & -\gamma_N\mathbf{I}
\end{bmatrix} < \mathbf{0}.$$

Pre-and post-multiplying $\mathbf{Y}_D > 0$ by $\mathbf{\Pi}_{2_D}^T$ and $\mathbf{\Pi}_{2_D}$, respectively, and the above constraint by diag $(\mathbf{\Pi}_{2_D}^T, \mathbf{I}, \mathbf{I})$ and diag $(\mathbf{\Pi}_{2_D}, \mathbf{I}, \mathbf{I})$, respectively, the LMIs become affine in controller and observer parameters.

■

A.2 Proof of Matching Condition

Assume that $\mathbf{H}_r$ has full rank ($\mathbf{H}_r^T\mathbf{H}_r$ is positive definite) and $(\mathbf{A}, \mathbf{H}_r)$ is detectable [83]. With $\mathbf{G} = \mathbf{B}$, some constraints in the LMI formulation of (A-4) are

$$\gamma > 0, \quad \mathbf{R}_1 > 0, \quad \mathbf{X}_r > 0, \quad \mathbf{Y}_r > 0,$$

$$\mathbf{A}\mathbf{X}_r + \mathbf{X}_r\mathbf{A}^T - \hat{\mathbf{C}}_r - \hat{\mathbf{C}}_r^T + \mathbf{B}\mathbf{B}^T + \frac{\mathbf{X}_r\mathbf{H}_r^T\mathbf{H}_r\mathbf{X}_r}{\gamma} < 0, \tag{A-6}$$

$$\mathbf{Y}_r\mathbf{A} + \hat{\mathbf{B}}_r\mathbf{C} + (\mathbf{Y}_r\mathbf{A} + \hat{\mathbf{B}}_r\mathbf{C})^T + \mathbf{Y}_r\mathbf{B}\mathbf{B}^T\mathbf{Y}_r + \frac{\mathbf{H}_r^T\mathbf{H}_r}{\gamma} < 0, \tag{A-7}$$

$$(\mathbf{A} + \mathbf{B}\mathbf{K})\mathbf{R}_1 + \mathbf{R}_1(\mathbf{A} + \mathbf{B}\mathbf{K})^T + \frac{\mathbf{R}_1\mathbf{H}_r^T\mathbf{H}_r\mathbf{R}_1}{\gamma} < 0. \tag{A-8}$$

The feasibility of (A-6) can be easily proved using the approach in [83]. To prove the feasibility of (A-7), consider the Riccati equation $\mathbf{A}^T\mathbf{Y}_m + \mathbf{Y}_m\mathbf{A} + \mathbf{Y}_m\mathbf{B}\mathbf{B}^T\mathbf{Y}_m + \frac{(\mathbf{H}_r^T\mathbf{H}_r+\epsilon\mathbf{C}^T\mathbf{C})}{\bar{\gamma}} = \mathbf{0}$, where $\epsilon > 0$ and $0 < \bar{\gamma} < \gamma$. Since $(\mathbf{A}, \mathbf{H}_r)$ and $(\mathbf{A}, \mathbf{C})$ are detectable, there always exist a unique $\mathbf{Y}_m > 0$ to the Riccati equation such that $(\mathbf{A} - \mathbf{B}\mathbf{B}^T\mathbf{Y}_m)$ is a stable matrix. Therefore, by choosing $\mathbf{Y}_r = \mathbf{Y}_m$ and $\hat{\mathbf{B}}_r = \frac{\epsilon\,\mathbf{C}^T}{2\gamma}$, a solution to the LMI for any $\gamma > 0$ can be achieved. Here, ϵ determines the convergence rate of observer. Finally, to prove feasibility of (A-8), consider the Lyapunov equation $\mathbf{A}_c^T\mathbf{R}_l + \mathbf{R}_l\mathbf{A}_c + \frac{\mathbf{H}_r^T\mathbf{H}_r}{\bar{\gamma}} = 0$, where $\mathbf{A}_c$ has all eigenvalues in the left half of s-plane. Since $\mathbf{H}_r^T\mathbf{H}_r > 0$, $\mathbf{A}_c$ is stable and $\mathbf{R}_l^{-1}\mathbf{A}_c^T + \mathbf{A}_c\mathbf{R}_l^{-1} + \frac{\mathbf{R}_l^{-1}\mathbf{H}_1^T\mathbf{H}_1\mathbf{R}_l^{-1}}{\gamma} < 0$, the choice of $\mathbf{R}_1 = \mathbf{R}_l^{-1}$and $\mathbf{A} + \mathbf{B}\mathbf{K} = \mathbf{A}_c$, leads to the solution of LMI for any $\gamma > 0$.

■

A.3 Proof of Theorem 2.2

With a Lyapunov function $v(\tilde{\mathbf{x}}) = \tilde{\mathbf{x}}^T\mathbf{P}\tilde{\mathbf{x}}$, the sufficient conditions for the stability in (2.30) are

$$\begin{aligned} \mathbf{P} &> \mathbf{0}, \\ \text{and } \tilde{\mathbf{x}}^T\hat{\mathbf{A}}_k^T\mathbf{P}\tilde{\mathbf{x}} + \mathbf{h}^T\mathbf{G}_k^T\mathbf{P}\tilde{\mathbf{x}} + \tilde{\mathbf{x}}^T\mathbf{P}\hat{\mathbf{A}}_k\tilde{\mathbf{x}} + \tilde{\mathbf{x}}^T\mathbf{P}\mathbf{G}_k\mathbf{h} &< \mathbf{0}. \end{aligned} \tag{A-9}$$

According to the S-procedure [14], when (2.29) is satisfied, condition (A-9) is equivalent to the existence of matrix $\mathbf{P}$ and a number $\tau > 0$ such that $\mathbf{P} > \mathbf{0}$ and

$$\begin{bmatrix} \hat{\mathbf{A}}_k^T\mathbf{P} + \mathbf{P}\hat{\mathbf{A}}_k + \tau\alpha^2\mathbf{H}_k^T\mathbf{H}_k & \mathbf{P}\mathbf{G}_k \\ \mathbf{G}_k^T\mathbf{P} & -\tau\mathbf{I} \end{bmatrix} < \mathbf{0}. \tag{A-10}$$

Using Schur's complement, (A-10) is equivalent to the existence of matrix $\mathbf{Y}$ satisfying

$$\mathbf{Y} > 0, \tag{A-11}$$

$$\begin{bmatrix} \hat{\mathbf{A}}_k\mathbf{Y} + \mathbf{Y}\hat{\mathbf{A}}_k^T & \mathbf{G}_k & \mathbf{Y}\mathbf{H}_k^T \\ \mathbf{G}_k^T & -\mathbf{I} & 0 \\ \mathbf{H}_k\mathbf{Y} & 0 & -\gamma\mathbf{I} \end{bmatrix} < 0, \tag{A-12}$$

where $\mathbf{Y} = \tau\mathbf{P}^{-1}$ and $\gamma = \frac{1}{\alpha^2}$. It is well known that α can be termed as degree of robustness; therefore, γ is a measure of the degree of robustness. The LMIs in (A-11) and (A-12) cannot be used to find the controller because it is not affine in controller parameters $\mathbf{A}_k$, $\mathbf{B}_k$, $\mathbf{C}_k$ and $\mathbf{D}_k$. Hence, the well-known "change of controller variables method" is used. If $\mathbf{A}$ and $\mathbf{A}_k$ are $n \times n$ and $n_k \times n_k$, respectively, partition $\mathbf{Y}$ and $\mathbf{Y}^{-1}$ as

$$\mathbf{Y} = \begin{bmatrix} \mathbf{X}_1 & \mathbf{M}_1 \\ \mathbf{M}_1^T & \mathbf{V}_1 \end{bmatrix}, \quad \mathbf{Y}^{-1} = \begin{bmatrix} \mathbf{Y}_1 & \mathbf{N}_1 \\ \mathbf{N}_1^T & \mathbf{U}_1 \end{bmatrix}, \tag{A-13}$$

where $\mathbf{X}_1$ and $\mathbf{Y}_1$ are $n \times n$ and symmetric, $\mathbf{M}_1$ and $\mathbf{N}_1$ are $n \times n_k$ and $\mathbf{Y} > \mathbf{0}$ implies $\mathbf{X}_1 > \mathbf{0}, \mathbf{Y}_1 > \mathbf{0}$. From $\mathbf{Y}^{-1}\mathbf{Y} = \mathbf{I}$, it can be derived that

$$\mathbf{Y}^{-1}\begin{bmatrix} \mathbf{X}_1 \\ \mathbf{M}_1^T \end{bmatrix} = \begin{bmatrix} \mathbf{I} \\ \mathbf{0} \end{bmatrix},$$

which leads to $\mathbf{Y}^{-1}\mathbf{\Pi}_1 = \mathbf{\Pi}_2$, where,

$$\mathbf{\Pi}_1 \triangleq \begin{bmatrix} \mathbf{X}_1 & \mathbf{I} \\ \mathbf{M}_1^T & \mathbf{0} \end{bmatrix}, \quad \mathbf{\Pi}_2 \triangleq \begin{bmatrix} \mathbf{Y}_1 & \mathbf{N}_1 \\ \mathbf{N}_1^T & \mathbf{U}_1 \end{bmatrix}\begin{bmatrix} \mathbf{X}_1 & \mathbf{I} \\ \mathbf{M}_1^T & \mathbf{0} \end{bmatrix} = \begin{bmatrix} \mathbf{I} & \mathbf{Y}_1 \\ \mathbf{0} & \mathbf{N}_1^T \end{bmatrix}. \tag{A-14}$$

Pre- and post multiplying (A-11) by $\mathbf{\Pi}_2^T$ and $\mathbf{\Pi}_2$, respectively and (A-12) by $\mathrm{diag}(\mathbf{\Pi}_2^T, \mathbf{I}, \mathbf{I})$ and $\mathrm{diag}(\mathbf{\Pi}_2, \mathbf{I}, \mathbf{I})$, respectively

$$\begin{aligned} \mathbf{\Pi}_2^T\mathbf{Y}\mathbf{\Pi}_2 &> \mathbf{0}, \\ \begin{bmatrix} \mathbf{\Pi}_2^T\hat{\mathbf{A}}_k\mathbf{Y}\mathbf{\Pi}_2 + \mathbf{\Pi}_2^T\mathbf{Y}\hat{\mathbf{A}}_k^T\mathbf{\Pi}_2 & \mathbf{\Pi}_2^T\mathbf{G}_k & \mathbf{\Pi}_2^T\mathbf{Y}\mathbf{H}_k^T \\ \mathbf{G}_k^T\mathbf{\Pi}_2 & -\mathbf{I} & \mathbf{0} \\ \mathbf{H}_k\mathbf{Y}\mathbf{\Pi}_2 & \mathbf{0} & -\gamma\mathbf{I} \end{bmatrix} &< \mathbf{0}. \end{aligned} \tag{A-15}$$

Now, straightforward calculation shows that

$$\begin{aligned} \mathbf{\Pi}_2^T\mathbf{Y}\mathbf{\Pi}_2 &= \begin{bmatrix} \mathbf{X}_1 & \mathbf{I} \\ \mathbf{I} & \mathbf{Y}_1 \end{bmatrix}, \quad \text{and} \\ \mathbf{\Pi}_2^T\hat{\mathbf{A}}_k\mathbf{Y}\mathbf{\Pi}_2 &= \begin{bmatrix} \mathbf{A}\mathbf{X}_1 + \mathbf{B}\hat{\mathbf{C}}_1 & \mathbf{A} + \mathbf{B}\hat{\mathbf{D}}_1\mathbf{C} \\ \hat{\mathbf{A}}_1 & \mathbf{Y}_1\mathbf{A} + \hat{\mathbf{B}}_1\mathbf{C} \end{bmatrix}, \end{aligned}$$

where

$$\begin{aligned} \hat{\mathbf{A}}_1 &\triangleq \mathbf{Y}_1^T(\mathbf{A} + \mathbf{B}\mathbf{D}_k\mathbf{C})\mathbf{X}_1 + \mathbf{N}_1\mathbf{B}_k\mathbf{C}\mathbf{X}_1 + \mathbf{Y}_1^T\mathbf{B}\mathbf{C}_k\mathbf{M}_1^T + \mathbf{N}_1\mathbf{A}_k\mathbf{M}_1^T, \\ \hat{\mathbf{B}}_1 &\triangleq \mathbf{Y}_1\mathbf{B}\mathbf{D}_k + \mathbf{N}_1\mathbf{B}_k, \ \hat{\mathbf{C}}_1 \triangleq \mathbf{D}_k\mathbf{C}\mathbf{X}_1 + \mathbf{C}_k\mathbf{M}_1^T, \ \hat{\mathbf{D}}_1 \triangleq \mathbf{D}_k. \end{aligned} \tag{A-16}$$

Hence,

$$\mathbf{\Pi}_2^T\hat{\mathbf{A}}_k\mathbf{Y}\mathbf{\Pi}_2 + \mathbf{\Pi}_2^T\mathbf{Y}\hat{\mathbf{A}}_k^T\mathbf{\Pi}_2 = \begin{bmatrix} \mathcal{F}_{11} & \mathcal{F}_{12} \\ \mathcal{F}_{12}^T & \mathcal{F}_{22} \end{bmatrix},$$

where

$$\begin{aligned} \mathcal{F}_{11} &\triangleq \mathbf{A}\mathbf{X}_1 + \mathbf{X}_1\mathbf{A}^T + \mathbf{B}\hat{\mathbf{C}}_1 + (\mathbf{B}\hat{\mathbf{C}}_1)^T, \ \mathcal{F}_{12} \triangleq \mathbf{A} + \hat{\mathbf{A}}_1^T + \mathbf{B}\hat{\mathbf{D}}_1\mathbf{C}, \\ \mathcal{F}_{22} &\triangleq \mathbf{Y}_1\mathbf{A} + \hat{\mathbf{B}}_1\mathbf{C} + \mathbf{A}^T\mathbf{Y}_1 + \mathbf{C}^T\hat{\mathbf{B}}_1^T. \end{aligned} \tag{A-17}$$

Furthermore,

$$\mathbf{\Pi}_2^T\mathbf{G}_k = \begin{bmatrix} \mathbf{I} & \mathbf{0} \\ \mathbf{Y}_1^T & \mathbf{N}_1 \end{bmatrix}\begin{bmatrix} \mathbf{G} \\ \mathbf{0} \end{bmatrix} = \begin{bmatrix} \mathbf{G} \\ \mathbf{Y}_1\mathbf{G} \end{bmatrix}, \quad \text{and}$$

$$\mathbf{\Pi}_2^T\mathbf{Y}\mathbf{H}_k^T = \mathbf{\Pi}_1^T\mathbf{H}_k^T = \begin{bmatrix} \mathbf{X}_1 & \mathbf{M}_1 \\ \mathbf{I} & \mathbf{0} \end{bmatrix}\begin{bmatrix} \mathbf{H}_1^T \\ \mathbf{0} \end{bmatrix} = \begin{bmatrix} \mathbf{X}_1\mathbf{H}_1^T \\ \mathbf{H}_1^T \end{bmatrix}.$$

This variable transformation makes the LMIs in (A-11) and (A-12) affine in the controller parameters. Since $\mathbf{X}_1$ and $\mathbf{Y}_1$ are symmetric matrices, $\mathbf{N}_1$ and $\mathbf{M}_1$ can be chosen square and non-singular such that $\mathbf{N}_1\mathbf{M}_1^T = \mathbf{I} - \mathbf{Y}_1\mathbf{X}_1$. Using the singular value decomposition

$$\left[\mathbf{\Sigma}\mathbf{\Lambda}\mathbf{\Phi}^T\right] = \text{svd}\left(\mathbf{I} - \mathbf{Y}_1\mathbf{X}_1\right).$$

Therefore, $\mathbf{N}_1$ and $\mathbf{M}_1$ can be calculated as

$$\mathbf{N}_1\mathbf{M}_1^T = \mathbf{\Sigma}\mathbf{\Lambda}\mathbf{\Phi}^T,\ \mathbf{N}_1 = \mathbf{\Sigma}\mathbf{\Lambda}^{\frac{1}{2}},\ \mathbf{M}_1 = \mathbf{\Phi}\mathbf{\Lambda}^{\frac{1}{2}}. \tag{A-18}$$

This allows to calculate $\mathbf{A}_k$, $\mathbf{B}_k$, $\mathbf{C}_k$ and $\mathbf{D}_k$ from (A-16)

$$\begin{aligned}
\mathbf{D}_k &= \hat{\mathbf{D}}_1, \\
\mathbf{C}_k &= \left(\hat{\mathbf{C}}_1 - \hat{\mathbf{D}}_1\mathbf{C}\mathbf{X}_1\right)\left(\mathbf{M}_1^T\right)^{-1}, \\
\mathbf{B}_k &= \left(\mathbf{N}_1\right)^{-1}\left(\hat{\mathbf{B}}_1 - \mathbf{Y}_1\mathbf{B}\hat{\mathbf{D}}_1\right), \\
\mathbf{A}_k &= \left(\mathbf{N}_1\right)^{-1}\left(\hat{\mathbf{A}}_1 - \mathbf{Y}_1\mathbf{A}\mathbf{X}_1 - \mathbf{Y}_1\mathbf{B}\hat{\mathbf{C}}_1 - \mathbf{N}_1\mathbf{B}_k\mathbf{C}\mathbf{X}_1\right)\left(\mathbf{M}_1^T\right)^{-1}.
\end{aligned}$$

■

A.4 Proof of Theorem 2.3

The mathematical treatment follows along the same lines as in Theorem 2.2. From (A-11) and (A-12), it is easy to say that the sufficient conditions of the closed loop system in (2.41) to be asymptotically stable under the quadratic constraint in (2.42) are

$$\mathbf{Y}_D > 0, \tag{A-19}$$

$$\begin{bmatrix} (\hat{\mathbf{A}}_{D_k}\mathbf{Y}_D + \mathbf{Y}_D\hat{\mathbf{A}}_{D_k}^T) & \mathbf{G}_{D_k} & \mathbf{Y}_D\mathbf{H}_{1_k}^T & \dots & \mathbf{Y}_D\mathbf{H}_{N_k}^T \\ \star & -\mathbf{I} & \mathbf{0} & \dots & \mathbf{0} \\ \star & \star & -\gamma_1\mathbf{I} & \dots & \mathbf{0} \\ \vdots & \vdots & \vdots & \ddots & \vdots \\ \star & \star & \star & \dots & -\gamma_N\mathbf{I} \end{bmatrix} < 0. \tag{A-20}$$

Similar to Theorem 2.2, defining new variables as in (A-13) and (A-14),

$$\begin{aligned}
\mathbf{Y}_i &\triangleq \begin{bmatrix} \mathbf{X}_{1_i} & \mathbf{M}_i \\ \mathbf{M}_i^T & \mathbf{V}_i \end{bmatrix},\ \mathbf{Y}_i^{-1} \triangleq \begin{bmatrix} \mathbf{Y}_{1_i} & \mathbf{N}_i \\ \mathbf{N}_i^T & \mathbf{U}_i \end{bmatrix},\ \mathbf{\Pi}_{2_i} \triangleq \begin{bmatrix} \mathbf{I} & \mathbf{Y}_{1_i} \\ \mathbf{0} & \mathbf{N}_i^T \end{bmatrix}, \\
\hat{\mathbf{A}}_i &\triangleq \mathbf{Y}_{1_i}^T\left(\mathbf{A}_i + \mathbf{B}_i\mathbf{D}_{k_i}\mathbf{C}_i\right)\mathbf{X}_{1_i} + \mathbf{N}_i\mathbf{B}_{k_i}\mathbf{C}_i\mathbf{X}_{1_i} + \mathbf{Y}_{1_i}^T\mathbf{B}_i\mathbf{C}_{k_i}\mathbf{M}_i^T \\
&\quad + \mathbf{N}_i\mathbf{A}_{k_i}\mathbf{M}_i^T, \\
\hat{\mathbf{B}}_i &\triangleq \mathbf{Y}_{1_i}\mathbf{B}_i\mathbf{D}_{k_i} + \mathbf{N}_i\mathbf{B}_{k_i},\ \hat{\mathbf{C}}_i \triangleq \mathbf{D}_{k_i}\mathbf{C}_i\mathbf{X}_{1_i} + \mathbf{C}_{k_i}\mathbf{M}_i^T,\ \hat{\mathbf{D}}_i \triangleq \mathbf{D}_{k_i},
\end{aligned} \tag{A-21}$$

where $\mathbf{X}_{1_i}$ and $\mathbf{Y}_{1_i}$ are $n_i \times n_i$ and symmetric matrices, $\mathbf{M}_i$ and $\mathbf{N}_i$ are $n_i \times n_{k_i}$ and $\mathbf{Y}_i > 0$ implies $\mathbf{X}_{1_i} > 0$, $\mathbf{Y}_{1_i} > 0$. Hence, for the overall system

$$\mathbf{Y}_D = \text{diag}(\mathbf{Y}_1, \mathbf{Y}_2, \ldots, \mathbf{Y}_N), \quad \mathbf{\Pi}_{2_D} = \text{diag}(\mathbf{\Pi}_{2_1}, \mathbf{\Pi}_{2_2}, \ldots, \mathbf{\Pi}_{2_N}),$$

and straightforward calculation shows that

$$\begin{aligned}
\mathbf{\Pi}_{2_D}^T \mathbf{Y}_D \mathbf{\Pi}_{2_D} &= \text{diag}\left[\begin{pmatrix} \mathbf{X}_{1_1} & \mathbf{I} \\ \mathbf{I} & \mathbf{Y}_{1_1} \end{pmatrix}, \ldots, \begin{pmatrix} \mathbf{X}_{1_N} & \mathbf{I} \\ \mathbf{I} & \mathbf{Y}_{1_N} \end{pmatrix}\right], \\
\mathbf{\Pi}_{2_D}^T \mathbf{G}_{D_k} &= \text{diag}\left[\begin{pmatrix} \mathbf{G}_1 \\ \mathbf{Y}_{1_1}\mathbf{G}_1 \end{pmatrix}, \ldots, \begin{pmatrix} \mathbf{G}_N \\ \mathbf{Y}_{1_N}\mathbf{G}_N \end{pmatrix}\right], \\
\mathbf{\Pi}_{2_i}^T \hat{\mathbf{A}}_{k_i} \mathbf{Y}_i \mathbf{\Pi}_{2_i} &= \begin{bmatrix} \mathbf{A}_i\mathbf{X}_{1_i} + \mathbf{B}_i\hat{\mathbf{C}}_i & \mathbf{A}_i + \mathbf{B}_i\hat{\mathbf{D}}_i\mathbf{C}_i \\ \hat{\mathbf{A}}_i & \mathbf{Y}_{1_i}\mathbf{A}_i + \hat{\mathbf{B}}_i\mathbf{C}_i \end{bmatrix}, \\
\mathbf{\Pi}_{2_D}^T (\hat{\mathbf{A}}_{D_k}\mathbf{Y}_D + \mathbf{Y}_D\hat{\mathbf{A}}_{D_k}^T)\mathbf{\Pi}_{2_D} &= \text{diag}\left[\begin{pmatrix} (\mathcal{F}_{11})_1 & (\mathcal{F}_{12})_1 \\ (\mathcal{F}_{12})_1^T & (\mathcal{F}_{22})_1 \end{pmatrix}, \ldots, \right. \\
&\qquad \left. \begin{pmatrix} (\mathcal{F}_{11})_N & (\mathcal{F}_{12})_N \\ (\mathcal{F}_{12})_N^T & (\mathcal{F}_{22})_N \end{pmatrix}\right],
\end{aligned}$$

where

$$\begin{aligned}
(\mathcal{F}_{11})_i &\triangleq \mathbf{A}_i\mathbf{X}_{1_i} + \mathbf{X}_{1_i}\mathbf{A}_i^T + \mathbf{B}_i\hat{\mathbf{C}}_i + (\mathbf{B}_i\hat{\mathbf{C}}_i)^T, \\
(\mathcal{F}_{12})_i &\triangleq \mathbf{A}_i + \hat{\mathbf{A}}_i^T + \mathbf{B}_i\hat{\mathbf{D}}_i\mathbf{C}_i, \\
(\mathcal{F}_{22})_i &\triangleq \mathbf{Y}_{1_i}\mathbf{A}_i + \hat{\mathbf{B}}_i\mathbf{C}_i + \mathbf{A}_i^T\mathbf{Y}_{1_i} + \mathbf{C}_i^T\hat{\mathbf{B}}_i^T.
\end{aligned}$$

For two interconnected subsystems, the structure of $\mathbf{H}_{1_k}^T$ will be

$$\begin{bmatrix} \mathbf{h}_{11} & 0 & \mathbf{h}_{12} & 0 \\ 0 & 0 & 0 & 0 \\ \mathbf{h}_{12} & 0 & \mathbf{h}_{22} & 0 \\ 0 & 0 & 0 & 0 \end{bmatrix}, \text{ which gives } \mathbf{\Pi}_{2_D}^T \mathbf{Y}_D \mathbf{H}_{1_k}^T = \begin{bmatrix} \mathbf{X}_{1_1}\mathbf{h}_{11} & 0 & \mathbf{X}_{1_1}\mathbf{h}_{12} & 0 \\ \mathbf{h}_{11} & 0 & \mathbf{h}_{12} & 0 \\ \mathbf{X}_{1_2}\mathbf{h}_{12} & 0 & \mathbf{X}_{1_2}\mathbf{h}_{22} & 0 \\ \mathbf{h}_{12} & 0 & \mathbf{h}_{22} & 0 \end{bmatrix}.$$

Pre- and post multiplying (A-19) by $\mathbf{\Pi}_{2_D}^T$ and $\mathbf{\Pi}_{2_D}$, respectively and (A-20) by $\text{diag}(\mathbf{\Pi}_{2_D}^T, \mathbf{I}, \mathbf{I})$ and $\text{diag}(\mathbf{\Pi}_{2_D}, \mathbf{I}, \mathbf{I})$, respectively and adding pole placement constraints, the result follows.

■

A.5 Proof of Theorem 3.1

Consider a quadratic Lyapunov function $v = \mathbf{x}_{cl}^T\mathbf{P}\mathbf{x}_{cl}$. The sufficient conditions for stability of the closed loop system can be expressed as $\mathbf{P} > 0$ (positive definite), and

$$\begin{aligned}
\dot{v} &= \dot{\mathbf{x}}_{cl}^T\mathbf{P}\mathbf{x}_{cl} + \mathbf{x}_{cl}^T\mathbf{P}\dot{\mathbf{x}}_{cl} = \mathbf{x}_{cl}^T\hat{\mathbf{A}}_D^T\mathbf{P}\mathbf{x}_{cl} + \mathbf{h}_r^T(\mathbf{x}_{cl})\mathbf{P}\mathbf{x}_{cl} + \mathbf{x}_{cl}^T\mathbf{P}\hat{\mathbf{A}}_D\mathbf{x}_{cl} \\
&\quad + \mathbf{x}_{cl}^T\mathbf{P}\mathbf{h}_r(\mathbf{x}_{cl}) < 0.
\end{aligned}$$

The above inequality can be written as

$$\begin{bmatrix} \mathbf{x}_{cl}^T & \mathbf{h}_r^T(\mathbf{x}_{cl}) \end{bmatrix} \begin{bmatrix} \hat{\mathbf{A}}_D^T\mathbf{P} + \mathbf{P}\hat{\mathbf{A}}_D & \mathbf{P} \\ \star & \mathbf{0} \end{bmatrix} \begin{bmatrix} \mathbf{x}_{cl} \\ \mathbf{h}_r(\mathbf{x}_{cl}) \end{bmatrix} < \mathbf{0}, \tag{A-22}$$

and the nonlinear quadratic bound in (3.5) or (3.7) is equivalent to

$$\begin{bmatrix} \mathbf{x}_{cl}^T & \mathbf{h}_r^T(\mathbf{x}_{cl}) \end{bmatrix} \begin{bmatrix} \alpha^2\mathbf{H}_l^T\mathbf{H}_l & \mathbf{0} \\ \mathbf{0} & -\mathbf{I} \end{bmatrix} \begin{bmatrix} \mathbf{x}_{cl} \\ \mathbf{h}_r(\mathbf{x}_{cl}) \end{bmatrix} \geq \mathbf{0}. \tag{A-23}$$

Combination of (A-22) and (A-23) according to the S-procedure gives $\mathbf{P} > 0$ and

$$\begin{bmatrix} \mathbf{x}_{cl}^T & \mathbf{h}_r^T(\mathbf{x}_{cl}) \end{bmatrix} \begin{bmatrix} \hat{\mathbf{A}}_D^T\mathbf{P} + \mathbf{P}\hat{\mathbf{A}}_D + \tau\alpha^2\mathbf{H}_l^T\mathbf{H}_l & \mathbf{P} \\ \star & -\tau\mathbf{I} \end{bmatrix} \begin{bmatrix} \mathbf{x}_{cl} \\ \mathbf{h}_r(\mathbf{x}_{cl}) \end{bmatrix} < 0. \tag{A-24}$$

The parameter τ allows the control engineers to combine several quadratic inequalities into a single inequality. Since, $-\tau\mathbf{I} < 0$, from (A-24), the conditions for stability are $\mathbf{P} > 0$ and

$$\begin{bmatrix} \hat{\mathbf{A}}_D^T\mathbf{P} + \mathbf{P}\hat{\mathbf{A}}_D + \tau\alpha^2\mathbf{H}_l^T\mathbf{H}_l & \mathbf{P} \\ \star & -\tau\mathbf{I} \end{bmatrix} < \mathbf{0}. \tag{A-25}$$

Pre- and post multiplying $\mathbf{P} > 0$ by $\tau\mathbf{P}^{-1}$ and $\tau\mathbf{P}^{-1}$, respectively and (A-25) by diag $(\tau\mathbf{P}^{-1}, I)$ and diag $(\tau\mathbf{P}^{-1}, I)$, respectively, the new relations are

$$\tau\mathbf{P}^{-1}(\mathbf{P})\tau\mathbf{P}^{-1} > 0, \quad \begin{bmatrix} \tau\mathbf{P}^{-1}(\hat{\mathbf{A}}_D^T\mathbf{P} + \mathbf{P}\hat{\mathbf{A}}_D + \tau\alpha^2\mathbf{H}_l^T\mathbf{H}_l)\tau\mathbf{P}^{-1} & \tau\mathbf{I} \\ \star & -\tau\mathbf{I} \end{bmatrix} < 0.$$

Since, τ is a positive scalar, defining $\mathbf{Y} = \tau\mathbf{P}^{-1}$, the conditions are $\mathbf{Y} > 0$ and

$$\begin{bmatrix} \mathbf{Y}\hat{\mathbf{A}}_D^T + \hat{\mathbf{A}}_D\mathbf{Y} + \alpha^2\mathbf{Y}\mathbf{H}_l^T\mathbf{H}_l\mathbf{Y} & \mathbf{I} \\ \star & -\mathbf{I} \end{bmatrix} < 0. \tag{A-26}$$

This LMI cannot be used to compute the controller parameters because it is not affine in $\mathbf{K}_d$. Therefore, using the Schur's complement, (A-26) can be written as

$$\hat{\mathbf{A}}_D\mathbf{Y} + \mathbf{Y}\hat{\mathbf{A}}_D^T + \frac{1}{\gamma}\mathbf{Y}\mathbf{H}_l^T\mathbf{H}_l\mathbf{Y} + \mathbf{I} < 0,$$

where $\gamma = \frac{1}{\alpha^2}$. It should be noted that the inequality is in the form of $\mathbf{\Psi} + \mathbf{S} + \mathbf{S^T} < 0$, with $\mathbf{\Psi} = \mathbf{I} + \frac{1}{\gamma}\mathbf{Y}\mathbf{H}_l^T\mathbf{H}_l\mathbf{Y}$. Therefore, application of the reciprocal projection lemma gives

$$\begin{bmatrix} \mathbf{I} + \frac{1}{\gamma}\mathbf{Y}\mathbf{H}_l^T\mathbf{H}_l\mathbf{Y} + \mathbf{X} - (\mathbf{W} + \mathbf{W}^T) & \mathbf{Y}\hat{\mathbf{A}}_D^T + \mathbf{W}^T \\ \star & -\mathbf{X} \end{bmatrix} < 0, \tag{A-27}$$

where $\mathbf{X}$ can be any given positive definite matrix and $\mathbf{W}$ is a decision variable. Hence, selecting $\mathbf{X} = \mathbf{I}$ and pre- and post- multiplying by diag$(\mathbf{Y}^{-1}, \mathbf{I})$ and diag$(\mathbf{Y}^{-1}, \mathbf{I})$, respectively

$$\begin{bmatrix} \mathbf{Y}^{-1}\mathbf{Y}^{-1} + \frac{1}{\gamma}\mathbf{H}_l^T\mathbf{H}_l + \mathbf{Y}^{-1}(\mathbf{I} - \mathbf{W} - \mathbf{W}^T)\mathbf{Y}^{-1} & \hat{\mathbf{A}}_D^T + \mathbf{Y}^{-1}\mathbf{W}^T \\ \star & -\mathbf{I} \end{bmatrix} < 0.$$

This can be expanded as

$$\begin{bmatrix} \frac{1}{\gamma}\mathbf{H}_l^T\mathbf{H}_l + \mathbf{Y}^{-1}(\mathbf{I}-\mathbf{W}-\mathbf{W}^T)\mathbf{Y}^{-1} & \hat{\mathbf{A}}_D^T + \mathbf{Y}^{-1}\mathbf{W}^T \\ \star & -\mathbf{I} \end{bmatrix} - \begin{bmatrix} \mathbf{Y}^{-1} \\ 0 \end{bmatrix}(-\mathbf{I})^{-1} \times \begin{bmatrix} \mathbf{Y}^{-1} & 0 \end{bmatrix} < 0.$$

Since, this inequality is in the form of $\Phi_{11} - \Phi_{12}\Phi_{22}^{-1}\Phi_{12}^T < 0$, application of the Schur's complement method gives

$$\begin{bmatrix} \frac{1}{\gamma}\mathbf{H}_l^T\mathbf{H}_l + \mathbf{Y}^{-1}(\mathbf{I}-\mathbf{W}-\mathbf{W}^T)\mathbf{Y}^{-1} & \hat{\mathbf{A}}_D^T + \mathbf{Y}^{-1}\mathbf{W}^T & \mathbf{Y}^{-1} \\ \star & -\mathbf{I} & 0 \\ \star & \star & -\mathbf{I} \end{bmatrix} < 0.$$

Again, expanding

$$\begin{bmatrix} \mathbf{Y}^{-1}(\mathbf{I}-\mathbf{W}-\mathbf{W}^T)\mathbf{Y}^{-1} & \hat{\mathbf{A}}_D^T + \mathbf{Y}^{-1}\mathbf{W}^T & \mathbf{Y}^{-1} \\ \star & -\mathbf{I} & 0 \\ \star & \star & -\mathbf{I} \end{bmatrix} - \begin{bmatrix} \mathbf{H}_l^T \\ 0 \\ 0 \end{bmatrix}(-\gamma\mathbf{I})^{-1} \times \begin{bmatrix} \mathbf{H}_l & 0 & 0 \end{bmatrix} < 0,$$

and applying the Schur's complement method

$$\begin{bmatrix} \mathbf{Y}^{-1}\mathbf{Y}^{-1} - \mathbf{Y}^{-1}\mathbf{M} - \mathbf{M}^T\mathbf{Y}^{-1} & \hat{\mathbf{A}}_D^T + \mathbf{M}^T & \mathbf{Y}^{-1} & \mathbf{H}_l^T \\ \star & -\mathbf{I} & 0 & 0 \\ \star & \star & -\mathbf{I} & 0 \\ \star & \star & \star & -\gamma\mathbf{I} \end{bmatrix} =$$

$$\begin{bmatrix} (\mathbf{Y}^{-1}-\mathbf{M}^T)(\mathbf{Y}^{-1}-\mathbf{M}) - \mathbf{M}^\mathbf{T}\mathbf{M} & \hat{\mathbf{A}}_D^T + \mathbf{M}^T & \mathbf{Y}^{-1} & \mathbf{H}_l^T \\ \star & -\mathbf{I} & 0 & 0 \\ \star & \star & -\mathbf{I} & 0 \\ \star & \star & \star & -\gamma\mathbf{I} \end{bmatrix} < 0,$$

where $\mathbf{M} = \mathbf{W}\mathbf{Y}^{-1}$. Finally, the above inequality can be written as

$$\begin{bmatrix} -\mathbf{M}^\mathbf{T}\mathbf{M} & \hat{\mathbf{A}}_D^T + \mathbf{M}^T & \mathbf{Y}^{-1} & \mathbf{H}_l^T \\ \star & -\mathbf{I} & 0 & 0 \\ \star & \star & -\mathbf{I} & 0 \\ \star & \star & \star & -\gamma\mathbf{I} \end{bmatrix} - \begin{bmatrix} \mathbf{Y}^{-1} - \mathbf{M}^T \\ 0 \\ 0 \\ 0 \end{bmatrix}(-\mathbf{I})^{-1} \times \begin{bmatrix} \mathbf{Y}^{-1} - \mathbf{M} & 0 & 0 & 0 \end{bmatrix} < 0,$$

which gives

$$\begin{bmatrix} -\mathbf{M}^T\mathbf{M} & \hat{\mathbf{A}}_D^T + \mathbf{M}^T & \mathbf{Y}^{-1} & \mathbf{H}_l^T & \mathbf{Y}^{-1} - \mathbf{M}^T \\ \star & -\mathbf{I} & 0 & 0 & 0 \\ \star & \star & -\mathbf{I} & 0 & 0 \\ \star & \star & \star & -\gamma\mathbf{I} & 0 \\ \star & \star & \star & \star & -\mathbf{I} \end{bmatrix} < 0. \qquad \text{(A-28)}$$

Substituting $\mathbf{Q} = \mathbf{M}^T\mathbf{M}$, $\mathbf{X}_P = \mathbf{Y}^{-1}$ and $\hat{\mathbf{A}}_D^T = \mathbf{A}_0^T + \bar{\mathbf{C}}^T\mathbf{K}_d^T\bar{\mathbf{B}}^T$, the result follows.

■

A.6 Proof of the Block Diagonal Approximation

It is straightforward to show that finding a structured $\tilde{\mathbf{G}}_1(s)$ such that $\bar{\sigma}[\mathbf{D}_r(\mathbf{G}_1(j\omega) - \tilde{\mathbf{G}}_1(j\omega))\mathbf{D}_r^{-1}] < \gamma$ is equivalent to solving the following optimization problem (after applying some transformations on the on the standard $\mathcal{H}_\infty$ result [91])

$$\begin{aligned} & \min \ \gamma \\ & \text{subject to } \mathbf{P} > 0, \\ & \begin{bmatrix} \mathbf{A}_{cl}^T\mathbf{P} + \mathbf{P}\mathbf{A}_{cl} & \mathbf{P}\mathbf{B}_{cl}\mathbf{D}_r^{-1} & \mathbf{C}_{cl}^T\mathbf{D}_r^T \\ \star & -\gamma\mathbf{I} & (\mathbf{D}_r^{-1})^T\mathbf{D}\mathbf{D}_r^T \\ \star & \star & -\gamma\mathbf{I} \end{bmatrix} < 0. \end{aligned} \tag{A-29}$$

Pre- and Post multiplying (A-29) by diag $(\mathbf{I}, \mathbf{D}_r^T, \mathbf{D}_r^T)$ and diag $(\mathbf{I}, \mathbf{D}_r, \mathbf{D}_r)$, respectively

$$\mathbf{P} > 0, \quad \begin{bmatrix} \mathbf{A}_{cl}^T\mathbf{P} + \mathbf{P}\mathbf{A}_{cl} & \mathbf{P}\mathbf{B}_{cl} & \mathbf{C}_{cl}^T\mathbf{H} \\ \star & -\gamma\mathbf{H} & \mathbf{D}_{cl}^T\mathbf{H} \\ \star & \star & -\gamma\mathbf{H} \end{bmatrix} < 0, \tag{A-30}$$

where $\mathbf{H} = \mathbf{D}_r^T\mathbf{D}_r$. It is clear that the optimization problem involves bilinear terms at each position. Pre- and post multiplying (A-30) by diag $(\mathbf{P}^{-1}, \mathbf{I}, \mathbf{I})$ and diag $(\mathbf{P}^{-1}, \mathbf{I}, \mathbf{I})$, respectively, the conditions are equivalent to

$$\mathbf{Y} > 0, \text{ and } \begin{bmatrix} \mathbf{Y}\mathbf{A}_{cl}^T + \mathbf{A}_{cl}\mathbf{Y} & \mathbf{B}_{cl} & \mathbf{Y}\mathbf{C}_{cl}^T\mathbf{H} \\ \star & -\gamma\mathbf{H} & \mathbf{D}_{cl}^T\mathbf{H} \\ \star & \star & -\gamma\mathbf{H} \end{bmatrix} < 0,$$

where $\mathbf{Y} = \mathbf{P}^{-1}$. This can be expanded using the Schur's complement method [14] as

$$\begin{bmatrix} \mathbf{Y}\mathbf{A}_{cl}^T + \mathbf{A}_{cl}\mathbf{Y} + \frac{\mathbf{Y}\mathbf{C}_{cl}^T\mathbf{H}\mathbf{C}_{cl}\mathbf{Y}}{\gamma} & \mathbf{B}_{cl} + \frac{\mathbf{Y}\mathbf{C}_{cl}^T\mathbf{H}\mathbf{D}_{cl}}{\gamma} \\ \star & -\gamma\mathbf{H} + \frac{\mathbf{D}_{cl}^T\mathbf{H}\mathbf{D}_{cl}}{\gamma} \end{bmatrix} < 0,$$

and further into

$$\begin{aligned} & \mathbf{Y}\mathbf{A}_{cl}^T + \mathbf{A}_{cl}\mathbf{Y} + \frac{\mathbf{Y}\mathbf{C}_{cl}^T\mathbf{H}\mathbf{C}_{cl}\mathbf{Y}}{\gamma} + \left(\mathbf{B}_{cl} + \frac{\mathbf{Y}\mathbf{C}_{cl}^T\mathbf{H}\mathbf{D}_{cl}}{\gamma}\right) \\ & \times \left(\gamma\mathbf{H} - \frac{\mathbf{D}_{cl}^T\mathbf{H}\mathbf{D}_{cl}}{\gamma}\right)^{-1} \left(\mathbf{B}_{cl}^T + \frac{\mathbf{D}_{cl}^T\mathbf{H}\mathbf{C}_{cl}\mathbf{Y}}{\gamma}\right) < 0, \end{aligned} \tag{A-31}$$

$$\left(-\gamma\mathbf{H} + \frac{\mathbf{D}_{cl}^T\mathbf{H}\mathbf{D}_{cl}}{\gamma}\right) < 0. \tag{A-32}$$

Now, it is well known that according to the reciprocal projection lemma [4], the following conditions are equivalent

1. $\Psi + \mathbf{S} + \mathbf{S}^T < 0$.
2. For any given positive-definite matrix $\mathbf{X}$, the LMI problem

$$\begin{bmatrix} \Psi + \mathbf{X} - (\mathbf{W} + \mathbf{W}^T) & \mathbf{S}^T + \mathbf{W}^T \\ \star & -\mathbf{X} \end{bmatrix} < 0$$

is feasible with respect to $\mathbf{W}$, where $\mathbf{W}$ is a decision variable.

Therefore, applying this lemma to the inequality in (A-31)

$$\begin{bmatrix} \mathcal{F}_{11}+\mathbf{X}-(\mathbf{W}+\mathbf{W}^T) & \mathbf{Y}\mathbf{A}_{cl}^T+\mathcal{F}_{12}+\mathbf{W}^T \\ \star & -\mathbf{X} \end{bmatrix} < \mathbf{0}, \tag{A-33}$$

where

$$\begin{aligned} \mathcal{F}_{11} &= \frac{\mathbf{Y}\mathbf{C}_{cl}^T\mathbf{H}\mathbf{D}_{cl}}{\gamma}\left(\gamma\mathbf{H}-\frac{\mathbf{D}_{cl}^T\mathbf{H}\mathbf{D}_{cl}}{\gamma}\right)^{-1}\frac{\mathbf{D}_{cl}^T\mathbf{H}\mathbf{C}_{cl}\mathbf{Y}}{\gamma}+\frac{\mathbf{Y}\mathbf{C}_{cl}^T\mathbf{H}\mathbf{C}_{cl}\mathbf{Y}}{\gamma} \\ &\quad +\mathbf{B}_{cl}\left(\gamma\mathbf{H}-\frac{\mathbf{D}_{cl}^T\mathbf{H}\mathbf{D}_{cl}}{\gamma}\right)^{-1}\mathbf{B}_{cl}^T, \\ \mathcal{F}_{12} &= \frac{\mathbf{Y}\mathbf{C}_{cl}^T\mathbf{H}\mathbf{D}_{cl}}{\gamma}\left(\gamma\mathbf{H}-\frac{\mathbf{D}_{cl}^T\mathbf{H}\mathbf{D}_{cl}}{\gamma}\right)^{-1}\mathbf{B}_{cl}^T. \end{aligned}$$

Since, $\mathbf{X}$ can be any given positive definite matrix and $\mathbf{B}_{cl}\left(\gamma\mathbf{H}-\frac{\mathbf{D}_{cl}^T\mathbf{H}\mathbf{D}_{cl}}{\gamma}\right)^{-1}\mathbf{B}_{cl}^T$ is symmetric, in most of the cases, the parameters $(\mathbf{B}_d, \mathbf{D}_d)$, γ, $\mathbf{H}$ and $\mathbf{X}$ can be designed such that

$$\mathbf{X}+\mathbf{B}_{cl}\left(\gamma\mathbf{H}-\frac{\mathbf{D}_{cl}^T\mathbf{H}\mathbf{D}_{cl}}{\gamma}\right)^{-1}\mathbf{B}_{cl}^T=\mathbf{I}. \tag{A-34}$$

This selection is done to decouple the design variables from the positive definite matrix $\mathbf{Y}$. If, in some cases, this is not satisfied, then similar to [108], a large decision variable λ can *always* be selected such that positive definiteness of

$$\mathbf{X}=\lambda\mathbf{I}-\mathbf{B}_{cl}\left(\gamma\mathbf{H}-\frac{\mathbf{D}_{cl}^T\mathbf{H}\mathbf{D}_{cl}}{\gamma}\right)^{-1}\mathbf{B}_{cl}^T \tag{A-35}$$

is guaranteed.

Case I: With the selection in (A-34), (A-33) is equivalent to

$$\begin{bmatrix} \mathbf{I}+\mathcal{Z}_{11}-(\mathbf{W}+\mathbf{W}^T) & \mathbf{Y}\mathbf{A}_{cl}^T+\mathcal{Z}_{12}+\mathbf{W}^T \\ \star & -\mathbf{I}+\mathbf{B}_{cl}\left(\gamma\mathbf{H}-\frac{\mathbf{D}_{cl}^T\mathbf{H}\mathbf{D}_{cl}}{\gamma}\right)^{-1}\mathbf{B}_{cl}^T \end{bmatrix} < \mathbf{0},$$

where $\mathcal{Z}_{11} = \frac{\mathbf{Y}\mathbf{C}_{cl}^T\mathbf{H}\mathbf{D}_{cl}}{\gamma}\left(\gamma\mathbf{H}-\frac{\mathbf{D}_{cl}^T\mathbf{H}\mathbf{D}_{cl}}{\gamma}\right)^{-1}\frac{\mathbf{D}_{cl}^T\mathbf{H}\mathbf{C}_{cl}\mathbf{Y}}{\gamma}+\frac{\mathbf{Y}\mathbf{C}_{cl}^T\mathbf{H}\mathbf{C}_{cl}\mathbf{Y}}{\gamma}$, $\mathcal{Z}_{12} = \frac{\mathbf{Y}\mathbf{C}_{cl}^T\mathbf{H}\mathbf{D}_{cl}}{\gamma}\left(\gamma\mathbf{H}-\frac{\mathbf{D}_{cl}^T\mathbf{H}\mathbf{D}_{cl}}{\gamma}\right)^{-1}\mathbf{B}_{cl}^T$. Pre- and post multiplying by diag $(\mathbf{Y}^{-1},\mathbf{I})$ and diag $(\mathbf{Y}^{-1},\mathbf{I})$, respectively and expanding the above inequality

$$\begin{bmatrix} \mathbf{Y}^{-1}\mathbf{Y}^{-1}+\frac{\mathbf{C}_{cl}^T\mathbf{H}\mathbf{C}_{cl}}{\gamma}-\mathbf{Y}^{-1}\mathbf{M}-\mathbf{M}^T\mathbf{Y}^{-1} & \mathbf{A}_{cl}^T+\mathbf{M}^T \\ \star & -\mathbf{I} \end{bmatrix} - \begin{bmatrix} \frac{\mathbf{C}_{cl}^T\mathbf{H}\mathbf{D}_{cl}}{\gamma} \\ \mathbf{B}_{cl} \end{bmatrix}$$
$$\times\left(-\gamma\mathbf{H}+\frac{\mathbf{D}_{cl}^T\mathbf{H}\mathbf{D}_{cl}}{\gamma}\right)^{-1}\begin{bmatrix} \frac{\mathbf{D}_{cl}^T\mathbf{H}\mathbf{C}_{cl}}{\gamma} & \mathbf{B}_{cl}^T \end{bmatrix} < \mathbf{0},$$

where $\mathbf{M}=\mathbf{W}\mathbf{Y}^{-1}$. Using the Schur's complement

$$\begin{bmatrix} \mathbf{Y}^{-1}(\mathbf{Y}^{-1}-\mathbf{M})-\mathbf{M}^T\mathbf{Y}^{-1}+\frac{\mathbf{C}_{cl}^T\mathbf{H}\mathbf{C}_{cl}}{\gamma} & \mathbf{A}_{cl}^T+\mathbf{M}^T & \frac{\mathbf{C}_{cl}^T\mathbf{H}\mathbf{D}_{cl}}{\gamma} \\ \star & -\mathbf{I} & \mathbf{B}_{cl} \\ \star & \star & -\gamma\mathbf{H}+\frac{\mathbf{D}_{cl}^T\mathbf{H}\mathbf{D}_{cl}}{\gamma} \end{bmatrix} < 0.$$

This inequality can be further expanded as

$$\begin{bmatrix} \mathbf{Y}^{-1}\mathbf{Y}^{-1} - \mathbf{Y}^{-1}\mathbf{M} - \mathbf{M}^T\mathbf{Y}^{-1} & \mathbf{A}_{cl}^T + \mathbf{M}^T & 0 \\ \star & -\mathbf{I} & \mathbf{B}_{cl} \\ \star & \star & -\gamma\mathbf{H} \end{bmatrix} + \begin{bmatrix} \mathbf{C}_{cl}^T\mathbf{H} \\ 0 \\ \mathbf{D}_{cl}^T\mathbf{H} \end{bmatrix}$$
$$\times(\gamma\mathbf{H})^{-1}\begin{bmatrix} \mathbf{H}\mathbf{C}_{cl} & 0 & \mathbf{H}\mathbf{D}_{cl} \end{bmatrix} < 0, \tag{A-36}$$

which is equivalent to

$$\begin{bmatrix} 2\mathbf{X}_P\mathbf{X}_P + \mathbf{M}^T\mathbf{M} - \mathbf{Q} & \mathbf{A}_{cl}^T + \mathbf{M}^T & 0 & \mathbf{C}_{cl}^T\mathbf{H} \\ \star & -\mathbf{I} & \mathbf{B}_{cl} & 0 \\ \star & \star & -\gamma\mathbf{H} & \mathbf{D}_{cl}^T\mathbf{H} \\ \star & \star & \star & -\gamma\mathbf{H} \end{bmatrix} < 0, \tag{A-37}$$

where $\mathbf{X}_P = \mathbf{Y}^{-1}$ and $\mathbf{Q} = (\mathbf{X}_P + \mathbf{M})^T(\mathbf{X}_P + \mathbf{M})$. Finally, applying the Schur's complement method to the inequality in (A-37) and relaxing the equality constraint

$$\begin{bmatrix} -\mathbf{Q} & \mathbf{A}_{cl}^T + \mathbf{M}^T & 0 & \mathbf{C}_{cl,h}^T & \sqrt{2}\mathbf{X}_P & \mathbf{M}^T \\ \star & -\mathbf{I} & \mathbf{B}_{cl} & 0 & 0 & 0 \\ \star & \star & -\gamma\mathbf{H} & \mathbf{D}_{cl,h}^T & 0 & 0 \\ \star & \star & \star & -\gamma\mathbf{H} & 0 & 0 \\ \star & \star & \star & \star & -\mathbf{I} & 0 \\ \star & \star & \star & \star & \star & -\mathbf{I} \end{bmatrix} < 0,$$
$$\begin{bmatrix} \mathbf{Q} & \mathbf{X}_P + \mathbf{M}^T \\ \star & \mathbf{I} \end{bmatrix} \geq 0, \tag{A-38}$$

where $\mathbf{Q} = (\mathbf{X}_P + \mathbf{M})^T(\mathbf{X}_P + \mathbf{M})$ corresponds to the boundary of the convex set in (A-38). Moreover, the inequality $\left(-\gamma\mathbf{H} + \frac{D_{cl}^T\mathbf{H}\mathbf{D}_{cl}}{\gamma}\right) < 0$ is equivalent to

$$\begin{bmatrix} -\gamma\mathbf{H} & \mathbf{D}_{cl}^T\mathbf{H} \\ \star & -\gamma\mathbf{H} \end{bmatrix} < 0.$$

■